Peptidic Neuropeptide Y Y_4 Receptor Agonists: Synthesis, Pharmacology and Stability

DISSERTATION
ZUR ERLANGUNG DES DOKTORGRADES DER NATURWISSENSCHAFTEN
(DR. RER. NAT.)
AN DER FAKULTÄT FÜR CHEMIE UND PHARMAZIE
DER UNIVERSITÄT REGENSBURG

vorgelegt von Albert Owusu Gattor

aus Accra, Ghana

im Jahr 2025

This thesis was prepared between September 2020 and March 2025 under the supervision of Prof. Dr. Max Keller at the Institute of Pharmacy, Faculty of Chemistry and Pharmacy, University of Regensburg.

The application for promotion was submitted on 15th April, 2025.

Date of the oral examination:	28th May, 2025
Chairman of the examination board:	Prof. Dr. Steffen Pockes
First reviewer:	Prof Dr. Max Keller
Second reviewer:	Prof. Dr. Patrick Vanderheyden
Third examiner:	Prof. Dr. Joachim Wegener

To my sisters, Winnie & Ella

Imagination is everything.

It is the preview of life's coming attractions

– Albert Einstein

Acknowledgement

I would like to express my heartfelt gratitude to everyone who has supported me throughout the journey of my dissertation.

First and foremost, I extend my sincerest thanks to my advisor, Prof. Dr. Max Keller, whose guidance and expertise have been invaluable in shaping my research and academic growth. His unwavering support, scientific advice on all aspects of my research, as well as his support in the preparation of the manuscripts and the constructive review of the work, has brought me this far.

I would also like to thank:

Prof. Dr. Pierre Koch for his invaluable support,

Prof. Dr. Miguel Castanho and Dr. Marco Cavacao for facilitating and supervising my research stay at the Institute of Molecular Medicine at the University of Lisbon in Portugal and to the whole research group for making my research stay fruitful,

The Research Training Group 1910 “Medicinal chemistry of selective GPCR ligands”, funded by the German Research Foundation (DFG), for the financing of the research stay,

Ms. Maria Beer-Krön for her kind support in cell culture, for conducting the cAMP and some radioligand binding assays as well, and for her willingness to allow me to practice German with her. Ms. Susanne Bollwein, and Ms. Brigitte Wenzl for their unwavering support in the performance of the radioligand competition binding assays,

Mr. Franz Wiesenmayer for his support in obtaining the rat brains and intestines for the autoradiography studies, Dr. Lisa Schindler and Franziska Schettler for the cryosectioning of the organs for the autoradiographic study,

Mr. Fritz Kastner and Mr. Josef Kiermaier for their expert support regarding the evaluation of NMR and mass spectra, as well as for the prompt processing of the measurement orders,

Mr. Peter Richthammer for his friendliness and technical support and Ms. Silvia Heinrich for her reliable support in organizational and bureaucratic matters.

I would also like to acknowledge my colleagues at the Lehrstuhl Koch for their camaraderie and collaboration, which fostered a stimulating intellectual environment. I would also like to thank you all for all the good moments we shared.

Lastly, I extend my heartfelt thanks to my family and friends for their unwavering support and understanding during this challenging yet rewarding endeavor.

Me Da Mo Nyinaa Ase !!!

Publications, presentations, and professional training

Publications (peer-reviewed articles; published prior to the submission of this thesis)

Schettler, F.; **Gattor, A. O.**; Koch, P.; Keller, M. Characterization of [^{3}H]propionylated human peptide YY – a new probe for neuropeptide Y Y_2 receptor binding studies. *ACS Pharmacol. Transl. Sci.* 2025, *8* (3), 785-799. DOI: 10.1021/acsptsci.4c00666.

Ertl, F. J.; Kopanchuk, S.; Dijon, N. C.; Veiksina, S.; Tahk, M. J.; Laasfeld, T.; Schettler, F.; **Gattor, A. O.**; Hubner, H.; Archipowa, N.*;* Köckenberger, J.; Heinrich, M. R.; Gmeiner, P.; Kutta, R. J.; Holliday, N. D.; Rinken, A.; and Keller, M. Dually labeled neurotensin NTS_1R ligands for probing radiochemical and fluorescence-based binding assays. *J. Med. Chem.* 2024, *67* (18), 16664-16691. DOI: 10.1021/acs.jmedchem.4c01470.

Gleixner, J.; Kopanchuk, S.; Gratz, L.; Tahk, M. J.; Laasfeld, T.; Veiksina, S.; Horing, C.; **Gattor, A. O.**; Humphrys, L. J.; Müller, C.*;* Archipowa, N.*;* Köckenberger, J.; Heinrich, M. R.; Kutta, R. J.; Rinken, A.; and Keller M. Illuminating neuropeptide Y Y_4 receptor binding: fluorescent cyclic peptides with subnanomolar binding affinity as novel molecular tools. *ACS Pharmacol. Transl. Sci.* 2024, *7* (4), 1142-1168. DOI: 10.1021/acsptsci.4c00013.

Gleixner, J.[#]; **Gattor, A. O.**[#]; Humphrys, L. J.; Brunner, T.; Keller, M. [^{3}H]UR-JG102–a radiolabeled cyclic peptide with high affinity and excellent selectivity for the neuropeptide Y Y_4 receptor. *J. Med. Chem.* 2023, *66* (19), 13788-13808. DOI: 10.1021/acs.jmedchem.3c01224. [#]Equally contributed.

Plut, E.; Calderon, J. C.; Stanojlovic, V.; **Gattor, A. O.**; Horing, C.; Humphrys, L. J.; Konieczny, A.; Kerres, S.; Schubert, M.; Keller, M.*;* Cabrele, C.; Clark, T.; and Reiser, Oliver. Stereochemistry-driven interactions of α,γ-peptide ligands with the neuropeptide Y Y_4 Receptor. *J. Med. Chem.* 2023, *66* (14), 9642-9657. DOI: 10.1021/acs.jmedchem.3c00363.

Konieczny, A.; Conrad, M.; Ertl, F. J.; Gleixner, J.; **Gattor, A. O.**; Grätz, L.; Schmidt, M. F.; Neu, E.; Horn, A. H. C.; Wifling, D.*;* Gmeiner, P.; Clark, T.; Sticht, H.; and Keller, M. N-Terminus to arginine side-chain cyclization of linear peptidic neuropeptide Y Y_4 receptor ligands results in picomolar binding constants. *J. Med. Chem.* 2021, *64* (22), 16746-16769. DOI: 10.1021/acs.jmedchem.1c01574.

Poster presentations (only contributions as presenting author are listed)

Gattor, A. O.; Gleixner, J.; Keller, M. [^{3}H]UR-JG102 – A new molecular tool for binding studies at the neuropeptide Y Y_4 receptor in sodium-containing buffers. *Summer School Medicinal Chemistry* - DPhG (2023, Regensburg, Germany).

Gattor, A. O.; Gleixner, J.; Keller, M. [^{3}H]UR-JG102 – A new molecular tool for binding studies at the neuropeptide Y Y_4 receptor in sodium-containing buffers. *Annual Meeting of the German Pharmaceutical Society* - DPhG (2022, Marburg, Germany).

Oral presentation

Gattor, A. O. Making Santa Slim Again. *25. Regensburger Weihnachtskolloquium-Instiitut für Organische Chemie*. (December 2023, Regensburg, Germany)

Gattor, A. O. Peptidic NPY Y_4 receptor ligands: design strategies for stable analogs and characterizing the high-affinity [^{3}H]UR-JG102. *Annual retreat of the research training group 1910 "Medicinal chemistry of selective GPCR ligands"* (2022, Fensterbach, Germany)

Gattor, A. O. Peptidic NPY Y_4 receptor ligands: degradation in human plasma and design strategies for stable analogs. *Annual retreat of the research training group 1910 "Medicinal chemistry of selective GPCR ligands"* (2021, Regensburg, Germany)

Professional training

Seminar: Radioanalytical working methods for Pharmacists and Scientists (June 2022, Regensburg).

Member of the research training group 1910 "Medicinal chemistry of selective GPCR ligands" funded by Deutsche Forschungsgemeinschaft (DFG) (2020-2023)

Table of Contents

Chapter 1

General Introduction

1.1 Overview of neuropeptide Y receptor family and their ligands

1.1.1 Neuropeptide Y receptor family

The neuropeptide Y (NPY) receptor (YR) family, since its discovery in mammals, has been shown to be involved in several important physiological activities due to the abundance of their endogenous ligands —NPY, pancreatic polypeptide (PP), peptide YY (PYY) and their derivatives— in both the central nervous system (CNS) and peripheral tissues.[1, 2] This receptor family is made up of 6 subtypes, which include the Y_1, Y_2, Y_4, Y_5, and Y_6 receptors, with the latter not being functional in humans.[1] Homologs of some of these subtypes, for example, Y_1, have also been found in other vertebrates and insects such as zebrafish, frogs, and drosophila, indicating their shared common evolutionary ancestry.[1, 3] The neuropeptide Y receptors belong to the rhodopsin-like family of GPCRs and mainly couple to the $G_{i/o}$ family of G-proteins, inhibiting adenyl cyclase activity upon activation.[3, 4] Nonetheless, some studies have also shown that these receptors can also couple to G_q and G_s family of G-proteins in some cell types such as muscles, which may transduce its signaling through the activation of phospholipase C or adenyl cyclase, respectively.[5, 6]

The physiological distribution of the NPY receptors has been extensively investigated, focusing on their gene and protein expression in humans and other mammals, such as rodents. Transcriptomic, immunogenic, and autoradiographic studies, among others, have shown the expression of the various YR subtypes in the CNS and peripheral tissues. The Y_1 subtype is expressed in the CNS, blood vessels, heart, airways, GIT, adrenal, and pancreatic glands, while for the Y_2 subtype, expression is majorly seen in the CNS.[3, 7-12] The Y_4 subtype, previously known as polypeptide 1 receptor (PP1R) due to its preference for PP, is mainly localized in the guts, with some detections in the testes, adipocytes, skin, kidney, and in some regions of the CNS.[3, 13-15] The Y_5 subtype is also expressed in the CNS, intestine, ovary, testis, skeletal muscles, liver, and heart.[12, 16] In contrast, the Y_6 subtype was shown to be a pseudogene in humans and monkeys but functionally expressed in the brains of rodents and rabbits.[3, 16-19]

1.1.2 The endogenous ligands of NPY receptors (YRs)

The endogenous ligands of the NPY receptor family consist of the NPY, which is mainly present in the CNS; PP, found predominantly in the periphery and, to some

extent, in the CNS; and PYY, which can be found in both the CNS and peripheral tissues.[20] All these peptides consist of 36 amino acids, differing in composition at a few positions (Figure 1.1), and in turn, have similar amino acid residues in distinct positions resulting in their characteristic hairpin PP-fold structure (consisting of an alpha helix motif, a β-turn, and a random coil end) (Figures 1.1 and 1.2). Furthermore, they all exhibit an amidated C-terminus, enhancing their stability against enzymatic (carboxypeptidase) degradation,[21] and as such, are classified as the NPY peptide family. Despite these similarities, NPY is referred to as a neurotransmitter due to its abundance and activity in the CNS. In contrast, PYY and PP are generally recognized as gut hormones owing to their presence and activities in the GIT.[22, 23] Endogenous derivatives of these ligands (such as NPY_{3-35} and PYY_{3-36}) are also found in human blood circulation, formed by *in vivo* enzymatic activities that typically result in truncation at the N-terminus.[24, 25] Depending on the number of the N-terminal residues removed, the receptor binding of these truncated peptides may be altered moderately or substantially.[14, 26] For example, removal of the first N-terminal residue (Tyr^1) of NPY to produce $NPY_{2–36}$ leads to a substantial loss of binding affinity.[16] In contrast, the removal of the two N-terminal residues (Tyr^1 and Pro^2) to obtain NPY_{3-36} significantly increases its Y_2R binding affinity.[15, 16]

Neuropeptide Y receptor activation by these peptides or their truncated derivatives can be directly and indirectly linked to regulating food intake, blood pressure, memory retention, etc. As such, it can be associated with the pathophysiology of obesity, seizures, feeding disorders, inflammation, mood disorders, circadian rhythm, pain, drug addiction, GI functions, and cardiac complications.[1, 27] This highlights the therapeutic potential of these receptors and their respective endogenous ligands.

Due to their structural similarities, the NPY family of receptors and peptides form a multiligand/multi-receptor system. All the NPY peptides can bind to the different YR subtypes at high affinities except for the Y_4 subtype, which preferentially binds to PP. A notable example is NPY's ability to bind to only Y_1R, Y_2R, and Y_5R with high affinity.[3, 28, 29] This multiligand/multi-receptor system has made it challenging to identify the specific roles of each subtype in the aforementioned physiological processes. Despite the general lack of YR binding selectivity by the NPY peptides, several radioligand binding studies have shown that their binding affinities to the different NPY receptor subtypes vary considerably.[3, 22] Leveraging this, along with recent developments in

subtype-selective YR agonists and antagonists, has facilitated detailed studies of some of the receptor subtypes. Among those studied, the NPY receptor subtypes Y_1 and Y_2 have been much investigated and well understood. On the contrary, the Y_4 and Y_5 subtypes have been the least studied, with limited knowledge about their expression and physiological relevance in the CNS or peripheral tissues.

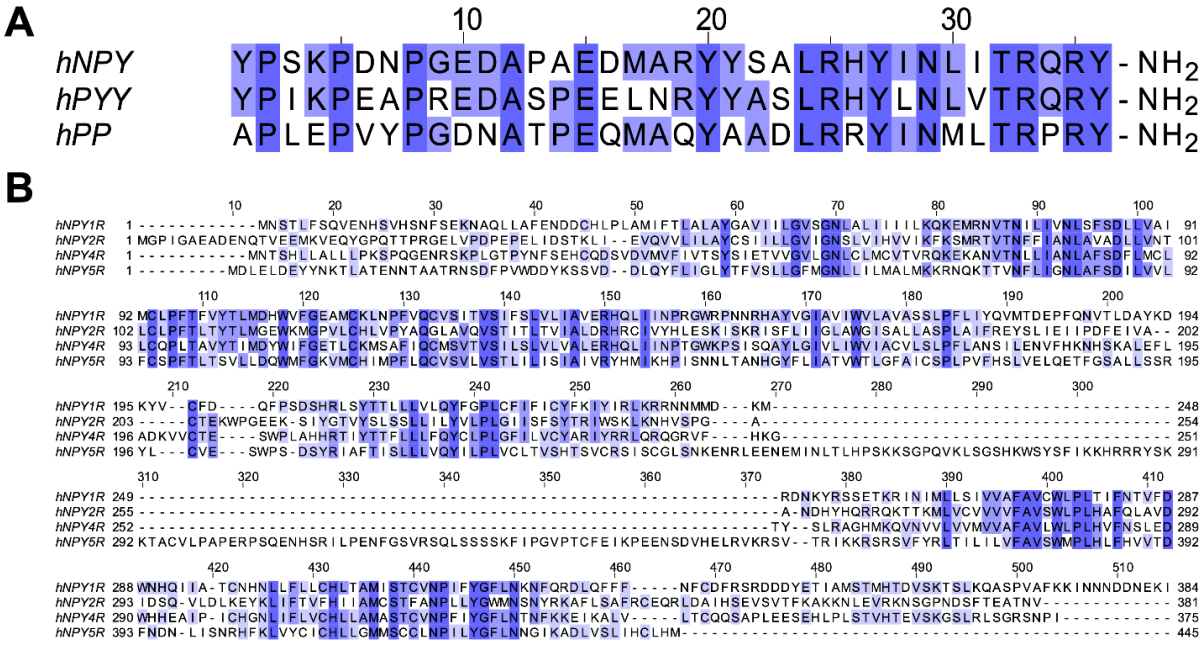

Figure 1.1. Amino acid sequence alignment of (A) human NPY, PYY, PP, and (B) the different human YR subtypes. Amino acid similarities are highlighted in blue (the color intensity directly correlates with amino acid similarities in the individual positions).

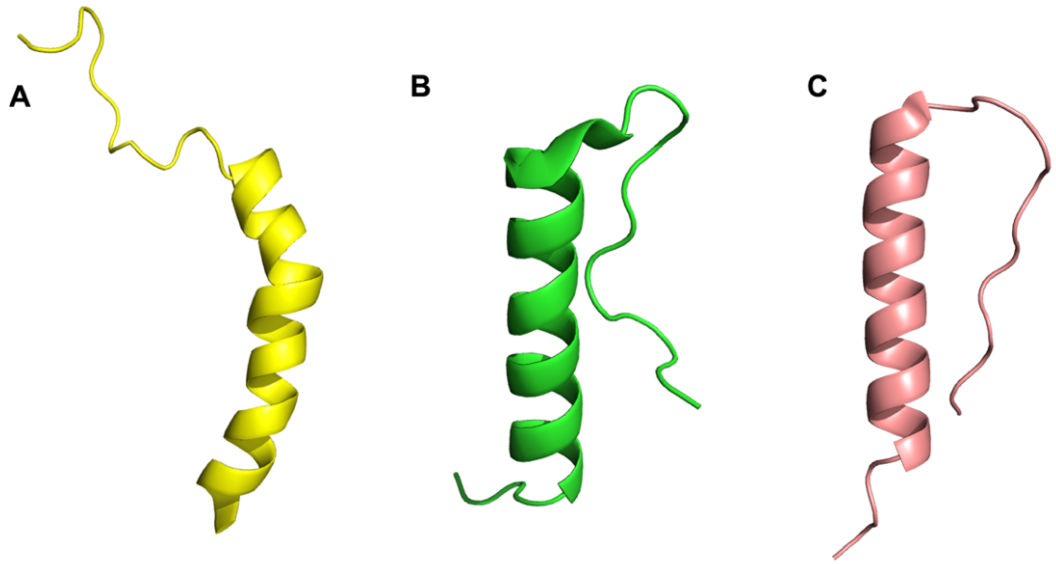

Figure 1.2. Secondary peptide structures of human NPY (A, PDB:1RON), PYY (B, PDB:2DEZ), and PP (C, PDB:7X9C) showing the similar hairpin PP-fold. The α-helix motif is made of the amino acids in positions 12-35 for NPY, 12-31 for PYY, and 13-31 for PP.

1.2 The NPY Y_4 receptor (Y_4R)

1.2.1 Expression and regional distributions of Y_4R

The Y_4R, like other receptor subtypes in the NPY family, is a seven-transmembrane monomeric protein (composed of 375 amino acids in humans) that primarily couples with the $G_{i/o}$ family of G-proteins ($G_{i/o}$-proteins). It is encoded by an 8kb long gene located on chromosome 10q11.22, which is not clustered with the genes encoding the other YR subtypes.[30, 31] Compared to the other three functional NPY family receptor subtypes, the Y_4 subtype is the least conserved among species and the fastest-evolving receptor subtype.[19] A sequence comparison study of the different receptor subtypes indicates that Y_4 is more closely related to Y_1 and Y_6 than to Y_2 and Y_5.[3, 32]

Several functional and non-functional variants of the *NPY4R* gene have been identified on the human chromosome.[30, 33] On the gene level, 12 naturally occurring single nucleotide variant forms of the receptor have been identified in a study of the Swedish population.[33] Out of these 12 single nucleotide variants, seven were shown to be functionally similar to the wild type in this study, while the other five were functionally inactive. At the mRNA level, three possible splice variants have been identified based on the three exons contained in the *NPY4R* gene (Ensembl database - GRCh38.p5).

As part of understanding and linking the molecular signaling of the Y_4R to its possible physiological functions, there is a need to identify where these receptors are localized. Several studies using ligand binding techniques (such as autoradiography), in situ hybridization, and immunohistochemistry have detected significant receptor expressions in some areas of the CNS and the peripheral tissues of humans and other mammals (Table 1.1). In humans, Y_4R is expressed in peripheral tissues, including the stomach, pancreas, small intestine, colon, adrenal glands, prostate, and skin epidermis.[12, 17, 34] In the CNS, Y_4R expression can be seen in the hypothalamus, thalamus, midbrain, and medulla oblongata.[12] Table 1.1 summarizes various Y_4R expression sites found in humans and rodents. It is important to note that, given the limitations of the methods used to detect Y_4R expression, such as the likely insensitivity of the detection probes to lowly expressed proteins or to the low copies of DNA or RNA, as well as their low reproducibility,[41, 42] generalizing the potential role of Y_4R in relation to their expression sites, particularly across species, should be

approached with caution as the regional distribution and localization of the Y_4R may vary among different species.[10, 12]

Table 1.1. Selected mRNA and protein expression sites of Y_4R in humans and rodents and the methods used

Expression sites	Species	Methods used to determine expression	References
Peripheral Tissues			
Pancreas, small intestine, colon, prostate, stomach, epidermal skin, adrenal glands	human	Northern blotting, immunoblotting, immunohistochemistry, immunolocalization, immunoreactivity	Gregor *et al.*[34], Aragon *et al.*[17], Dumont *et. al.*[35], Fagerberg *et al.*[12]
Intestine, testes, lungs, adrenal glands, arteries	rats	RT-PCR, Northern blot	Goumain *et al.*[36], Lundell *et al.*[37], Barriors *et al.*[18]
Central nervous system (CNS)			
Hypothalamus, thalamus, medulla	human	Immunohistochemistry	Fagerberg *et al.*[12]
Brainstem, hippocampus, hypothalamus, and striatum	mice	Immunoblotting	Aragon *et al.*[17]
Hypothalamus, vagus nerves, ventrolateral medulla, dorsal motor nucleus of vagus, area postrema, olfactory tubercle, interpeduncular nucleus and nucleus tractus solitarius	rats	*In situ* hybridization, autoradiography, immunocytochemistry	Whitcomb *et al.*[38], Stanley *et al.*[39], Campbell *et al.*[40]

1.2.2 Structure, signaling, and potential therapeutic relevance of human Y_4R

1.2.2.1 Structure and signaling

As a plasma membrane-bound GPCR, the Y_4R, consists of seven transmembrane helices, three intracellular loops (ICL1-3), and three extracellular loops (ECL1-3) (Figure 1.3).[43] With its N-terminus positioned on the extracellular side and the C-terminus on the intracellular side, the N-terminus of the receptor is involved in PP binding. The C-terminus, on the other hand, participates in interactions with effector proteins such as $G_{i/o}$-proteins and arrestin.[44, 45]

Findings from a cryo-EM structure of Y_4R have shown that the orthosteric binding pocket of Y_4R, located within the transmembrane (TM) helical bundle, is mainly formed by the TM2 to TM6 and the receptor's ECL2-3.[46] The study also revealed that upon

binding of the preferred Y_4R endogenous ligand PP in the orthosteric binding pocket, the α-helical region of PP leans against the receptor's N-terminus and makes extensive contact with the second and third extracellular loops (ECL2 and ECL3), while the peptide's N-terminus points towards the extracellular tip of TM5. These interactions and conformational changes also lead to an outward shift of TM6 and an inward movement of TM7, forming a cavity on the intracellular side of the receptor for binding of the $G\alpha_{i/o}$ subunit of the heterotrimeric $G_{i/o}$-proteins.

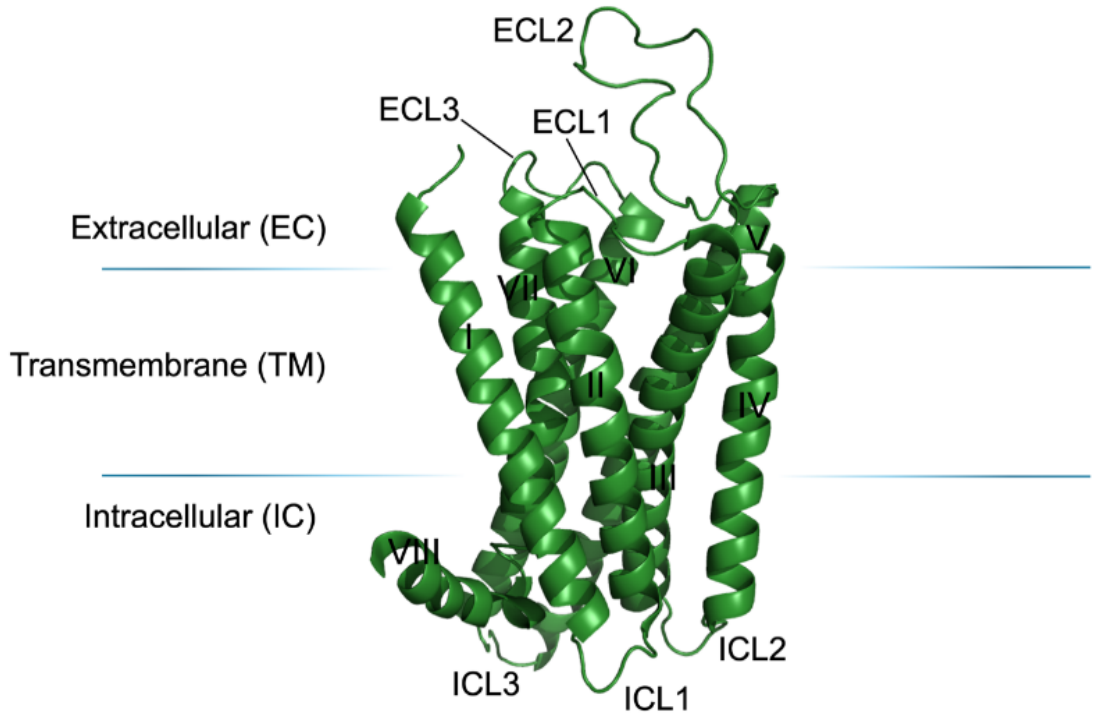

Figure 1.3. A cryo-EM structure of human Y_4R (PDB:7X9C) presented as cartoon. Image represents the innervation of the receptor through a membrane showing the seven transmembrane helices linked by three intracellular loops (ICL1-3) and three extracellular loops (ECL1-3).

These conformational changes, indicating the active state of the Y_4R, allow for the activation of the $G_{i/o}$-protein upon binding in the cavity. The $G_{i/o}$-protein consists of three subunits in complex: $G\alpha_{i/o}$, Gβ, and Gγ.[47] In its inactive state, it is bound to guanine diphosphate (GDP). It acts as a guanine nucleotide exchange factor (GEF) that induces the release of GDP to bind guanine triphosphate (GTP) to the $G\alpha_{i/o}$ subunit when complexed with Y_4R.[46, 48, 49] This leads to the dissociation of the $G\alpha_{i/o}$ subunit from the tightly bound Gβγ subunits, with $G\alpha_{i/o}$ and Gβγ complex functioning as separate effector proteins.[47] The $G\alpha_{i/o}$ subunit acts by inhibiting the activity of plasma membrane-bound adenyl cyclase (AC), which is known to convert adenosine

triphosphate (ATP) to cyclic adenosine monophosphate (cAMP), thereby reducing the intracellular cAMP levels in the cell.[47, 50] This lower cAMP level leads to a decrease in protein kinase A (PKA) activity, further affecting downstream signaling. The Gβγ subunits of the $G_{i/o}$-protein (functional when in complex with each other) also inhibit enzymes such as phospholipase C as well as Ca^{2+} channels and consequently Ca^{2+} influx, while stimulating GIRK (G protein-activated inwardly-rectifying K^+) channels.[6, 51, 52] These activities of the Gβγ subunits results in the modulation of membrane potentials and cellular excitability.

The activation of Y_4R, like all GPCRs, is typically followed by desensitization to decrease further stimulation or prevent overstimulation and maintain cellular homeostasis.[53] Receptor desensitization helps in regulating receptor sensitivity as well as the signaling duration. A primary mechanism for GPCR desensitization involves the phosphorylation of the intracellular side of the receptor by G protein-coupled receptor kinases (GRKs), followed by the binding of arrestins to these areas.[45, 54] This ultimately prevents the binding and further activation of G-proteins while facilitating the receptor's internalization. The internalized receptor bound to the activating ligand in the endosome is then dephosphorylated, while the ligand typically dissociates from it at the same time. Subsequently, the receptor is recycled back to the cell surface or degraded in the lysosomes.[55, 56] Another means of GPCR desensitization, but less common, is the phosphorylation-independent mechanism, where specific GRKs bind to the intracellular side of the receptor together with the G-proteins, thereby attenuating the receptor signaling.[57] The Y_4R is known to undergo agonist-induced and arrestin-dependent internalization, as a means of desensitization, with the rate of this desensitization directly correlating with the agonist's binding affinity.[58]

1.2.2.2 Potential therapeutic relevance of Y_4R agonism and antagonism

While the connection between Y_4R signaling and its physiological implications is not well understood, it is clear that YR activity influences regulatory functions tied to vital processes such as food intake, energy balance, gastrointestinal motility, reproductive functions, anxiety, and stress modulation.

Y_4R agonism. While Y_4R activation has been associated with regulating several physiological processes, most studies have focused solely on their role in the treatment of obesity. The potential therapeutic role of Y_4R in treating obesity can be

attributed to its ability to reduce food intake and appetite, given its high expression in peripheral tissues involved in digestion and areas of the brain known to regulate appetite and energy expenditure metabolism.[12] As expected, studies in mice over-expressing PP, the preferred endogenous agonist of Y_4R, led to reduced food intake and gastric emptying.[59, 60] In addition, mRNA expression of grehlin and orexin, the hunger hormones, in these rodents were significantly reduced. In another mice study, intraperitoneal injections of a high-affinity Y_4R peptidic agonist, BVD-74D, also suppressed food intake and body weight gain in the mice.[28, 61, 62] In humans, a study in patients with Prader–Willi syndrome (PWS) characterized by childhood-onset hyperphagia and morbid obesity showed that two times intravenous infusions of pancreatic polypeptide significantly reduced their food intake and led to weight loss.[63] A similar effect was also observed in a study with healthy volunteers.[64] Intravenous administration of PP an hour before their meal ingestion led to a reduction in their food intake. With these studies emphasizing the reduced food intake effect mediated by the activation of peripheral Y_4R, studies involving the central injection of PP directly into the dorsal vagal complex, led to reduced gastric emptying, gastric motility, and gastric acid secretion, all of which influence satiety, reducing appetite and in turn, food intake.[39, 65]

Y_4R antagonism. Despite the aforementioned therapeutic potentials of Y_4R agonists in treating obesity with respect to reducing food intake and appetite, a few studies involving Y_4R knockout obese or healthy mice indicated that antagonizing Y_4R or Y_4R/Y_2R activity could also help treat obesity by reducing adiposity, fat mass, and body weight.[66-68] A study[67] involving obese mice, which are known to be infertile due to the underdevelopment of reproductive organs and spermatogenesis,[69] revealed that the deletion of Y_4R led to an increase in testosterone levels as well as increased seminal vesicle and testis weight in males. In obese female mice, fertility was restored with improvement in mammary gland development. These findings highlight the therapeutic significance of Y_4R antagonism in treating obesity and infertility in obese people while also illustrating the complexity of Y_4R activity. However, it is important to note that studies using knockout mice may lead to misleading conclusions about the target gene's functions. This is due to the compensatory changes that are likely to occur in other genes or pathways, which can conceal the effects of the knockout gene.[70]

1.2.3 Y_4R Ligands

1.2.3.1 Endogenous ligands and their derivatives

Given that all members of the NPY peptides and their N-terminally truncated derivatives, such as NPY_{2-36} and PYY_{3-36}, could bind to Y_4R, their ability to act as endogenous Y_4R agonists may depend on their physiological concentrations relative to their Y_4R binding affinities as seen for most peptide hormones.[71-73] Thus, with the exception of PP, most of these peptides may not act as Y_4R agonist physiologically due to their low Y_4R binding affinities and physiological concentrations.[2, 20 74, 75] Y_4R binding studies of the NPY peptides showed that NPY and PYY similarly bind to Y_4R in the micromolar to nanomolar concentration range, while PP binds in the picomolar range.[76] Additionally, NPY, PYY, and PP derivatives exhibit reduced affinities toward Y_4R (up to 1,000-fold) compared to their parent peptides.[77, 78] Some studies have concluded that the distinct binding profiles of these peptides to Y_4R can be attributed to the amino acid residues in positions 31 and 34 of the C-terminus and those in positions 1 and 2 of the N-terminus (Figure 1.1A).[2, 79, 80] In addition, structural binding studies of PP to Y_4R have shown that the amino acid residues in the C-terminal pentapeptide sequence of PP, specifically the Arg residues in positions 33 and 35, are also essential for binding.[81, 82] Unlike the other endogenous ligands, these residues in PP, upon binding in the orthosteric Y_4R binding pocket, interact with crucial residues of TMs 2–7, like $Asp^{6.59}$ and $Asn^{7.32}$ necessary for inducing the receptor's active conformation.[83]

With the physiological levels of NPY peptides ranging between 0.01–0.4 nM, these findings imply that PP is the primary activator of Y_4R *in vivo*.[74, 75, 84, 85] It is worth mentioning that, for PP and PYY, these physiological levels are solely from their production and secretion in the periphery, as there is currently no evidence of their expression in the CNS of humans or other mammals.[86-88]

1.2.3.2 Non-endogenous ligands

So far, few reported ligands have been developed for Y_4R compared to the other YR subtypes. Some of these reported peptidic or peptidic-like ligands are based on the C-terminal pentapeptide sequence of NPY peptides and known Y_1R ligands because the Y_1R shares a high sequence similarity to Y_4R.[28, 29, 89, 90] One such ligand is BVD-74D, a selective Y_4R agonist, which was derived from the dimeric peptidic Y_1R antagonist

GR231118, represents a dimer of the pentapeptide (Tyr-Arg-Leu-Arg-Tyr-NH_2) (Figure 1.4A).[89] BVD-74D shows a very high Y_4R binding affinity (K_i (hY_4R): 0.05 nM).[28]

Serving as a lead structure, several monomeric and dimeric analogs of BVD-74D showing Y_4R binding affinities in the picomolar to nanomolar range and partial Y_4R agonism were developed. These include the recently reported dimeric ligand UR-KK200, which has the diaminosuberic acid linker replaced by an achiral octanedioic acid linker;[91] the dimeric UR-KK193, which has a modified moiety of GR231118 and an acylated diaminosuberic acid linker;[91] and the N-terminally acetylated hexapeptide UR-KK236, a monomeric derivative of the dimeric pentapeptide, BVD-47D (see structures in Figure 1.4A).[92]

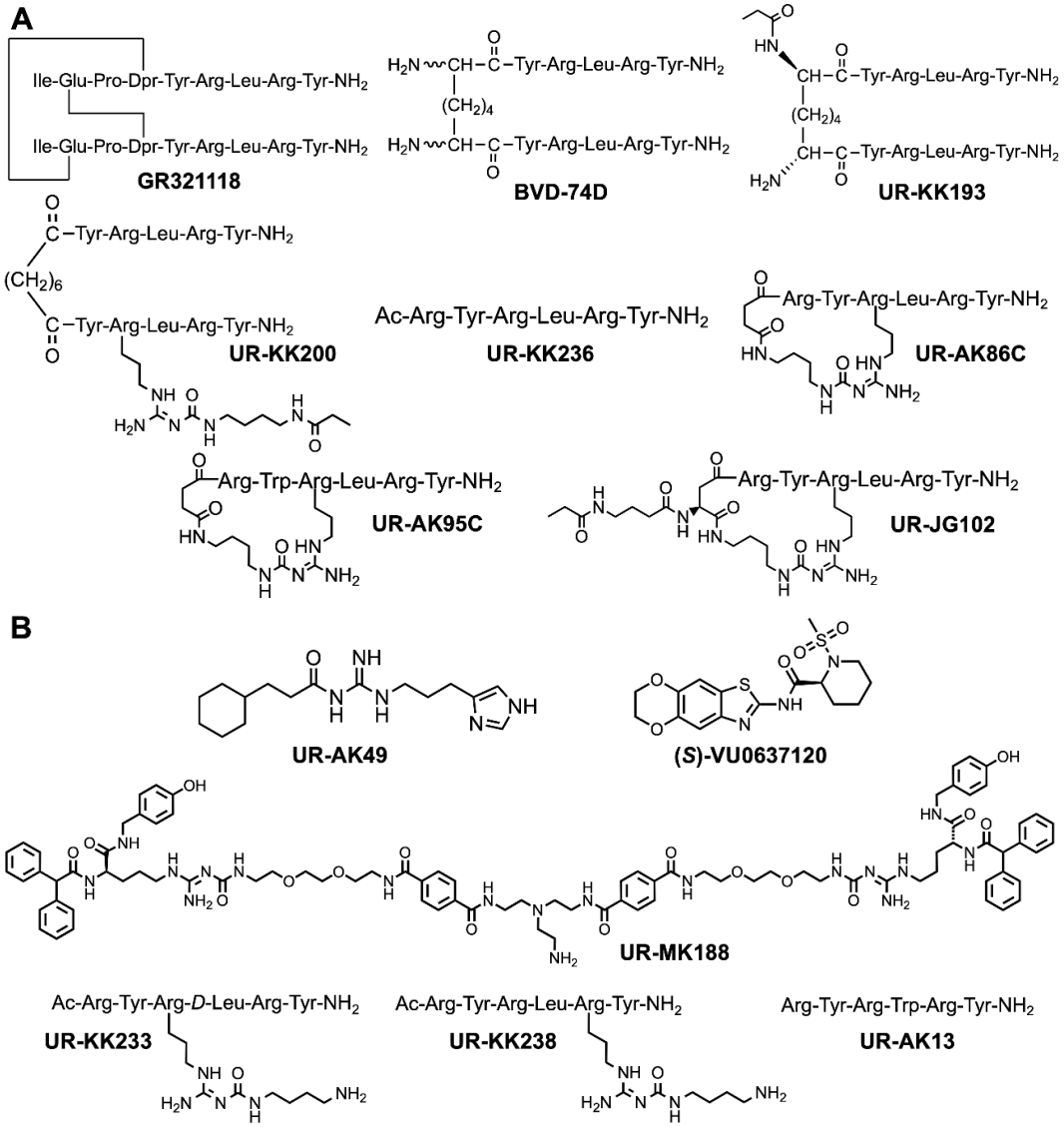

Figure 1.4. Structures of synthesized low molecular weight (A) agonists and (B) antagonists.

Further advancement aimed at obtaining small molecular weight agonists resulted in the synthesis of several linear and cyclic oligopeptides derived from UR-KK236.[29, 92, 93] Out of these, high Y_4R affinity cyclic hexapeptide partial agonists, UR-AK86C, UR-AK95C, and UR-JG102, with the potential of being lead structures for drug development, were reported (Figure 1.4A).[93, 94] The cyclization of these peptides was made possible by introducing a succinyl or aspartyl residue at the N-terminus of the peptide and replacing the Arg in position 3 with an amine-functionalized N^{ω}-carbamoylated Arg.[93, 95] Despite UR-AK86C, UR-AK95C, and UR-JG102 being cyclized, they exhibited low stability in human plasma (half-lives ca. 2 h).[93] The synthesis of UR-KK236 derivatives in search of potent agonists and antagonists also led to weak binding but Y_4R selective peptidic antagonists (e.g., UR-KK233[92], UR-KK238[92], and UR-AK13[29]), which represent potential structure-lead candidates for the development of Y_4R antagonists (Figure 1.4B).

Regarding the synthesis of non-peptidic ligands for Y_4R, several agonists, including a series of adipic acids amides and (*R,R*)-diaminocyclohexanes, have been reported.[103, 104] However, there is no information on their characterization and Y_4R binding affinities apart from their agonistic potencies in cAMP assays (EC_{50} ranging from 1 nM to 1 µM). With respect to the development of non-peptidic Y_4R antagonists, only three, i.e., UR-AK49, UR-MK188, and (*S*)-VU0637120, have been reported (Figure 1.4B).[101, 102] UR-AK49, an acylguanidine with an imidazole ring and a cyclohexyl moiety, was the first antagonist to be reported but exhibited a very weak binding affinity to Y_4R ($pK_i = 4.1$). In contrast, UR-MK188, obtained by dimerizing the known argininamide-type Y_1R antagonist BIBP3226 via the guanidine group, emerged as the first antagonist for Y_4R, exhibiting moderate binding affinity ($pK_i = 6.7$).[101] Notably, while the (*R*,*R*)-configured compound UR-MK188 also binds to Y_1R with an affinity in the nanomolar range, its (*S*,*S*)-configured enantiomer UR-MEK388, exhibiting Y_4R binding affinity comparable to that of UR-MK188, does not bind to Y_1R ($pK_i < 5.5$).[101] (*S*)-VU0637120, on the other hand, was the first Y_4R selective negative allosteric modulator to be reported with an inhibition constant also in the micromolar range ($pIC_{50} = 5.6$).[102] Binding in an allosteric site located below the orthosteric binding pocket, this antagonist decreased Y_4R activation in a concentration-dependent manner. An overview of some selected Y_4R ligands with their binding affinities is provided in Table 1.2.

Table 1.2. A summary of Y_4R ligands and their binding affinities

Ligand	Types	Y_4R binding affinity (pK_i /pIC_{50})	References
hPP	endogenous peptidic agonist	8.7–10.9 10.1–10.3*	Bard *et al*.[2], Lundell *et al*.[96], Tough *et al*.[97], Yan *et al*.[98], Gleixner *et al*.[94]
hPP_{2-36}	endogenous peptidic agonist	10.1*	Bard *et al*.[2]
hPP_{13-36}	peptidic agonist	7.1*	Bard *et al*.[2]
hNPY	endogenous peptidic agonist	8.0 8.7*	Lundell *et al*.[96], Bard *et al*.[2]
$hNPY_{2-36}$	endogenous peptidic agonist	7.8*	Bard *et al*.[2]
[Leu^{31},Pro^{34}]hNPY	peptidic agonist	7.7	Lundell *et al*.[96],
hPYY	endogenous peptidic agonist	8.8 9.0*	Lundell *et al*.[96], Bard *et al*.[2]
$hPYY_{3-36}$	endogenous peptidic agonist	7.9*	Bard *et al*.[2]
[Pro^{34}]hPYY	peptidic agonist	8.9*	Tough *et al*.[97]
GR321118	peptidic agonist	9.4 9.8*	Daniel *et al*.[99], Tough *et al*.[97]
BVD-74D	peptidic agonist	9.3–10.3	Balasubramaniam *et al*.[28], Kuhn *et al*.[91]
UR-KK193	peptidic agonist	8.2–9.5	Kuhn *et al*.[91]
UR-KK200	peptidic agonist	8.9–9.2	Kuhn *et al*.[91]
UR-KK236	peptidic agonist	8.5	Kuhn *et al*.[92]
UR-AK86C	peptidic agonist	10.4	Konieczny *et al*.[93]
UR-AK95C	peptidic agonist	10.5	Konieczny *et al*.[93]
UR-JG102	peptidic agonist	10.5	Gleixner *et al*.[94]
UR-AK49	non-peptidic antagonist	4.1	Ziemek *et al*.[100]
UR-MK188	non-peptidic antagonist	6.7	Keller *et al*.[101]
(S)-VU0637120	non-peptidic antagonist	5.6	Schüß *et al*.[102]
UR-KK233[a]	peptidic antagonist	6.6	Kuhn *et al*.[92]
UR-KK238[b]	peptidic antagonist	6.3	Kuhn *et al*.[92]
UR-AK13	peptidic antagonist	7.5	Konieczny *et al*.[29]

*Binding assay was performed in the presence of Na^+ (10–150 mM); [a]Peptide **40** and [b]Peptide **37** in Kuhn *et al*.[92]

1.3 Objectives and scope of the thesis

The neuropeptide Y family of receptors, comprising Y_1R, Y_2R, Y_4R, and Y_5R, is involved in several physiological processes, including regulating anxiety, emotions, hormone secretion, blood pressure, food intake, and energy expenditure.[22, 105-107] With the Y_4R subtype being known for its effect on food intake and body weight, it has been considered a potential therapeutic target for the treatment or management of obesity, a global health problem associated with several non-communicable diseases.[62, 68, 108-111] Consequently, several ligands that target this receptor as a potential therapeutic option have been developed.

As the design and development of Y_4R ligands require the determination of their Y_4R binding affinities, there is a need for labeled Y_4R ligands that can be used as molecular tools or probes in binding assays. This has resulted in the development of several radioligands and fluorescently labeled ligands for ligand binding studies at Y_4R. Most of these reported probes are derivatives of endogenous Y_4R agonists. Some examples include [^{125}I]PP, [^{125}I]PYY, [^{3}H]UR-KK193, [^{3}H]UR-KK200 and [^{3}H]UR-JG102. Prior to the recent report of the very high-affinity Y_4R radioligand [^{3}H]UR-JG102, most ligand binding studies were conducted in sodium-free assay conditions to minimize the consumption of radioligand, as almost all of them showed lower binding affinities in the presence of sodium, which is physiologically relevant. Given that [^{3}H]UR-JG102 represents a tool to study Y_4R-ligand binding in the presence of sodium at physiological levels, which means physiological-like conditions, one aim of this thesis was to characterize Y_4R binding of this radioligand (saturation binding, binding kinetics) in both sodium-free and sodium-containing buffer (*Chapter 2*), as well as to evaluate its use in radioligand competition binding assays (*Chapter 2*) and autoradiographic studies (*Chapter 3*).

In addition to the demand for high-affinity and selective Y_4R molecular probes, there is also a need for plasma-stable Y_4R ligands with high binding affinity for potential *in vivo* studies. So far, all reported peptidic Y_4R agonists with high binding affinity display shorter half-lives in human plasma similar to PP.[28, 93, 111, 112] As such, this thesis also aimed at developing plasma-stable analogs of the cyclic peptidic Y_4R agonist UR-AK86C due to its ease of synthesis, high Y_4R selectivity, and picomolar Y_4R binding affinity (pK_i = 10.13). This cyclic hexapeptide has also been shown to exhibit partial Y_4R agonism with a potency similar to that of PP (e.g., cAMP assay: pEC_{50} = 9.82 vs.

9.85). Prior to this, amide bonds in UR-AK86C susceptible to hydrolysis, and the corresponding proteases had to be identified. Based on the results from this investigation, plasma-stable analogs of UR-AK86C had to be developed by employing N^{α}-methylation, amino acid replacement, and peptide backbone extension strategies. Subsequently, the obtained peptide analogs had to be characterized in well-established YR radioligand binding assays to determine their binding affinities and selectivities for Y_4R as well as in a cAMP-based functional assay to assess their agonistic effect on Y_4R by determining their potencies and efficacies (*Chapter 4*). Furthermore, the plasma stabilities (half-lives) of these peptide analogs in human plasma were also determined (*Chapter 4*). Additional analogs of UR-AK86C with increased lipophilicity had to be synthesized by either substituting the strongly basic guanidine groups of the Arg residues in the peptide with weakly basic N^{ω}-carbamoylguanidine moieties or by conjugating the peptide with a lipophilic moiety, such as fluorescent dyes, to facilitate their translocation across hydrophobic barriers like cell membranes. These analogs with reduced hydrophilicity had to be characterized in the same manner as the plasma-stable analogs in addition to determining their n-octanol/water distribution coefficients and their ability to penetrate across endothelial cells (*Chapter 5*).

Lastly, this thesis also aimed to provide a comprehensive overview of binding of the endogenous peptides NPY, PYY, and PP, along with some selected YR antagonists, to human YRs in both sodium-free and sodium-containing buffers (*Chapter 6*). This was performed to explore the effect of sodium on the binding of ligands to YRs.

1.4 References

(1) Walther, C.; Morl, K.; Beck-Sickinger, A. G. Neuropeptide Y receptors: ligand binding and trafficking suggest novel approaches in drug development. *J. Pept. Sci.* 2011, *17* (4), 233-246. DOI: 10.1002/psc.1357.

(2) Bard, J. A.; Walker, M. W.; Branchek, T. A.; Weinshank, R. L. Cloning and functional expression of a human Y_4 subtype receptor for pancreatic polypeptide, neuropeptide Y, and peptide YY. *J. Biol. Chem.* 1995, *270* (45), 26762-26765. DOI: 10.1074/jbc.270.45.26762.

(3) Michel, M. C.; Beck-Sickinger, A.; Cox, H.; Doods, H. N.; Herzog, H.; Larhammar, D.; Quirion, R.; Schwartz, T.; Westfall, T. XVI. International Union of Pharmacology recommendations for the nomenclature of neuropeptide Y, peptide YY, and pancreatic polypeptide receptors. *Pharmacol. Rev.* 1998, *50* (1), 143-150.

(4) Cabrele, C.; Langer, M.; Bader, R.; Wieland, H. A.; Doods, H. N.; Zerbe, O.; Beck-Sickinger, A. G. The first selective agonist for the neuropeptide YY_5 receptor increases food intake in rats. *J. Biol. Chem.* 2000, *275* (46), 36043-36048. DOI: 10.1074/jbc.M000626200.

(5) Misra, S.; Murthy, K. S.; Zhou, H.; Grider, J. R. Coexpression of Y_1, Y_2, and Y_4 receptors in smooth muscle coupled to distinct signaling pathways. *J. Pharmacol. Exp. Ther.* 2004, *311* (3), 1154-1162. DOI: 10.1124/jpet.104.071415.

(6) de Oliveira, P. G.; Ramos, M. L. S.; Amaro, A. J.; Dias, R. A.; Vieira, S. I. $G_{i/o}$-Protein Coupled Receptors in the Aging Brain. *Front. Aging Neurosci.* 2019, *11*, 89. DOI: 10.3389/fnagi.2019.00089.

(7) Wharton, J.; Gordon, L.; Byrne, J.; Herzog, H.; Selbie, L. A.; Moore, K.; Sullivan, M. H. F.; Elder, M. G.; Moscoso, G.; Taylor, K. M.*; et al.* Expression of the human neuropeptide tyrosine Y_1 receptor. *PNAS USA* 1993, *90*, 687 - 691.

(8) Eva, C.; Serra, M.; Mele, P.; Panzica, G.; Oberto, A. Physiology and gene regulation of the brain NPY Y_1 receptor. *Front. Neuroendocrinol.* 2006, *27* (3), 308-339. DOI: 10.1016/j.yfrne.2006.07.002.

(9) Dumont, Y.; St-Pierre, J.-A.; Quirion, R. Comparative autoradiographic distribution of neuropeptide Y Y-1 receptors visualized with the Y_1 receptor agonist [^{125}I][Leu^{31}, Pro^{34}]PYY and the non-peptide antagonist [^{3}H]BIBP3226. *NeuroReport* 1996, *7* (4), 901-904. DOI: 10.1097/00001756-199603220-00013.

(10) Dumont, Y.; Jacques, D.; Bouchard, P.; Quirion, R. m. Species differences in the expression and distribution of the neuropeptide Y Y_1, Y_2, Y_4, and Y_5 receptors in rodents, guinea pig, and primates brains. *J. Comp. Neurol.* 1998, *402* (3), 372-384. DOI: 10.1002/(sici)1096-9861(19981221)402:3<372::Aid-cne6>3.0.Co;2-2.

(11) Widdowson, P. S. Quantitative receptor autoradiography demonstrates a differential distribution of neuropeptide-Y Y_1 and Y_2 receptor subtypes in human and rat brain. *Brain Res.* 1993, *631* (1), 27-38. DOI: 10.1016/0006-8993(93)91182-R.

(12) Fagerberg, L.; Hallström, B. M.; Oksvold, P.; Kampf, C.; Djureinovic, D.; Odeberg, J.; Habuka, M.; Tahmasebpoor, S.; Danielsson, A.; Edlund, K.*; et al.* Analysis of the human tissue-specific expression by Genome-wide integration of transcriptomics and antibody-based proteomics*. *Mol. Cell. Proteom.* 2014, *13* (2), 397-406. DOI: 10.1074/mcp.M113.035600.

(13) Larsen, P. J.; Kristensen, P. The neuropeptide Y (Y_4) receptor is highly expressed in neurones of the rat dorsal vagal complex. *Brain Res. Mol.* 1997, *48* (1), 1-6. DOI: 10.1016/s0169-328x(97)00069-7.

(14) Michel, M. C.; Schlicker, E.; Fink, K.; Boublik, J. H.; Gothert, M.; Willette, R. N.; Daly, R. N.; Hieble, J. P.; Rivier, J. E.; Motulsky, H. J. Distinction of NPY receptors in vitro and in vivo. I. NPY-(18-36) discriminates NPY receptor subtypes in vitro. *Am. J. Physiol.* 1990, *259* (1 Pt 1), E131-139. DOI: 10.1152/ajpendo.1990.259.1.E131.

(15) Grandt, D.; Schimiczek, M.; Rascher, W.; Feth, F.; Shively, J.; Lee, T. D.; Davis, M. T.; Reeve, J. R.; Michel, M. C. Neuropeptide $Y_{3–36}$ is an endogenous ligand selective for Y_2 receptors. *Regul. Pept.* 1996, *67* (1), 33-37. DOI: 10.1016/S0167-0115(96)00104-8.

(16) Pedragosa-Badia, X.; Stichel, J.; Beck-Sickinger, A. G. Neuropeptide Y receptors: how to get subtype selectivity. *Front. Endocrinol. (Lausanne)* 2013, *4*, article 5. DOI: 10.3389/fendo.2013.00005.

(17) Aragon, F.; Karaca, M.; Novials, A.; Maldonado, R.; Maechler, P.; Rubi, B. Pancreatic polypeptide regulates glucagon release through PPYR1 receptors expressed in mouse and human alpha-cells. *Biochim. Biophys. Acta* 2015, *1850* (2), 343-351. DOI: 10.1016/j.bbagen.2014.11.005.

(18) Barrios, V. E.; Sun, J.; Douglass, J.; Toombs, C. F. Evidence of a specific pancreatic polypeptide receptor in rat arterial smooth muscle. *Peptides* 1999, *20* (9), 1107-1113. DOI: 10.1016/S0196-9781(99)00106-0.

(19) Wraith, A.; Tornsten, A.; Chardon, P.; Harbitz, I.; Chowdhary, B. P.; Andersson, L.; Lundin, L. G.; Larhammar, D. Evolution of the neuropeptide Y receptor family: gene and chromosome duplications deduced from the cloning and mapping of the five receptor subtype genes in pig. *Genome Res.* 2000, *10* (3), 302-310. DOI: 10.1101/gr.10.3.302.

(20) Kim, W.; Fiori, J. L.; Shin, Y. K.; Okun, E.; Kim, J. S.; Rapp, P. R.; Egan, J. M. Pancreatic polypeptide inhibits somatostatin secretion. *FEBS Lett.* 2014, *588* (17), 3233-3239. DOI: 10.1016/j.febslet.2014.07.005.

(21) Cerdá-Reverter, J. M.; Larhammar, D. Neuropeptide Y family of peptides: structure, anatomical expression, function, and molecular evolution. *Biochem. Cell Biol.* 2000, *78* (3), 371-392. DOI: 10.1139/o00-004 %M 10949087.

(22) Brothers, S. P.; Wahlestedt, C. Therapeutic potential of neuropeptide Y (NPY) receptor ligands. *EMBO Mol. Med.* 2010, *2* (11), 429-439. DOI: 10.1002/emmm.201000100.

(23) Holzer, P.; Reichmann, F.; Farzi, A. Neuropeptide Y, peptide YY and pancreatic polypeptide in the gut-brain axis. *Neuropeptides* 2012, *46* (6), 261-274. DOI: 10.1016/j.npep.2012.08.005.

(24) Grandt, D.; Schimiczek, M.; Beglinger, C.; Layer, P.; Goebell, H.; Eysselein, V. E.; Reeve, J. R. Two molecular forms of Peptide YY (PYY) are abundant in human blood: characterization of a radioimmunoassay recognizing PYY_{1-36} and PYY_{3-36}. *Regul. Pept.* 1994, *51* (2), 151-159. DOI: 10.1016/0167-0115(94)90204-6.

(25) Abid, K.; Rochat, B.; Lassahn, P.-G.; Stöcklin, R.; Michalet, S.; Brakch, N.; Aubert, J.-F.; Vatansever, B.; Tella, P.; De Meester, I.*; et al.* Kinetic study of neuropeptide Y (NPY) proteolysis in blood and identification of NPY_{3-35}: a new peptide generated by plasma kallikrein. *J. Biol. Chem.* 2009, *284* (37), 24715-24724. DOI: 10.1074/jbc.M109.035253 (acccessed 2025/03/06).

(26) Borowsky, B.; Walker, M. W.; Bard, J.; Weinshank, R. L.; Laz, T. M.; Vaysse, P.; Branchek, T. A.; Gerald, C. Molecular biology and pharmacology of multiple NPY Y_5 receptor species homologs. *Regul. Pept.* 1998, *75-76*, 45-53. DOI: 10.1016/s0167-0115(98)00052-4.

(27) Silva, A. P.; Cavadas, C.; Grouzmann, E. Neuropeptide Y and its receptors as potential therapeutic drug targets. *Clin. Chim. Acta* 2002, *326* (1-2), 3-25. DOI: 10.1016/S0009-8981(02)00301-7.

(28) Balasubramaniam, A.; Mullins, D. E.; Lin, S.; Zhai, W.; Tao, Z.; Dhawan, V. C.; Guzzi, M.; Knittel, J. J.; Slack, K.; Herzog, H.*; et al.* Neuropeptide Y (NPY) Y_4 receptor selective agonists based on NPY_{32-36}: development of an anorectic Y_4 receptor selective agonist with picomolar affinity. *J. Med. Chem.* 2006, *49* (8), 2661-2665. DOI: 10.1021/jm050907d.

(29) Konieczny, A.; Braun, D.; Wifling, D.; Bernhardt, G.; Keller, M. Oligopeptides as neuropeptide Y Y_4 receptor ligands: identification of a high-affinity tetrapeptide agonist and a hexapeptide antagonist. *J. Med. Chem.* 2020, *63*, 8198-8215. DOI: 10.1021/acs.jmedchem.0c00426.

(30) Darby, K.; Eyre, H. J.; Lapsys, N.; Copeland, N. G.; Gilbert, D. J.; Couzens, M.; Antonova, O.; Sutherland, G. R.; Jenkins, N. A.; Herzog, H. Assignment of the Y_4 receptor gene (PPYR1) to human chromosome 10q11.2 and mouse chromosome 14. *Genomics* 1997, *46* (3), 513-515. DOI: 10.1006/geno.1997.5071.

(31) Lutz, C. M.; Richards, J. E.; Scott, K. L.; Sinha, S.; Yang-Feng, T. L.; Frankel, W. N.; Thompson, D. A. Neuropeptide Y receptor genes mapped in human and mouse: receptors with high affinity for pancreatic polypeptide are not clustered with receptors specific for neuropeptide Y and peptide YY. *Genomics* 1997, *46* (2), 287-290. DOI: 10.1006/geno.1997.5024.

(32) Larhammar, D.; Salaneck, E. Molecular evolution of NPY receptor subtypes. *Neuropeptides* 2004, *38* (4), 141-151. DOI: 10.1016/j.npep.2004.06.002.

(33) Shebanits, K.; Vasile, S.; Xu, B.; Gutiérrez-de-Terán, H.; Larhammar, D. Functional characterization *in vitro* of twelve naturally occurring variants of the human pancreatic polypeptide receptor NPY4R. *Neuropeptides* 2019, *76*, 101933. DOI: 10.1016/j.npep.2019.05.004.

(34) Gregor, P.; Millham, M. L.; Feng, Y.; DeCarr, L. B.; McCaleb, M. L.; Cornfield, L. J. Cloning and characterization of a novel receptor to pancreatic polypeptide, a member of the neuropeptide Y receptor family. *FEBS Lett.* 1996, *381* (1-2), 58-62. DOI: 10.1016/0014-5793(96)00067-1 From NLM.

(35) Dumont, Y.; Bastianetto, S.; Duranton, A.; Breton, L.; Quirion, R. Immunohistochemical distribution of neuropeptide Y, peptide YY, pancreatic polypeptide-like immunoreactivity and their receptors in the epidermal skin of healthy women. *Peptides* 2015, *70*, 7-16. DOI: 10.1016/j.peptides.2015.05.002.

(36) Goumain, M.; Voisin, T.; Lorinet, A.-M.; Laburthe, M. Identification and distribution of mRNA encoding the Y_1, Y_2, Y_4, and Y_5 receptors for peptides of the PP-fold family in the rat intestine and colon. *Biochem. Biophys. Res. Commun.* 1998, *247* (1), 52-56. DOI: 10.1006/bbrc.1998.8647.

(37) Lundell, I.; Statnick, M. A.; Johnson, D.; Schober, D. A.; Starback, P.; Gehlert, D. R.; Larhammar, D. The cloned rat pancreatic polypeptide receptor exhibits profound differences to the orthologous receptor. *PNAS USA* 1996, *93* (10), 5111-5115. DOI: 10.1073/pnas.93.10.5111.

(38) Whitcomb, D. C.; Puccio, A. M.; Vigna, S. R.; Taylor, I. L.; Hoffman, G. E. Distribution of pancreatic polypeptide receptors in the rat brain. *Brain Res.* 1997, *760* (1), 137-149. DOI: 10.1016/S0006-8993(97)00295-3.

(39) Stanley, B. G.; Magdalin, W.; Seirafi, A.; Thomas, W. J.; Leibowitz, S. F. The perifornical area: the major focus of (a) patchily distributed hypothalamic neuropeptide Y-sensitive feeding system(s). *Brain Res.* 1993, *604* (1), 304-317. DOI: 10.1016/0006-8993(93)90382-W.

(40) Campbell, R. E.; Smith, M. S.; Allen, S. E.; Grayson, B. E.; Ffrench-Mullen, J. M.; Grove, K. L. Orexin neurons express a functional pancreatic polypeptide Y_4 receptor. *J. Neurosci.* 2003, *23* (4), 1487-1497. DOI: 10.1523/JNEUROSCI.23-04-01487.2003.

(41) Jensen, E. Technical review: In situ hybridization. *Anat. Rec. (Hoboken)* 2014, *297* (8), 1349-1353. DOI: 10.1002/ar.22944.

(42) De Matos, L. L.; Trufelli, D. C.; De Matos, M. G. L.; Da Silva Pinhal, M. A. Immunohistochemistry as an important tool in biomarkers detection and clinical practice. *Biomark. Insights* 2010, *5*, BMI.S2185. DOI: 10.4137/bmi.S2185.

(43) Schüß, C.; Behr, V.; Beck-Sickinger, A. G. Illuminating the neuropeptide Y_4 receptor and its ligand pancreatic polypeptide from a structural, functional, and therapeutic perspective. *Neuropeptides* 2024, *105*, 102416. DOI: 10.1016/j.npep.2024.102416.

(44) Edward Zhou, X.; Melcher, K.; Eric Xu, H. Structural biology of G protein-coupled receptor signaling complexes. *Protein Sci.* 2019, *28* (3), 487-501. DOI: 10.1002/pro.3526.

(45) Gurevich, V. V.; Gurevich, E. V. GPCR Signaling Regulation: The Role of GRKs and Arrestins. *Front. pharmacol.* 2019, *10*, Review. DOI: 10.3389/fphar.2019.00125.

(46) Tang, T.; Tan, Q.; Han, S.; Diemar, A.; Lobner, K.; Wang, H.; Schuss, C.; Behr, V.; Morl, K.; Wang, M.*; et al.* Receptor-specific recognition of NPY peptides revealed by structures of NPY receptors. *Sci. Adv.* 2022, *8* (18), eabm1232. DOI: 10.1126/sciadv.abm1232.

(47) Syrovatkina, V.; Alegre, K. O.; Dey, R.; Huang, X.-Y. Regulation, signaling, and physiological functions of G-proteins. *J. Mol. Biol.* 2016, *428* (19), 3850-3868. DOI: 10.1016/j.jmb.2016.08.002.

(48) Zhang, M.; Chen, T.; Lu, X.; Lan, X.; Chen, Z.; Lu, S. G protein-coupled receptors (GPCRs): advances in structures, mechanisms and drug discovery. *Signal Transduct. Target. Ther.* 2024, *9* (1), 88. DOI: 10.1038/s41392-024-01803-6.

(49) Simon, M. I.; Strathmann, M. P.; Gautam, N. Diversity of G proteins in signal transduction. *Science* 1991, *252* (5007), 802-808. DOI: 10.1126/science.1902986.

(50) McCudden, C. R.; Hains, M. D.; Kimple, R. J.; Siderovski, D. P.; Willard, F. S. G-protein signaling: back to the future. *Cell. Mol. Life Sci.* 2005, *62* (5), 551-577. DOI: 10.1007/s00018-004-4462-3.

(51) Dupré, D. J.; Robitaille, M.; Rebois, R. V.; Hébert, T. E. The role of Gβγ subunits in the organization, assembly, and function of GPCR signaling complexes. *Annu. Rev. Pharmacool. Toxicol.* 2009, *49* (Volume 49, 2009), 31-56. DOI: 10.1146/annurev-pharmtox-061008-103038.

(52) Kehrl, J. H. Heterotrimeric G protein signaling: roles in immune function and fine-tuning by RGS proteins. *Immunity* 1998, *8* (1), 1-10.

(53) Gainetdinov, R. R.; Premont, R. T.; Bohn, L. M.; Lefkowitz, R. J.; Caron, M. G. Desensitization of G protein–coupled receptors and neuronal functions. *Annu. Rev. Neurosci.* 2004, *27* (Volume 27, 2004), 107-144. DOI: 10.1146/annurev.neuro.27.070203.144206.

(54) Chen, Q.; Tesmer, J. J. G. G protein–coupled receptor interactions with arrestins and GPCR kinases: the unresolved issue of signal bias. *J. Biol. Chem.* 2022, *298* (9), 102279. DOI: 10.1016/j.jbc.2022.102279.

(55) Böhm, S. K.; Grady, E. F.; Bunnett, N. W. Regulatory mechanisms that modulate signalling by G-protein-coupled receptors. *Biochem. J.* 1997, *322* (1), 1-18. DOI: 10.1042/bj3220001 (acccessed 2/27/2025).

(56) Ferguson, S. S. G.; Caron, M. G. G protein-coupled receptor adaptation mechanisms. *Semin. Cell Dev. Biol.* 1998, *9* (2), 119-127. DOI: 10.1006/scdb.1997.0216.

(57) Ferguson, S. S. G. Phosphorylation-independent attenuation of GPCR signalling. *Trends Pharmacol. Sci.* 2007, *28* (4), 173-179. DOI: 10.1016/j.tips.2007.02.008 (acccessed 2025/02/27).

(58) Parker, M. S.; Lundell, I.; Parker, S. L. Internalization of pancreatic polypeptide Y_4 receptors: correlation of receptor intake and affinity. *Eur. J. Pharmacol.* 2002, *452* (3), 279-287. DOI: 10.1016/S0014-2999(02)02339-7.

(59) Ueno, N.; Inui, A.; Iwamoto, M.; Kaga, T.; Asakawa, A.; Okita, M.; Fujimiya, M.; Nakajima, Y.; Ohmoto, Y.; Ohnaka, M.*; et al.* Decreased food intake and body weight in pancreatic polypeptide-overexpressing mice. *Gastroenterology* 1999, *117* (6), 1427-1432. DOI: 10.1016/s0016-5085(99)70293-3.

(60) Asakawa, A.; Inui, A.; Yuzuriha, H.; Ueno, N.; Katsuura, G.; Fujimiya, M.; Fujino, M. A.; Niijima, A.; Meguid, M. M.; Kasuga, M. Characterization of the

effects of pancreatic polypeptide in the regulation of energy balance. *Gastroenterology* 2003, *124* (5), 1325-1336. DOI: 10.1016/s0016-5085(03)00216-6.

(61) Balasubramaniam, A.; Joshi, R.; Su, C.; Friend, L. A.; James, J. H. Neuropeptide Y (NPY) Y_2 receptor-selective agonist inhibits food intake and promotes fat metabolism in mice: combined anorectic effects of Y_2 and Y_4 receptor-selective agonists. *Peptides* 2007, *28* (2), 235-240. DOI: 10.1016/j.peptides.2006.08.041.

(62) Li, J. B.; Asakawa, A.; Terashi, M.; Cheng, K.; Chaolu, H.; Zoshiki, T.; Ushikai, M.; Sheriff, S.; Balasubramaniam, A.; Inui, A. Regulatory effects of Y_4 receptor agonist (BVD-74D) on food intake. *Peptides* 2010, *31*, 1706-1710. DOI: 10.1016/j.peptides.2010.06.011.

(63) Berntson, G. G.; Zipf, W. B.; O'Dorisio, T. M.; Hoffman, J. A.; Chance, R. E. Pancreatic polypeptide infusions reduce food intake in Prader-Willi syndrome. *Peptides* 1993, *14* (3), 497-503. DOI: 10.1016/0196-9781(93)90138-7.

(64) Jesudason, D. R.; Monteiro, M. P.; McGowan, B. M. C.; Neary, N. M.; Park, A. J.; Philippou, E.; Small, C. J.; Frost, G. S.; Ghatei, M. A.; Bloom, S. R. Low-dose pancreatic polypeptide inhibits food intake in man. *Br. J. Nutr.* 2007, *97* (3), 426-429. DOI: 10.1017/S0007114507336799 From Cambridge University Press Cambridge Core.

(65) McTigue, D. M.; Chen, C. H.; Rogers, R. C.; Stephens, R. L. Intracisternal rat pancreatic polypeptide stimulates gastric emptying in the rat. *Am. J. Physiol. Regul. Integr. Comp. Physiol.* 1995, *269* (1), R167-R172. DOI: 10.1152/ajpregu.1995.269.1.R167.

(66) Sainsbury, A.; Baldock, P. A.; Schwarzer, C.; Ueno, N.; Enriquez, R. F.; Couzens, M.; Inui, A.; Herzog, H.; Gardiner, E. M. Synergistic effects of Y_2 and Y_4 receptors on adiposity and bone mass revealed in double knockout mice. *Mol. Cell. Biol.* 2003, *23* (15), 5225-5233. DOI: 10.1128/MCB.23.15.5225-5233.2003.

(67) Sainsbury, A.; Schwarzer, C.; Couzens, M.; Jenkins, A.; Oakes, S. R.; Ormandy, C. J.; Herzog, H. Y_4 receptor knockout rescues fertility in ob/ob mice. *Genes Dev.* 2002, *16* (9), 1077-1088. DOI: 10.1101/gad.979102.

(68) Lee, N. J.; Enriquez, R. F.; Boey, D.; Lin, S.; Slack, K.; Baldock, P. A.; Herzog, H.; Sainsbury, A. Synergistic attenuation of obesity by Y_2- and Y_4-receptor double knockout in ob/ob mice. *Nutrition* 2008, *24* (9), 892-899. DOI: 10.1016/j.nut.2008.06.019.

(69) Caprio, M.; Fabbrini, E.; Isidori, A. M.; Aversa, A.; Fabbri, A. Leptin in reproduction. *Trends Endocrinol. Metab.* 2001, *12* (2), 65-72. DOI: 10.1016/S1043-2760(00)00352-0.

(70) Eisener-Dorman, A. F.; Lawrence, D. A.; Bolivar, V. J. Cautionary insights on knockout mouse studies: the gene or not the gene? *Brain Behav. Immun.* 2009, *23* (3), 318-324. DOI: 10.1016/j.bbi.2008.09.001.

(71) Badin, A.-S.; Morrill, P.; Devonshire, I. M.; Greenfield, S. A. (II) Physiological profiling of an endogenous peptide in the basal forebrain: age-related

bioactivity and blockade with a novel modulator. *Neuropharmacology* 2016, *105*, 47-60. DOI: 10.1016/j.neuropharm.2016.01.012.

(72) Tinoco, A. D.; Saghatelian, A. Investigating endogenous peptides and peptidases using peptidomics. *Biochemistry* 2011, *50* (35), 7447-7461. DOI: 10.1021/bi200417k.

(73) Foster, S. R.; Hauser, A. S.; Vedel, L.; Strachan, R. T.; Huang, X.-P.; Gavin, A. C.; Shah, S. D.; Nayak, A. P.; Haugaard-Kedström, L. M.; Penn, R. B.*; et al.* Discovery of human signaling systems: pairing peptides to G Protein-Coupled receptors. *Cell* 2019, *179* (4), 895-908.e821. DOI: 10.1016/j.cell.2019.10.010.

(74) Fletcher, M. A.; Rosenthal, M.; Antoni, M.; Ironson, G.; Zeng, X. R.; Barnes, Z.; Harvey, J. M.; Hurwitz, B.; Levis, S.; Broderick, G.*; et al.* Plasma neuropeptide Y: a biomarker for symptom severity in chronic fatigue syndrome. *Behav. Brain Funct.* 2010, *6* (1), 76. DOI: 10.1186/1744-9081-6-76.

(75) Lettgen, B.; Wagner, S.; Hänze, J.; Lang, R. E.; Rascher, W. Elevated plasma concentration of neuropeptide Y in adolescents with primary hypertension. *J. Hum. Hypertens.* 1994, *8* (5), 345-349. PubMed.

(76) Beck-Sickinger, A. G.; Colmers, W. F.; Cox, H. M.; Doods, H. N.; Herzog, H.; Larhammar, D.; Michel, M. C.; Quirion, R.; Schwartz, T.; Westfall, T. Neuropeptide Y receptors in GtoPdb v.2023.1. *IUPHAR/BPS GtoPdb CITE* 2023, *2023* (1). DOI: 10.2218/gtopdb/F46/2023.1 (acccessed 2025/03/10).

(77) Gehlert, D. R.; Schober, D. A.; Gackenheimer, S. L.; Beavers, L.; Gadski, R.; Lundell, I.; Larhammar, D. [^{125}I]Leu^{31}, Pro^{34}-PYY is a high affinity radioligand for rat PP1/Y_4 and Y_1 receptors: evidence for heterogeneity in pancreatic polypeptide receptors. *Peptides* 1997, *18* (3), 397-401. DOI: 10.1016/s0196-9781(96)00346-4.

(78) Walker, M. W.; Smith, K. E.; Bard, J.; Vaysse, P. J.; Gerald, C.; Daouti, S.; Weinshank, R. L.; Branchek, T. A. A structure-activity analysis of the cloned rat and human Y_4 receptors for pancreatic polypeptide. *Peptides* 1997, *18* (4), 609-612. DOI: 10.1016/s0196-9781(97)00070-3.

(79) Fuhlendorff, J.; Gether, U.; Aakerlund, L.; Langeland-Johansen, N.; Thøgersen, H.; Melberg, S.; Olsen, U.; Thastrup, O.; Schwartz, T. [Leu^{31},Pro^{34}]neuropeptide Y: A specific Y_1 receptor agonist. *PNAS USA* 1990, *87*, 182-186.

(80) Eriksson, H.; Berglund, M. M.; Holmberg, S. K.; Kahl, U.; Gehlert, D. R.; Larhammar, D. The cloned guinea pig pancreatic polypeptide receptor Y_4 resembles more the human Y_4 than does the rat Y_4. *Regul. Pept.* 1998, *75-76*, 29-37. DOI: 10.1016/s0167-0115(98)00050-0.

(81) Cabrele, C.; Beck-Sickinger, A. G. Molecular characterization of the ligand–receptor interaction of the neuropeptide Y family. *J. Pept. Sci.* 2000, *6* (3), 97-122. DOI: 10.1002/(SICI)1099-1387(200003)6:3<97::AID-PSC236>3.0.CO;2-E.

(82) Pedragosa-Badia, X.; Sliwoski, G. R.; Dong Nguyen, E.; Lindner, D.; Stichel, J.; Kaufmann, K. W.; Meiler, J.; Beck-Sickinger, A. G. Pancreatic polypeptide

is recognized by two hydrophobic domains of the human Y_4 receptor binding pocket. *J. Biol. Chem.* 2014, *289* (9), 5846-5859. DOI: 10.1074/jbc.M113.502021.

(83) Lindner, D.; Stichel, J.; Beck-Sickinger, A. G. Molecular recognition of the NPY hormone family by their receptors. *Nutrition* 2008, *24* (9), 907-917. DOI: 10.1016/j.nut.2008.06.025.

(84) Dyzma, M.; Boudjeltia, K. Z.; Faraut, B.; Kerkhofs, M. Neuropeptide Y and sleep. *Sleep Med. Rev.* 2010, *14* (3), 161-165. DOI: 10.1016/j.smrv.2009.09.001.

(85) Guo, Y.; Ma, L.; Enriori, P. J.; Koska, J.; Franks, P. W.; Brookshire, T.; Cowley, M. A.; Salbe, A. D.; DelParigi, A.; Tataranni, P. A. Physiological evidence for the involvement of peptide YY in the regulation of energy homeostasis in humans. *Obesity* 2006, *14* (9), 1562-1570. DOI: 10.1038/oby.2006.180.

(86) DiMaggio, D. A.; Chronwall, B. M.; Buchanan, K.; O'Donohoue, T. L. Pancreatic polypeptide immunoreactivity in rat brain is actually neuropeptide Y. *Neuroscience* 1985, *15* (4), 1149-1157. DOI: 10.1016/0306-4522(85)90259-3.

(87) Whitcomb, D. C.; Taylor, I. L.; Vigna, S. R. Characterization of saturable binding sites for circulating pancreatic polypeptide in rat brain. *Am. J. Physiol.* 1990, *259* (4 Pt 1), G687-691. DOI: 10.1152/ajpgi.1990.259.4.G687.

(88) Pieribone, V. A.; Brodin, L.; Friberg, K.; Dahlstrand, J.; Soderberg, C.; Larhammar, D.; Hokfelt, T. Differential expression of mRNAs for neuropeptide Y-related peptides in rat nervous tissues: possible evolutionary conservation. *J. Neurosci.* 1992, *12* (9), 3361-3371. DOI: 10.1523/jneurosci.12-09-03361.1992.

(89) Parker, E. M.; Babij, C. K.; Balasubramaniam, A.; Burrier, R. E.; Guzzi, M.; Hamud, F.; Gitali, M.; Rudinski, M. S.; Tao, Z.; Tice, M.*; et al.* GR231118 (1229U91) and other analogues of the C-terminus of neuropeptide Y are potent neuropeptide Y Y_1 receptor antagonists and neuropeptide Y Y_4 receptor agonists. *Eur. J. Pharmacol.* 1998, *349* (1), 97-105. DOI: 10.1016/s0014-2999(98)00171-x.

(90) Berlicki, Ł.; Kaske, M.; Gutiérrez-Abad, R.; Bernhardt, G.; Illa, O.; Ortuño, R. M.; Cabrele, C.; Buschauer, A.; Reiser, O. Replacement of Thr^{32} and Gln^{34} in the C-terminal neuropeptide Y fragment 25–36 by cis-cyclobutane and cis-cyclopentane β-amino acids shifts selectivity toward the Y_4 receptor. *J. Med. Chem.* 2013, *56*, 8422-8431. DOI: 10.1021/jm4008505.

(91) Kuhn, K. K.; Ertl, T.; Dukorn, S.; Keller, M.; Bernhardt, G.; Reiser, O.; Buschauer, A. High affinity agonists of the neuropeptide Y (NPY) Y_4 receptor derived from the C-terminal pentapeptide of human pancreatic polypeptide (hPP): synthesis, stereochemical discrimination, and radiolabeling. *J. Med. Chem.* 2016, *59*, 6045-6058. DOI: 10.1021/acs.jmedchem.6b00309.

(92) Kuhn, K. K.; Littmann, T.; Dukorn, S.; Tanaka, M.; Keller, M.; Ozawa, T.; Bernhardt, G.; Buschauer, A. In search of NPY Y_4R antagonists: incorporation of carbamoylated arginine, aza-amino acids, or d-amino acids into oligopeptides derived from the C-termini of the endogenous agonists. *ACS Omega* 2017, *2*, 3616-3631. DOI: 10.1021/acsomega.7b00451.

(93) Konieczny, A.; Conrad, M.; Ertl, F. J.; Gleixner, J.; Gattor, A. O.; Grätz, L.; Schmidt, M. F.; Neu, E.; Horn, A. H. C.; Wifling, D.*; et al.* N-Terminus to arginine side-chain cyclization of linear peptidic neuropeptide Y Y_4 receptor ligands results in picomolar binding constants. *J. Med. Chem.* 2021, *64* (22), 16746-16769. DOI: 10.1021/acs.jmedchem.1c01574.

(94) Gleixner, J.; Gattor, A. O.; Humphrys, L. J.; Brunner, T.; Keller, M. [^{3}H]UR-JG102-a radiolabeled cyclic peptide with high affinity and excellent selectivity for the neuropeptide Y Y_4 receptor. *J. Med. Chem.* 2023, *66* (19), 13788-13808. DOI: 10.1021/acs.jmedchem.3c01224.

(95) Keller, M.; Kuhn, K. K.; Einsiedel, J.; Hübner, H.; Biselli, S.; Mollereau, C.; Wifling, D.; Svobodová, J.; Bernhardt, G.; Cabrele, C.*; et al.* Mimicking of arginine by functionalized N^{ω}-carbamoylated arginine as a new broadly applicable approach to labeled bioactive peptides: high affinity angiotensin, neuropeptide Y, neuropeptide FF, and neurotensin receptor ligands as examples. *J. Med. Chem.* 2016, *59* (5), 1925-1945. DOI: 10.1021/acs.jmedchem.5b01495.

(96) Lundell, I.; Blomqvist, A. G.; Berglund, M. M.; Schober, D. A.; Johnson, D.; Statnick, M. A.; Gadski, R. A.; Gehlert, D. R.; Larhammar, D. Cloning of a human receptor of the NPY receptor family with high affinity for pancreatic polypeptide and peptide YY. *J. Biol. Chem.* 1995, *270* (49), 29123-29128. DOI: 10.1074/jbc.270.49.29123.

(97) Tough, I. R.; Holliday, N. D.; Cox, H. M. Y_4 receptors mediate the inhibitory responses of pancreatic polypeptide in human and mouse colon mucosa. *J. Pharmacol. Exp. Ther.* 2006, *319* (1), 20-30. DOI: 10.1124/jpet.106.106500.

(98) Yan, H.; Yang, J.; Marasco, J.; Yamaguchi, K.; Brenner, S.; Collins, F.; Karbon, W. Cloning and functional expression of cDNAs encoding human and rat pancreatic polypeptide receptors. *PNAS USA* 1996, *93* (10), 4661-4665. DOI: 10.1073/pnas.93.10.4661.

(99) Daniels, A. J.; Matthews, J. E.; Slepetis, R. J.; Jansen, M.; Viveros, O. H.; Tadepalli, A.; Harrington, W.; Heyer, D.; Landavazo, A.; Leban, J. J. High-affinity neuropeptide Y receptor antagonists. *PNAS* 1995, *92* (20), 9067-9071. DOI: doi:10.1073/pnas.92.20.9067.

(100) Ziemek, R.; Schneider, E.; Kraus, A.; Cabrele, C.; Beck-Sickinger, A. G.; Bernhardt, G.; Buschauer, A. Determination of affinity and activity of ligands at the human neuropeptide Y Y_4 receptor by flow cytometry and aequorin luminescence. *J. Recept. Signal Transduct.* 2007, *27*, 217-233. DOI: 10.1080/10799890701505206.

(101) Keller, M.; Kaske, M.; Holzammer, T.; Bernhardt, G.; Buschauer, A. Dimeric argininamide-type neuropeptide Y receptor antagonists: chiral discrimination between Y_1 and Y_4 receptors. *Biorg. Med. Chem.* 2013, *21* (21), 6303-6322. DOI: 10.1016/j.bmc.2013.08.065.

(102) Schüß, C.; Vu, O.; Schubert, M.; Du, Y.; Mishra, N. M.; Tough, I. R.; Stichel, J.; Weaver, C. D.; Emmitte, K. A.; Cox, H. M.*; et al.* Highly selective Y_4 receptor antagonist binds in an allosteric binding pocket. *J. Med. Chem.* 2021, *64* (5), 2801-2814. DOI: 10.1021/acs.jmedchem.0c02000.

(103) Sun, C.; Ewing William, R.; Bolton Scott, A.; Gu, Z.; Huang, Y.; Murugesan, N.; Zhu, Y. Substituted adipic acid amides and uses thereof. WO WO 2012/125622 A1, 2012.

(104) Ewing William, R.; Zhu, Y.; Sun, C.; Huang, Y.; Karatholuvhu Maheswaran, S.; Bolton Scott, A.; Pasunoori, L.; Mandal Sunil, K.; Sher Philip, M. Diaminocyclohexane compounds and uses thereof. US US 2013/0184284 A1, 2013.

(105) Heilig, M. The NPY system in stress, anxiety and depression. *Neuropeptides* 2004, *38* (4), 213-224. DOI: 10.1016/j.npep.2004.05.002.

(106) Vona-Davis, L. C.; McFadden, D. W. NPY family of hormones: clinical relevance and potential use in gastrointestinal disease. *Curr. Top. Med. Chem.* 2007, *7* (17), 1710-1720. DOI: 10.2174/156802607782340966.

(107) Zukowska, Z.; Feuerstein, G. Z. *NPY family of peptides in neurobiology, cardiovascular and metabolic disorders: from genes to therapeutics*; Birkhäuser Basel, 2006. DOI: 10.1007/3-7643-7417-9.

(108) Lin, S.; Shi, Y. C.; Yulyaningsih, E.; Aljanova, A.; Zhang, L.; Macia, L.; Nguyen, A. D.; Lin, E. J.; During, M. J.; Herzog, H.*; et al.* Critical role of arcuate Y_4 receptors and the melanocortin system in pancreatic polypeptide-induced reduction in food intake in mice. *PLoS One* 2009, *4* (12), e8488. DOI: 10.1371/journal.pone.0008488.

(109) Sainsbury, A.; Shi, Y. C.; Zhang, L.; Aljanova, A.; Lin, Z.; Nguyen, A. D.; Herzog, H.; Lin, S. Y_4 receptors and pancreatic polypeptide regulate food intake via hypothalamic orexin and brain-derived neurotropic factor dependent pathways. *Neuropeptides* 2010, *44* (3), 261-268. DOI: 10.1016/j.npep.2010.01.001.

(110) Blüher, M. Obesity: global epidemiology and pathogenesis. *Nat. Rev. Endocrinol.* 2019, *15* (5), 288-298. DOI: 10.1038/s41574-019-0176-8.

(111) Yulyaningsih, E.; Zhang, L.; Herzog, H.; Sainsbury, A. NPY receptors as potential targets for anti-obesity drug development. *Br. J. Pharmacol.* 2011, *163* (6), 1170-1202. DOI: 10.1111/j.1476-5381.2011.01363.x.

(112) Cuenco, J.; Minnion, J.; Tan, T.; Scott, R.; Germain, N.; Ling, Y.; Chen, R.; Ghatei, M.; Bloom, S. Degradation paradigm of the gut hormone, pancreatic polypeptide, by hepatic and renal peptidases. *Endocrinol.* 2017, *158* (6), 1755-1765. DOI: 10.1210/en.2016-1827 (acccessed 4/2/2025).

Chapter 2

Characterization of Y_4R binding of [^{3}H]UR-JG102

Note: Prior to the submission of this thesis, the content of this chapter, except for the cellular internalization studies, was published in collaboration with partners:

Gleixner, J.[#], Gattor, A. O.[#], Humphrys, L. J., Brunner, T., & Keller, M. (2023). [^{3}H]UR-JG102–A Radiolabeled Cyclic Peptide with High Affinity and Excellent Selectivity for the Neuropeptide Y Y_4 Receptor. *J. Med. Chem.*, 66(19), 13788-13808. [#]Equally contributed

2.1 Introduction

The neuropeptide Y Y_4 receptor (Y_4R) is a receptor subtype belonging to the neuropeptide Y (NPY) family of receptors (YRs). Found in both the central nervous system and in peripheral tissues, this family is a member of the rhodopsin-like superfamily of G-protein coupled receptors (GPCRs) and comprises three other functional subtypes, namely the Y_1R, Y_2R, and Y_5R.[1-4] All YRs can be activated by either neuropeptide Y (NPY), peptide YY (PYY), or pancreatic polypeptide (PP), which all represent homologous, linear 36 amino acid peptides, thereby forming a multi-ligand and -receptor system.[5, 6] Upon activation, they primarily couple to $G_{i/o}$-type G-proteins in mammalian cells, mediating a reduction in cAMP production. Nonetheless, a few studies have shown that they could also couple to other G-proteins, such as the G_q-type in some mammalian smooth muscle cells.[7]

In humans, the Y_4R subtype is preferentially activated by PP, and its activation regulates food intake, gastrointestinal motility, pancreatic secretion, and anxiolysis.[2, 8-12] This suggests that the Y_4R can serve as a potential drug target for the treatment of metabolic diseases such as obesity. As such, molecular tools are needed to help study and develop therapeutics for it.

Until recently, only ^{125}I-labeled peptides ([^{125}I]hPP,[13-16] [^{125}I]rPP,[13, 17] [^{125}I]pPYY,[15, 17, 18] [Leu^{31},Pro^{34}]hPYY,[19] and [^{125}I]GR231118[20]) were used as radiochemical molecular tools to study Y_4R binding. However, among other drawbacks like the low half-life of 59.4 days of these radioligands and their high susceptibility to radiation-induced destruction, labeling the peptides with ^{125}I at their tyrosine residues could drastically change their physicochemical properties and pharmacological profile.[21] Also, it could result in a mixture of differently labeled species (both mono or di-iodinated) due to the presence of several tyrosine residues in the peptides.[22]

Consequently, these limitations have led to the development of several tritium-labeled Y_4R binding peptides: the hPP derivative [^{3}H]**2.1**,[23] which is labeled at a lysine residue; the dimeric pentapeptide [^{3}H]**2.2**,[24] bearing a tritiated propionyl moiety at the 2,6-diaminosuberyl linker; and the dimeric pentapeptide [^{3}H]**2.3**,[24] labeled via an N^{ω}-carbamoylated arginine (Figure 2.1).

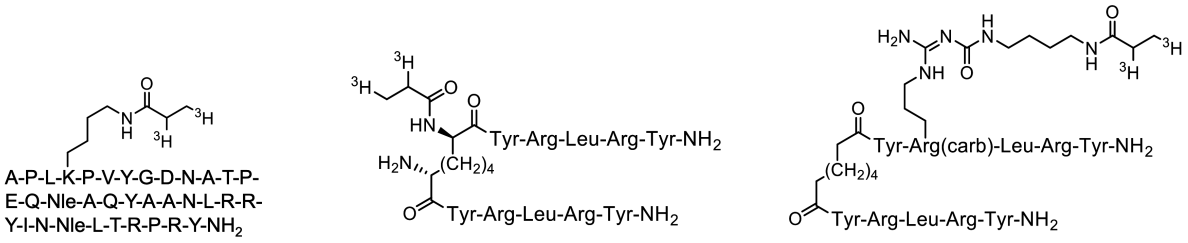

[^{3}H]propionyl-[Lys^4,Nle^{17,30}]hPP ([^{3}H]**2.1**)
K_d (hY$_4$R): 1.1 nM[a] (Na^+-free)[c]
K_d (hY$_4$R): 20.9 nM[a] (150 mM Na^+)[d]

[^{3}H]UR-KK193 ([^{3}H]**2.2**)
K_d (hY$_4$R): 0.67 nM[b] (Na^+-free)[c]
K_d (hY$_4$R): 9.8 nM[b] (140 mM Na^+)[e]

[^{3}H]UR-KK200 ([^{3}H]**2.3**)
K_d (hY$_4$R): 0.67 nM[b] (Na^+-free)[c]

Arg(carb) = N^{ω}-carbamoylated arginine

Figure 2.1. Structures and Y$_4$R affinities (K_d values) of reported tritium-labeled Y$_4$R ligands. [a]Dukorn *et al.*[23] [b]Kuhn *et al.*[24] [c]Determined in a hypotonic, sodium-free HEPES buffer. [d]Determined in an isotonic HEPES buffer containing 150 mM sodium. [e]Determined in Leibovitz's L-15 medium containing 140 mM sodium.

Nevertheless, these tritiated radioligands exhibit low binding affinities (K_d values > 10 nM) in binding studies conducted under sodium-containing or physiological-like conditions. This limitation makes them unsuitable probes for such conditions due to potential high unspecific binding and high radioligand consumption.[23, 24] However, these radioligands normally show higher binding affinities under sodium-free conditions. Thus, the majority of the reported Y$_4$R binding studies with these radioligands are conducted in hypotonic, sodium-free HEPES buffer typically containing 25 or 50 mM HEPES, 2.5 mM $CaCl_2$, and 1 mM $MgCl_2$.[11, 13-16, 19, 24-30] This change in binding affinity under the two different conditions is probably due to the negative allosteric modulation of GPCRs by sodium ions that stabilizes the inactive receptor conformation, resulting in lower affinities of agonists that prefer the active receptor conformation.[31, 32]

In an attempt to develop a suitable tritiated Y$_4$R radioligand that shows high Y$_4$R affinity in sodium-containing buffer and suitable for use under physiological conditions, several derivatives of the recently discovered Y$_4$R partial agonist UR-AK86C (**2.4**),[30] a cyclic hexapeptide exhibiting very high Y$_4$R affinity (K_i = 0.048 nM, sodium-free buffer) were synthesized. Out of these, UR-JG102 (**2.5**), a derivative in which the succinyl moiety in the macrocycle of **2.4** is replaced by *β*-D-aspartate, the latter carrying a propionylated 4-aminobutyryl substituent, was obtained as the "cold" form of a potential tritium-labeled peptide showing high selectivity and high affinity for the Y$_4$R. Subsequently, the tritiated analog of **2.5**, [^{3}H]UR-JG102 ([^{3}H]**2.5**), was prepared as a Y$_4$R radioligand (Figure 2.2). This chapter focuses on the characterization of

[^{3}H]**2.5** by Y_4R saturation binding, binding kinetics, competition binding, and receptor internalization.

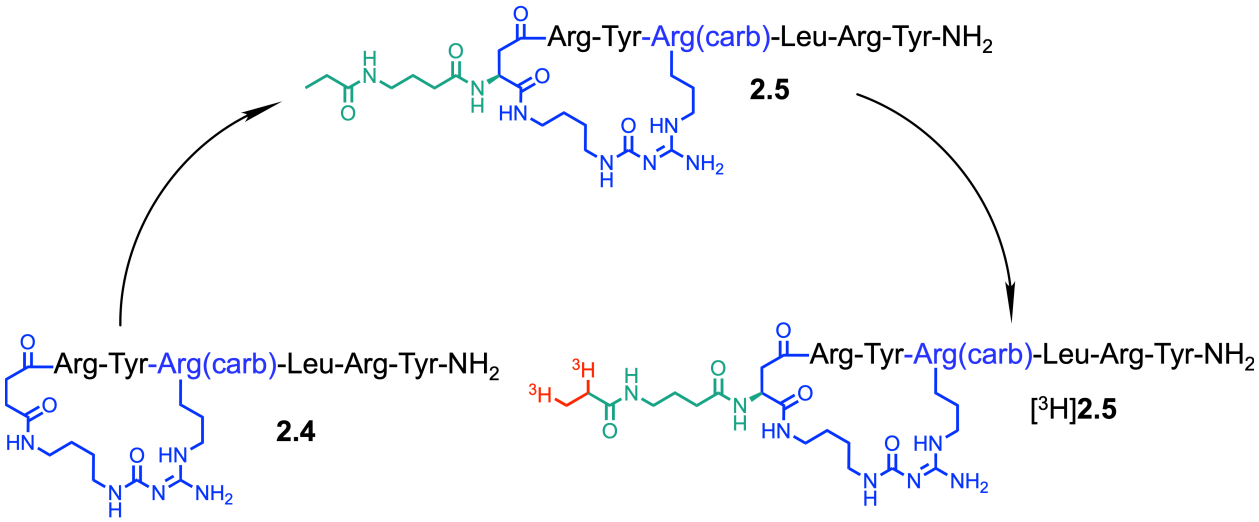

Arg(carb) = N^{ω}-carbamoylated arginine

Figure 2.2. Structures of UR-AK86C (**2.4**), **2.5** (an analog of **2.4** with a propionylated γ-aminobutyryl linker-green), and the radioligand [^{3}H]**2.5** labeled via a [^{3}H]propionyl moiety.

2.2 Materials and Methods

2.2.1 Materials

Human pancreatic polypeptide (hPP) and porcine neuropeptide Y (pNPY) were purchased from Synpeptide (Shanghai, China). Bacitracin and bovine serum albumin (BSA) were obtained from Serva (Heidelberg, Germany). Fetal bovine serum (FBS) was purchased from Pan-Biotech (Aidenbach, Germany). The Y_2R antagonist BIIE0246 was obtained from Boehringer Ingelheim (Ingelheim, Germany). The syntheses of the Y_1R antagonist BIBO3304,[33] **2.4**,[30] [^{3}H]UR-MK299[34] (molar activity: 1.81 TBq/mmol), and [^{3}H]UR-KK200[24] (molar activity: 0.98 TBq/mmol) were described previously. [^{3}H]Propionyl-pNPY (molar activity: 1.39 TBq/mmol) was prepared according to a previously reported procedure[34] with minor modifications that were described elsewhere.[35] Compounds **2.5** and [^{3}H]**2.5**[30, 36] were prepared according to reported procedures. Ultrapure water was consistently used for the preparation of stock solutions, buffers, and eluents for HPLC. Polypropylene reaction vessels (1.5 and 2 mL) from Sarstedt (Nümbrecht, Germany) were used to keep stock solutions.

2.2.2 Methods

2.2.2.1 Cell Culture

Cells were cultured in T25, T75, or T175 tissue culture flasks (Sarstedt, Nümbrecht, Germany) in a humidified atmosphere (95% air, 5% CO_2) at 37 °C. SK-N-MC neuroblastoma cells (obtained from the American Type Culture Collection, ATCC HTB-10) were maintained in EMEM supplemented with 5% FBS. CHO-hY_2R cells (obtained from PerkinElmer, Rodgau, Germany) were cultured in Ham's F-12 supplemented with 5% FBS and G418 (400 µg/mL). CHO-hY_4-G_{qi5}-mtAEQ cells[26] were cultured in HAM's F-12 supplemented with 10% FBS, hygromycin (400 µg/mL), zeocin (250 µg/mL), and G418 (400 µg/mL). HEC-1B-hY_5 cells[37] were maintained in EMEM supplemented with 5% FBS and G418 (400 µg/mL).

2.2.2.2 Buffers and Media Used for Binding and Functional Assays

Buffer I (used for binding experiments at Y_4R (sodium-free conditions) and Y_2R): a hypotonic sodium-free HEPES buffer (25 mM HEPES, 2.5 mM $CaCl_2$, 1 mM $MgCl_2$, pH 7.4) supplemented with 1% BSA (Serva, Heidelberg, Germany) and 0.1 mg/mL bacitracin (Serva). *Buffer II* (used for binding experiments at Y_1R and Y_5R): an isotonic

sodium-containing HEPES buffer (10 mM HEPES, 150 mM NaCl, 25 mM $NaHCO_3$, 2.5 mM $CaCl_2$, 5 mM KCl, pH 7.4) supplemented with 1% BSA. *DPBS* (used for binding studies at Y_4R in the presence of sodium): Dulbecco's phosphate-buffered saline with calcium and magnesium (1.8 mM $CaCl_2$, 2.68 mM KCl, 1.47 mM KH_2PO_4, 3.98 mM $MgSO_4$, 153 mM NaCl, 8.06 mM Na_2HPO_4, pH 7.4) supplemented with 1% BSA and 0.1 mg/mL bacitracin.

2.2.2.3 Radioligand Binding Assays

All radioligand binding assays were performed at intact Y receptor-expressing cells at 23 ± 2 °C. The radiochemical competition binding assays used to study Y_1, Y_2, Y_4, and Y_5 receptor binding of peptide **2.5**, were recently validated by the determination of binding affinities of the reference ligands pNPY (Y_1R, Y_2R, and Y_5R)[30] and hPP (Y_4R).[36] The obtained Y receptor affinities were in good agreement with previously reported binding affinities [for determined and reference pK_i or K_i values of pNPY (Y_1, Y_2, Y_5) see Konieczny *et al.*;[30] determined pK_i of hPP (hY_4R): 10.02,[36] previously reported pK_i value of hPP (hY_4R): 9.62,[26] previously reported K_i value of hPP (hY_4R): 0.023 nM[38]].

Y_1R binding. Competition binding assays at Y_1R-expressing SK-N-MC neuroblastoma cells were performed as previously described using [^{3}H]UR-MK299 as radioligand (concentration: 0.15 nM) (see structure in Figure A2.1, *Section 2.6 Appendix*).[34] Prior to the competition binding experiments, the K_d value of [^{3}H]UR-MK299 was redetermined by saturation binding at SK-N-MC cells according to the reported protocol (data not shown).[34] The obtained K_d value amounted to 0.054 ± 0.006 nM (mean value ± SEM from four independent determinations performed in triplicate), being in excellent agreement with the originally reported dissociation constant (K_d = 0.044 nM) determined with the same batch of [^{3}H]UR-MK299.[34] Due to low radioligand displacement by compound **2.5**, no curve fitting was performed.

Y_2R binding. Competition binding assays at CHO-hY_2R cells were performed as previously described using [^{3}H]propionyl-pNPY (K_d = 0.14 nM, concentration: 0.5 nM) as radioligand (see structure in Figure A2.1, *Section 2.6 Appendix*).[29] Due to low radioligand displacement by compound **2.5**, no curve fitting was performed.

*Y_4R binding using [^{3}H]**2.3** as radioligand*. Competition binding experiments at CHO-hY_4-G_{qi5}-mtAEQ cells[26] using [^{3}H]**2.3** ([^{3}H]UR-KK200) as radioligand (K_d = 0.67 nM,

concentration: 1.0 nM)[24] were performed as previously described.[30] Binding data (dpm) were normalized (100% = bound radioligand in the absence of competitor; 0% = unspecific binding), plotted as % over log(concentration of competitor), and analyzed by a four-parameter logistic fit (log(inhibitor) vs response – variable slope; GraphPad Prism 5, GraphPad Software, San Diego, CA) to obtain pIC_{50} and IC_{50} values, which were converted to pK_i and K_i values according to the Cheng-Prusoff equation[39] (logarithmic form in the case of pK_i values).

Y_5R binding. Competition binding studies at HEC-1B-hY_5R cells[37] were performed as previously described[24] using [^{3}H]propionyl-pNPY (K_d = 11 nM,[23] concentration: 5 nM) as radioligand. Due to low radioligand displacement by compound **2.5**, no curve fitting was performed.

*Y_4R binding assays with [^{3}H]**2.5***. Y_4R binding studies with [^{3}H]**2.5** were performed at intact CHO-hY_4-G_{qi5}-mtAEQ cells[26] at 24 ± 2 °C. All experiments (saturation and competition binding, association and dissociation kinetics) were performed in triplicate with cell suspensions prepared with *buffer I* or with *DPBS*. Cell suspensions were prepared as follows: cells were grown in T75 flasks to reach a confluency of 70–90% on the day of the experiment. The culture medium was aspirated, and the adherent cells were washed twice with *buffer I* or *DPBS* (in this case, both buffers were not supplemented with BSA and bacitracin). The cells were covered with BSA- and bacitracin-free *buffer I* or *DPBS* and scraped off the flask followed by centrifugation at 300 g at rt for 5 min. The supernatant was discarded, and the cells were resuspended in *buffer I* or *DPBS* (containing BSA and bacitracin) at varying densities (100,000–500,000 cells/mL) depending on the receptor expression (in higher passages, expression is decreased) and the type of experiment (for saturation binding experiments a low density was used to reduce the extent of ligand depletion). For all binding experiments, the same filtration procedure for separating free radioligand from cell-bound radioligand and for measuring the activity of the latter was used: after completed incubation, cells were collected on GF/C filter mats (0.26 mm; Whatman, Maidstone, UK) (pretreated with 0.3% polyethylenimine for 30 min) using a Brandel harvester for 96-well plates (Brandel, Gaithersburg, MD), and the wells of the plate and the cells on the filter mat were immediately washed twice with ice-cold PBS. Filter pieces for each well were punched out and transferred into flexible 96-well sample plates (Part No.1450-401; PerkinElmer, Rodgau, Germany) followed by the addition

of Rotiscint Routine (Carl Roth, Karlsruhe, Germany) (200 µL). The plates were sealed with a transparent sealing tape (Greiner Bio-One EASYseal, part no. 676001; Greiner Bio-One, Frickenhausen, Germany), shaken in the dark for at least 3 h, and kept in the dark (without shaking) for at least one more hour before measurement. Radioactivity (dpm) was measured with a MicroBeta2 plate counter equipped with six pairs of photomultiplier tubes (PerkinElmer).

Saturation binding experiments. The wells of a polypropylene round-bottom 96-well plate (polypropylene HTS microtiter plate, Brand, Wertheim, Germany) were prefilled with freshly prepared cell suspension (160 µL) followed by the addition of 20 µL of *buffer I* or *DPBS* (determination of total binding) or 20 µL of a 10 µM solution of hPP in *buffer I* or *DPBS* (final concentration: 1 µM) (determination of unspecific binding), and the addition of 20 µL of a 10-fold concentrated (compared to the final concentration) solution of [^{3}H]**2.5** in *buffer I* or *DPBS*. Samples were incubated under shaking for 2 h followed by cell harvesting and further processing as described afore. Specific binding data, obtained by subtracting triplicate radioactivity (dpm) mean values of unspecific binding from triplicate radioactivity (dpm) mean values of total binding, were plotted against the free radioligand concentration and analyzed by a two-parameter equation describing hyperbolic single-site binding (one-site, specific binding, GraphPad Prism 5) to obtain K_d values. The free concentration of [^{3}H]**2.5** (nM) was calculated by subtracting the amount of specifically bound [^{3}H]**2.5** (nM) (calculated from specifically bound [^{3}H]**2.5** in dpm, the molar activity and the volume per well) from the total concentration of [^{3}H]**2.5**.

Association experiments. The wells of a polypropylene round-bottom 96-well plate (Brand) were prefilled with freshly prepared cell suspension (160 µL). 20 µL of *buffer I* or *DPBS* (determination of total binding) or 20 µL of a solution of hPP in *buffer I* (0.75 µM) or *DPBS* (2.5 µM) (final concentrations: 0.075 and 0.25 µM, respectively) (determination of unspecific binding) were added, followed by the addition of 20 µL of a 0.15 nM (*buffer I*) or 0.5 nM (*DPBS*) solution of [^{3}H]**2.5** (final concentrations: 0.015 and 0.05 nM, respectively). Each association experiment was set up on one 96-well plate. Samples were incubated under shaking for different periods of time. The samples of the different time points were prepared in reversed order (longest incubation time first, shortest incubation time last) so that the cells of all samples could be collected simultaneously with the harvester (method described above). The studied

timespan was 1–150 min for both buffers. Specific binding data of association experiments performed in *buffer I*, obtained by subtracting triplicate radioactivity (dpm) mean values of unspecific binding from triplicate radioactivity (dpm) mean values of total binding, were plotted against the time and analyzed by a two-parameter equation describing an exponential rise to a maximum (one-phase association, Y_0 constrained to zero, GraphPad Prism 5) to yield the observed association rate constants k_{obs}. To calculate mean values in % (*cf*. Figure 2.5B), specific binding data were normalized based on the corresponding B_{eq} value. In the case of *DBPS*, the association of [^{3}H]**2.5** was clearly biphasic, reaching a first, well-pronounced plateau at approximately 10 min, followed by a second association phase starting at ca. 20 min (Figure 2.5B). Therefore, specific binding data of [^{3}H]**2.5** were separately analyzed for the time intervals 0–20 min and 20–150 min. The dataset 0–20 min was analyzed by a three-parameter equation describing an exponential rise to a maximum (one-phase association, Y_0 constrained to zero, GraphPad Prism 5) to yield the observed association rate constants $k_{obs,fast}$. The dataset 20–150 min was analyzed by a four-parameter equation describing an exponential rise to a maximum starting from a plateau (plateau followed by one-phase association, X_0 constrained to 20 min, Y_0 constrained to the plateau value obtained by fitting of the 0–20 min dataset, GraphPad Prism 5) to yield the observed association rate constants $k_{obs,slow}$. To calculate mean values in % (*cf*. Figure 2.5B), specific binding data were normalized based on the B_{eq} value obtained by fitting the 20–150 min dataset. In addition to non-linear data fitting, data were fitted linearly by plotting $\ln[B_{eq}/(B_{eq} - B_t)]$ against the time (*cf*. Figure 2.5B).

Dissociation experiments. The wells of a polypropylene round-bottom 96-well plate (Brand) were prefilled with freshly prepared cell suspension (160 µL). 20 µL of *buffer I* or *DPBS* (determination of total binding) or 20 µL of a solution of hPP in *buffer I* (0.5 µM) or *DPBS* (2.5 µM) (final concentrations: 50 and 250 nM, respectively) (determination of unspecific binding) were added, followed by the addition of 20 µL of a 0.5 nM (*buffer I*) or 5 nM (*DPBS*) solution of [^{3}H]**2.5** (final concentrations: 0.05 and 0.5 nM, respectively) to start the preincubation. Each dissociation experiment was set up on one 96-well plate. Samples were incubated under shaking for 20 min (*DPBS*) or 2 h (*buffer I*, *DPBS*), followed by the addition of 20 µL of a 5 µM (*buffer I* and *DPBS*) solution of hPP (start of the dissociation) and continued shaking. The samples of the different time points were prepared in reversed order (preincubation with the

radioligand was started 20 min or 2 h before the start of the dissociation) so that the cells of all samples could be collected simultaneously with the harvester (method described above). The studied dissociation periods were 0-150 min (*DPBS*, 20 min preincubation) or 0–240 min (*buffer I*, *DPBS*, 2 h preincubation). Specific binding data, obtained by subtracting triplicate radioactivity (dpm) mean values of unspecific binding from triplicate radioactivity (dpm) mean values of total binding, were plotted against the time and analyzed by a three-parameter equation, describing a potentially incomplete monophasic exponential decline (one phase decay, GraphPad Prism 5) to obtain k_{off} values. The mean ± SEM of the plateau values from individual experiments proved to be significantly different from zero (one-tailed t-test, $P > 0.05$) throughout. Thus, re-analysis of the data using a two-parameter equation (complete monophasic exponential decline) was not performed. To calculate mean values in % (*cf*. Figure 2.5C), binding data were normalized based on the specifically bound ligand (B) at t = 0 (B_0). In addition to non-linear data fitting, data were fitted linearly by plotting $\ln[(B_t - B_{plataeu})/(B_0 - B_{plateau})]$ against the time (*cf*. Figure 2.5C).

Calculation of the association rate constants (k_{on}) and the kinetically derived dissociation constants K_d(kin). The association rate constants were calculated according to the equation $k_{on} = (k_{obs} - k_{off})/[\text{radioligand}]$, where [radioligand] represents the concentration of the [^{3}H]**2.5** used for association experiments. Kinetically derived dissociation constants K_d(kin) of [^{3}H]**2.5** were calculated according to $K_d(\text{kin}) = k_{off}/k_{on}$.

Competition binding experiments. The wells of a polypropylene round-bottom 96-well plate (Brand) were prefilled with freshly prepared cell suspension (160 µL). 20 µL of a 10-fold concentrated (relative to the final concentration) solution of the compound of interest in *buffer I* or *DPBS*, and 20 µL of a 10-fold concentrated solution of [^{3}H]**2.5** in *buffer I* or *DPBS* were added (used concentrations of [^{3}H]**2.5**: 0.03 nM in *buffer I* and 0.25 or 0.3 µM in *DPBS*). To determine total binding in the absence of a competitor, 20 µL of *buffer I* or *DPBS* were added, followed by the addition of 20 µL of the aforementioned radioligand solution. To determine unspecific binding, 20 µL of a 0.3 µM solution of hPP in *buffer I* or 20 µL of a 2.5–3 µM solution of hPP in *DPBS* (final concentrations: 30 and 250–300 nM, respectively) and 20 µL of the aforementioned radioligand solution were added. Samples were incubated under shaking for 2 h followed by cell harvesting and further processing as described afore. Binding data

(dpm) were normalized (100% = totally bound radioligand in the absence of competitor; 0% = unspecific binding), plotted as % over log(concentration of competitor), and analyzed by a four-parameter logistic fit (log(inhibitor) vs response – variable slope; GraphPad Prism 5) to obtain pIC_{50} and IC_{50} values, which were converted to pK_i and K_i values according to the Cheng-Prusoff equation (logarithmic form in the case of pK_i values).

2.2.2.4 Acid wash internalization studies

To estimate cell surface-bound and internalized radioligand, saturation binding experiments were performed with [^{3}H]**2.5** at adherent CHO-hY_4-G_{qi5}-mtAEQ cells as described below:

A day prior to the experiment, CHO cells were seeded in a 96-well Primaria plate (Corning Life Sciences, Durham, United States) at a density of 200,000 cells/well. Shortly before the experiment, the culture medium was aspirated, and the cells were washed twice with 200 µL of *DPBS* (in this case, the buffer was not supplemented with BSA and bacitracin) followed by pre-filling of the wells with 180 µL of *DPBS* supplemented with 1% BSA and 100 mg/µL Bacitracin for wells designated for the determination of total binding and 160 µL for the wells assigned for determination of unspecific binding. To determine total binding, 20 µL of 10-fold concentrated solutions of [^{3}H]**2.5** (compared to the final concentrations) were prepared and added to each well to a final sample volume of 200 µL. For the determination of unspecific binding, 20 µL of a 10-fold concentrated solution of hPP in DPBS (compared to the final concentrations) was added to designated wells prior to the addition of the radioligand.

The following acid wash procedure was applied for the two types of internalization assays performed: After the incubation, the wells were aspirated, and the cells were washed twice with 200 µL ice-cold PBS. This was followed by treating the cells with 150 µL of ice-cold acid strip buffer (50 mM glycine and 125 mM NaCl in H_2O, pH 3.0) for 5 min. The acid strip buffer was aspirated and collected in a 96-well round bottom polypropylene plate. The treatment with ice-cold acid-strip buffer (150 µL, 5 min incubation) was repeated, and the washings from each well (representing the surface-bound [^{3}H]**2.5**) were combined in the 96-well polypropylene plate. They were later transferred into 5 mL polypropylene tubes containing 3 mL Rotiscint Routine (Carl

Roth, Karlsruhe, Germany), followed by measurement of the radioactivity (dpm) in a PerkinElmer Liquid Scintillation Analyzer (Tri-Carb 3100TR).

After the treatment with acid strip buffer, the cells were lysed by adding 25 µL of lysis solution (8 M urea, 3 M acetic acid, 1% Triton-X-100 in water) and incubated on a shaker at rt for at least 40 min. The lysates (representing internalized [^{3}H]**2.5**) were transferred into a 96-well sample plate (Part no. 1450-401; PerkinElmer), followed by the washing of the wells with 25 µL of lysis solution (washings combined with the lysates). 200 µL of Rotiscint Routine (Carl Roth) were added to each well, and the surface of the plate was cleaned with a paper towel (wetted with 70% ethanol) to remove possible spills of the scintillation cocktail. The plate was then sealed with a transparent sealing tape (Greiner Bio-One EASYseal, part no. 676001; Greiner Bio-One, Frickenhausen, Germany) and shaken in the dark for at least 2 h. After shaking, the plate was measured for radioactivity (dpm) using a MicroBeta2 plate counter equipped with six pairs of photomultiplier tubes (PerkinElmer).

Triplicate radioactivity (dpm) mean values of unspecific binding were subtracted from triplicate radioactivity (dpm) mean values of total binding to obtain specific binding data for both surface-bound [^{3}H]**2.5** (acid strip washings) and internalized [^{3}H]**2.5** (cell lysate). The percent amount of internalized radioligand was determined as a percentage of total specific binding which is the sum of specific binding data for both surface-bound and internalized [^{3}H]**2.5**.

Saturation binding experiments in adherent CHO-hY_4-G_{q15}-mtAEQ cells. To determine total binding, 20 µL of 10-fold concentrated solutions of [^{3}H]**2.5** in DPBS (compared to the final concentrations) was added, whereas for the determination of unspecific binding, 20 µL of a 10 µM solution of hPP in DPBS (final concentrations: 1 µM) was added to designated wells prior to the addition of the radioligand. Samples were incubated under shaking for 2 h followed by further processing as described afore.

Concentration-dependent internalization. To determine the total binding, 20 µL of 10-fold concentrated serially diluted solutions of [^{3}H]**2.5** in *DPBS* with final concentrations ranging from 0.01 nM to 4 nM were added to the respective wells. For unspecific binding, 20 µL of hPP in 100-fold excess of the radioligand in *DPBS* were first added to the respective wells, followed by the addition of 20 µL of the serially diluted solutions

of [^{3}H]**2.5**. The plates were gently shaken for 1.5 h, followed by further processing of the samples as described afore.

Time-dependent internalization. For the determination of total binding, 20 µL of 10-fold concentrated solution of [^{3}H]**2.5** in *DPBS* were added to the respective wells, resulting in a final concentration of 2 nM. The unspecific binding was determined by adding 20 µL of 0.2 µM of hPP into corresponding wells before the addition of [^{3}H]**2.5**. 20 µL of a 20 nM solution of [^{3}H]**2.5** in *DPBS* were added to the respective wells (final concentration of [^{3}H]**2.5**: 2 nM) followed by incubation under gentle shaking at rt (24 ± 3 °C) for different times (1, 3, 6, 12, 25, 45, 70, and 90 min). After incubation, further processing was performed as described afore.

2.2.2.5 Calculation of propagated errors

Propagated errors were calculated according to the general equation (maximum error propagation):

$$\Delta z = \left|\frac{\partial f}{\partial x_1}\right| \Delta x_1 + \left|\frac{\partial f}{\partial x_2}\right| \Delta x_2 + \ldots$$

f: function of x_1, x_2, etc. ($f(x_1, x_2, \ldots) = z$); Δx_1, Δx_2: error (in this work represented by the SEM or a propagated error) of x_1 and x_2; Δz: (propagated) error of z.

2.3 Results and Discussion

2.3.1 Peptide 2.5 is highly selective towards Y_4R

The YR binding profile of **2.5** was determined by competition binding studies at all human Y receptors using previously validated assays and the respective radioligands for the different receptor subtypes. Y_1R binding was determined at hY_1R-expressing SK-N-MC neuroblastoma cells in sodium-containing buffer using [^{3}H]UR-MK299[34] as radioligand. Binding to the Y_2 and Y_5 subtypes was investigated at intact CHO-hY_2R cells in a sodium-free buffer and at HEC-1B-hY_5R cells in a sodium-containing buffer, respectively, using the radioligand [^{3}H]propionyl-pNPY.[24, 37] In the case of Y_4R, the competition binding assay was performed with CHO-hY_4-G_{qi5}-mtAEQ cells in sodium-free buffer using the radioligand [^{3}H]UR-KK200.[30] The results from these binding studies show that the parent peptide **2.4** and peptide **2.5** exhibit very low affinities to Y_1R, Y_2R, and Y_5R, and as such, the pK_i values could not be determined within the applied concentration range reaching up to 10 µM (Table 2.1).

Table 2.1. Y receptor binding data of hPP, **2.4** and **2.5**.

Compd.	pK_i ± SEM / K_i [nM]				Selectivity towards Y_4R, ratio K_i ($Y_{1,2,5}R$) / K_i (Y_4R)		
	hY_1R^a	hY_2R^b	hY_4R^c	hY_5R^d	Y_1R	Y_2R	Y_5R
hPP	6.4 / 440[e]	<5.5 / >3000[e]	10.02 ± 0.06 / 0.10[f]	7.8 / 17[e]	>630	>4300	>20
2.4	<5.5 / >3000[g]	<5 / >10000[g]	10.36 ± 0.11 / 0.048[g]	<5.5 / >3000[g]	>60000	>200000	>60000
2.5	<6 / >1000	<5.5 / >3000	10.5 ± 0.1 / 0.036	<6 / >1000	>27000	>83000	>83000

[a]Determined by competition binding at SK-N-MC neuroblastoma cells using [^{3}H]UR-MK299 (K_d = 0.054 nM, c = 0.15 nM) as radioligand (see structure in Figure A2.1, *Section 2.6 Appendix*). [b]Determined by competition binding with [^{3}H]propionyl-pNPY (K_d = 0.14 nM,[29] c = 0.5 nM) at CHO-hY_2R cells (see radioligand structure in Figure A2.1, *Section 2.6 Appendix*). [c]Determined by competition binding at CHO-hY_4-G_{qi5}-mtAEQ cells using [^{3}H]**2.3** ([^{3}H]UR-KK200) (K_d = 0.67 nM,[24] c = 1 nM) as radioligand (see structure in Figure 2.1). [d]Determined by competition binding at HEC-1B-hY_5R cells using [^{3}H]propionyl-pNPY (K_d = 11 nM,[23] c = 5 nM) as radioligand. [e]Berlicki *et al.* (reported K_i values were converted to pK_i values)[27] [f]Wirth *et al.*[36] [g]Konieczny *et al.*[30] Data represent mean values ± SEM (pK_i) or mean values (K_i) from three to five independent experiments performed in triplicate.

Peptides **2.4** and **2.5** exhibited at least 3000-fold higher Y_4R affinity compared to the subtypes Y_1, Y_2, and Y_5. Moreover, in comparison to hPP, **2.5** appears to be more selective towards the Y_4R as it shows lower affinity to Y_1R and Y_5R (K_i > 1000 nM). Overall, the Y_4R selectivity of peptide **2.5** (and predictively of [^{3}H]**2.5**), proved to be very high (> 27,000-fold over Y_1, Y_2, and Y_5 receptors). The investigation of **2.5** in different functional Y_4R assays (Ca^{2+} aequorin assay, miniG_{si} recruitment assay, cAMP CAMYEN assay) revealed that this cyclic peptide represents a partial Y_4R agonist with efficacies of 60–83% (data not shown).[40]

2.3.2 [^{3}H]**2.5** binds in a saturable manner at Y_4R under physiological-like conditions

Saturation binding studies with [^{3}H]**2.5** were conducted with cell suspensions of intact Chinese hamster ovary (CHO) cells stably expressing the hY_4R in hypotonic sodium-free buffer (*buffer I*) as well as in an isotonic buffer containing 153 mM sodium (*DPBS*) (for detailed buffer compositions see *Section 2.2.2.2*). In both buffers, binding of [^{3}H]**2.5** to the hY_4R was saturable, yielding average K_d values of 12 pM and 110 pM for *buffer I* and *DPBS*, respectively (Figure 2.3, Table 2.1). The saturability of this radioligand was also confirmed in saturation binding studies using adherent, intact Chinese hamster ovary (CHO) cells stably expressing the hY_4R in *DPBS* (average K_d = 650 pM) (see Figure A2.2, *Section 2.6 Appendix*). The slight difference in K_d could be attributed to the extracellular microenvironment of adherent cells known to have extracellular matrices (ECM) that can affect ligand-receptor interactions.[41, 42] Another possible explanation could be the effect of the type of plate used and the material it is made of.

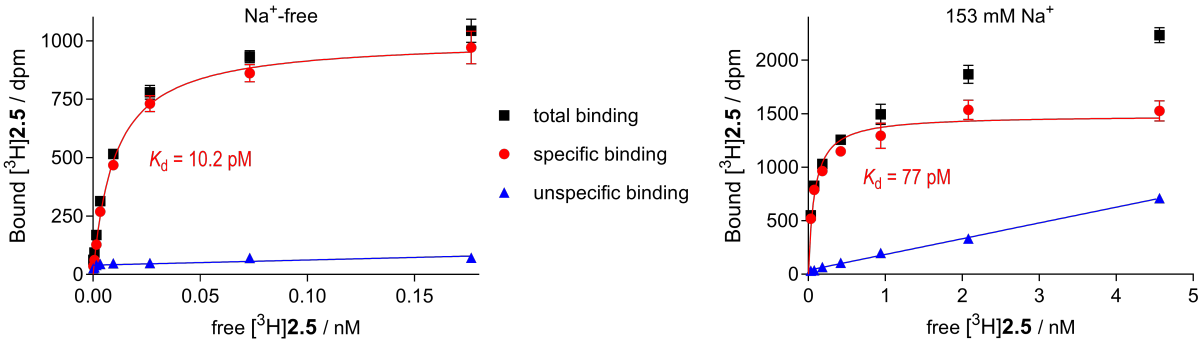

Figure 2.3. Representative Y_4R binding isotherms (specific binding) of [^{3}H]**2.5** obtained from saturation binding experiments performed with intact CHO-hY_4-G_{qi5}-mtAEQ cells in sodium-free and sodium-containing buffer at 24 ± 2 °C. Unspecific binding was determined in the presence of 1 µM hPP. Experiments were performed in triplicate. Total and unspecific binding data represent mean values ± SEM. Specific binding data represent calculated values ± propagated error.

Due to the high binding affinities, unspecific binding amounted to less than 10% at a radioligand concentration corresponding to the K_d value. As observed for the previously described tritiated Y_4R radioligands [^{3}H]**2.1** and [^{3}H]**2.2** (*cf.* Figure 2.1), the Y_4R affinity of [^{3}H]**2.5** was lower in sodium-containing buffer compared to *buffer I* (about a factor of 10). Notably, the affinity of [^{3}H]**2.5** in the presence of 153 mM sodium (K_d = 0.11 nM) was still higher than the Y_4R affinity of [^{3}H]**2.1** and [^{3}H]**2.2** in hypotonic sodium-free buffer (K_d = 1.1 nM and 0.67 nM, respectively).

2.3.3 Binding kinetics of [^{3}H]2.5 at Y_4R exhibit both biphasic association and dissociation under physiological-like conditions

Following the saturation binding assays, the Y_4R binding kinetics of [^{3}H]**2.5** were investigated using the same cell line and buffer conditions. In *buffer I*, the radioligand showed a monophasic association, whereas in *DPBS,* a clear biphasic association was observed, with the initial phase plateauing after around 10 min and the second phase starting and plateauing after 20 min and 75 min, respectively (Figure 2.4A). For the initial phase that showed fast association, the plateau amounted to approximately 70% in relation to the plateau of the second association phase. The data suggest that the biphasic character of the association of [^{3}H]**2.5** to Y_4R in sodium-containing buffer can be attributed to the presence of sodium. Seemingly, when sodium is present at a physiological concentration, two subpopulations of Y_4R exist. As many class A GPCRs bind sodium ions as an allosteric modulator stabilizing the inactive receptor conformation,[31, 32] these subpopulations could be explained by an incomplete occupation of the sodium binding site of Y_4R at the used sodium concentration (153 mM). This is supported by the reported measurement of the melting temperature of the A_{2A} adenosine receptor in the absence of sodium, at 150 mM NaCl and 500 mM NaCl, showing that the melting temperature of the receptor further decreased by increasing the sodium concentration from 150 to 500 mM (note: sodium destabilizes the receptor protein).[32] With sodium being known to stabilize the inactive conformation of GPCRs, which is characterized by a more open passage to the ligand binding pocket,[31, 32] the initial association phase likely represents the binding of the radioligand to the subpopulation of receptors that have sodium bound, as such making the receptor more accessible for the ligand. At the same time, the agonist is loosely held by the receptor, which is in accordance with the faster dissociation of [^{3}H]**2.5** (compared to sodium-free conditions) observed in sodium-containing buffer initiated after 20 min or 2 h of preincubation (Figure 2.4B). Consequently, the second slow association phase could represent the binding to the non-sodium-bound receptor subpopulation. This is also supported by the monophasic association curve from studies in sodium-free *buffer I,* which is nearly superimposed with the curve of the slow association phase from studies in *DPBS* (Figure 2.4A).

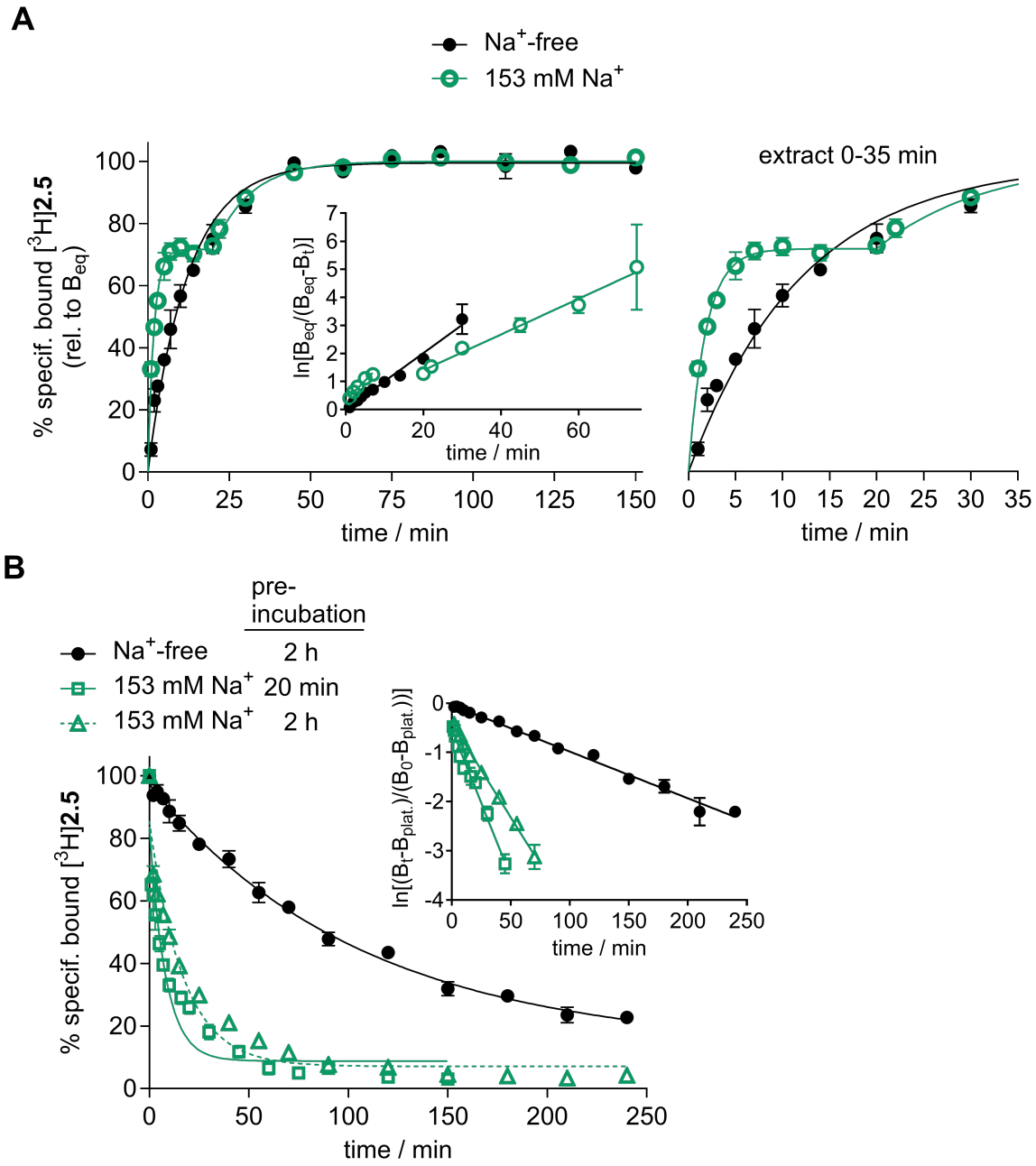

Figure 2.4. Y_4R binding characteristics of [^{3}H]**2.5** studied in sodium-free and sodium-containing buffer at 24 ± 2 °C using intact CHO-hY_4-G_{qi5}-mtAEQ cells. (A) Association of [^{3}H]**2.5** (c = 0.015 nM (Na^+-free) or 0.05 nM (153 mM Na^+) to the Y_4R. In sodium-containing buffer (*DPBS*), [^{3}H]**2.5** exhibited a biphasic association kinetics. Inset: linearized data. Data represent mean values ± SEM from three or four independent experiments, each performed in triplicate. For k_{obs} and k_{on} values, see Table 2.2. (B) Dissociation of [^{3}H]**2.5** from the Y_4R. Concentration of [^{3}H]**2.5** used for the preincubation: 0.05 nM (Na^+-free), 0.5 nM (153 mM Na^+). Plateau values of the three-parameter fits (monophasic exponential decline): 13% (Na^+-free), 8% (153 mM Na^+, 20 min preincubation), and 7% (153 mM Na^+, 2 h preincubation). Inset: linearized data. Data represent mean values ± SEM from three or four independent experiments each performed in triplicate. For k_{off} values, see Table 2.2.

Table 2.2. Y_4R binding data of [^{3}H]**2.5** determined at 24 ± 2 °C using CHO-hY_4-G_{qi5}-mtAEQ cells.

Buffer	Saturation binding	Binding kinetics			
	pK_d / K_d [nM][a]	k_{obs} [min^{-1}][b]	k_{off} [min^{-1}][c]	k_{on} [nM^{-1}·min^{-1}][d]	K_d(kin) [nM][e]
buffer I (sodium-free)	10.92 ± 0.06 / 0.012	0.071 ± 0.008	0.0094 ± 0.0004	4.1 ± 0.6	0.0023 ± 0.0004
DPBS (153 mM Na^+)	9.98 ± 0.06 / 0.11	fast: 0.54 ± 0.03	20 min preincubation: 0.12 ± 0.02	fast: 8.4 ± 0.9	0.014 ± 0.003[f]
		slow: 0.093 ± 0.006	2 h preincubation: 0.059 ± 0.001	slow: 0.7 ± 0.2	0.09 ± 0.02[g]

[a]Equilibrium dissociation constants expressed as pK_d and K_d; mean values ± SEM (pK_d) or mean values (K_d) from four independent experiments (performed in triplicate). [b]Observed association rate constants obtained by monophasic fitting (in the case of *DPBS*, the fast and slow component were fitted separately); mean values ± SEM from three or four independent experiments (performed in triplicate). [c]Dissociation rate constants obtained from three-parameter monophasic fits, mean values ± SEM from three or four independent experiments (performed in triplicate). [d]Association rate constants ± propagated error calculated from k_{obs}, the respective k_{off} value, and the ligand concentration used for the association studies. [e]Kinetically derived dissociation constants ± propagated error calculated from k_{off} and k_{on}. [f]Calculated from $k_{off(20\ min\ preincub.)}$ and $k_{on,fast}$. [g]Calculated from $k_{off(2\ h\ preincub.)}$ and $k_{on,slow}$.

In view of this, the slower association of [^{3}H]**2.5** observed in *buffer I* can be explained by the spatially more restricted passage to the ligand binding pocket in the receptor.[31, 32] Once it enters the binding pocket, the ligand is more tightly bound in the absence of sodium, and this is corroborated by the markedly slower dissociation of [^{3}H]**2.5** from Y_4R in *buffer I* (Figure 2.4B). An alternative explanation for the biphasic association curve could possibly be the internalization of the agonist-bound Y_4R impacting the association kinetics from 20 min onward (Figure 2.4A). The removal of occupied Y_4R from the cell surface would lead to a reoccupation of unoccupied Y_4R at the cell surface, resulting in the second slow association phase. To test this hypothesis, association experiments were conducted with [^{3}H]**2.5** in *DPBS* at 4 °C precluding receptor internalization. As the K_d of [^{3}H]**2.5** in *DPBS* was higher at a low temperature (average K_d = 0.86 nM, *cf*. Figure 2.5A), the association studies at 4 °C were performed with a radioligand concentration of 0.2 nM instead of 0.05 nM (24 °C).

The results clearly showed an initial fast association plateauing at a similar time as observed at 24 °C (Figure 2.5B). In contrast to the studies at 24 °C, the first association phase was followed by two more phases, which could be due to a splitting of the second phase observed at 24 °C into two phases. Nonetheless, the association studies at 4 °C did not support the hypothesis that the biphasic association of [^{3}H]**2.5** in *DPBS* at 24 °C is caused by internalization of Y_4R induced by binding of the partial agonist [^{3}H]**2.5**.

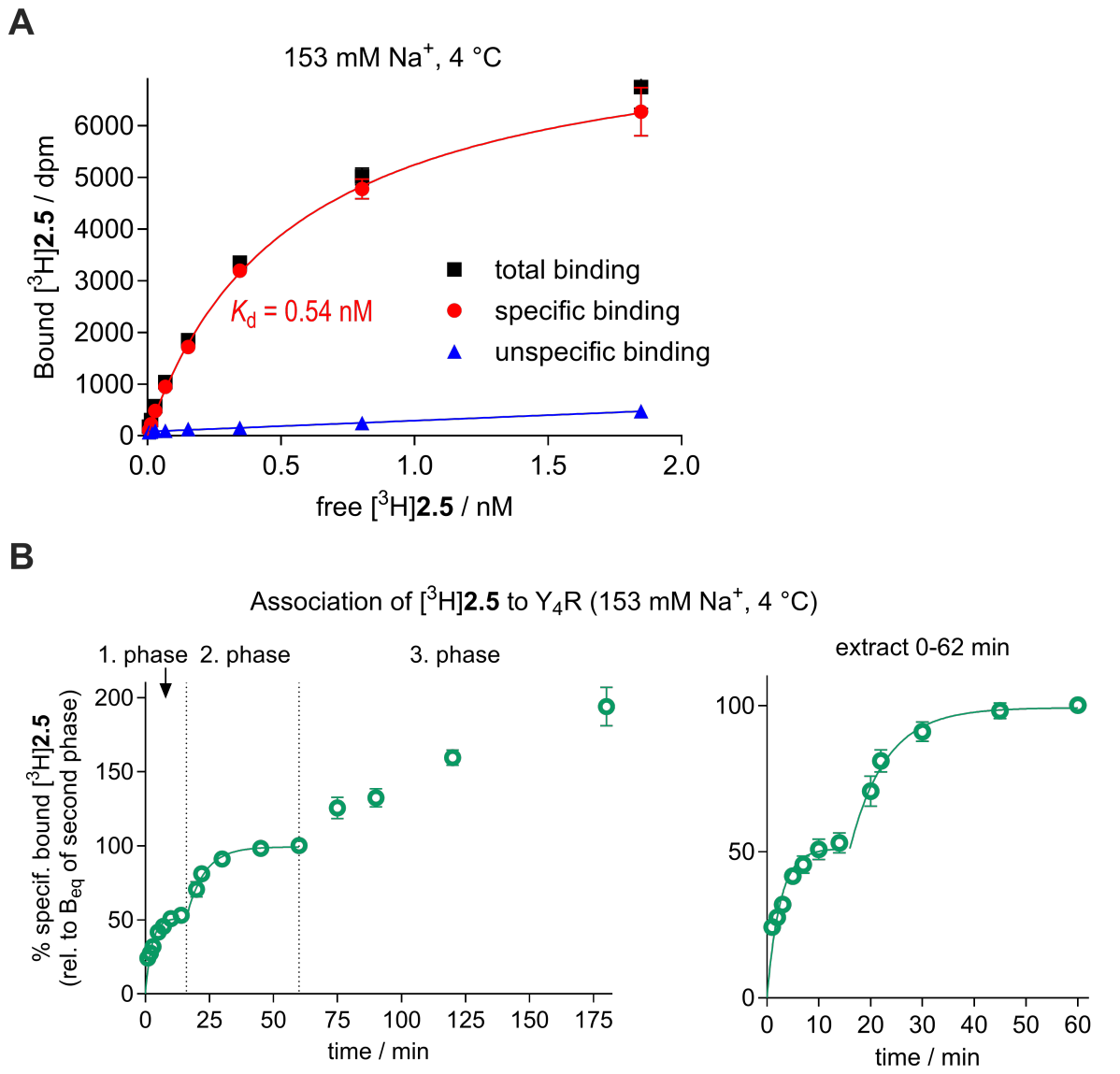

Figure 2.5. Y_4R binding characteristics of [^{3}H]**2.5** studied in sodium-containing buffer (*DPBS*) at 4 °C using intact CHO-hY_4-G_{qi5}-mtAEQ cells. (A) Representative Y_4R binding isotherm (specific binding) of [^{3}H]**2.5** obtained from a saturation binding experiment. Total and unspecific binding data represent mean values ± SEM. Specific binding data represent calculated values ± propagated error. The mean pK_d value of [^{3}H]**2.5**, obtained from four independent experiments (each performed in triplicate at 4 °C) amounted to 9.15 ± 0.16 (mean value ± SEM). The mean K_d value was 0.86 nM. (B) Association of [^{3}H]**2.5** (c = 0.2 nM) to the hY_4R. In contrast to association studies in *DPBS* at 24 °C (*cf.* Figure 2.4A), the association kinetics of [^{3}H]**2.5** appeared to be triphasic at 4 °C. Specific binding was normalized based on the B_{eq} value obtained by fitting of the 20–60 min dataset (second phase). Data represent mean values ± SEM from five independent experiments, each performed in triplicate. The k_{obs} values of the first and second phases amounted to 0.5 ± 0.1 min^{-1} and 0.15 ± 0.03 min^{-1} (mean values ± SEM from five independent experiments).

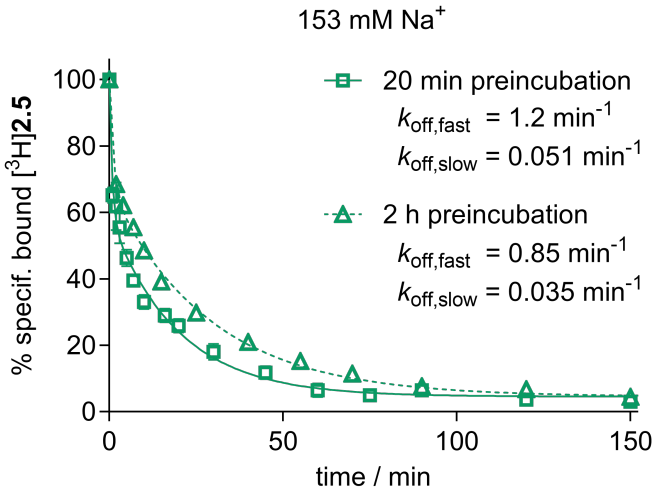

Figure 2.6. Biphasic fitting (two-phase decay, GraphPad Prism 5) of the data obtained from Y_4R dissociation experiments with [^{3}H]**2.5** performed in *DPBS* with 20 min or 2 h preincubation (data taken from Figure 2.4B). Presented are mean values ± SEM from three independent experiments (performed in triplicate).

Dissociation studies with [^{3}H]**2.5** in sodium-free *buffer I* revealed a monophasic dissociation of the radioligand from Y_4R (Figure 2.4B). In contrast, fitting of the data obtained from dissociation experiments in *DPBS* using different preincubation periods (20 min and 2 h) revealed a biphasic character (F-test one-phase decay vs two-phase decay gave P values < 0.001 favoring the two-phase model, GraphPad Prism 5, GraphPad Software, San Diego, CA) being similar for both preincubation conditions (Figure 2.6).

However, the $k_{off,fast}$ values resulting from the biphasic fits were higher than the $k_{obs,fast}$ value from the association studies, precluding a calculation of the association rate constant k_{on} and, in turn, the kinetically derived dissociation constant K_d(kin). Therefore, as an approximation, these data were also fitted using an equation describing a monophasic decline (Figure 2.4B). Regarding the dissociation initiated after 2 h of preincubation, covering both the fast and slow associations, one might expect a more pronounced biphasic character of the dissociation curve compared to the dissociation started after 20 min of preincubation, covering only the initial fast association. However, similar curves were obtained for the dissociation of [^{3}H]**2.5** initiated after 20 min or 2 h of preincubation (Figures 2.4B and 2.6), suggesting an equalization of the initially distinguishable receptor populations driven by the binding of the agonist [^{3}H]**2.5** to Y_4R. As **2.5** acts as a partial Y_4R agonist (results not shown), this equalization could be explained by a partial collapse of the sodium binding pocket

upon agonist binding in contrast to a complete collapse as proposed for full agonists,[31] allowing sodium to reside in the receptor and even to enter the receptor while the partial agonist is bound. This hypothesis is supported by recent molecular dynamics simulations performed for the A_{2A} adenosine receptor, which suggest the existence of multiple sodium binding sites in the receptor, justifying a possible coexistence of agonist and sodium ions in the receptor and an entry of sodium ions in the ligand-bound receptor protein.[43] To note, the binding kinetics of the radiolabeled hPP derivative [^{3}H]**2.1** (*cf*. Figure 2.1), also studied in sodium-free and sodium-containing buffer, showed monophasic association and dissociation curves for both conditions.[23] This indicates a more complex interaction of **2.5** with Y_4R compared to hPP and confirms once more that each ligand-receptor complex exhibits its own individual characteristics. In addition to the effect of sodium, the observed biphasic dissociation of [^{3}H]**2.5** from Y_4R could also be explained by ligand-driven conformational adjustments of the binding pocket affecting residence time,[44] or by a high affinity of the peptide ligand to the vestibule of the receptor as identified for binding of arginine vasopressin to the V_2 vasopressin receptor.[45] This would result in the coexistence of different types of ligand-receptor complexes (occupation of the vestibule vs occupation of the orthosteric site), potentially showing different dissociation kinetics. Nonetheless, as the dissociation rate constants of the second slow phase ($k_{off,slow}$ = 0.051 and 0.035 min^{-1}, respectively, Figure 2.4B) were not far from the k_{off} value obtained from dissociation studies in sodium-free *buffer I* (k_{off} = 0.0094 min^{-1}, Table 2.2), the second slow dissociation phase might predominantly represent dissociation of [^{3}H]**2.5** from sodium-free Y_4R. In both buffers, the monophasic analyses of the dissociation data gave curve plateaus significantly different from zero (one-tailed t-test, $P < 0.05$). However, the plateaus, which represent the undissociated, potentially internalized radioligand, were below 14%, implying that Y_4R binding of [^{3}H]**2.5** was largely reversible. This is a favorable feature with respect to the application of [^{3}H]**2.5** in competition binding assays. For *buffer I*, the kinetically derived dissociation constant K_d(kin), defined as k_{off}/k_{on}, was five times lower than the K_d value obtained from saturation binding experiments (Table 2.2). This minor discrepancy might arise from the slow dissociation kinetics of [^{3}H]**2.5** in *buffer I* (*cf*. Figure 2.4B) and the incubation time of 2 h applied for saturation binding studies not allowing complete equilibrium. In the case of *DPBS*, the K_d(kin) (88 pM) was in good agreement with the equilibrium K_d (110 pM) when considering the $k_{on,slow}$ value and the k_{off} value from dissociation

experiments applying a preincubation period of 2 h (Table 2.2). This indicates that Y_4R binding of [^{3}H]**2.5** in *DPBS* largely follows the law of mass action for an incubation time of 2 h.

2.3.4 [^{3}H]2.5 can be used as a probe in Y_4R competition binding assays

Finally, the suitability of [^{3}H]**2.5** to serve as a molecular tool for the determination of Y_4R binding affinities was explored by conducting competition binding experiments with hPP, and **2.2–2.5** in *buffer I* and *DPBS* using the same cell line as for saturation binding and kinetic studies. The obtained radioligand displacement curves are shown in Figure 2.7, and the K_i values are summarized in Table 2.3.

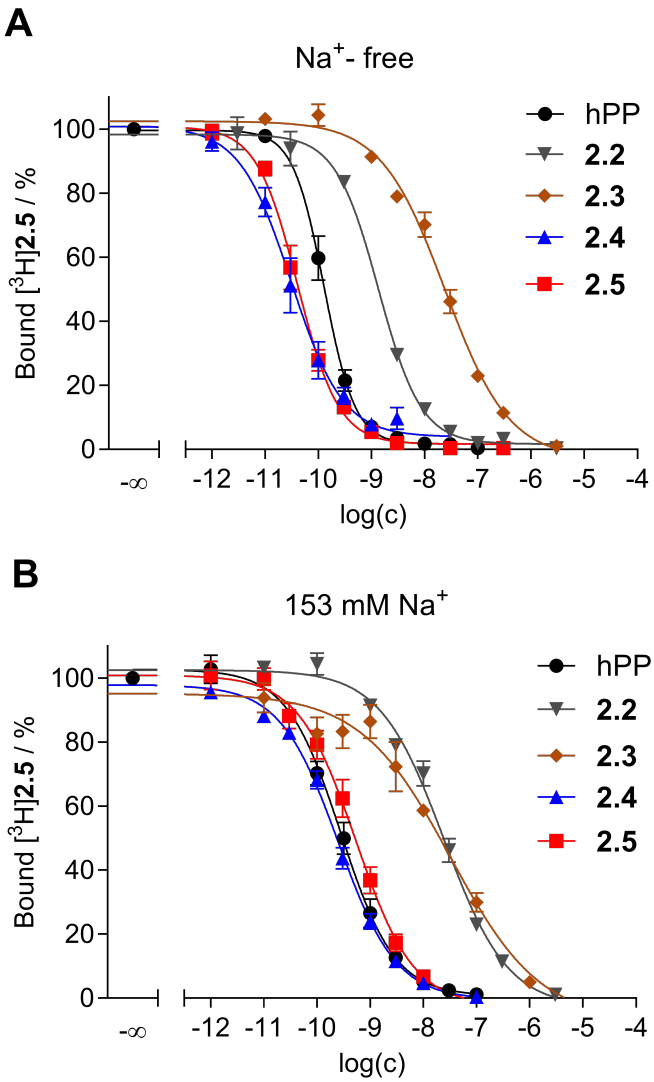

Figure 2.7. Radioligand displacement curves from competition binding experiments performed with [^{3}H]**2.5** and hPP, **2.2**, **2.3**, **2.4** or **2.5** at intact CHO-hY_4-G_{qi5}-mtAEQ cells using (A) a sodium-free or (B) a sodium-containing buffer. Used concentrations of [^{3}H]**2.5**: 30 pM (A), 250 pM (hPP, **2.3–2.5** in B) and 300 pM (**2.2** in B). Data represent mean values ± SEM from at least three independent experiments performed in triplicate.

Table 2.3. Overview of hY_4R binding affinities of hPP and **2.2-2.5**.

Compd.	Hypotonic sodium-free buffer		Isotonic sodium-containing buffer	
	pK_i / K_i [nM][a]	literature (K_i in nM)	pK_i / K_i [nM][a]	literature (K_i in nM)
hPP	10.44 ± 0.07 / 0.037	0.10[b] 0.24[c] 0.023[d]	10.08 ± 0.12 / 0.088	10.41[e]
2.2	9.41 ± 0.01 / 0.39	0.87[f] 0.32[f]	7.99 ± 0.07 / 11	6.3[f]
2.3	9.68 ± 0.30 / 0.41	1.2[f] 0.66[f]	8.18 ± 0.06 / 6.7	n.a.
2.4	11.04 ± 0.16 / 0.011	0.048[g]	10.13 ± 0.07 / 0.076	n.a.
2.5	11.05 ± 0.10 / 0.010	n.a.	9.79 ± 0.09 / 0.17	n.a.

[a]Determined by competition binding at CHO-hY_4-G_{qi5}-mtAEQ cells using [^{3}H]**2.5** as radioligand; mean values ± SEM (pK_i) or mean values (K_i) from two (**2.2** Na^+-free), three (hPP, **2.2** and **2.3** with Na^+), four (**2.4**, **2.5** with Na^+) or five (**2.3** Na^+-free, **2.5** Na^+-free) independent experiments performed in triplicate. [b]Wirt *et al.*[36] [c]Ziemek *et al.* (reported pK_i of 9.62 was converted to K_i).[26] [d]Gehlert *et al*.[38] [e]Eriksson *et. al.*[14] [f]Kuhn *et al*.[24] [g]Konieczny *et al*.[30] n.a. not available.

The determined Y_4R affinities of hPP and **2.2**–**2.4** were consistent with the reported binding data (Table 2.3). Likewise, the obtained K_i values of **2.5** were in line with the K_d values resulting from saturation binding with [^{3}H]**2.5** (*buffer I*: K_d = 12 pM, K_i = 10 pM, *DPBS*: K_d = 110 pM, K_i = 170 pM). Notably, the Y_4R affinities of **2.2–2.4** and **2.5** determined in *DPBS* were significantly lower compared to those in *buffer I* (factor of 7–28). On the contrary, this difference in Y_4R affinities was less pronounced (factor of 2.5) in the case of hPP. Taken together, the competition binding studies with [^{3}H]**2.5** showed that this radioligand is well suited for the determination of Y_4R binding affinities of Y_4R ligands targeting the orthosteric binding site.

2.3.5 Binding of [^{3}H]2.5 to Y_4R induces receptor internalization

Agonist radioligands, either full or partial, are known to only label a subpopulation (2%–68%) of the receptor population compared to their antagonist counterpart.[46] Moreover, high-affinity agonists can generally induce rapid receptor internalization due to the persistent stimulation of the receptor, resulting in receptor desensitization as a part of the regulation of signaling transduction.[47-49] Thus, for the suitability of high-affinity radioligands as probes in competition binding assays, a slow internalization in low amounts is favorable as the cellular uptake of receptor and radioligand could affect the accuracy of the inhibition constant (K_i) of the ligands to be determined. To investigate the internalization of Y_4R occupied by [^{3}H]**2.5** under physiological-like conditions (sodium-containing buffer), intact adherent CHO-hY_4-G_{qi5}-mtAEQ cells were incubated at room temperature with [^{3}H]**2.5** followed by washing with low pH buffer (acid strip buffer) to remove all extracellularly bound ligand. The applied concentration range for [^{3}H]**2.5** was 0.011–4 nM.

Results from this showed that about 5-30% of the ligand-receptor complex was internalized depending on the concentration of the radioligand used. The amounts internalized at the very low concentrations (0.011 and 0.025 nM) were about 5%. The amount of internalized radioligand then further increased with increasing receptor occupancy, reaching a maximum of 28 ± 2% (mean value ± SEM from three independent experiments performed in triplicate) (Figure 2.8A). This indicated that internalization depends on the receptor occupancy, being high and close to saturation at high ligand concentrations.

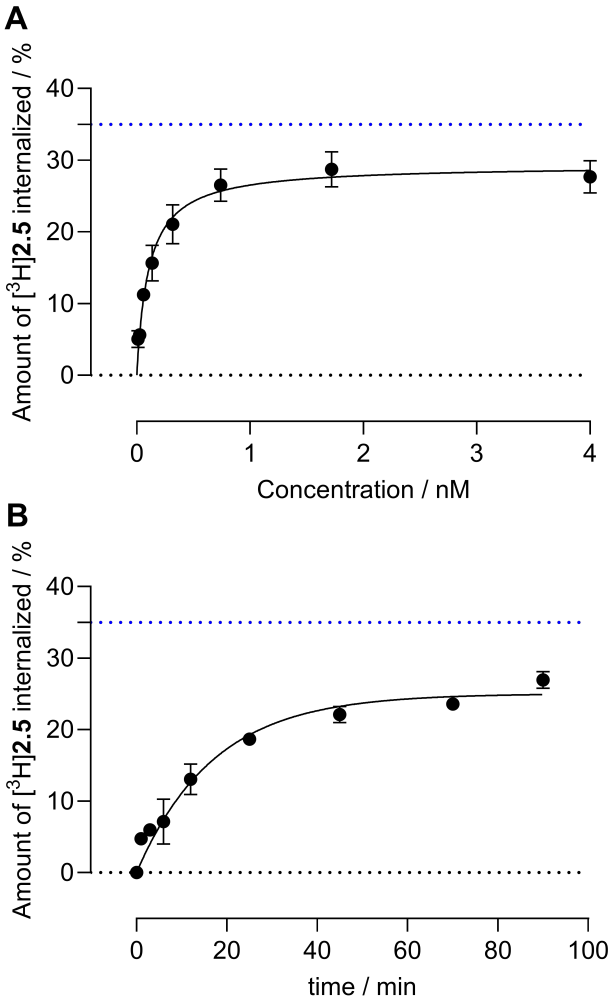

Figure 2.8. Internalization of radioligand [^{3}H]**2.5** in intact CHO-hY_4-G_{qi5}-mtAEQ cells studied in a sodium-containing buffer at 24 ± 2 °C. (A) Effect of the radioligand concentration on the amount internalized after 1.5 h of incubation. (B) Effect of the incubation time on the amount of radioligand internalized using a radioligand concentration of 2 nM. Data represent mean values ± SEM from at least three independent experiments performed in triplicate.

To estimate the rate of internalization, the cells were then incubated with 2 nM [^{3}H]**2.5** (within the concentration range where the amount of internalized Y_4R-[^{3}H]**2.5** complex

plateaus) for up to 90 min at rt. The amount of internalized [^{3}H]**2.5** increased exponentially, reaching an average of 27% after 90 min (Figure 2.8B). Although this implies that the rate of internalization for [^{3}H]**2.5** is very slow, it is important to note that this rate could increase at increasing temperatures above rt, as studies have shown that above 10 °C, any increase in temperature is known to directly correlate to observed increases in the rate of internalization.[50, 51]

Overall, these findings indicate that the amount of internalized Y_4R-[^{3}H]**2.5** complex is low and concentration-dependent, while the rate of internalization is slow at room temperature (binding assays' temperature). Nonetheless, this concentration dependency should have a negligible effect on the radioligand's Y_4R binding kinetics and affinity determined in sodium-containing buffer at room temperature. This can be corroborated by the similar association kinetics of [^{3}H]**2.5** studied at rt and at 4 °C (Figures 2.4A and 2.5B). Furthermore, this is also supported by reported K_i values of hPP in assays using membrane preparations being similar to that obtained using [^{3}H]**2.5** as a probe.[11, 52] This characteristic adds to the suitability of [^{3}H]**2.5** as a competitor in binding assays.

2.4 Conclusion

Until now, hypotonic sodium-free buffers have been widely used for Y_4R binding assays since most of the used radioligands, representing peptidic Y_4R agonists, show higher Y_4R affinity under sodium-free conditions, accounting for a lower consumption of radioligand and lower unspecific binding. However, binding studies for the development of therapeutics acting at Y_4R should be performed under physiological-like conditions using sodium-containing buffers. The newly developed Y_4R radioligand [^{3}H]UR-JG102 ([^{3}H]**2.5**) shows unprecedented Y_4R affinity in the presence of sodium (K_d = 0.11 nM) compared to the reported tritiated Y_4R radioligands and exhibits a lower molecular weight compared to all previously reported radiolabeled Y_4R ligands. Benefits associated with the use of [^{3}H]**2.5** are low consumption of radioligand and low unspecific binding due to the low concentrations needed. Low unspecific binding, in turn, is advantageous with respect to robustness and reproducibility. Consequently, [^{3}H]**2.5** represents a useful radioligand for Y_4R binding studies in buffers containing sodium at physiological concentrations that have been neglected in the past. Moreover, as [^{3}H]**2.5** also shows superb Y_4R selectivity, this radioligand is considered an excellent tool for the investigation of Y_4R protein expression in tissues, for example, by autoradiography.

2.5 References

(1) Michel, M. C.; Beck-Sickinger, A.; Cox, H.; Doods, H. N.; Herzog, H.; Larhammar, D.; Quirion, R.; Schwartz, T.; Westfall, T. XVI. International Union of Pharmacology recommendations for the nomenclature of neuropeptide Y, peptide YY, and pancreatic polypeptide receptors. *Pharmacol. Rev.* 1998, *50* (1), 143-150.

(2) Sainsbury, A.; Shi, Y.-C.; Zhang, L.; Aljanova, A.; Lin, Z.; Nguyen, A. D.; Herzog, H.; Lin, S. Y_4 receptors and pancreatic polypeptide regulate food intake via hypothalamic orexin and brain-derived neurotropic factor dependent pathways. *Neuropeptides* 2010, *44*, 261-268. DOI: 10.1016/j.npep.2010.01.001.

(3) Whitcomb, D. C.; Taylor, I. L.; Vigna, S. R. Characterization of saturable binding sites for circulating pancreatic polypeptide in rat brain. *Am. J. Physiol.* 1990, *259* (4 Pt 1), G687-691. DOI: 10.1152/ajpgi.1990.259.4.G687.

(4) Fagerberg, L.; Hallstrom, B. M.; Oksvold, P.; Kampf, C.; Djureinovic, D.; Odeberg, J.; Habuka, M.; Tahmasebpoor, S.; Danielsson, A.; Edlund, K.*; et al.* Analysis of the human tissue-specific expression by genome-wide integration of transcriptomics and antibody-based proteomics. *Mol. Cell. Proteomics* 2014, *13* (2), 397-406. DOI: 10.1074/mcp.M113.035600.

(5) Pedragosa-Badia, X.; Stichel, J.; Beck-Sickinger, A. G. Neuropeptide Y receptors: how to get subtype selectivity. *Front. Endocrinol. (Lausanne)* 2013, *4*, article 5. DOI: 10.3389/fendo.2013.00005.

(6) Tang, T.; Tan, Q.; Han, S.; Diemar, A.; Lobner, K.; Wang, H.; Schuss, C.; Behr, V.; Morl, K.; Wang, M.*; et al.* Receptor-specific recognition of NPY peptides revealed by structures of NPY receptors. *Sci. Adv.* 2022, *8* (18), eabm1232. DOI: 10.1126/sciadv.abm1232.

(7) Misra, S.; Murthy, K. S.; Zhou, H.; Grider, J. R. Coexpression of Y1, Y2, and Y4 receptors in smooth muscle coupled to distinct signaling pathways. *J. Pharmacol. Exp. Ther.* 2004, *311* (3), 1154-1162. DOI: 10.1124/jpet.104.071415.

(8) Ueno, N.; Inui, A.; Iwamoto, M.; Kaga, T.; Asakawa, A.; Okita, M.; Fujimiya, M.; Nakajima, Y.; Ohmoto, Y.; Ohnaka, M.*; et al.* Decreased food intake and body weight in pancreatic polypeptide-overexpressing mice. *Gastroenterology* 1999, *117* (6), 1427-1432. DOI: 10.1016/s0016-5085(99)70293-3.

(9) Schmidt, P. T.; Naslund, E.; Gryback, P.; Jacobsson, H.; Holst, J. J.; Hilsted, L.; Hellstrom, P. M. A role for pancreatic polypeptide in the regulation of gastric emptying and short-term metabolic control. *J. Clin. Endocrinol. Metab.* 2005, *90* (9), 5241-5246. DOI: 10.1210/jc.2004-2089.

(10) Batterham, R. L.; Le Roux, C. W.; Cohen, M. A.; Park, A. J.; Ellis, S. M.; Patterson, M.; Frost, G. S.; Ghatei, M. A.; Bloom, S. R. Pancreatic polypeptide reduces appetite and food intake in humans. *J. Clin. Endocrinol. Metab.* 2003, *88* (8), 3989-3992. DOI: 10.1210/jc.2003-030630.

(11) Balasubramaniam, A.; Mullins, D. E.; Lin, S.; Zhai, W.; Tao, Z.; Dhawan, V. C.; Guzzi, M.; Knittel, J. J.; Slack, K.; Herzog, H.*; et al.* Neuropeptide Y (NPY) Y_4 receptor selective agonists based on NPY_{32-36}: development of an anorectic

Y_4 receptor selective agonist with picomolar affinity. *J. Med. Chem.* 2006, *49* (8), 2661-2665. DOI: 10.1021/jm050907d.

(12) Li, J. B.; Asakawa, A.; Terashi, M.; Cheng, K.; Chaolu, H.; Zoshiki, T.; Ushikai, M.; Sheriff, S.; Balasubramaniam, A.; Inui, A. Regulatory effects of Y_4 receptor agonist (BVD-74D) on food intake. *Peptides* 2010, *31*, 1706-1710. DOI: 10.1016/j.peptides.2010.06.011.

(13) Yan, H.; Yang, J.; Marasco, J.; Yamaguchi, K.; Brenner, S.; Collins, F.; Karbon, W. Cloning and functional expression of cDNAs encoding human and rat pancreatic polypeptide receptors. *PNAS USA* 1996, *93* (10), 4661-4665. DOI: 10.1073/pnas.93.10.4661.

(14) Eriksson, H.; Berglund, M. M.; Holmberg, S. K.; Kahl, U.; Gehlert, D. R.; Larhammar, D. The cloned guinea pig pancreatic polypeptide receptor Y_4 resembles more the human Y_4 than does the rat Y_4. *Regul. Pept.* 1998, *75-76*, 29-37. DOI: 10.1016/s0167-0115(98)00050-0.

(15) Berglund, M. M.; Lundell, I.; Eriksson, H.; Soll, R.; Beck-Sickinger, A. G.; Larhammar, D. Studies of the human, rat, and guinea pig Y_4 receptors using neuropeptide Y analogues and two distinct radioligands. *Peptides* 2001, *22* (3), 351-356. DOI: 10.1016/s0196-9781(01)00337-0.

(16) Parker, M. S.; Sah, R.; Sheriff, S.; Balasubramaniam, A.; Parker, S. L. Internalization of cloned pancreatic polypeptide receptors is accelerated by all types of Y_4 agonists. *Regul. Pept.* 2005, *132* (1-3), 91-101. DOI: 10.1016/j.regpep.2005.09.008.

(17) Walker, M. W.; Smith, K. E.; Bard, J.; Vaysse, P. J.; Gerald, C.; Daouti, S.; Weinshank, R. L.; Branchek, T. A. A structure-activity analysis of the cloned rat and human Y_4 receptors for pancreatic polypeptide. *Peptides* 1997, *18* (4), 609-612. DOI: 10.1016/s0196-9781(97)00070-3.

(18) Dautzenberg, F. M.; Higelin, J.; Pflieger, P.; Neidhart, W.; Guba, W. Establishment of robust functional assays for the characterization of neuropeptide Y (NPY) receptors: identification of 3-(5-benzoyl-thiazol-2-ylamino)-benzonitrile as selective NPY type 5 receptor antagonist. *Neuropharmacol.* 2005, *48* (7), 1043-1055. DOI: 10.1016/j.neuropharm.2005.01.020.

(19) Gehlert, D. R.; Schober, D. A.; Gackenheimer, S. L.; Beavers, L.; Gadski, R.; Lundell, I.; Larhammar, D. [^{125}I]Leu^{31}, Pro^{34}-PYY is a high affinity radioligand for rat PP1/Y_4 and Y_1 receptors: evidence for heterogeneity in pancreatic polypeptide receptors. *Peptides* 1997, *18* (3), 397-401. DOI: 10.1016/s0196-9781(96)00346-4.

(20) Dumont, Y.; Quirion, R. [^{125}I]-GR231118: a high affinity radioligand to investigate neuropeptide Y Y_1 and Y_4 receptors. *Br. J. Pharmacol.* 2000, *129* (1), 37-46. DOI: 10.1038/sj.bjp.0702983.

(21) Mantyh, P. W. Autoradiographic localization and characterization of receptor binding sites in the brain and peripheral tissues. In *Receptor Localization: Ligand Autoradiography*, Leslie, F. M., Altar, C. A. Eds.; Vol. 13; Alan R. Liss Inc., 1988; pp 9-36.

(22) de Blois, E.; Chan, H. S.; Breeman, W. A. Iodination and stability of somatostatin analogs: comparison of iodination techniques. a practical overview. *Curr. Top. Med. Chem.* 2012, *12* (23), 2668-2676. DOI: 10.2174/1568026611212230004.

(23) Dukorn, S.; Littmann, T.; Keller, M.; Kuhn, K.; Cabrele, C.; Baumeister, P.; Bernhardt, G.; Buschauer, A. Fluorescence- and radiolabeling of [Lys^{4},Nle^{17},^{30}]hPP yields molecular tools for the NPY Y_4 receptor. *Bioconjug. Chem.* 2017, *28*, 1291-1304. DOI: 10.1021/acs.bioconjchem.7b00103.

(24) Kuhn, K. K.; Ertl, T.; Dukorn, S.; Keller, M.; Bernhardt, G.; Reiser, O.; Buschauer, A. High affinity agonists of the neuropeptide Y (NPY) Y_4 receptor derived from the C-terminal pentapeptide of human pancreatic polypeptide (hPP): synthesis, stereochemical discrimination, and radiolabeling. *J. Med. Chem.* 2016, *59*, 6045-6058. DOI: 10.1021/acs.jmedchem.6b00309.

(25) Lundell, I.; Statnick, M. A.; Johnson, D.; Schober, D. A.; Starback, P.; Gehlert, D. R.; Larhammar, D. The cloned rat pancreatic polypeptide receptor exhibits profound differences to the orthologous receptor. *PNAS USA* 1996, *93* (10), 5111-5115. DOI: 10.1073/pnas.93.10.5111.

(26) Ziemek, R.; Schneider, E.; Kraus, A.; Cabrele, C.; Beck-Sickinger, A. G.; Bernhardt, G.; Buschauer, A. Determination of affinity and activity of ligands at the human neuropeptide Y Y_4 receptor by flow cytometry and aequorin luminescence. *J. Recept. Signal Transduct.* 2007, *27*, 217-233. DOI: 10.1080/10799890701505206.

(27) Berlicki, Ł.; Kaske, M.; Gutiérrez-Abad, R.; Bernhardt, G.; Illa, O.; Ortuño, R. M.; Cabrele, C.; Buschauer, A.; Reiser, O. Replacement of Thr^{32} and Gln^{34} in the C-terminal neuropeptide Y fragment 25–36 by cis-cyclobutane and cis-cyclopentane β-amino acids shifts selectivity toward the Y_4 receptor. *J. Med. Chem.* 2013, *56*, 8422-8431. DOI: 10.1021/jm4008505.

(28) Kuhn, K. K.; Littmann, T.; Dukorn, S.; Tanaka, M.; Keller, M.; Ozawa, T.; Bernhardt, G.; Buschauer, A. In search of NPY Y_4R antagonists: incorporation of carbamoylated arginine, aza-amino acids, or d-amino acids into oligopeptides derived from the C-termini of the endogenous agonists. *ACS Omega* 2017, *2*, 3616-3631. DOI: 10.1021/acsomega.7b00451.

(29) Konieczny, A.; Braun, D.; Wifling, D.; Bernhardt, G.; Keller, M. Oligopeptides as neuropeptide Y Y_4 receptor ligands: identification of a high-affinity tetrapeptide agonist and a hexapeptide antagonist. *J. Med. Chem.* 2020, *63*, 8198-8215. DOI: 10.1021/acs.jmedchem.0c00426.

(30) Konieczny, A.; Conrad, M.; Ertl, F. J.; Gleixner, J.; Gattor, A. O.; Grätz, L.; Schmidt, M. F.; Neu, E.; Horn, A. H. C.; Wifling, D.*; et al.* N-Terminus to arginine side-chain cyclization of linear peptidic neuropeptide Y Y_4 receptor ligands results in picomolar binding constants. *J. Med. Chem.* 2021, *64* (22), 16746-16769. DOI: 10.1021/acs.jmedchem.1c01574.

(31) Katritch, V.; Fenalti, G.; Abola, E. E.; Roth, B. L.; Cherezov, V.; Stevens, R. C. Allosteric sodium in class A GPCR signaling. *Trends Biochem. Sci.* 2014, *39*, 233-244. DOI: 10.1016/j.tibs.2014.03.002.

(32) White, K. L.; Eddy, M. T.; Gao, Z.-G.; Han, G. W.; Lian, T.; Deary, A.; Patel, N.; Jacobson, K. A.; Katritch, V.; Stevens, R. C. Structural connection between

activation microswitch and allosteric sodium site in GPCR signaling. *Structure* 2018, *26*, 259-269. DOI: 10.1016/j.str.2017.12.013.

(33) Keller, M.; Erdmann, D.; Pop, N.; Pluym, N.; Teng, S.; Bernhardt, G.; Buschauer, A. Red-fluorescent argininamide-type NPY Y_1 receptor antagonists as pharmacological tools. *Biorg. Med. Chem.* 2011, *19* (9), 2859-2878. DOI: 10.1016/j.bmc.2011.03.045.

(34) Keller, M.; Weiss, S.; Hutzler, C.; Kuhn, K. K.; Mollereau, C.; Dukorn, S.; Schindler, L.; Bernhardt, G.; König, B.; Buschauer, A. N^{ω}-Carbamoylation of the argininamide moiety: an avenue to insurmountable NPY Y_1 receptor antagonists and a radiolabeled selective high-affinity molecular tool ([^{3}H]UR-MK299) with extended residence time. *J. Med. Chem.* 2015, *58*, 8834-8849. DOI: 10.1021/acs.jmedchem.5b00925.

(35) Müller, C.; Gleixner, J.; Tahk, M.-J.; Kopanchuk, S.; Laasfeld, T.; Weinhart, M.; Schollmeyer, D.; Betschart, M. U.; Lüdeke, S.; Koch, P.*; et al.* Structure-based design of high-affinity fluorescent probes for the neuropeptide Y Y_1 receptor. *J. Med. Chem.* 2022, *65* (6), 4832-4853. DOI: 10.1021/acs.jmedchem.1c02033.

(36) Wirth, U.; Erl, J.; Azzam, S.; Höring, C.; Skiba, M.; Singh, R.; Hochmuth, K.; Keller, M.; Wegener, J.; König, B. Monitoring the reversibility of GPCR signaling by combining photochromic ligands with label-free impedance analysis. *Angew. Chem. Int. Ed.* 2023, *62* (21), e202215547. DOI: 10.1002/anie.202215547.

(37) Moser, C.; Bernhardt, G.; Michel, J.; Schwarz, H.; Buschauer, A. Cloning and functional expression of the hNPY Y_5 receptor in human endometrial cancer (HEC-1B) cells. *Can. J. Physiol. Pharmacol.* 2000, *78* (2), 134-142. DOI: 10.1139/y99-125 %M 10737676.

(38) Gehlert, D. R.; Schober, D. A.; Beavers, L.; Gadski, R.; Hoffman, J. A.; Smiley, D. L.; Chance, R. E.; Lundell, I.; Larhammar, D. Characterization of the peptide binding requirements for the cloned human pancreatic polypeptide-preferring receptor. *Mol. Pharmacol.* 1996, *50* (1), 112-118.

(39) Cheng, Y.; Prusoff, W. H. Relationship between the inhibition constant (K_I) and the concentration of inhibitor which causes 50 per cent inhibition (I_{50}) of an enzymatic reaction. *Biochem. Pharmacol.* 1973, *22*, 3099-3108. DOI: 10.1016/0006-2952(73)90196-2.

(40) Gleixner, J.; Gattor, A. O.; Humphrys, L. J.; Brunner, T.; Keller, M. [^{3}H]UR-JG102-A Radiolabeled Cyclic Peptide with High Affinity and Excellent Selectivity for the Neuropeptide Y Y_4 Receptor. *J. Med. Chem.* 2023, *66* (19), 13788-13808. DOI: 10.1021/acs.jmedchem.3c01224.

(41) Sun, A. R.; Hengst, R. M.; Young, J. L. All the small things: nanoscale matrix alterations in aging tissues. *Curr. Opin. Cell Biol.* 2024, *87*, 102322. DOI: 10.1016/j.ceb.2024.102322.

(42) Huang, C. J.; Tseng, P. Y.; Chang, Y. C. Effects of extracellular matrix protein functionalized fluid membrane on cell adhesion and matrix remodeling. *Biomaterials* 2010, *31* (27), 7183-7195. DOI: 10.1016/j.biomaterials.2010.05.076.

(43) Hu, X.; Smith, M. D.; Humphreys, B. M.; Green, A. T.; Parks, J. M.; Baudry, J. Y.; Smith, J. C. Ligand-dependent sodium ion dynamics within the A_{2A} adenosine receptor: a molecular dynamics study. *J. Phys. Chem. B* 2019, *123* (38), 7947-7954. DOI: 10.1021/acs.jpcb.9b04474.

(44) Copeland, R. A. Conformational adaptation in drug-target interactions and residence time. *Future Med. Chem.* 2011, *3* (12), 1491-1501. DOI: 10.4155/fmc.11.112.

(45) Saleh, N.; Saladino, G.; Gervasio, F. L.; Haensele, E.; Banting, L.; Whitley, D. C.; Sopkova-de Oliveira Santos, J.; Bureau, R.; Clark, T. A three-site mechanism for agonist/antagonist selective binding to vasopressin receptors. *Angew. Chem. Int. Ed. Engl.* 2016, *55* (28), 8008-8012. DOI: 10.1002/anie.201602729.

(46) Kenakin, T. Differences between natural and recombinant G protein-coupled receptor systems with varying receptor/G protein stoichiometry. *Trends Pharmacol. Sci.* 1997, *18* (12), 456-464. DOI: 10.1016/s0165-6147(97)01136-x.

(47) Cescato, R.; Schulz, S.; Waser, B.; Eltschinger, V.; Rivier, J. E.; Wester, H. J.; Culler, M.; Ginj, M.; Liu, Q.; Schonbrunn, A.*; et al.* Internalization of sst_2, sst_3, and sst_5 receptors: effects of somatostatin agonists and antagonists. *J. Nucl. Med.* 2006, *47* (3), 502-511.

(48) Sander, C. Y.; Hooker, J. M.; Catana, C.; Rosen, B. R.; Mandeville, J. B. Imaging agonist-induced D2/D3 receptor desensitization and internalization *in vivo* with PET/fMRI. *Neuropsychopharmacol.* 2016, *41* (5), 1427-1436. DOI: 10.1038/npp.2015.296.

(49) Gurevich, V. V.; Pals-Rylaarsdam, R.; Benovic, J. L.; Hosey, M. M.; Onorato, J. J. Agonist-receptor-arrestin, an alternative ternary complex with high agonist affinity. *J. Biol. Chem.* 1997, *272* (46), 28849-28852. DOI: 10.1074/jbc.272.46.28849.

(50) Weigel, P. H.; Oka, J. A. Temperature dependence of endocytosis mediated by the asialoglycoprotein receptor in isolated rat hepatocytes. Evidence for two potentially rate-limiting steps. *J. Biol. Chem.* 1981, *256* (6), 2615-2617. DOI: 10.1016/s0021-9258(19)69656-0.

(51) Zhang, A.; Guan, Y.; Xu, L. X. Theoretical study on temperature dependence of cellular uptake of QDs nanoparticles. *J. Biomech. Eng.* 2011, *133* (12), 124502. DOI: 10.1115/1.4005481.

(52) Parker, E. M.; Babij, C. K.; Balasubramaniam, A.; Burrier, R. E.; Guzzi, M.; Hamud, F.; Gitali, M.; Rudinski, M. S.; Tao, Z.; Tice, M.*; et al.* GR231118 (1229U91) and other analogues of the C-terminus of neuropeptide Y are potent neuropeptide Y Y_1 receptor antagonists and neuropeptide Y Y_4 receptor agonists. *Eur. J. Pharmacol.* 1998, *349* (1), 97-105. DOI: 10.1016/s0014-2999(98)00171-x.

2.6 Appendix

2.6.1 Figure A2.1–A2.2

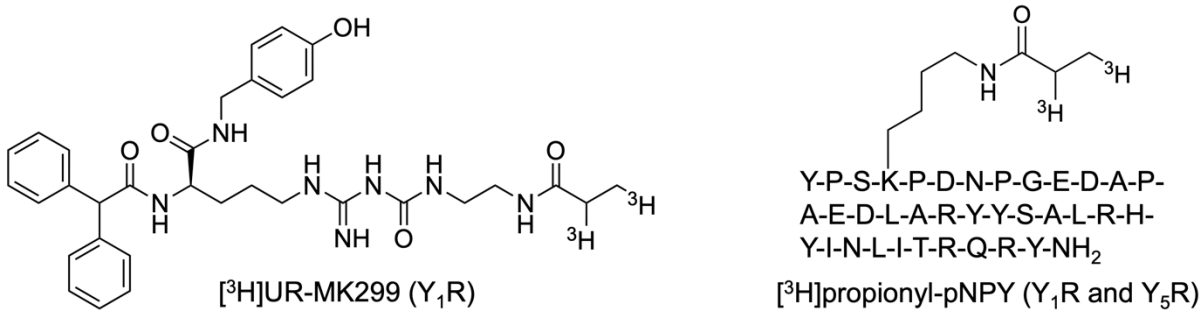

Figure A2.1. Structures of the tritiated Y_1R, Y_2R, and Y_5R radioligands used in this study.

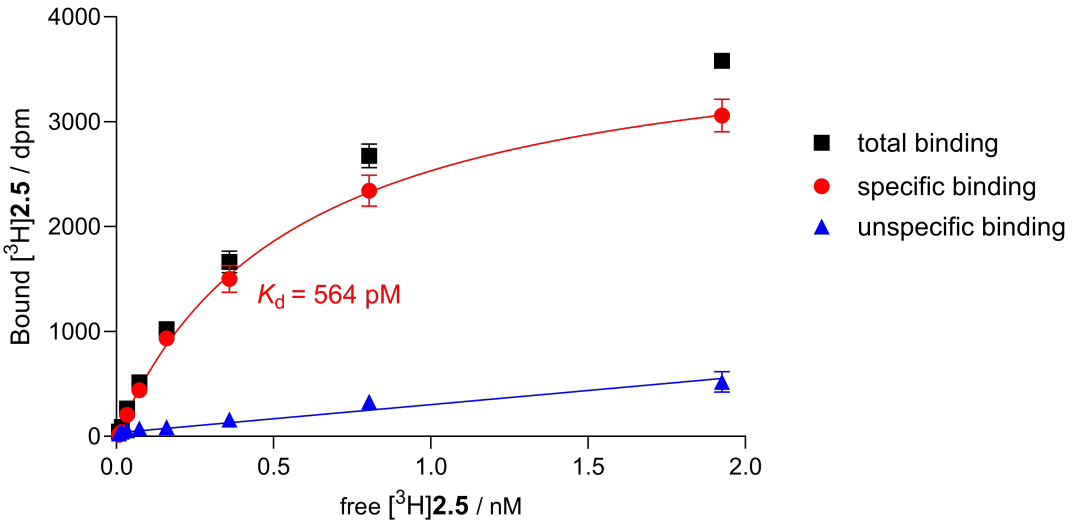

Figure A2.2. A representative Y_4R binding isotherm (specific binding) of [^{3}H]**2.5** obtained from saturation binding experiments performed with adherent CHO-hY_4-G_{qi5}-mtAEQ cells in sodium-containing buffer (DPBS) at 24 ± 2 °C. Unspecific binding was determined in the presence of 1 µM hPP. Experiments were performed in triplicate. Total and unspecific binding data represent mean values ± SEM. Specific binding data represent calculated values ± propagated error.

Chapter 3

Autoradiographic Investigation of Y_4R Expression in Rat Brains and Gastrointestinal Tract Tissues Using [^{3}H]UR-JG102

3.1 Introduction

The neuropeptide Y family of receptors to which the Y_4 receptor (Y_4R) belongs is generally distributed throughout the central nervous system (CNS) and peripheral tissues. This family of receptors plays a critical role in several essential physiological functions, including regulating pain, appetite, emotion, memory, anxiety, and energy balance.[1-5] The Y_4R, in particular, has been shown to play a significant role in regulating feeding, gastrointestinal motility, and energy homeostasis through its activation in the CNS and peripheral tissues.[3, 6-8] Nevertheless, it is still one of the least comprehensively studied of the NPY family of receptors, with limited information about its exact expression and distribution, especially in the CNS.

Several studies aimed at determining Y_4R protein expression and localization in mammals indicate that it is predominantly found in the gastrointestinal tract (GIT), notably the small intestine and colon, as well as on the skin, muscles, and specific brain regions, which include the hippocampus, basal ganglia, hypothalamus, and brain stem.[3, 9-11] Most of these studies utilized immunoassays, employing polyclonal antibodies against Y_4R due to their specificity and sensitivity.[12] Although immunoassays offer advantages for the precise estimation and detection of the target proteins, they also have limitations. These limitations include the high background and unspecific staining from the use of polyclonal antibodies, their unsuitability for receptors in low concentration, the intra- and interobserver variability due to the subjective nature of visual assessments, potential false-negatives, cross-reactivity issues, and poor reproducibility.[12, 13] These factors can affect the accuracy and interpretation of the obtained results. With respect to Y_4R expression in the brain, a few of the studies utilized the more precise and sensitive method of autoradiography, in which iodinated radioligands such as ^{125}I-PP and ^{125}I-PYY_{3-36} were used to investigate Y_4R expression.[10, 14-16] Some of these studies revealed defined expression of Y_4R within the interpeduncular nucleus (IPN) structure of the midbrain and areas of the brain stem, particularly in structures of the dorsal vagal complex (DVC).[10, 14, 15] Although autoradiography is suited for qualitatively and quantitatively detecting receptors of low concentration, the use of iodinated radioligands usually presents a challenge due to possible contamination by free iodine or iodine isotopes. This generally leads to self-absorption, a phenomenon where emitted radiation from a radioactive source is partially absorbed by the tissue before its detection, and in turn,

reduces the image resolutions needed for accurate interpretations.[17-19] To mitigate these drawbacks, tritiated radioligands, which have high molar activity and emit short-length β^- particles, are usually used to enhance the image resolution.[18, 20-22]

Therefore, to help contribute to addressing the current research gap on the expression of Y_4R in the brain, this study was designed to preliminarily investigate the expression of Y_4R in the brains of Wistar rats using the recently reported tritiated radioligand, [^{3}H]UR-JG102 ([^{3}H]**2.5**), known for its high binding affinity and selectivity for human Y_4R.[23] This study is the first to investigate Y_4R expression in rat tissues using a tritiated radioligand. To detect Y_4Rs in the brain, autoradiographic binding studies using [^{3}H]**2.5** (see structure in Figure 2.2; *Chapter 2*) were performed on adult male and female rat brain sections representative of the various brain regions. Additionally, the suitability of [^{3}H]**2.5** to be used in this autoradiographic study to explore Y_4R expression was investigated in intestinal tissues from the rats, known to express the receptor in high amounts.

3.2 Materials and Methods

3.2.1 Materials

A complementary DNA (cDNA) of a rat (*Rattus norvegicus*) untagged clone of neuropeptide Y Y_4 receptor was purchased from OriGene Technologies GmbH (Herford, Germany). Human pancreatic polypeptide (hPP) was from SynPeptide (Shanghai, China). The syntheses of UR-AK86C[24] and [^{3}H]UR-JG102 ([^{3}H]**2.5**) (molar activity: 3.44 TBq/mmol)[23] were reported elsewhere. Bacitracin and bovine serum albumin (BSA) were from Serva (Heidelberg, Germany). Fetal bovine serum (FBS) was purchased from Pan-Biotech (Aidenbach, Germany). 1.5 and 2 mL polypropylene reaction vessels with screw caps from Süd-Laborbedarf (Gauting, Germany) were used for the preparation and storage of stock solutions. 1.5 or 2 mL polypropylene reaction vessels from Sarstedt (Nümbrecht, Germany) were used for the preparation of diluted solutions. Ultrapure water was used to prepare stock solutions and buffers.

3.2.2 Methods

3.2.2.1 Cell culture

Cells were cultured in T75 or T175 flasks (Sarstedt, Nümbrecht, Germany) in a humidified atmosphere (95% air, 5% CO_2) at 37 °C. CHO cells (obtained from PerkinElmer, Rodgau, Germany) were maintained in Ham's F-12 supplemented with 10% FBS. CHO-rY_4 cells were cultured in HAM's F-12 supplemented with 10% FBS and G418 (600 µg/mL).

3.2.2.2 Molecular cloning

All enzymes and molecular biology reagents were from New England Biolabs (Frankfurt am Main, Germany). The pcDNA3.1$_{neo}$-rY_4R plasmid was generated using standard restriction cloning techniques with pcDNA3.1$_{neo}$ as the vector and complementary DNA of rat untagged clone of neuropeptide Y Y_4 receptor (rY_4R-cDNA) as insert. The pcDNA3.1$_{neo}$ vector contains the selectable markers ampicillin resistance genes and neomycin resistance genes for the selection and maintenance of the transformed *E. coli* cells and transfected mammalian cells, respectively.

To insert the rY_4R-cDNA into the vector, flanking *HindIII* and *ApaI* restriction enzyme sites were added to it via polymerase chain reaction (PCR) with Phusion polymerase using the complementary forward (*gatcaagcttccaccATGAATACCTCTCATTTCTTGG*)

and reverse (*gatcgggccctcTATGAAGTTAGACTTGCTACC*) primers. A Kozak sequence was included in the forward primer to improve the translation of the rY_4R protein in mammalian cells. The PCR product was purified by gel electrophoresis to obtain inserts flanked with *HindIII* and *ApaI* sites. This insert and vector were then digested with *HindIII* and *ApaI* restriction enzymes and repurified by gel electrophoresis before their ligation with T4 DNA ligase overnight at 16 °C. The ligated cDNA was transformed into Top10F' *E. coli* cells (made competent in-house). Positive bacterial colonies were first extracted in a mini-prep from overnight cultures (Miniprep Kit, Nippon Genetics, Düren, Germany) and then maxi-prepped for use in mammalian cells (Maxiprep Kit, Qiagen, Hilden, Germany).

DNA concentration was quantified by UV-Vis absorbance using a NanoDrop spectrophotometer (Fisher Scientific, Schwerte, Germany), and the pcDNA3.1_{neo}-rY_4R sequence was confirmed by DNA sequencing (Eurofins Genomics, Ebersberg, Germany).

3.2.2.3 Generation of the stable CHO-rY_4R cell line

CHO-rY_4R stable cells were generated as a pooled population. 1 mL of CHO wild-type cells in suspension (200,000 cells/mL) was seeded into a T25 flask in HAM-F12 supplemented with 10% FBS. The following day, cells were transfected with 4 µg of pcDNA3.1_{neo}-rY_4R using the XtremeGene HP transfection reagent (Merck, Darmstadt, Germany) according to the manufacturer's protocol. Cells were passaged after 48 h and grown under selective pressure for a week at a high G418 concentration (1,000 µg/mL). Thereafter, cells were cultured at 600 µg/mL G418 for maintained selection pressure.

3.2.2.4 Radioligand saturation binding experiments

Y_4R saturation binding studies were performed in triplicate at 24 ± 2 °C as previously reported by Gleixner *et al*.[23], with a minor modification: which is using stably transfected intact CHO-rY_4R cells instead of CHO-hY_4-G_{qi5}-mtAEQ cells. Cell suspensions (50,000–100,000 cells/mL) for the binding experiments were prepared in Dulbecco's phosphate-buffered saline (*DPBS*) (1.8 mM $CaCl_2$, 2.68 mM KCl, 1.47 mM KH_2PO_4, 3.98 mM $MgSO_4$, 137 mM NaCl, 8.06 mM Na_2HPO_4, pH 7.4) supplemented with 1% BSA and 0.1 mg/mL bacitracin. Specific binding data, obtained by subtracting triplicate radioactivity (dpm) mean values of unspecific binding from triplicate

radioactivity (dpm) mean values of total binding, were plotted against the free radioligand concentration. The plots were analyzed using a two-parameter equation describing hyperbolic single-site binding (one-site, specific binding, GraphPad Prism 10) to obtain K_d values. The free concentration of [^{3}H]**2.5** (nM) was calculated by subtracting the amount of specifically bound [^{3}H]**2.5** (nM) (calculated from specifically bound [^{3}H]**2.5** in dpm, the molar activity, and the volume per well) from the total concentration of [^{3}H]**2.5**. Propagated errors were calculated as described by Gleixner *et al*.[23]

3.2.2.5 *In-vitro* autoradiography

Adult male and female Wistar rats (4–5 months; 215–390 g) were from the Central Animal Facility of the University of Regensburg. Animals were kept under specified pathogen-free (SPF) conditions at 23 °C, 55% relative humidity in stainless steel cages with sawdust bedding, fed with standard laboratory chow, and had access to tap water ad libitum. The rats were sacrificed by cervical dislocation under CO_2, after which the whole brains, sections of the small intestines (duodenum, jejunum, and ileum), and mid-section of the colon were carefully cut out, rinsed with PBS, and immediately frozen in Tissue-Tek with the help of dry ice, and stored at –80 °C. On the day of the experiment, cryosections (12 µm) of these organs were obtained at –16 °C using a 2800 Frigocut E freezing microtome (Leica Biosystems, Nussloch, Germany). Two, three, or four adjacent sections were mounted on a microscopic slide (75 × 25 × 1 mm, Superfrost Plus, Breda, The Netherlands), and the slides were kept for 1–2 min in a chamber of 100% humidity (quadriPERM culture dishes; Sarstedt, Nümbrecht, Germany). This step and the following steps were carried out at room temperature. After the short incubation period, the tissue sections were carefully covered with 800 µL of binding buffer (the same buffer used for saturation binding studies) and kept in the chamber for 5–10 min. The binding buffer was carefully removed (slides were put uprightly lengthwise on a paper towel for ca. 1 min), and the slides were placed back in a chamber of 100% humidity. The sections were then carefully covered with binding buffer (800 µL) containing 0.3 nM of radioligand [^{3}H]**2.5** to determine total binding or with binding buffer (800 µL) containing 0.3 nM [^{3}H]**2.5**, 0.3 µM hPP, and 0.03 µM UR-AK86C to determine unspecific binding. The sections were incubated in a humidity chamber for 60 min (during incubation, the chamber was slightly tilted every 5 min to carefully move the binding buffer on the sections). After

incubation, a large part of the binding buffer was drained, and the slides were immersed three times into ice-cold PBS (three separate vessels, each for 10 s), followed by immersion in ice-cold distilled water for 10 s. The slides were put uprightly lengthwise on a paper towel for 10 min, the remaining liquid at the edge of the slides was removed, and the slides were kept in a desiccator over P_4O_{10} for at least 24 h. The slides were set in close contact with a TR 2025 E Cytiva BAS storage phosphor screen (20 × 25 cm, Fisher Scientific, Schwerte, Germany) using an X-ray film cassette and stored in the dark for 21–28 days. Autoradiographic images were generated from the screen using a Typhoon FLA 9500 or 3000 biomolecular imager (GE Healthcare Life Sciences) at a resolution of 25 µm and a photomultiplier voltage of 1000 V.

3.3 Results and Discussions

3.3.1 [^{3}H]2.5 exhibits a very high binding affinity to rat Y_4R (rY_4R)

A prerequisite for a radioligand to be used in exploring the expression of a target receptor in tissues or organs in autoradiographic binding studies is its binding affinity to the receptor. This affects the choice of radioligand concentration, which determines the occupancy of receptor binding sites as well as the extent of unspecific binding and, in turn, the accuracy and reliability of the results.[25] Although [^{3}H]**2.5** binds to the human Y_4R with high affinity (K_d = 110 pM), its binding affinity to Y_4R of other species' origin may differ.[26] Thus, saturation binding experiments were conducted using Chinese hamster ovary (CHO) cells stably transfected with rat Y_4R (CHO-rY_4R) to determine the binding affinity (K_d) of [^{3}H]**2.5** to rY_4R.

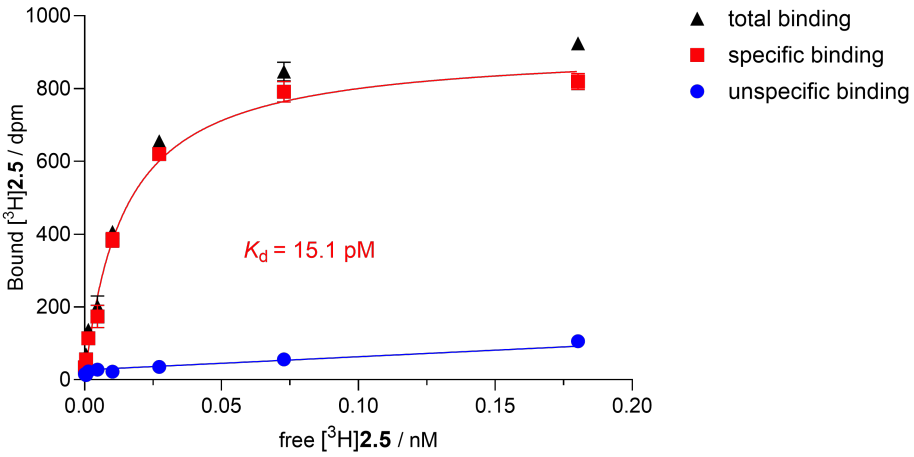

Figure 3.1. Representative Y_4R binding isotherm (specific binding) of [^{3}H]**2.5** obtained from saturation binding experiments at 24 ± 2 °C using intact CHO-rY_4R cells. The average K_d value determined from five independent experiments was 16 ± 0.002 pM. Unspecific binding was determined in the presence of 1 µM hPP. Total and unspecific binding data represent mean values ± SEM. Specific binding data represent calculated values ± propagated error. Propagated error was calculated as described by Gleixner *et al*.[23]

The results from these experiments showed a saturable binding of [^{3}H]**2.5** to rY_4R, yielding an average K_d value of 16 pM (Figure 3.1). Unspecific binding was less than 10% at the radioligand concentration corresponding to the K_d value. This could be a result of the high binding affinity observed. Compared to the hY_4R binding affinity of [^{3}H]**2.5** in sodium-containing buffer reported by Gleixner *et al*.[23], the affinity of [^{3}H]**2.5** to rY_4R was about 7-fold higher (K_d = 110 pM vs 16 pM). This can be explained by the

differences in the protein structure of the receptor between rats and humans due to evolution.[27, 28]

3.3.2 Varying levels of Y_4R expression are seen in the different rat brain regions

In autoradiographic studies, the relative distribution of a target receptor in a tissue usually correlates to the specific binding of the radioligand in this tissue, which cannot be measured directly.[29] Hence, to investigate the expression of Y_4R in rat brains, brain cryosections (12 µm) on glass slides were incubated with [^{3}H]**2.5** in the absence (determination of total binding) and presence of the competitors hPP and UR-AK86C (determination of unspecific binding) and, subsequently incubated in the dark in contact with a tritium-sensitive phosphor screen as described in the *Section 3.2.2.5*. The cryosections used in this study comprised the sagittal and coronal sections of various brain regions, including those already identified to express the Y_4R or suggested to exert effects attributed to Y_4R activation in both *in vitro* and *in vivo* studies.

Autoradiographic images of the sections generated from the screen were further processed to obtain images showing binding in a rainbow color gradient (blue colors in the color spectrum correlate with low radioligand binding, whereas red colors indicate high radioligand binding) to aid in interpreting the varying levels of radioligand binding. To simplify the correlation of the coronal sections to the various rat brain regions, the rat brain was divided into three main segments: the forebrain consisting of the frontal cortex and olfactory nucleus; the interbrain made of the caudal cortex, hippocampus, thalamus, hypothalamus, midbrain and the anterior parts of the pons; and the hindbrain which include the posterior parts of the pons, cerebellum, and medulla oblongata (Figure 3.2).

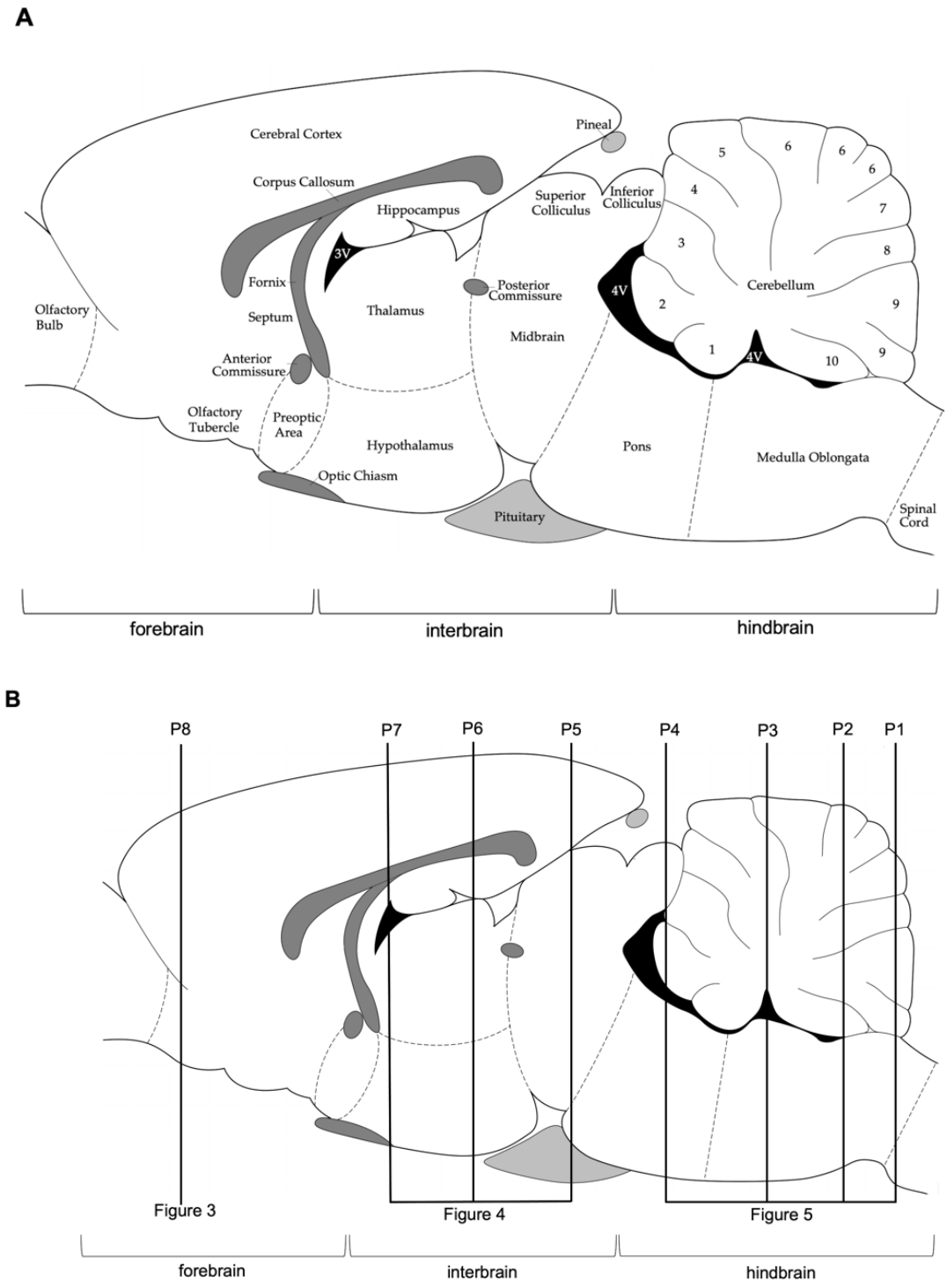

Figure 3.2. Schematic sagittal diagrams of a rat brain divided into three main parts: the forebrain, interbrain, and hindbrain. (A) A labeled diagram of the rat brain. (B) A diagram showing planes of the coronal sections, P, which approximately corresponds to the brain sections shown in Figures 3.3, 3.4, and 3.5). Diagrams are adapted from Paxinos and Watson.[30]

The autoradiographic images obtained from rat brain sections showed varying levels of binding of [^{3}H]**2.5** in several regions of the brain. Sections from the forebrain containing the frontal cortex and olfactory nucleus showed very low to no specific binding of [^{3}H]**2.5** when the total and unspecific binding were compared (Figure 3.3). Sections consisting of the rostral parts of the interbrain showed moderate to low [^{3}H]**2.5** binding in the areas of the parietal-temporal cortex, thalamus, hypothalamus, and hippocampus (Figure 3.4). High specific binding of [^{3}H]**2.5** was observed on sections with the posterior area of the interbrain containing structures from the midbrain (Figure 3.4C). Similarly, a high specific [^{3}H]**2.5** binding was also seen on the sections of the hindbrain containing the cerebellum and brain stem, particularly in the region of the medulla (Figure 3.5). Sagittal sections around the midline of a female Wistar rat brain somewhat confirmed the binding of [^{3}H]**2.5** in the structures mentioned above (Figure 3.6).

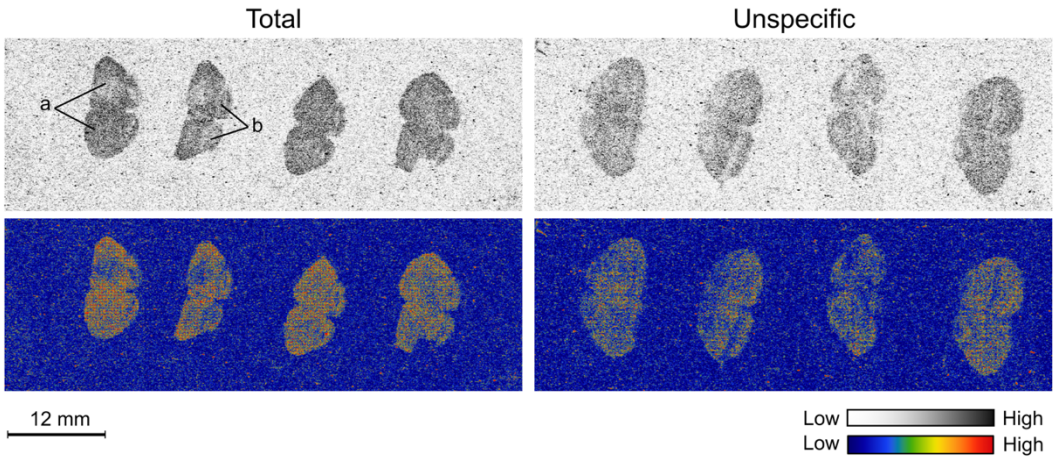

Figure 3.3. Autoradiographic images of coronal sections from the forebrain segment (P8) of a male Wistar rat brain labeled by incubation with 0.3 nM of [^{3}H]**2.5**. Each section is represented by the total and unspecific binding of [^{3}H]**2.5** in greyscale and color images. Images show the [^{3}H]**2.5** binding sites in sections of the forebrain with (a) frontal cortex and (b) olfactory nucleus.

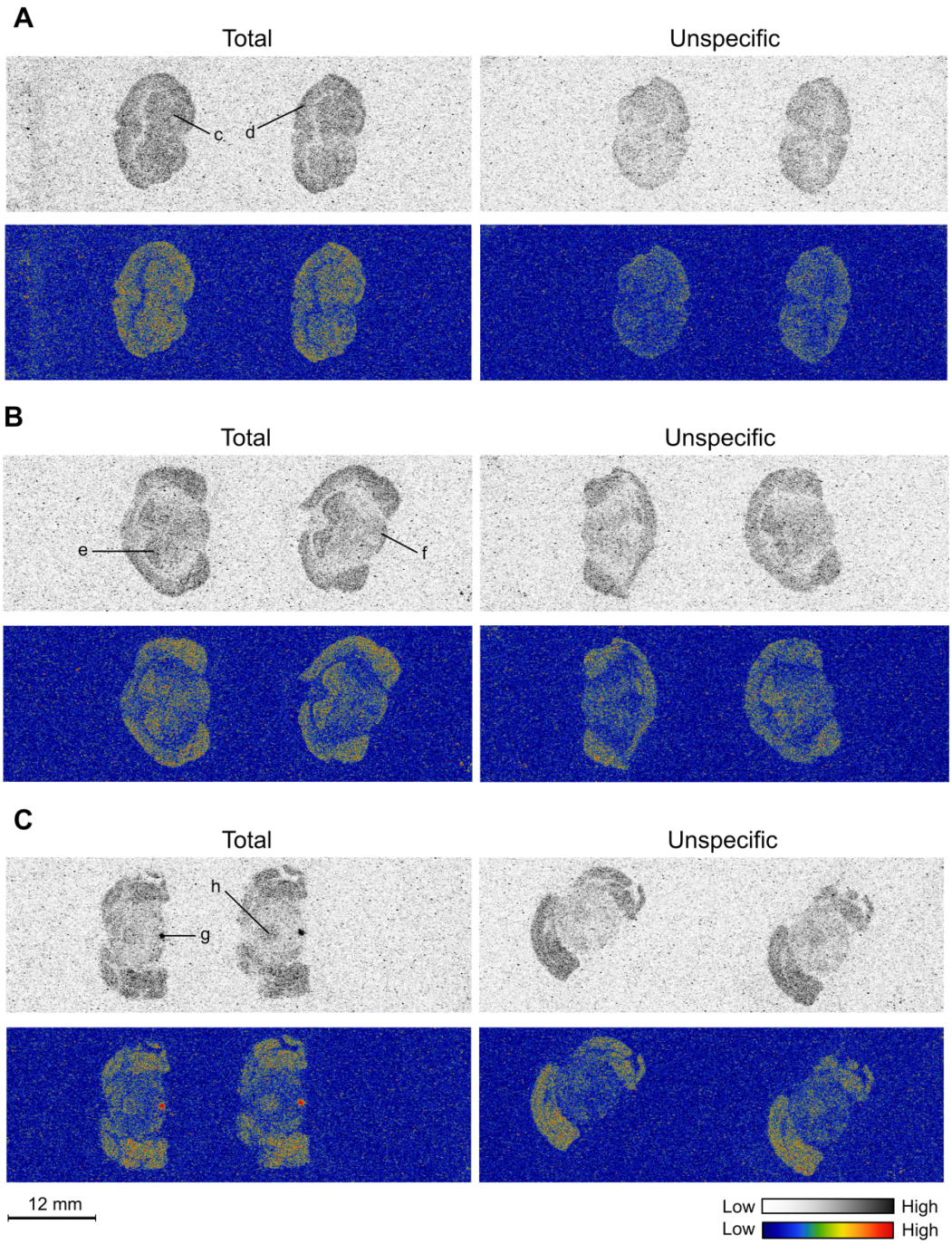

Figure 3.4. Autoradiographic images of coronal sections from the interbrain segment of a male Wistar rat brain labeled by incubation with 0.3 nM of [^{3}H]**2.5**. Each section is represented by the total and unspecific binding of [^{3}H]**2.5** in greyscale and color images. (A) Images represent [^{3}H]**2.5** binding in the rostral parts of the interbrain (P7). The binding of [^{3}H]**2.5** can be seen in the (c) thalamus and (d) parietal-temporal cortex. (B–C) Images represent [^{3}H]**2.5** binding in the posterior area of the interbrain (P5 and P6). The binding of [^{3}H]**2.5** can be seen in the structures of the (e) hippocampus, (f) hypothalamus (arcuate nucleus), (g) interpeduncular nucleus, and (h) periaqueductal gray.

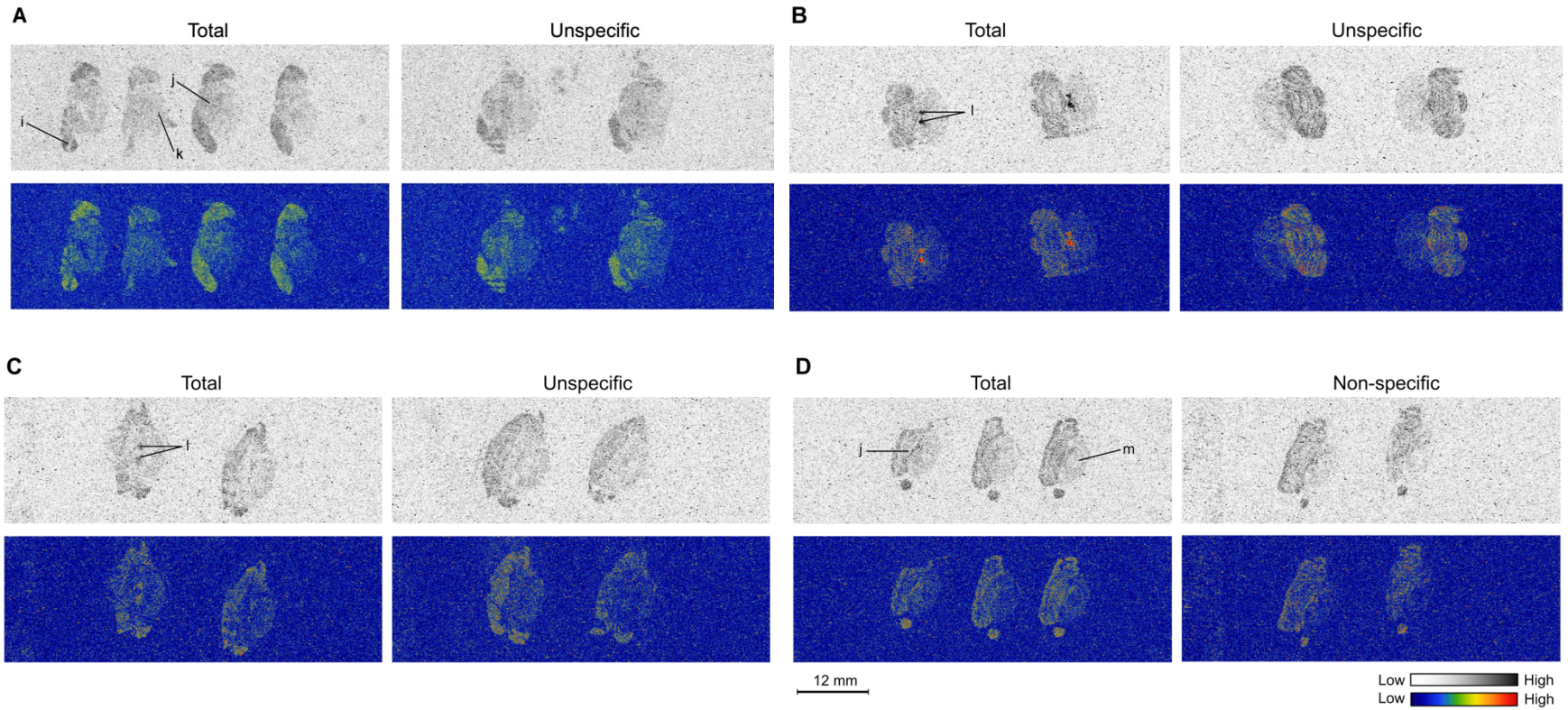

Figure 3.5. Autoradiographic images of coronal sections from the hindbrain segment of both male and female Wistar rat brains labeled by incubation with 0.3 nM of [^{3}H]**2.5**. Each section is represented by the total and unspecific binding of [^{3}H]**2.5** in greyscale and color images. (A) Images represent sections containing anterior parts (P4) of the female hindbrain, which includes the (i) inferior colliculus, (j) cerebellum, and (l) pons region brain stem. (B–C) Images represent [^{3}H]**2.5** binding in the mid parts of the male hindbrain (P2 and P3). Specific binding of [^{3}H]**2.5** can be seen in the medulla, specifically in the (l) dorsal vagal complex structure consisting of area postrema, nucleus tractus solitarius, and dorsal motor nucleus. (D) Images represent sections containing the posterior parts (P1) of the female hindbrain, which include the (i) cerebellum and (m) caudal part of the brain stem. Low to no binding of the radioligand can be seen comparing total to unspecific binding.

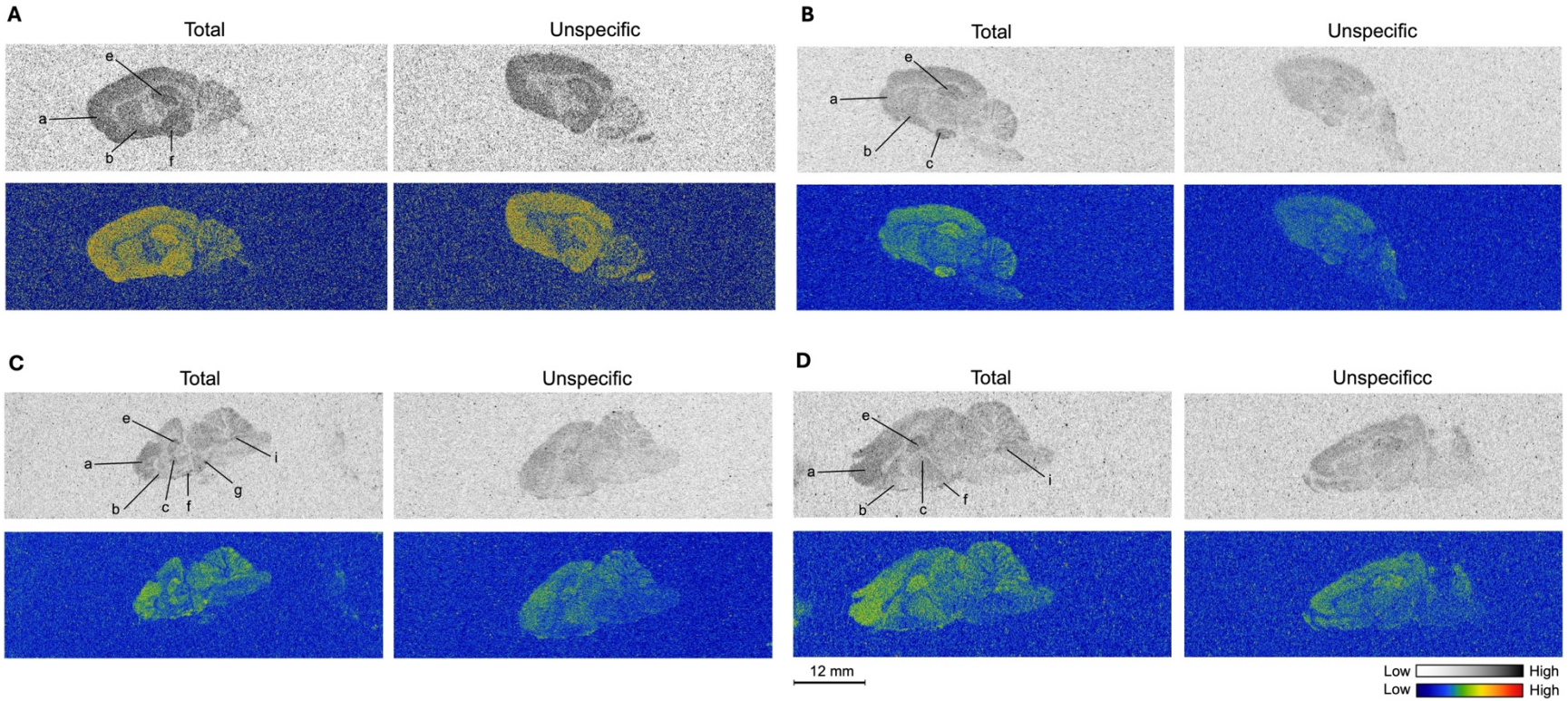

Figure 3.6. Autoradiographic images of sagittal sections from the mid-line of a female Wistar rat brain labeled by incubation with 0.3 nM of [^{3}H]**2.5**. Each section is represented by the total and unspecific binding of [^{3}H]**2.5** in greyscale and color images. Images represent sections (A) 4 mm, (B) 2 mm away from the right hemisphere mid-line of the brain, and sections (C) 1.5 mm, and (D) 3.5 mm away from the left hemisphere.

Focusing on the coronal sections of the rat brain, the total binding of [^{3}H]**2.5** was higher than the unspecific binding of [^{3}H]**2.5** within regions of the hypothalamus, midbrain, and medulla oblongata, indicating Y_4R expression in these brain regions (Figures 3.4B–C and 3.5B–C). The highest binding of the radioligand [^{3}H]**2.5** was observed in the interpeduncular nucleus (IPN) structure of the midbrain and in the dorsal vagal complex (DVC) of the medulla oblongata (Figures 3.4C and 3.5B–C). The expression of Y_4R in these structures has been confirmed in several studies and is linked to the regulation of feeding and digestion.[9, 10, 15] The IPN is part of the limbic system associated with the modulation of anhedonia-like behaviors, memory, reward processing as well as motivational behaviors.[31-35] Several studies have shown that it regulates emotional and behavioral responses, food-seeking behaviors, and sleep.[36-38] Additionally, it could be indirectly involved in regulating hunger and satiety since neurons in the IPN function in conjunction with neurons in the hypothalamus that are directly involved in this regulatory role.[39] The DVC, on the other hand, is shown to regulate various autonomic functions of the parasympathetic nervous system, such as gastrointestinal function and stress response.[40-42] This complex consists of several individual structures, namely, the area postrema (AP), nucleus tractus solitarius (NTS), and dorsal motor nucleus (DMV); which helps maintain body and energy homeostasis by either monitoring blood circulating nutrients and hormones, including those responsible for thirst and hunger or integrating sensory information from the body and coordinating the brain's responses to that effect.[43, 44] Thus, they control gastric motility and secretions, bronchoconstriction, and heart rate as well as process taste information, thereby contributing to the perception of flavors and the regulation of feeding behaviors.[41, 45-47] With respect to the hypothalamus, binding of [^{3}H]**2.5** to this region was moderately low and not well defined, although several transcriptomic and autoradiographic studies have indicated the expression of Y_4R in neurons from the hypothalamic regions.[7, 8, 10] However, [^{3}H]**2.5** binding sites can fairly be seen in the arcuate nucleus (Arc) of the hypothalamus (Figure 3.4B) associated with the regulation of energy expenditure, appetite, reproductive behavior, and sleep.[8, 10]

In the sections of rat brains containing the frontal cortex, olfactory nucleus, thalamus, and hippocampus, binding of [^{3}H]**2.5** was either very low or nonexistent, as the images from total and unspecific binding were not easily distinguishable (Figures 3.3, 3.4A, 3.5A, and 3.5D). Although several transcriptomic and proteomic studies in addition to

autoradiographic studies, identified Y_4R expression in these regions,[7, 9, 10, 48, 49] the inability to clearly confirm the presence of Y_4R by binding of [^{3}H]**2.5** in this study, despite the high binding affinity and selectivity of [^{3}H]**2.5**, might be attributed to the high concentration of the radioligand (ca. 19-fold of the K_d of rY_4R) used. This can increase unspecific binding and, as such, lead to a high background noise in the generated image, making it difficult to observe specific binding.[17-19] Another explanation could be the possible downregulation of the receptor due to their diet and rearing conditions or the possibility of different single-nucleotide variants of Y_4R existing in these regions.[50-53] For the latter, findings from a study using 12 different naturally occurring single-nucleotide variants of Y_4R showed that the binding of the endogenous ligand, PP, to these receptor variants, was significantly different.[54]

Regardless of these findings, [^{3}H]**2.5** appears to be suited for use in autoradiographic Y_4R binding studies. This suitability was further tested by investigating the binding of [^{3}H]**2.5** to sections of Wistar rat colons and small intestines (duodenum, jejunum, and ileum), well known to express the Y_4R.[55-57] The results indicated a high binding of [^{3}H]**2.5** in the small intestine and colon sections for both male and female Wistar rats (Figure 3.7). Generally, in the sections of duodenum, jejunum, and ileum, similar levels of [^{3}H]**2.5** binding can be seen for both total and unspecific binding, i.e., Y_4R expression was not distinctly evident in these tissues (Figure 3.7A-C). This could also be attributed to the previously stated reasons. Contrary to the duodenum, jejunum, and ileum, the total binding of [^{3}H]**2.5** to the sections of the colon was clearly higher than the unspecific binding of [^{3}H]**2.5** in the outer regions of the sections (Figure 3.7D). This confirms Y_4R expression in the colon of male and female Wistar rats. Overall, the detected Y_4R expression in the intestines is comparable to the literature[55, 58, 59] and, to some extent, confirms the suitability of this radioligand in autoradiography. Nonetheless, when using [^{3}H]**2.5** in autoradiographic binding studies, it will be important to optimize the experimental method, time of incubation, and concentration.

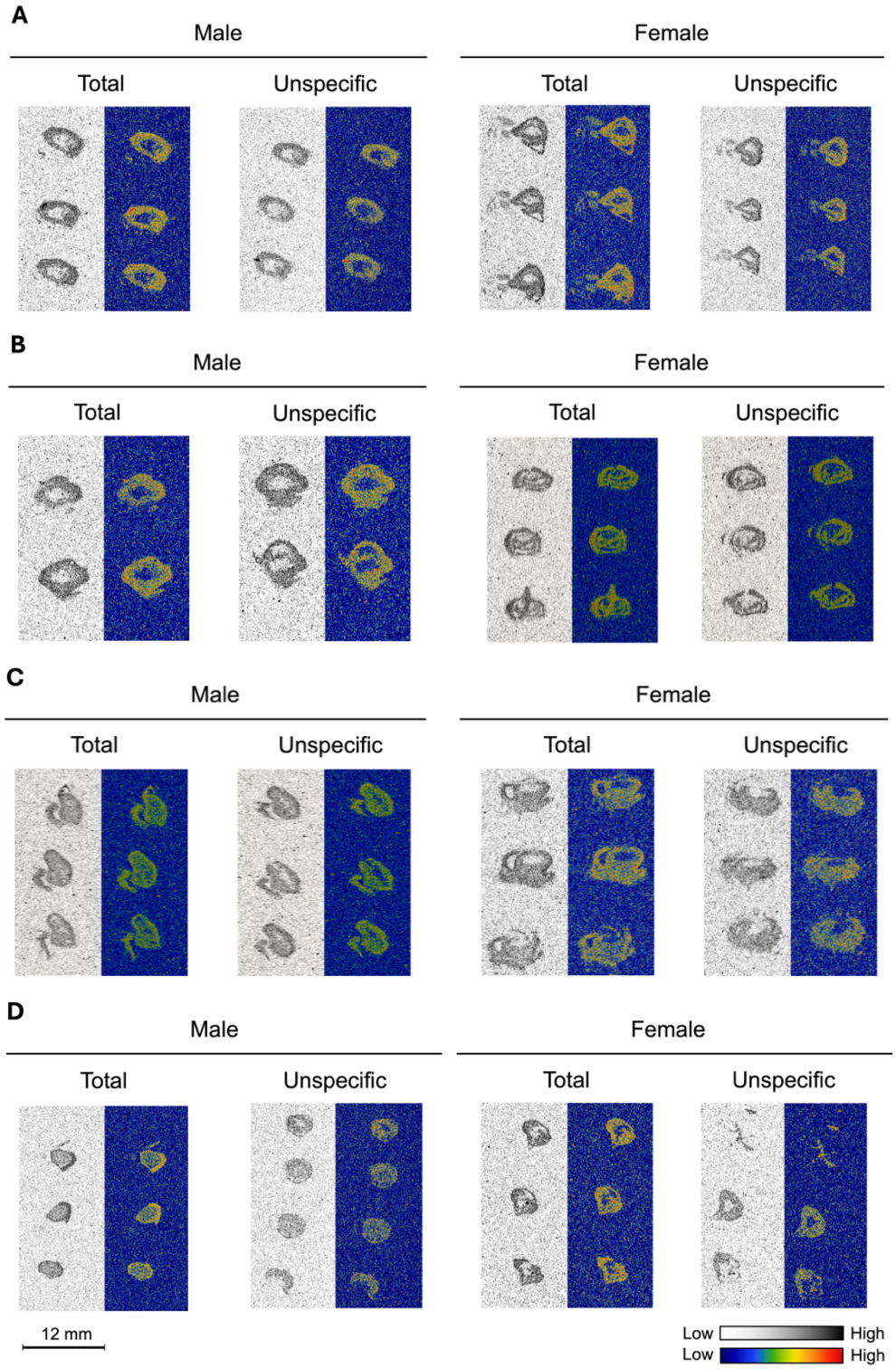

Figure 3.7. Autoradiographic images of coronal sections from the duodenum, jejunum, and ileum segments of small intestines and colons of Wistar rats incubated with 0.3 nM of [^{3}H]**2.5**. Each section is represented by the total and unspecific binding of [^{3}H]**2.5** in greyscale and color images. Images represent [^{3}H]**2.5** binding sites in the (A) duodenum, (B) jejunum, (C) ileum, and (D) colon.

3.4 Conclusion

So far, autoradiographic studies on Y_4R expression in mammalian brains have used iodinated radioligands, which tend to produce low-resolution autoradiographic images. As a result, tritiated radioligands are generally preferred, as they produce higher spatial resolutions. This study appears to be the first to examine Y_4R expression in rat brains and intestines using a tritiated radioligand, i.e., the recently reported tritium-labeled Y_4R ligand [^{3}H]UR-JG102 ([^{3}H]**2.5**).

Results from this autoradiographic study on Wistar rat brains and intestines using [^{3}H]**2.5** as a radioligand with high Y_4R binding affinity and selectivity, show distinct Y_4R expressions in the hypothalamus; midbrain region of the brain, largely in the interpeduncular nucleus (IPN) where a high level of Y_4R expression was found; and in the medulla, primarily within the dorsal vagal complex (DVC) where high levels of Y_4R expression were also located. Furthermore, very low to no expression of Y_4R can be seen in the frontal cortex, olfactory nucleus, thalamus, and hippocampus regions of the brain, as well as in both the small intestine and colon. These findings are generally in agreement with those reported in the literature. However, for the observed low to no Y_4R expressions in the frontal cortex, olfactory nucleus, thalamus, and hippocampus regions, there is a need for further studies to validate them, e.g., by using varying radioligand concentrations. These findings also suggest that [^{3}H]**2.5** is suitable for autoradiographic binding studies aiming at the identification of Y_4R in organs. Nonetheless, additional studies may be needed to determine the optimal conditions for its application, along with confirming the assignment of the targeted organ regions by histological staining techniques. In summary, the present study confirms the presence of Y_4R in the IPN, DVC, hypothalamus, and colon, supporting previous studies on the role of Y_4R in regulating feeding and gastrointestinal functions.

3.5 References

(1) Pedrazzini, T.; Pralong, F.; Grouzmann, E. Neuropeptide Y: the universal soldier. *Cell. Mol. Life Sci.* 2003, *60* (2), 350-377. DOI: 10.1007/s000180300029.

(2) Heilig, M. The NPY system in stress, anxiety and depression. *Neuropeptides* 2004, *38* (4), 213-224. DOI: 10.1016/j.npep.2004.05.002.

(3) Schüß, C.; Behr, V.; Beck-Sickinger, A. G. Illuminating the neuropeptide Y_4 receptor and its ligand pancreatic polypeptide from a structural, functional, and therapeutic perspective. *Neuropeptides* 2024, *105*, 102416. DOI: 10.1016/j.npep.2024.102416.

(4) Brothers, S. P.; Wahlestedt, C. Therapeutic potential of neuropeptide Y (NPY) receptor ligands. *EMBO Mol. Med.* 2010, *2* (11), 429-439. DOI: 10.1002/emmm.201000100.

(5) Diaz-del Castillo, M.; Woldbye, D. P. D.; Heegaard, A. M. Neuropeptide Y and its involvement in chronic pain. *Neuroscience* 2018, *387*, 162-169. DOI: 10.1016/j.neuroscience.2017.08.050.

(6) Asakawa, A.; Inui, A.; Yuzuriha, H.; Ueno, N.; Katsuura, G.; Fujimiya, M.; Fujino, M. A.; Niijima, A.; Meguid, M. M.; Kasuga, M. Characterization of the effects of pancreatic polypeptide in the regulation of energy balance. *Gastroenterology* 2003, *124* (5), 1325-1336. DOI: 10.1016/s0016-5085(03)00216-6.

(7) Campbell, R. E.; Smith, M. S.; Allen, S. E.; Grayson, B. E.; Ffrench-Mullen, J. M.; Grove, K. L. Orexin neurons express a functional pancreatic polypeptide Y_4 receptor. *J. Neurosci.* 2003, *23* (4), 1487-1497. DOI: 10.1523/JNEUROSCI.23-04-01487.2003.

(8) Lin, S.; Shi, Y. C.; Yulyaningsih, E.; Aljanova, A.; Zhang, L.; Macia, L.; Nguyen, A. D.; Lin, E. J.; During, M. J.; Herzog, H.*; et al.* Critical role of arcuate Y_4 receptors and the melanocortin system in pancreatic polypeptide-induced reduction in food intake in mice. *PLoS One* 2009, *4* (12), e8488. DOI: 10.1371/journal.pone.0008488.

(9) Fagerberg, L.; Hallstrom, B. M.; Oksvold, P.; Kampf, C.; Djureinovic, D.; Odeberg, J.; Habuka, M.; Tahmasebpoor, S.; Danielsson, A.; Edlund, K.*; et al.* Analysis of the human tissue-specific expression by genome-wide integration of transcriptomics and antibody-based proteomics. *Mol. Cell. Proteomics* 2014, *13* (2), 397-406. DOI: 10.1074/mcp.M113.035600.

(10) Whitcomb, D. C.; Puccio, A. M.; Vigna, S. R.; Taylor, I. L.; Hoffman, G. E. Distribution of pancreatic polypeptide receptors in the rat brain. *Brain Res.* 1997, *760* (1-2), 137-149. DOI: 10.1016/s0006-8993(97)00295-3.

(11) Gehlert, D. R.; Schober, D. A.; Gackenheimer, S. L.; Beavers, L.; Gadski, R.; Lundell, I.; Larhammar, D. [^{125}I]Leu^{31}, Pro^{34}-PYY is a high affinity radioligand for rat PP1/Y_4 and Y_1 receptors: evidence for heterogeneity in pancreatic polypeptide receptors. *Peptides* 1997, *18* (3), 397-401. DOI: 10.1016/s0196-9781(96)00346-4.

(12) Mebratie, D. Y.; Dagnaw, G. G. Review of immunohistochemistry techniques: applications, current status, and future perspectives. *Semin. Diagn. Pathol.* 2024, *41* (3), 154-160. DOI: 10.1053/j.semdp.2024.05.001.

(13) Hoofnagle, A. N.; Wener, M. H. The fundamental flaws of immunoassays and potential solutions using tandem mass spectrometry. *J. Immunol. Methods* 2009, *347* (1-2), 3-11. DOI: 10.1016/j.jim.2009.06.003.

(14) Whitcomb, D. C.; Taylor, I. L.; Vigna, S. R. Characterization of saturable binding sites for circulating pancreatic polypeptide in rat brain. *Am. J. Physiol.* 1990, *259* (4 Pt 1), G687-691. DOI: 10.1152/ajpgi.1990.259.4.G687.

(15) Dumont, Y.; Moyse, E.; Fournier, A.; Quirion, R. Distribution of peripherally injected peptide YY ([^{125}I]PYY_{3-36}) and pancreatic polypeptide ([^{125}I]hPP) in the CNS: enrichment in the area postrema. *J. Mol. Neurosci.* 2007, *33* (3), 294-304. DOI: 10.1007/s12031-007-9007-9.

(16) Shetzline, M. A.; Zipf, W. B.; Nishikawara, M. T. Pancreatic polypeptide: identification of target tissues using an *in vivo* radioreceptor assay. *Peptides* 1998, *19* (2), 279-289. DOI: 10.1016/s0196-9781(97)00372-0.

(17) Feucht, H. H.; Zollner, B.; Laufs, R. Comparison of conventional autoradiography with a new DNA enzyme immunoassay for the detection of hepatitis C virus-polymerase chain reaction amplification products. *J. Virol. Methods* 1995, *55* (1), 105-110. DOI: 10.1016/0166-0934(95)00049-z.

(18) McEwen, A.; Henson, C. Quantitative whole-body autoradiography: past, present and future. *Bioanalysis* 2015, *7* (5), 557-568. DOI: 10.4155/bio.15.9.

(19) Griem-Krey, N.; Klein, A. B.; Herth, M.; Wellendorph, P. Autoradiography as a simple and powerful method for visualization and characterization of pharmacological targets. *J. Vis. Exp.* 2019, (145). DOI: 10.3791/58879.

(20) Shaffer, C. L.; Gunduz, M.; Thornburgh, B. A.; Fate, G. D. Using a tritiated compound to elucidate its preclinical metabolic and excretory pathways *in vivo*: exploring tritium exchange risk. *Drug Metab. Dispos.* 2006, *34* (9), 1615-1623. DOI: 10.1124/dmd.106.010934.

(21) Potchoiba, M. J.; Nocerini, M. R. Utility of whole-body autoradioluminography in drug discovery for the quantification of tritium-labeled drug candidates. *Drug Metab. Dispos.* 2004, *32* (10), 1190-1198. DOI: 10.1124/dmd.32.10.

(22) Caro, L. G. High-resolution autoradiogaphy. II. The problem of resolution. *J. Cell Biol.* 1962, *15* (2), 189-199. DOI: 10.1083/jcb.15.2.189.

(23) Gleixner, J.; Gattor, A. O.; Humphrys, L. J.; Brunner, T.; Keller, M. [^{3}H]UR-JG102–A radiolabeled cyclic peptide with high affinity and excellent selectivity for the neuropeptide Y Y_4 receptor. *J. Med. Chem.* 2023, *66* (19), 13788-13808. DOI: 10.1021/acs.jmedchem.3c01224.

(24) Konieczny, A.; Conrad, M.; Ertl, F. J.; Gleixner, J.; Gattor, A. O.; Grätz, L.; Schmidt, M. F.; Neu, E.; Horn, A. H. C.; Wifling, D.*; et al.* N-Terminus to arginine side-chain cyclization of linear peptidic neuropeptide Y Y_4 receptor ligands results in picomolar binding constants. *J. Med. Chem.* 2021, *64* (22), 16746-16769. DOI: 10.1021/acs.jmedchem.1c01574.

(25) Pavey, G. M.; Copolov, D. L.; Dean, B. High-resolution phosphor imaging: validation for use with human brain tissue sections to determine the affinity and density of radioligand binding. *J. Neurosci. Methods* 2002, *116* (2), 157-163. DOI: 10.1016/s0165-0270(02)00036-5.

(26) Tough, I. R.; Holliday, N. D.; Cox, H. M. Y_4 receptors mediate the inhibitory responses of pancreatic polypeptide in human and mouse colon mucosa. *J. Pharmacol. Exp. Ther.* 2006, *319* (1), 20-30. DOI: 10.1124/jpet.106.106500.

(27) Markov, G. V.; Paris, M.; Bertrand, S.; Laudet, V. The evolution of the ligand/receptor couple: a long road from comparative endocrinology to comparative genomics. *Mol. Cell. Endocrinol.* 2008, *293* (1-2), 5-16. DOI: 10.1016/j.mce.2008.06.011.

(28) Bridgham, J. T.; Carroll, S. M.; Thornton, J. W. Evolution of hormone-receptor complexity by molecular exploitation. *Science* 2006, *312* (5770), 97-101. DOI: 10.1126/science.1123348.

(29) Lever, S. Z.; Fan, K. H.; Lever, J. R. Tactics for preclinical validation of receptor-binding radiotracers. *Nucl. Med. Biol.* 2017, *44*, 4-30. DOI: 10.1016/j.nucmedbio.2016.08.015.

(30) Paxinos, G.; Watson, C. *The rat brain in stereotaxic coordinates*; Academic Press, 1998.

(31) Mai, J. K.; Ashwell, K. W. S. CHAPTER 3 - Fetal Development of the Central Nervous System. In *The Human Nervous System (Second Edition)*, Paxinos, G., Mai, J. K. Eds.; Academic Press, 2004; pp 49-94.

(32) Chao, O. Y.; Nikolaus, S.; Yang, Y. M.; Huston, J. P. Neuronal circuitry for recognition memory of object and place in rodent models. *Neurosci. Biobehav. Rev.* 2022, *141*, 104855. DOI: 10.1016/j.neubiorev.2022.104855.

(33) McLaughlin, I.; Dani, J. A.; De Biasi, M. The medial habenula and interpeduncular nucleus circuitry is critical in addiction, anxiety, and mood regulation. *J. Neurochem.* 2017, *142 Suppl 2* (Suppl 2), 130-143. DOI: 10.1111/jnc.14008.

(34) Xu, C.; Sun, Y.; Cai, X.; You, T.; Zhao, H.; Li, Y.; Zhao, H. Medial habenula-interpeduncular nucleus circuit contributes to Anhedonia-like behavior in a rat model of depression. *Front. behav. neurosci.* 2018, *12*, 238. DOI: 10.3389/fnbeh.2018.00238.

(35) Kobayashi, Y.; Sano, Y.; Vannoni, E.; Goto, H.; Suzuki, H.; Oba, A.; Kawasaki, H.; Kanba, S.; Lipp, H. P.; Murphy, N. P.*; et al.* Genetic dissection of medial habenula-interpeduncular nucleus pathway function in mice. *Front. behav. neurosci.* 2013, *7*, 17. DOI: 10.3389/fnbeh.2013.00017.

(36) Ables, J. L.; Park, K.; Ibanez-Tallon, I. Understanding the habenula: a major node in circuits regulating emotion and motivation. *Pharmacol. Res.* 2023, *190*, 106734. DOI: 10.1016/j.phrs.2023.106734.

(37) Chen, W. Y.; Peng, X. L.; Deng, Q. S.; Chen, M. J.; Du, J. L.; Zhang, B. B. Role of olfactorily responsive neurons in the right dorsal habenula-ventral interpeduncular nucleus pathway in food-seeking behaviors of larval zebrafish. *Neurosci. J.* 2019, *404*, 259-267. DOI: 10.1016/j.neuroscience.2019.01.057.

(38) Cherng, B. W.; Islam, T.; Torigoe, M.; Tsuboi, T.; Okamoto, H. The dorsal lateral habenula-interpeduncular nucleus pathway is essential for left-right-dependent decision making in zebrafish. *Cell Rep.* 2020, *32* (11), 108143. DOI: 10.1016/j.celrep.2020.108143.

(39) Li, S. Y.; Cao, J. J.; Tan, K.; Fan, L.; Wang, Y. Q.; Shen, Z. X.; Li, S. S.; Wu, C.; Zhou, H.; Xu, H. T. CRH neurons in the lateral hypothalamic area regulate feeding behavior of mice. *Curr. Biol.* 2023, *33* (22), 4827-4843 e4827. DOI: 10.1016/j.cub.2023.09.050.

(40) Grijalva, C. V.; Novin, D. The role of the hypothalamus and dorsal vagal complex in gastrointestinal function and pathophysiology. *Ann. N. Y. Acad. Sci.* 1990, *597*, 207-222. DOI: 10.1111/j.1749-6632.1990.tb16169.x.

(41) Williams, D. L.; Kaplan, J. M.; Grill, H. J. The role of the dorsal vagal complex and the vagus nerve in feeding effects of melanocortin-3/4 receptor stimulation. *Endocrinology* 2000, *141* (4), 1332-1337. DOI: 10.1210/endo.141.4.7410.

(42) Leslie, R. A. Neuroactive substances in the dorsal vagal complex of the medulla oblongata: nucleus of the tractus solitarius, area postrema, and dorsal motor nucleus of the vagus. *Neurochem. Int.* 1985, *7* (2), 191-211. DOI: 10.1016/0197-0186(85)90106-8.

(43) Price, C. J.; Hoyda, T. D.; Ferguson, A. V. The area postrema: a brain monitor and integrator of systemic autonomic state. *Neuroscientist* 2008, *14* (2), 182-194. DOI: 10.1177/1073858407311100.

(44) Young, A. A. Brainstem sensing of meal-related signals in energy homeostasis. *Neuropharmacol.* 2012, *63* (1), 31-45. DOI: 10.1016/j.neuropharm.2012.03.019.

(45) AbuAlrob, M. A.; Tadi, P. Neuroanatomy, Nucleus Solitarius. In *StatPearls*, 2025.

(46) Holtmann, G.; Talley, N. J. The stomach-brain axis. *Best Pract. Res. Clin. Gastroenterol.* 2014, *28* (6), 967-979. DOI: 10.1016/j.bpg.2014.10.001.

(47) Cutsforth-Gregory, J. K.; Benarroch, E. E. Nucleus of the solitary tract, medullary reflexes, and clinical implications. *Neurology* 2017, *88* (12), 1187-1196. DOI: 10.1212/WNL.0000000000003751.

(48) Sainsbury, A.; Shi, Y.-C.; Zhang, L.; Aljanova, A.; Lin, Z.; Nguyen, A. D.; Herzog, H.; Lin, S. Y_4 receptors and pancreatic polypeptide regulate food intake via hypothalamic orexin and brain-derived neurotropic factor dependent pathways. *Neuropeptides* 2010, *44*, 261-268. DOI: 10.1016/j.npep.2010.01.001.

(49) Sjöstedt, E.; Zhong, W.; Fagerberg, L.; Karlsson, M.; Mitsios, N.; Adori, C.; Oksvold, P.; Edfors, F.; Limiszewska, A.; Hikmet, F.*; et al.* An atlas of the protein-coding genes in the human, pig, and mouse brain. *Science* 2020, *367* (6482), eaay5947. DOI: doi:10.1126/science.aay5947.

(50) The status, quality, and expansion of the NIH full-length cDNA project: The mammalian gene collection (MGC). *Genome Res.* 2004, *14* (10b), 2121-2127. DOI: 10.1101/gr.2596504.

(51) Yan, H.; Yang, J.; Marasco, J.; Yamaguchi, K.; Brenner, S.; Collins, F.; Karbon, W. Cloning and functional expression of cDNAs encoding human and rat pancreatic polypeptide receptors. *PNAS USA* 1996, *93* (10), 4661-4665. DOI: 10.1073/pnas.93.10.4661.

(52) Bard, J. A.; Walker, M. W.; Branchek, T. A.; Weinshank, R. L. Cloning and functional expression of a human Y_4 subtype receptor for pancreatic polypeptide, neuropeptide Y, and peptide YY. *J Biol Chem* 1995, *270* (45), 26762-26765. DOI: 10.1074/jbc.270.45.26762.

(53) Chen, S.; Xiang, H.; Zhang, H.; Zhu, X.; Wang, D.; Wang, J.; Yin, T.; Liu, L.; Kong, M.; Li, H.*; et al.* Rearing system causes changes of behavior, microbiome, and gene expression of chickens. *Poult. Sci.* 2019, *98* (9), 3365-3376. DOI: 10.3382/ps/pez140.

(54) Shebanits, K.; Vasile, S.; Xu, B.; Gutierrez-de-Teran, H.; Larhammar, D. Functional characterization *in vitro* of twelve naturally occurring variants of the human pancreatic polypeptide receptor NPY_4R. *Neuropeptides* 2019, *76*, 101933. DOI: 10.1016/j.npep.2019.05.004.

(55) Goumain, M.; Voisin, T.; Lorinet, A. M.; Laburthe, M. Identification and distribution of mRNA encoding the Y_1, Y_2, Y_4, and Y_5 receptors for peptides of the PP-fold family in the rat intestine and colon. *Biochem. Biophys. Res. Commun.* 1998, *247* (1), 52-56. DOI: 10.1006/bbrc.1998.8647.

(56) Gregor, P.; Millham, M. L.; Feng, Y.; DeCarr, L. B.; McCaleb, M. L.; Cornfield, L. J. Cloning and characterization of a novel receptor to pancreatic polypeptide, a member of the neuropeptide Y receptor family. *FEBS Lett.* 1996, *381* (1-2), 58-62. DOI: 10.1016/0014-5793(96)00067-1 From NLM.

(57) Lundell, I.; Statnick, M. A.; Johnson, D.; Schober, D. A.; Starback, P.; Gehlert, D. R.; Larhammar, D. The cloned rat pancreatic polypeptide receptor exhibits profound differences to the orthologous receptor. *PNAS USA* 1996, *93* (10), 5111-5115. DOI: 10.1073/pnas.93.10.5111.

(58) Cox, H. M. Neuropeptide Y receptors; antisecretory control of intestinal epithelial function. *Auton. Neurosci.* 2007, *133* (1), 76-85. DOI: 10.1016/j.autneu.2006.10.005.

(59) Hyland, N. P.; Cox, H. M. NPY-Like Peptides, Y Receptors and Gastrointestinal Function. In *Neuropeptide Y and Related Peptides*, Michel, M. C. Ed.; Springer Berlin Heidelberg, 2004; pp 389-408.

Chapter 4

Synthesis and Characterization of Plasma-stable Analogs of the Y_4R Agonist UR-AK86C

Note: In this chapter, all induced fit docking (IFD) experiments were conducted by Simon Gross. The section on "Angiotensin-converting enzyme is responsible for degrading UR-AK86C (**2.4**)" was published in the *Journal of Medicinal Chemistry*, prior to the submission of this thesis. (reused with permission from ACS, Copyright 2021:

Konieczny, A., Conrad, M., Ertl, F. J., Gleixner, J., Gattor, A. O., Grätz, L., Schmidt, M. F., Neu, E., Horn, A. H. C., Wifling, D., Gmeiner, P., Clark, T., Sticht, H. & Keller, M. (2021). N-terminus to arginine side-chain cyclization of linear peptidic neuropeptide Y Y_4 receptor ligands result in picomolar binding constants. *J. Med. Chem., 64(22), 16746-16769*.

4.1 Introduction

In recent times, research into the use of bioactive peptides as candidates in drug development has gathered momentum due to their appealing pharmacological profile and inherent properties, often leading to safe and efficacious therapeutics.[1] The surge in these studies has led to the identification and characterization of several peptide hormones and their receptors, as well as the development of modified and synthetic analogs of these hormones.[2-5] Although most bioactive peptide ligands or their synthetic/modified analogs exhibit high potency, selectivity, and favorable biosafety profiles, they are often known to show very low stability *in vivo.* In humans, this low stability often results from the proteolytic degradation of these peptides or their analogs by active proteases present in the body, as well as their rapid renal clearance.[5, 6]

The human neuropeptide Y Y_4 receptor (hY_4R) is a peptide hormone-activated receptor whose activation has been shown to have a direct and indirect therapeutic effect on regulating food intake and weight loss; thus, it could be targeted for the treatment of obesity and other diet-related diseases.[7-10] As a potential therapeutic target, several potent peptidic ligands targeting this receptor have been developed. Some of these include oligopeptides, which mimic the C-terminus of pancreatic polypeptide (PP).[11-15]

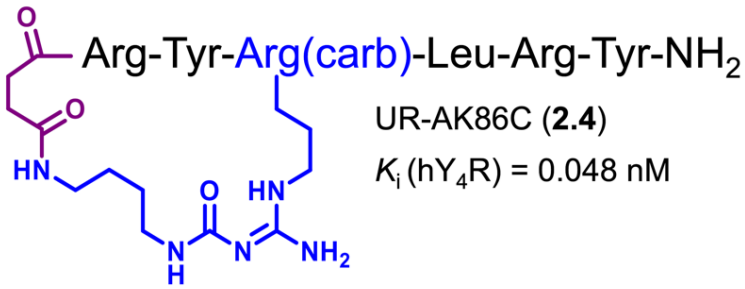

Figure 4.1. Structure of the parent peptide UR-AK86C (**2.4**)

Among these, the UR-AK86C (**2.4**; Figure 4.1), a highly Y_4R selective and potent cyclic hexapeptide, stands out as a lead structure for developing drug candidates targeting the hY_4R. In comparison to human PP, **2.4** is a partial agonist in functional assays with a similar binding affinity.[16] Despite its selectivity and potency, *in vitro* stability studies in human plasma revealed a moderately low half-life (ca. 2 h). Given this low half-life

of **2.4** *in vitro*, it is likely that its stability *in vivo* would be even lower, possibly due to factors such as cellular degradation activities as seen in endothelial cells and hepatocytes.[17, 18] Hence, there is a compelling need to develop derivatives of **2.4** that exhibit improved proteolytic stability.

Regarding the development of analogs of **2.4** with improved plasma stability, the major challenge is maintaining high Y_4R binding affinity and potency. Generally, to improve the plasma stability of a biologically active peptide, structural activity relationship (SAR) studies for the identification of chemical groups responsible for its biological activity are conducted. This is followed by identifying regions of the peptides susceptible to proteolytic cleavage and proteases involved in the degradation. Next, medicinal chemistry strategies such as peptide bond modification, the use of peptidomimetics, and amino acid replacement, among others, are employed to improve the peptide's stability.[19-22]

This study focused on improving the plasma stability of **2.4** while retaining its biological activity by first identifying the peptide bonds in **2.4** susceptible to proteolysis and the protease responsible for its degradation. Potential plasma-stable analogs of hexapeptide **2.4** were subsequently synthesized using commonly known chemical strategies and insights from previously conducted SAR studies.

4.2 Materials and Methods

4.2.1 Materials

The protected amino acids Fmoc-Tyr(tBu)-OH and Fmoc-Arg(Pbf)-OH were purchased from Carbolution Chemicals (St. Ingbert, Germany). Fmoc-Cpg-OH, Fmoc-β-Homo-Tyr(tBu)-OH, and Fmoc-β-Homo-Arg(Pbf)-OH were obtained from BLD Pharma (Reinbek, Germany). Fmoc-Sieber-PS-resin (0.61 mmol/g), HBTU, *N*-methyl-2-pyrrolidinone (NMP) for peptide synthesis, Fmoc-Gln-OH, Fmoc-Asn-OH, Fmoc-allo-Ile-OH, and PyBOP were obtained from Iris Biotech (Marktredwitz, Germany). Fmoc-*N*-Me-Arg(Pbf)-OH, Fmoc-Tle-OH (Fmoc-α-*tert*-butylglycine), Fmoc-Leu-OH, Fmoc-Phe-OH, Fmoc-His(Trt)-OH, Oxyma pure, *N,N'*-diisopropylcarbodiimide (DIC), Ramage amide resin (0.66 mmol/g), gradient grade MeOH for HPLC, and trifluoroacetic acid (TFA) were from Merck (Darmstadt, Germany). HOBt hydrate, succinic anhydride, and dichloromethane (CH_2Cl_2) were purchased from Acros Organics/Fisher Scientific (Nidderau, Germany). Fmoc-α-Me-Leu-OH and *N,N*-diisopropylethylamine (DIPEA) were obtained from ABCR (Karlsruhe, Germany). DMF for peptide synthesis, absolute EtOH, gradient grade acetonitrile (MeCN) for HPLC, forskolin, and piperidine were from Sigma-Aldrich (Taufkirchen, Germany). Human pancreatic polypeptide (hPP) and porcine neuropeptide Y (pNPY) were from SynPeptide (Shanghai, China). Coelenterazine h was purchased from Biotrend (Cologne, Germany). Bacitracin and bovine serum albumin (BSA) were from Serva (Heidelberg, Germany). Deuterated solvents were from Deutero (Kastellaun, Germany). Blood plasma was obtained by the collection of human blood from a healthy female donor in 5.5 mL heparinized plasma-monovettes followed by centrifugation at 1,200 g at 4 °C for 10 min. The supernatants were pooled in two 50-mL Falcon tubes and centrifuged again at 1,200 g at 4 °C for 10 min. The supernatant made of plasma was aliquoted and stored at −80 °C. Ultrapure water was consistently used for the preparation of stock solutions, buffers, and eluents for HPLC. Polypropylene reaction vessels (1.5 and 2 mL) from Sarstedt (Nümbrecht, Germany) were used to keep stock solutions and for small-scale reactions (e.g., activation of Fmoc-protected amino acids).

4.2.2 Methods

4.2.2.1 Mass spectrometry

High-resolution mass spectrometry (HRMS) was performed using an Agilent 6540 UHD accurate-mass Q-TOF LC/MS system coupled to an Agilent 1290 analytical HPLC system (Agilent Technologies. Santa Clara, CA) using an ESI source and the following LC method: column: Luna Omega C18, 1.6 µm, 50 × 2.1 mm (Phenomenex, Aschaffenburg, Germany), column temperature: 40 °C, solvent/linear gradient: 0−4 min: 0.1% aqueous HCOOH/MeCN supplemented with 0.1% HCOOH 95:5−2:98, 4−5 min: 2:98, flow: 0.6 mL/min.

4.2.2.2 NMR spectroscopy

NMR spectra were recorded on a Bruker AVANCE 600 instrument with a cryogenic probe (^{1}H: 600 MHz) (Bruker, Karlsruhe, Germany). NMR spectra were calibrated based on the solvent residual peaks (^{1}H-NMR, DMSO-d_6: δ = 2.50 ppm), and data are reported as follows: ^{1}H-NMR: chemical shift δ in ppm (multiplicity [s = singlet, d = doublet, t = triplet, m = multiplet, and br s = broad singlet], integral, coupling constant *J* in Hz).

4.2.2.3 Preparative HPLC

Preparative HPLC was performed with a Prep 150 LC system from Waters (Eschborn, Germany) comprising a Waters 2545 binary gradient module, a Waters 2489 UV/vis detector, and a Waters fraction collector III. A Gemini NX-C18, 5 µm, 250 mm × 21 mm (Phenomenex, Aschaffenburg, Germany) was used as a reversed-phase (RP) column at a flow rate of 20 mL/min using mixtures of 0.1% aqueous TFA and MeCN as the mobile phase. A detection wavelength of 220 nm was used throughout. Collected fractions were lyophilized using a Scanvac CoolSafe 100-9 freeze dryer (Labogene, Allerød, Denmark) equipped with an RZ 6 rotary vane vacuum pump (Vacuubrand, Wertheim, Germany).

4.2.2.4 Analytical HPLC

Analytical HPLC analysis was performed with a system from Agilent Technologies composed of a 1290 Infinity binary pump equipped with a degasser, a 1290 Infinity autosampler, a 1290 Infinity thermostatted column compartment, a 1260 Infinity diode array detector, and a 1260 Infinity fluorescence detector. A Kinetex-XB C18, 2.6 µm,

100 × 3 mm (Phenomenex) served as the stationary phase at a flow rate of 0.6 mL/min. Detection was performed at 220 nm, and the oven temperature was 25 °C. Mixtures of MeCN (A) and 0.04% aqueous TFA (B) were used as mobile phases. The following linear gradients were applied: compounds **4.2–4.10**: 0–14 min: A/B 5:95–25:75, 14–16 min: 25:75–95:5, 16–20 min: 95:5 (isocratic); compounds **4.11–4.14**: 0–14 min: A/B 10:90–30:70, 14–16 min: 30:70–95:5, 16–20 min: 95:5 (isocratic). The injection volume was 20 µL. Retention (capacity) factors *k* were calculated from the retention times t_R according to $k = (t_R - t_0)/t_0$ (t_0 = dead time).

4.2.2.5 General procedure for solid phase peptide synthesis (SPPS)

Peptides were synthesized either on Fmoc-Sieber-PS-resins or Ramage amide resins by the manual Fmoc strategy SPPS. 5 mL Injekt Solo (B. Braun, Melsungen, Germany) or NPRM-JECT (Henke Sass Wolf, Tuttlingen, Germany) syringes, equipped with polyethylene frits (pore size: 35 µm) (Roland Vetter Laborbedarf, Ammerbuch, Germany) were used as reaction vessels. DMF/NMP (8:2 v/v) was used as a solvent for the coupling reactions and the cleavage of Fmoc groups. For syntheses using Fmoc-Sieber-PS-resin, initial Fmoc deprotection, and swelling were performed by treating the resin with 20% piperidine in the solvent at rt for 2 × 20 min. In the case of Ramage amide resin, the resin was first allowed to swell in solvent for 45 min at rt, followed by initial Fmoc deprotection with 20% piperidine in solvent (2 × 20 min at rt). Protected amino acids (Fmoc-aa) were used in 5-fold excess and preactivated with HBTU (4.9 equiv.)/HOBt (5 equiv.)/DIPEA (10 equiv.) in polypropylene reaction vessels for at least 5 min prior to addition to the resin (volume of the solvent: ca. 2.2 mL/mmol Fmoc-aa). In the case of standard (natural) Fmoc-aa, “double” coupling (2 × 45 min) was performed at 35 °C. Special building block **4.1**[23] (Fmoc-Arg(carb)(Boc)-OH; Figure 4.2) was used in 3-fold excess, preactivated with HBTU (2.95 equiv.)/HOBt (3 equiv.)/DIPEA (6 equiv.) (volume of solvent: ca. 2.2 mL/mmol building block) and the reaction was performed at 35 °C for at least 4 h (maximum 18 h) for the first coupling followed by a second coupling for some peptides using 3-fold excess, preactivated with Oxyma Pure (3 equiv.)/DIC (3 equiv.) (volume of solvent: ca. 1.6 mL/mmol building block) also performed at 35 °C for at least 4 h. During coupling reactions, syringes were shaken using a Multi Reax shaker (Heidolph, Schwabach, Germany) covered with a box, which was equipped with a thermostat-controlled heater. After the completion of a Fmoc-aa coupling, the resin was washed

with solvent (4 ×) and treated with 20% piperidine in solvent at rt for 2 × 10 min, followed by washing of the resin with solvent (6 ×). After coupling and Fmoc deprotection of the final amino acid, the resin-bound completely elongated peptide was treated with succinic anhydrate (10 equiv)/DIPEA (10 equiv) in the solvent at 35 °C for 30 min.

For syntheses using Sieber resins, the resin was washed with solvent (6 ×) and CH_2Cl_2 (treated with K_2CO_3) (4 ×) after this treatment, followed by cleavage of the resin with CH_2Cl_2/TFA (3:1 v/v) at rt (2 × 20 min, performed in the syringe). After the completion of cleavage, the liquid from the resin was collected, and the resin was washed three times with CH_2Cl_2/TFA (3:1 v/v). The washings were collected and combined with the cleavage liquid in a 100 mL round-bottom flask, where the volatiles were removed by rotary evaporation. The residue was dissolved in TFA/H_2O (95:5 v/v), and the mixture was stirred at rt for 3–5 h (for full side chain deprotection). With respect to syntheses using Ramage amide resin, the resin was washed with solvent (6 ×) followed by treatment with TFA/TIPS/H_2O (95:2.5:2.5 v/v) at rt (2 × 30 min, performed in the syringe) to cleave peptides off the resin. The liquids from the cleavage were collected in a 100 mL round-bottom flask, and the resin was washed three times with the cleavage cocktail. The washings were added to the 100 mL round-bottom flask, and the combined mixture was directly stirred for at least 3–5 h.

After stirring, the volatiles were removed from the mixture by rotary evaporation, followed by the addition of 40–50 mL of water and lyophilization to obtain the crude peptide. The crude peptide was subsequently purified by preparative HPLC.

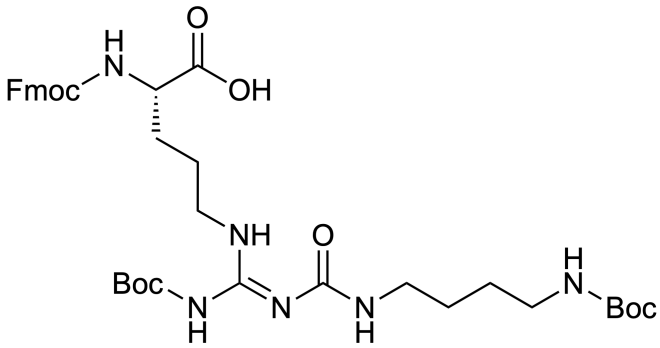

4.1, Fmoc-Arg(carb)(Boc)-OH

Figure 4.2. Structure of N^{ω}-carbamoylated arginine **4.1**[23] used in SPPS for the synthesis of linear precursor peptides.

4.2.2.6 Compound characterization

The linear precursor peptides **4.2a–4.14a** obtained from SPPS were characterized by HRMS, whereas their cyclic derivatives **4.2b–4.14b** were characterized by ^{1}H-NMR spectroscopy, HRMS, and RP-HPLC analysis. Additionally, ^{1}H-COSY NMR spectra were acquired for all cyclic peptides. The purity of all final compounds, determined by RP-HPLC (220 nm), was ≥ 95%. Annotation concerning the ^{1}H-NMR spectra (solvent: DMSO-d_6) of the peptides: to allow integration of the signals interfering with the broad water signal at ca. 3.33 ppm, ^{1}H-NMR spectra were additionally recorded in DMSO-d_6/D_2O (10:1 v/v) resulting in a total H-D exchange of the phenolic OH proton and NH protons of the (carbamoylated) guanidinium groups and no or a partial H-D exchange of amide NH protons. An overview of the analytical data of the peptides can be seen in *Section 4.6 Appendix* (Table A4.1 and A4.2). The peptide sequence of **4.2a–4.14a** and **4.2b–4.14b** can be seen in Table A4.1 and Figure 4.5, respectively.

4.2.2.7 Synthesis protocols and analytical data

(9S,12S,15S)-N-((S)-1-(((S)-1-(((S)-1-amino-3-(4-hydroxyphenyl)-1-oxopropan-2-yl)amino)-5-guanidino-1-oxopentan-2-yl)(methyl)amino)-4-methyl-1-oxopentan-2-yl)-15-(3-guanidinopropyl)-12-(4-hydroxybenzyl)-4-imino-2,11,14,17,20-pentaoxo-1,3,5,10,13,16,21-heptaazacyclopentacosane-9-carboxamide tris(hydrotrifluoroacetate) (**4.2b**). The linear precursor peptide **4.2a** (5.8 mg, 3.60 µmol, synthesized by SPPS), HOBt (2.7 mg, 0.018 mmol) and DIPEA (6.2 µL, 0.036 mmol) were dissolved in DMF/NMP 8:2 v/v (500 µL) in a 100 mL round-bottom flask. Under stirring, a solution of PyBOP (2.7 mg, 0.018 mmol) in DMF/NMP 8:2 v/v (500 µL) was added, and the mixture was stirred at rt overnight. 0.1% aqueous TFA (30 mL) was added, followed by freeze-drying and purification by preparative HPLC (gradient: 0–30 min: MeCN/0.1% aqueous TFA 5:95–30:70, t_R = 23 min) to yield **4.2b** as a white fluffy solid (4.4 mg, 80%). ^{1}H-NMR (600 MHz, DMSO-d_6): δ (ppm) 0.87–0.96 (m, 6H), 1.19–1.33 (m, 3H), 1.33–1.47 (m, 8H), 1.46–1.60 (m, 5H), 1.60–1.69 (m, 2H), 1.69–1.82 (m, 2H), 2.25–2.41 (m, 4H), 2.68–2.96 (m, 6H), 2.98–3.08 (m, 5H), 3.09–3.14 (m, 1H), 3.16–3.22 (m, 1H), 3.26–3.32 (m, 2H), 4.06 (br s, 1H), 4.26–4.48 (m, 3H), 4.58–4.65 (m, 1H), 4.87–4.95 (m, 1H), 6.57–6.61 (m, 1H), 6.62–6.67 (m, 4H), 6.67–7.09 (br s, 4H, interfering with the next two listed signals), 6.90–6.93 (m, 1H), 6.96–7.03 (m, 4H), 7.129–7.76 (br s, 4H, interfering with the next listed signal), 7.46–7.56 (m, 4H), 7.82–7.98 (m, 3H), 7.99–8.23 (m, 3H), 8.23–8.48 (m, 2H),

9.04–9.37 (m, 3H), 9.89–10.30 (m, 1H). HRMS (ESI): *m/z* $[M+2H]^{2+}$ calcd. for $[C_{52}H_{84}N_{18}O_{11}]^{2+}$ 568.3278, found: 568.3280. RP-HPLC (220 nm): > 96% (t_R = 10.9 min, *k* = 13.4). $C_{52}H_{82}N_{18}O_{11} \cdot C_6H_3F_9O_6$ (1135.34 + 342.07).

(9S,12S,15S)-N-((S)1-(((S)-1-(((S)-1-amino-3-(4-hydroxyphenyl)-1-oxopropan-2-yl)amino)-5-guanidino-1-oxopentan-2-yl)amino)-1-oxo-3-phenylpropan-2-yl)-15-(3-guanidinopropyl)-12-(4-hydroxybenzyl)-4-imino-2,11,14,17,20-pentaoxo-1,3,5,10,13,16,21-heptaazacyclopentacosane-9-carboxamide tris(hydrotrifluoroacetate) (**4.3b**). The linear precursor peptide **4.3a** (13.9 mg, 8.53 µmol), HOBt (6.5 mg, 0.043 mmol) and DIPEA (14.8 µL, 0.085 mmol) were dissolved in DMF/NMP 8:2 v/v (500 µL) in a 100 mL round-bottom flask. Under stirring, a solution of PyBOP (22.1 mg, 0.043 mmol) in DMF/NMP 8:2 v/v (500 µL) was added, and the mixture was stirred at rt overnight. 0.1% aqueous TFA (30 mL) was added followed by freeze-drying and purification by preparative HPLC (gradient: 0–14 min MeCN/0.1% aqueous TFA 5:95–25:75, t_R = 25 min) to yield **4.3b** as a white fluffy solid (9.8 mg, 76%).

^{1}H-NMR (600 MHz, DMSO-d_6): δ (ppm) 1.28–1.48 (m, 12H), 1.49–1.51 (m, 2H), 1.57–1.71 (m, 3H), 2.23–2.38 (m, 3H), 2.64–2.75 (m, 2H), 2.76–2.80 (m, 1H), 2.81–2.93 (m, 3H), 2.99–3.10 (m, 6H), 3.11–3.18 (m, 2H), 3.25 (br s, 2H), 4.1 (br s, 1H), 4.18–4.28 (m, 2H), 4.29–4.42 (m, 2H), 4.49–4.64 (m, 1H), 6.61–6.66 (m, 4H), 6.66–7.10 (br s, 4H, interfering with the next two listed signals), 6.99–7.01 (m, 4H), 7.06 (s, 1H), 7.10–7.77 (br s, 4H, interfering with the next four listed signals), 7.13–716 (m, 1H), 7.18–7.24 (m, 4H), 7.40 (s, 1H), 7.51–7.57 (m, 3H), 7.79–7.84 (m, 1H), 7.85–7.90 (m, 2H), 7.91–7.94 (m, 1H), 7.95–8.02 (m, 1H), 8.03–8.12 (m, 1H), 8.12–8.23 (m, 1H), 8.31 (br s, 2H), 8.81–9.70 (m, 3H), 10.2 (br s, 1H). HRMS (ESI): *m/z* $[M+3H]^{3+}$ calcd. for $[C_{54}H_{81}N_{18}O_{11}]^{3+}$ 385.8772, found: 385.8783. RP-HPLC (220 nm): > 97% (t_R = 10.9 min, *k* = 13.4). $C_{54}H_{78}N_{18}O_{11} \cdot C_6H_3F_9O_6$ (1155.33 + 342.07).

(S)-N^1-((S)-1-(((S)-1-amino-3-(4-hydroxyphenyl)-1-oxopropan-2-yl)amino)-5-guanidino-1-oxopentan-2-yl)-2-((9S,12S,15S)-15-(3-guanidinopropyl)-12-(4-hydroxybenzyl)-4-imino-2,11,14,17,20-pentaoxo-1,3,5,10,13,16,21-heptaazacyclopentacosane-9-carboxamido)pentanediamide tris(hydrotrifluoroacetate) (**4.4b**). The linear precursor peptide **4.4a** (10.1 mg, 6.27 µmol), HOBt (4.8 mg, 0.031 mmol) and DIPEA (10.8 µL, 0.062 mmol) were dissolved in DMF/NMP 8:2 v/v (500 µL) in a 100 mL round-bottom

flask. Under stirring, a solution of PyBOP (16.2 mg, 0.031 mmol) in DMF/NMP 8:2 v/v (500 µL) was added and the mixture was stirred at rt overnight. 0.1% aqueous TFA (30 mL) was added, followed by freeze-drying and purification by preparative HPLC (gradient: 0–30 min MeCN/0.1% aqueous TFA 10:90–25:75, t_R = 19 min) to yield **4.4b** as a white fluffy solid (3.8 mg, 41%).

^{1}H-NMR (600 MHz, DMSO-d_6): δ (ppm) 1.30–1.47 (m, 9H), 1.54 (s, 4H), 1.58–1.70 (s, 2H), 1.70–1.83 (m, 2H), 1.83–1.95 (m, 1H), 2.08–2.24 (m, 2H), 2.27–2.40 (m, 4H), 2.66–2.75 (m, 1H), 2.75–2.90 (m, 3H), 2.91–2.98 (m, 1H), 2.98–3.09 (m, 5H), 3.09–3.16 (m, 1H), 3.18–3.24 (m, 1H), 3.30 (br s, 2H), 4.07 (br s, 1H), 4.15–4.24 (m, 2H), 4.24–4.31 (m, 1H), 4.31–4.40 (m, 2H), 6.62–6.67 (m, 4H), 6.82 (m, 1H), 6.49–7.12 (br s, 4H, interfering with the next two listed signals), 6.98–7.00 (m, 2H), 7.02–7.04 (m, 2H), 7.07 (s, 1H), 7.12–7.66 (br s, 4H, interfering with the next four listed signals), 7.27 (s, 1H), 7.38 (s, 1H), 7.48–7.52 (m, 2H), 7.53–7.66 (br s, 1H), 7.74–7.84 (m, 1H), 7.85–7.95 (m, 2H), 7.95–8.08 (m, 3H), 8.16 (br s, 1H), 8.31 (br s, 2H), 8.90–9.55 (m, 3H), 10.13 (br s, 1H). HRMS (ESI): *m/z* $[M+3H]^{3+}$ calcd. for $[C_{50}H_{80}N_{19}O_{12}]^{3+}$ 379.5406, found: 379.5415. RP-HPLC (220 nm): > 97% (t_R = 7.4 min, k = 8.7). $C_{50}H_{77}N_{19}O_{12} \cdot C_6H_3F_9O_6$ (1136.29 + 342.07).

(S)-N^1-((S)-1-(((S)-1-amino-3-(4-hydroxyphenyl)-1-oxopropan-2-yl)amino)-5-guanidino-1-oxopentan-2-yl)-2-((9S,12S,15S)-15-(3-guanidinopropyl)-12-(4-hydroxybenzyl)-4-imino-2,11,14,17,20-pentaoxo-1,3,5,10,13,16,21-heptaazacyclopentacosane-9-carboxamido)succinamide tris(hydrotrifluoroacetate) (**4.5b**). The linear precursor peptide **4.5a** (24.1 mg, 15.10 µmol), HOBt (11.5 mg, 0.075 mmol) and DIPEA (26.3 µL, 0.15 mmol) were dissolved in DMF/NMP 8:2 v/v (500 µL) in a 100 mL round-bottom flask. Under stirring, a solution of PyBOP (39.2 mg, 0.075 mmol) in DMF/NMP 8:2 v/v (500 µL) was added, and the mixture was stirred at rt overnight. 0.1% aqueous TFA (30 mL) was added, followed by freeze-drying and purification by preparative HPLC (gradient: 0–30 min MeCN/0.1% aqueous TFA 10:90–25:75, t_R = 17 min) to yield **4.5b** as a white fluffy solid (10.0 mg, 45%).

^{1}H-NMR (600 MHz, DMSO-d_6): δ (ppm) 1.26–1.47 (m, 10H), 1.48–1.56 (m, 3H), 1.57–1.66 (m, 2H), 1.67–1.79 (m, 1H), 1.68–1.76 (m, 1H), 2.23–2.42 (m, 4H), 2.55–2.60 (m, 1H), 2.67–2.80 (m, 2H), 2.81–2.88 (m, 2H), 2.90–2.97 (m, 2H), 2.97–3.08 (m, 5H), 3.08–3.15 (m, 1H), 3.16–3.22 (m, 1H), 3.27 (br s, 2H), 3.96–4.06 (m, 1H), 4.06–4.17 (m, 1H), 4.18–4.27 (m, 1H), 4.27–4.42 (m, 2H), 4.47–4.60 (m, 1H), 6.63–6.67 (m, 4H),

6.54–7.17 (br s, 4H, interfering with the next three listed signals), 7.00–7.03 (m, 4H), 7.07 (s, 2H), 7.13 (s, 1H), 7.17–7.71 (br s, 4H, interfering with the next three listed signals), 7.47 (t, 1H, J = 5.5 Hz), 7.51–7.55 (m, 1H), 7.57 (s, 1H), 7.88 (br s, 1H), 7.93–7.98 (m, 1H), 7.98–8.05 (m, 2H), 8.05–8.13 (m, 2H), 8.15–8.27 (m, 1H), 8.27–8.56 (br s, 2H), 9.16 (br s, 3H), 10.18 (br s, 1H). HRMS (ESI): *m/z* $[M+3H]^{3+}$ calcd. for $[C_{49}H_{78}N_{19}O_{12}]^{3+}$ 374.8687, found: 374.8701. RP-HPLC (220 nm): > 97% (t_R = 7.1 min, k = 8.2). $C_{49}H_{75}N_{19}O_{12} \cdot C_6H_3F_9O_6$ (1122.26 + 342.07).

(9S,12S,15S)-N-((S)-1-(((S)-1-(((S)-1-amino-3-(4-hydroxyphenyl)-1-oxopropan-2-yl)amino)-5-guanidino-1-oxopentan-2-yl)amino)-3-(1H-imidazol-5-yl)-1-oxopropan-2-yl)-15-(3-guanidinopropyl)-12-(4-hydroxybenzyl)-4-imino-2,11,14,17,20-pentaoxo-1,3,5,10,13,16,21-heptaazacyclopentacosane-9-carboxamide tetrakis(hydrotrifluoroacetate) (**4.6b**). The linear precursor peptide **4.6a** (20.4 mg, 11.75 µmol), HOBt (9.6 mg, 0.062 mmol) and DIPEA (32.7 µL, 0.13 mmol) were dissolved in DMF/NMP 8:2 v/v (500 µL) in a 100 mL round-bottom flask. Under stirring, a solution of PyBOP (21.9 mg, 0.062 mmol) in DMF/NMP 8:2 v/v (500 µL) was added, and the mixture was stirred at rt overnight. 0.1% aqueous TFA (30 mL) was added, followed by freeze-drying and purification by preparative HPLC (gradient: 0–30 min MeCN/0.1% aqueous TFA 10:90–25:75, t_R = 18 min) to yield **4.6b** as a white fluffy solid (10.0 mg, 53%).

^{1}H-NMR (600 MHz, DMSO-d_6): δ (ppm) 1.32–1.47 (m, 9H), 1.51 (s, 4H), 1.59 (s, 1H), 1.62–1.68 (m, 1H), 1.68–1.76 (m, 1H), 2.28–2.42 (m, 4H), 2.68–2.74 (m, 1H), 2.74–2.81 (m, 1H), 2.82–2.89 (m, 2H), 2.89–2.98 (m, 2H), 2.98–3.15 (m, 7H), 3.16–3.24 (m, 1H), 3.28 (br s, 2H), 4.04 (br s, 1H), 4.18–4.28 (m, 2H), 4.28–4.40 (m, 2H), 4.51–4.67 (m, 1H), 6.61–6.66 (m, 4H), 6.66–7.16 (br s, 4H, interfering with the next two listed signals), 6.99–7.03 (m, 4H), 7.05 (s, 1H), 7.16–7.73 (br s, 4H, interfering with the next four listed signals), 7.29 (s, 1H), 7.40 (s, 1H), 7.55 (s, 1H), 7.56–7.63 (m, 2H), 7.93 (br s, 2H), 7.98–8.06 (m, 2H), 8.09 (t, 2H, J = 7.6 Hz), 8.14 (br s, 1H), 8.33 (br s, 2H), 8.93 (br s, 1H), 9.20 (br s, 3H), 10.33 (br s, 1H), 14.18 (br s, 2H). HRMS (ESI): *m/z* $[M+3H]^{3+}$ calcd. for $[C_{51}H_{79}N_{20}O_{11}]^{3+}$ 382.5407, found: 382.5411. RP-HPLC (220 nm): > 97% (t_R = 6.8 min, k = 8.0). $C_{51}H_{76}N_{20}O_{11} \cdot C_8H_4F_{12}O_8$ (1145.30 + 456.09).

(S)-N-((S)-1-(((S)-1-amino-3-(4-hydroxyphenyl)-1-oxopropan-2-yl)amino)-5-guanidino-1-oxopentan-2-yl)-1-((9S,12S,15S)-15-(3-guanidinopropyl)-12-(4-

hydroxybenzyl)-4-imino-2,11,14,17,20-pentaoxo-1,3,5,10,13,16,21-heptaazacyclopentacosane-9-carbonyl)pyrrolidine-2-carboxamide tris(hydrotrifluoroacetate) (**4.7b**). The linear precursor peptide **4.7a** (14.6 mg, 9.21 µmol), HOBt (7.1 mg, 0.046 mmol) and DIPEA (16.1 µL, 0.092 mmol) were dissolved in DMF/NMP 8:2 v/v (500 µL) in a 100 mL round-bottom flask. Under stirring, a solution of PyBOP (24.0 mg, 0.046 mmol) in DMF/NMP 8:2 v/v (500 µL) was added, and the mixture was stirred at rt overnight. 0.1% aqueous TFA (30 mL) was added followed by freeze-drying and purification by preparative HPLC (gradient: 0–30 min MeCN/0.1% aqueous TFA 10:90–25:75, t_R = 19 min) to yield **4.7b** as a white powder (9.0 mg, 68%).

^{1}H-NMR (600 MHz, DMSO-d_6): δ (ppm) 1.30–1.52 (m, 11H), 1.52–1.58 (m, 2H), 1.58–1.67 (m, 2H), 1.67–1.82 (m, 3H), 1.82–1.92 (m, 1H), 1.97–2.08 (m, 1H), 2.25–2.40 (m, 4H), 2.66–2.80 (m, 2H), 2.80–2.96 (m, 3H), 2.96–3.14 (m, 7H), 3.14–3.20 (m, 1H), 3.22–3.29 (m, 2H), 3.48 (br s, 2H), 4.07 (br s, 1H), 4.10–4.17 (m, 1H), 4.28–4.36 (m, 2H), 4.36–4.44 (m, 1H), 4.49–4.60 (m, 1H), 6.60–6.65 (m, 4H), 6.65–7.13 (br s, 4H, interfering with the next two listed signals), 6.96–7.00 (m, 4H), 7.08 (s, 1H), 7.13–7.79 (br s, 4H, interfering with the next three listed signals), 7.36 (s, 1H), 7.52 (s, 2H), 7.66 (d, 1H, J = 8.1 Hz), 7.79–7.97 (m, 2H), 8.00–8.16 (m, 3H), 8.32 (br s, 2H), 9.13 (br s, 1H), 9.19 (s, 1H), 9.22 (s, 1H), 10.06 (br s, 1H). HRMS (ESI): m/z $[M+3H]^{3+}$ calcd. for $[C_{50}H_{79}N_{18}O_{11}]^{3+}$ 369.2053, found: 369.2066. RP-HPLC (220 nm): > 97% (t_R = 8.4 min, k = 9.9). $C_{50}H_{76}N_{18}O_{11} \cdot C_6H_3F_9O_6$ (1105.27 + 342.07).

(9S,12S,15S)-N-((S)-1-(((S)-1-(((S)-1-amino-3-(4-hydroxyphenyl)-1-oxopropan-2-yl)amino)-5-guanidino-1-oxopentan-2-yl)amino)-3,3-dimethyl-1-oxobutan-2-yl)-15-(3-guanidinopropyl)-12-(4-hydroxybenzyl)-4-imino-2,11,14,17,20-pentaoxo-1,3,5,10,13,16,21-heptaazacyclopentacosane-9-carboxamide tris(hydrotrifluoroacetate) (**4.8b**). The linear precursor peptide **4.8a** (10.9 mg, 6.81 µmol), HOBt (5.2 mg, 0.034 mmol) and DIPEA (11.9 µL, 0.068 mmol) were dissolved in DMF/NMP 8:2 v/v (500 µL) in a 100 mL round-bottom flask. Under stirring, a solution of PyBOP (17.7 mg, 0.034 mmol) in DMF/NMP 8:2 v/v (500 µL) was added and the mixture was stirred at rt overnight. 0.1% aqueous TFA (30 mL) was added followed by freeze-drying and purification by preparative HPLC (gradient: 0–30 min MeCN/0.1% aqueous TFA 15:85–35:65, t_R = 11 min) to yield **4.8b** as a white fluffy solid (8.0 mg, 80%).

^{1}H-NMR (600 MHz, DMSO-d_6): δ (ppm) 0.89 (s, 9H), 1.31–1.48 (m, 9H), 1.48–1.58 (m, 4H), 1.58–1.66 (m, 2H), 1.70–1.78 (m, 1H), 2.21–2.41 (m, 4H), 2.68–2.79 (m, 2H), 2.79–2.87 (m, 2H), 2.87–2.95 (m, 1H), 2.98–3.09 (m, 5H), 3.09–3.20 (m, 2H), 3.27 (br s, 2H), 4.10 (m, 1H), 4.17–4.31 (m, 2H), 4.31–4.37 (m, 1H), 4.37–4.43 (m, 2H), 6.60–6.65 (m, 4H), 6.65–7.09 (br s, 4H, interfering with the next one listed signals), 6.96–7.01 (m, 5H), 7.09–7.73 (br s, 4H, interfering with the next three listed signals), 7.36 (s, 1H), 7.45–7.48 (m, 2H), 7.49–7.56 (m, 2H), 7.80–7.91 (m, 3H), 7.99–8.12 (m, 2H), 8.20–8.46 (m, 3H), 9.01–9.30 (m, 3H), 9.92 (br s, 1H). HRMS (ESI): *m/z* $[M+3H]^{3+}$ calcd. for $[C_{51}H_{83}N_{18}O_{11}]^{3+}$ 374.5491, found: 374.5500. RP-HPLC (220 nm): > 97% (t_R = 9.9 min, k = 12.1). $C_{51}H_{80}N_{18}O_{11} \cdot C_6H_3F_9O_6$ (1121.32 + 342.07).

(9S,12S,15S)-N-((S)-2-(((S)-1-(((S)-1-amino-3-(4-hydroxyphenyl)-1-oxopropan-2-yl)amino)-5-guanidino-1-oxopentan-2-yl)amino)-1-cyclopentyl-2-oxoethyl)-15-(3-guanidinopropyl)-12-(4-hydroxybenzyl)-4-imino-2,11,14,17,20-pentaoxo-1,3,5,10,13,16,21-heptaazacyclopentacosane-9-carboxamide tris(hydrotrifluoroacetate) (**4.9b**). The linear precursor peptide **4.9a** (7.8 mg, 4.83 µmol), HOBt (3.7 mg, 0.024 mmol) and DIPEA (8.4 µL, 0.048 mmol) were dissolved in DMF/NMP 8:2 v/v (500 µL) in a 100 mL round-bottom flask. Under stirring, a solution of PyBOP (12.6 mg, 0.024 mmol) in DMF/NMP 8:2 v/v (500 µL) was added and the mixture was stirred at rt overnight. 0.1% aqueous TFA (30 mL) was added followed by freeze-drying and purification by preparative HPLC (gradient: 0–30 min MeCN/0.1% aqueous TFA 10:90–35:65, t_R = 17 min) to yield **4.9b** as a white powder (4.3 mg, 60%).

^{1}H-NMR (600 MHz, DMSO-d_6): δ (ppm) 1.14–1.30 (m, 3H), 1.41 (s, 11H), 1.51 (s, 7H), 1.56–1.68 (m, 3H), 1.68–1.77 (m, 1H), 2.03–2.15 (m, 1H), 2.24–2.40 (m, 4H), 2.66–2.79 (m, 2H), 2.79–2.87 (m, 2H), 2.87–2.95 (m, 1H), 2.95–3.08 (m, 5H), 3.11 (br s, 1H), 3.15–3.20 (m, 1H), 3.24–3.28 (br s, 2H), 4.07 (br s, 1H), 4.14–4.25 (m, 2H), 4.27–4.40 (m, 3H), 6.58–6.65 (m, 4H), 6.65–7.08 (br s, 4H, interfering with the next two listed signals), 6.95–7.00 (m, 4H), 7.02 (s, 1H), 7.08–7.63 (br s, 4H, interfering with the next two listed signals), 7.36 (s, 1H), 7.51 (s, 2H), 7.71–7.80 (m, 2H), 7.82–7.95 (m, 2H), 8.01 (d, 1H, J = 7.8 Hz), 8.05–8.18 (m, 2H), 8.32 (s, 2H), 9.03–9.18 (m, 2H), 9.20 (s, 1H), 10.11 (br s, 1H). HRMS (ESI): m/z $[M+3H]^{3+}$ calcd. for $[C_{52}H_{83}N_{18}O_{11}]^{3+}$ 378.5491, found: 378.5503. RP-HPLC (220 nm): > 97% (t_R = 10.4 min, k = 12.6). $C_{52}H_{80}N_{18}O_{11} \cdot C_6H_3F_9O_6$ (1133.33 + 342.07).

(9S,12S,15S)-N-((2S,3R)-1-(((S)-1-(((S)-1-amino-3-(4-hydroxyphenyl)-1-oxopropan-2-yl)amino)-5-guanidino-1-oxopentan-2-yl)amino)-3-methyl-1-oxopentan-2-yl)-15-(3-guanidinopropyl)-12-(4-hydroxybenzyl)-4-imino-2,11,14,17,20-pentaoxo-1,3,5,10,13,16,21-heptaazacyclopentacosane-9-carboxamide tris(hydrotrifluoroacetate) (**4.10b**). The linear precursor peptide **4.10a** (14.1 mg, 8.84 µmol), HOBt (6.8 mg, 0.044 mmol) and DIPEA (15.4 µL, 0.088 mmol) were dissolved in DMF/NMP 8:2 v/v (500 µL) in a 100 mL round-bottom flask. Under stirring, a solution of PyBOP (23.0 mg, 0.044 mmol) in DMF/NMP 8:2 v/v (500 µL) was added, and the mixture was stirred at rt overnight. 0.1% aqueous TFA (30 mL) was added, followed by freeze-drying and purification by preparative HPLC (gradient: 0–30 min MeCN/0.1% aqueous TFA 5:95–25:75, t_R = 25 min) to yield **4.10b** as a white fluffy solid (10.6 mg, 82%).

^{1}H-NMR (600 MHz, DMSO-d_6): δ (ppm) 0.77 (d, 3H, J = 6.8 Hz), 0.84 (t, 3H, J = 7.4 Hz), 1.03–1.12 (m, 1H), 1.27–1.34 (m, 1H), 1.35–1.47 (m, 9H), 1.47–1.58 (m, 4H), 1.58–1.70 (m, 2H), 1.69–1.85 (m, 2H), 2.23–2.42 (m, 4H), 2.68–2.79 (m, 2H), 2.79–2.88 (m, 2H), 2.88–2.94 (m, 1H), 2.97–3.09 (m, 5H), 3.01–3.15 (m, 1H), 3.16–3.22 (m, 1H), 3.25–3.30 (br s, 2H), 4.09 (br s, 1H), 4.22–4.30 (m, 1H), 4.30–4.36 (m, 2H), 4.36–4.43 (m, 2H), 6.60–6.66 (m, 4H), 6.66–7.12 (br s, 4H, interfering with the next two listed signals), 6.96–7.01 (m, 4H), 7.04 (s, 1H), 7.12–7.78 (br s, 4H, interfering with the next three listed signals), 7.37 (s, 1H), 7.55 (s, 3H), 7.63–7.66 (m, 1H), 7.79–7.83 (m, 1H), 7.87 (s, 2H), 7.93–8.03 (m, 1H), 8.08 (s, 1H), 8.13–8.25 (m, 1H), 8.34 (br s, 2H), 9.03–9.35 (m, 3H), 9.95–10.37 (br s, 1H). HRMS (ESI): *m/z* $[M+3H]^{3+}$ calcd. for $[C_{51}H_{83}N_{18}O_{11}]^{3+}$ 374.5491, found: 374.5503. RP-HPLC (220 nm): > 97% (t_R = 8.9 min, k = 10.7). $C_{51}H_{80}N_{18}O_{11} \cdot C_6H_3F_9O_6$ (1121.32 + 342.07).

(9S,12S,15S)-N-((S)-1-(((S)-1-(((S)-1-amino-3-(4-hydroxyphenyl)-1-oxopropan-2-yl)amino)-6-guanidino-1-oxohexan-3-yl)amino)-4-methyl-1-oxopentan-2-yl)-15-(3-guanidinopropyl)-12-(4-hydroxybenzyl)-4-imino-2,11,14,17,20-pentaoxo-1,3,5,10,13,16,21-heptaazacyclopentacosane-9-carboxamide tris(hydrotrifluoroacetate) (**4.11b**). The linear precursor peptide **4.11a** (14.6 mg, 9.04 µmol), HOBt (6.9 mg, 0.045 mmol) and DIPEA (15.7 µL, 0.090 mmol) were dissolved in DMF/NMP 8:2 v/v (500 µL) in a 100 mL round-bottom flask. Under stirring, a solution of PyBOP (23.5 mg, 0.045 mmol) in DMF/NMP 8:2 v/v (500 µL) was added and the mixture was stirred at rt overnight. 0.1% aqueous TFA (30 mL) was added

followed by freeze-drying and purification by preparative HPLC (gradient: 0–30 min MeCN/0.1% aqueous TFA 10:90–25:75, t_R = 23 min) to yield **4.11b** as a white powder (5.1 mg, 38%).

^{1}H-NMR (600 MHz, DMSO-d_6): δ (ppm) 0.83 (d, 3H, J = 6.50 Hz), 0.91 (d, 3H, J = 6.64 Hz), 1.18–1.32 (m, 3H), 1.32–1.49 (m, 11H), 1.49–1.68 (m, 6H), 1.74 (m, 1H), 2.27–2.40 (m, 4H), 2.60–2.67 (m, 1H), 2.70–2.81 (m, 1H), 2.81–2.95 (m, 3H), 2.95–3.08 (m, 6H), 3.08–3.16 (m, 1H), 3.17–3.24 (m, 1H), 3.29 (br s, 2H), 3.93–3.99 (m, 1H), 4.05 (br s, 1H), 4.14–4.23 (m, 1H), 4.23–4.32 (m, 1H), 4.32–4.40 (m, 2H), 6.61–6.66 (m, 4H), 6.66–7.14 (br s, 4H, interfering with the next two listed signals), 6.99–7.02 (m, 4H), 7.04 (s, 1H), 7.14–7.82 (br s, 4H, interfering with the next four listed signals), 7.39 (s, 1H), 7.44–7.47 (m, 1H), 7.49–7.54 (m, 2H), 7.71–7.77 (m, 2H), 7.88–7.94 (m, 1H), 7.97 (s, 1H, J = 8.4 Hz), 8.00–8.10 (m, 1H), 8.16 (br s, 1H), 8.31 (br s, 2H), 9.01–9.40 (m, 3H), 10.07 (br s, 1H). HRMS (ESI): *m/z* $[M+3H]^{3+}$ calcd. for $[C_{52}H_{85}N_{18}O_{11}]^{3+}$ 379.2210, found: 379.2220. RP-HPLC (220 nm): > 97% (t_R = 9.8 min, k = 11.9). $C_{52}H_{82}N_{18}O_{11} \cdot C_6H_3F_9O_6$ (1135.34 + 342.07).

(9S,12S,15S)-N-((S)-1-(((S)-1-(((S)-4-amino-1-(4-hydroxyphenyl)-4-oxobutan-2-yl)amino)-5-guanidino-1-oxopentan-2-yl)amino)-4-methyl-1-oxopentan-2-yl)-15-(3-guanidinopropyl)-12-(4-hydroxybenzyl)-4-imino-2,11,14,17,20-pentaoxo-1,3,5,10,13,16,21-heptaazacyclopentacosane-9-carboxamide tris(hydrotrifluoroacetate) (**4.12b**). The linear precursor peptide **4.12a** (19.4 mg, 12.05 µmol), HOBt (9.3 mg, 0.060 mmol) and DIPEA (21.0 µL, 0.12 mmol) were dissolved in DMF/NMP 8:2 v/v (500 µL) in a 100 mL round-bottom flask. Under stirring, a solution of PyBOP (31.4 mg, 0.060 mmol) in DMF/NMP 8:2 v/v (500 µL) was added, and the mixture was stirred at rt overnight. 0.1% aqueous TFA (30 mL) was added, followed by freeze-drying and purification by preparative HPLC (gradient: 0–30 min MeCN/0.1% aqueous TFA 10:90–30:70, t_R = 19 min) to yield **4.12b** as a white powder (8.8 mg, 50%).

^{1}H-NMR (600 MHz, DMSO-d_6): δ (ppm) 0.83 (d, 3H, J = 6.50 Hz), 0.91 (d, 3H, J = 6.64 Hz), 1.30–1.50 (m, 12H), 1.54 (s, 3H), 1.58–1.71 (m, 3H), 1.71–1.85 (m, 1H), 2.07–2.20 (m, 2H), 2.24–2.44 (m, 4H), 2.55–2.61 (m, 2H), 2.71–2.80 (m, 1H), 2.84 (br s, 1H), 2.90–2.98 (m, 1H), 2.98–3.09 (m, 5H), 3.12 (br s, 1H), 3.29 (br s, 2H), 4.06 (br s, 1H), 4.10–4.23 (m, 2H), 4.23–4.33 (m, 2H), 4.33–4.37 (m, 2H), 4.37–4.43 (m, 1H), 6.50–7.13 (br s, 4H, interfering with the next four listed signals), 6.62–6.66

(m, 4H), 6.83 (s, 1H), 6.93 (d, 2H, *J* = 8.32 Hz), 7.00 (d, 2H, *J* = 8.32 Hz), 7.13–7.79 (br s, 4H, interfering with the next three listed signals), 7.29 (s, 1H), 7.48–7.52 (m, 2H), 7.55 (s, 1H), 7.79–7.83 (m, 1H), 7.85–8.00 (m, 4H), 8.00–8.12 (m, 1H), 8.12–8.23 (br s, 1H), 8.34 (s, 2H), 9.06–9.28 (m, 2H), 10.04 (s, 1H). HRMS (ESI): *m/z* $[M+3H]^{3+}$ calcd. for $[C_{52}H_{85}N_{18}O_{11}]^{3+}$ 379.2210, found: 379.2221. RP-HPLC (220 nm): > 97% (t_R = 10.5 min, *k* = 12.8). $C_{52}H_{82}N_{18}O_{11} \cdot C_6H_3F_9O_6$ (1135.34 + 342.07).

(9S,12S,15S)-N-((S)-2-(((S)-1-(((S)-1-amino-3-(4-hydroxyphenyl)-1-oxopropan-2-yl)amino)-6-guanidino-1-oxohexan-3-yl)amino)-1-cyclopentyl-2-oxoethyl)-15-(3-guanidinopropyl)-12-(4-hydroxybenzyl)-4-imino-2,11,14,17,20-pentaoxo-1,3,5,10,13,16,21-heptaazacyclopentacosane-9-carboxamide tris(hydrotrifluoroacetate) (**4.13b**). The linear precursor peptide **4.13a** (19.4 mg, 11.96 µmol), HOBt (9.2 mg, 0.060 mmol) and DIPEA (20.8 µL, 0.12 mmol) were dissolved in DMF/NMP 8:2 v/v (500 µL) in a 100 mL round-bottom flask. Under stirring, a solution of PyBOP (31.1 mg, 0.060 mmol) in DMF/NMP 8:2 v/v (500 µL) was added and the mixture was stirred at rt overnight. 0.1% aqueous TFA (30 mL) was added, followed by freeze-drying and purification by preparative HPLC (gradient: 0–30 min MeCN/0.1% aqueous TFA 10:90–25:75, t_R = 24 min) to yield **4.13b** as a white fluffy solid (10 mg, 56%).

^{1}H-NMR (600 MHz, DMSO-d_6): δ (ppm) 0.92–1.31 (m, 4H), 1.32–1.47 (m, 11H), 1.52 (s, 6H), 1.59–1.68 (s, 2H), 1.69–1.81 (m, 1H), 2.02–2.11 (m, 1H), 2.11–2.20 (m, 1H), 2.24–2.42 (m, 5H), 2.58–2.69 (m, 1H), 2.69–2.80 (m, 1H), 2.81–3.01 (m, 4H), 3.01–3.09 (m, 4H), 3.12 (br s, 1H), 3.16–3.23 (s, 1H), 3.29 (br s, 2H), 3.94–3.99 (m, 1H), 4.03–4.20 (m, 2H), 4.20–4.56 (m, 3H), 6.54–7.17 (br s, 4H, interfering with the next three listed signals), 6.62–6.66 (m, 4H), 6.98–7.02 (m, 4H), 7.05 (s, 1H), 7.17–7.69 (br s, 4H, interfering with the next three listed signals), 7.41 (s, 1H), 7.46–7.49 (m, 1H), 7.50–7.57 (m, 2H), 7.73 (d, 1H, *J* = 8.3 Hz), 7.84 (d, 1H, *J* = 8.3 Hz), 7.87–7.93 (m, 2H), 7.98 (d, 1H, *J* = 8.3 Hz), 8.04–8.22 (m, 2H), 8.32 (br s, 2H), 8.97–9.41 (m, 3H), 10.10 (s, 1H). HRMS (ESI): *m/z* $[M+3H]^{3+}$ calcd. for $[C_{53}H_{85}N_{18}O_{11}]^{3+}$ 383.2210, found: 383.2218. RP-HPLC (220 nm): > 97% (t_R = 11.7 min, *k* = 14.1). $C_{53}H_{82}N_{18}O_{11} \cdot C_6H_3F_9O_6$ (1147.35 + 342.07).

(9S,12S,15S)-N-((S)-2-(((S)-1-(((S)-4-amino-1-(4-hydroxyphenyl)-4-oxobutan-2-yl)amino)-6-guanidino-1-oxohexan-3-yl)amino)-1-cyclopentyl-2-oxoethyl)-15-(3-guanidinopropyl)-12-(4-hydroxybenzyl)-4-imino-2,11,14,17,20-pentaoxo-

1,3,5,10,13,16,21-heptaazacyclopentacosane-9-carboxamide (**4.14b**). The linear precursor peptide **4.14a** (20.4 mg, 12.46 µmol), HOBt (9.5 mg, 0.062 mmol) and DIPEA (21.7 µL, 0.13 mmol) were dissolved in DMF/NMP 8:2 v/v (500 µL) in a 100 mL round-bottom flask. Under stirring, a solution of PyBOP (21.7 mg, 0.062 mmol) in DMF/NMP 8:2 v/v (500 µL) was added, and the mixture was stirred at rt overnight. 0.1% aqueous TFA (30 mL) was added, followed by freeze-drying and purification by preparative HPLC (gradient: 0–30 min MeCN/0.1% aqueous TFA 10:90–25:75, t_R = 23 min) to yield **4.14b** as a white solid (13 mg, 69%).

^{1}H-NMR (600 MHz, DMSO-d_6): δ (ppm) 1.09–1.31 (m, 3H), 1.31–1.49 (m, 12H), 1.53 (s, 6H), 1.59–1.69 (s, 2H), 1.69–1.81 (m, 1H), 2.03–2.12 (m, 2H), 2.12–2.18 (m, 2H), 2.18–2.25 (m, 1H), 2.23–2.4 (m, 4H), 2.52–2.61 (m, 2H), 2.70–2.88 (m, 2H), 2.88–2.96 (m, 1H), 2.96–3.15 (m, 6H), 3.17–3.23 (s, 1H), 3.29 (br s, 2H), 3.93–4.03 (m, 1H), 4.05–4.10 (m, 2H), 4.14–4.18 (m, 1H), 4.31–4.38 (m, 2H), 6.62–6.66 (m, 4H), 6.66–7.12 (br s, 4H, interfering with the next three listed signals), 6.82 (s, 1H), 6.92–6.95 (m, 2H), 6.99–7.03 (s, 2H), 7.17–7.71 (br s, 4H, interfering with the next two listed signals), 7.41 (s, 1H), 7.51–7.57 (m, 3H), 7.71–7.79 (m, 2H), 7.79–7.86 (m, 1H), 7.86–8.01 (m, 2H), 8.04–8.21 (m, 2H), 8.33 (s, 2H), 9.04–9.37 (m, 3H), 10.20 (s, 1H). HRMS (ESI): *m/z* $[M+3H]^{3+}$ calcd. for $[C_{54}H_{87}N_{18}O_{11}]^{3+}$ 387.8929, found: 387.8936. RP-HPLC (220 nm): > 97% (t_R = 11.9 min, k = 14.4). $C_{54}H_{84}N_{18}O_{11} \cdot C_6H_3F_9O_6$ (1161.38 + 342.07).

4.2.2.8 Cell culture

Cells were cultured in T75 or T175 flasks (Sarstedt, Nümbrecht, Germany) in a humidified atmosphere (95% air, 5% CO_2) at 37 °C. SK-N-MC neuroblastoma cells (obtained from the American Type Culture Collection, ATCC HTB-10) were maintained in EMEM supplemented with 5% FBS. CHO-hY_2R cells (obtained from PerkinElmer, Rodgau, Germany) were cultured in Ham's F-12 supplemented with 5% FBS and G418 (400 µg/mL). CHO-hY_4-G_{qi5}-mtAEQ cells[24] were cultured in HAM's F-12 supplemented with 10% FBS, hygromycin (400 µg/mL), zeocin (250 µg/mL), and G418 (400 µg/mL). HEC-1B-hY_5 cells[25] were maintained in EMEM supplemented with 5% FBS and G418 (400 µg/mL).

4.2.2.9 Buffers and media used for binding and functional assays

Buffer II (used for binding experiments at the Y_1R, Y_2R, and Y_5R): an isotonic sodium-containing HEPES buffer (150 mM NaCl, 10 mM HEPES, 25 mM $NaHCO_3$, 2.5 mM $CaCl_2$, 5 mM KCl, pH 7.4) supplemented with 1% BSA. *DPBS* (used for binding studies at Y_4R): Dulbecco's phosphate-buffered saline with calcium and magnesium (1.8 mM $CaCl_2$, 2.68 mM KCl, 1.47 mM KH_2PO_4, 3.98 mM $MgSO_4$, 137 mM NaCl, 8.06 mM Na_2HPO_4, pH 7.4) supplemented with 1% BSA and 0.1 mg/mL bacitracin. L-15 medium (used for the CAMYEN assays): phenol red-free Leibovitz's L-15 medium (140 mM NaCl, 1.3 mM $CaCl_2$,1 mM $MgCl_2$, various amino acids and vitamins, pH 7.4) supplemented with 10 mM HEPES and 5% FBS.

4.2.2.10 Radioligand binding assays

Y_1R Binding. Competition binding experiments at Y_1R-expressing SK-N-MC neuroblastoma cells were performed in *buffer II* as described previously[26] using the radioligand [^{3}H]UR-MK299 (K_d = 0.058 nM,[27] used concentration: 0.075 nM) (see structure in Figure A2.1, *Section 2.6 Appendix*; *Chapter 2*). Experiments were performed in triplicate. Due to low radioligand displacement, no curve fitting was performed for the studied cyclic peptides **4.2b**, **4.4b–4.10b**, and **4.12b–4.14b**. In the case of **4.3b** and **4.11b**, radioligand displacement at the highest concentration amounted to at least 70%. The pIC_{50} value was obtained by plotting $\log[B/(B_0 - B)]$ (Hill plot; B denotes specifically bound radioligand in the presence of a competitor (values between 10% and 90%), and B_0 denotes the specifically bound radioligand in the absence of a competitor (B_0 = 100%)) over log(competitor concentration) followed by linear regression (pIC_{50} corresponds to the intercept with the X-axis; $\log[B/(B_0 - B)] = 0$). The pIC_{50} values were converted to IC_{50} values, followed by calculating K_i and pK_i values via the Cheng-Prusoff equation.[28]

Y_2R Binding. Competition binding experiments at CHO-hY_2R cells were performed in *buffer II* as previously reported using the radioligand [K^4-[^{3}H]propionyl]hPYY (K_d = 0.16 nM; concentration used: 0.3 nM) (see structure in Figure A4.1, *Section 4.6 Appendix*).[27] Experiments were performed in triplicate. Due to low radioligand displacement, no curve fitting was applied for the studied cyclic peptides **4.2b–4.14b**.

Y_4R Binding. Y_4R competition binding studies with [^{3}H]**2.5** ([^{3}H]UR-JG102; see structure in Figure 2.2, *Section 2.6 Appendix*; *Chapter 2*) were performed with

suspensions of intact CHO-hY_4-G_{qi5}-mtAEQ cells[24] in *DPBS,* as described by Gleixner *et al*.[29] Each experiment was carried out in triplicate. Total binding data (dpm) from radioligand competition binding experiments (including total binding in the absence of competitor) were plotted against log(concentration competitor) and analyzed by a four-parameter logistic equation (log(inhibitor) vs. response-variable slope, GraphPad Prism 10, GraphPad Software, San Diego, California, United States) followed by normalization (100% = 'top' of the four-parameter logistic fit, 0% = unspecifically bound radioligand) and analysis of the normalized data by a four-parameter logistic equation. pIC_{50} and IC_{50} values from individual experiments were converted to pK_i and K_i values according to the Cheng-Prusoff equation.[28]

Y_5R Binding. Competition binding experiments at HEC-1B-hY_5R cells[25] were performed in *buffer II* using the radioligand [^{3}H]propionyl-pNPY (K_d = 11 nM,[30] used concentration: 5 nM) (see structure in Figure A2.1, Section 2.6 Appendix; Chapter 2).[14] Experiments were performed in triplicate. Due to low radioligand displacement, no curve fitting was performed for cyclic peptides **4.2b–4.10b**, **4.12b**, and **4.13b**. In the case of **4.11b** and **4.14b**, radioligand displacement at the highest concentration amounted to at least 80%. The pIC_{50} value was obtained by plotting log[B/(B_0 − B)] (Hill plot; B denotes specifically bound radioligand in the presence of a competitor (values between 10% and 90%), and B_0 denotes the specifically bound radioligand in the absence of a competitor (B_0 = 100%)) over log(competitor concentration) followed by linear regression (pIC_{50} corresponds to the intercept with the X-axis; log[B/(B_0 − B)] = 0). The pIC_{50} values were converted to IC_{50} values, after which the K_i and pK_i values were computed using the Cheng-Prusoff equation.[28]

4.2.2.11 Y_4R cAMP CAMYEN-assay

The assay was performed with HEK293T-CAMEYN-hY_4R cells in agonist mode, as reported.[29] Experiments were performed in triplicate. Data were analyzed as reported[29] using GraphPad Prism 10 (GraphPad Software): raw BRET ratios were determined by dividing the acceptor fluorescence (520–580 nm) by the donor luminescence (< 470 nm). Baseline-corrected relative cAMP responses were calculated by dividing data by the buffer control (with no forskolin). The area under the curve for the 60 min read was taken for each agonist concentration and was normalized to the response of 1 µM hPP (100%) and the effect of 10 µM forskolin in the absence of agonist (0%). The normalized responses were plotted against

log[Y_4R agonist], and concentration-response curves were generated using the four-parameter logistic equation (GraphPad Prism 10) to obtain pEC_{50} values. Efficacies E_{max} corresponds to the upper plateaus of the normalized concentration-response curves.

4.2.2.12 *In vitro* human plasma stability assay

The stabilities of the peptides in human heparinized plasma were investigated in triplicate at 37 °C using a modified method described by Pegoli *et al*.[31] 1-Methyl-D-tryptophane (Sigma) (IS) was used as internal standard (note: as the purity of 1-methyl-D-tryptophane was < 95%, it was repurified by preparative HPLC to give a purity of > 99%, data not shown). For the plasma stability and recovery determination, the peptide concentration used was 40 µM. In contrast to the method described by Pegoli *et al*.,[31] for protein precipitation, 93 µL of ice-cold EtOH/MeCN (50:50 v/v) were added to 46 µL aliquots of plasma/PBS (136.9 mM NaCl, 2.68 mM KCl, 5.62 mM Na_2HPO_4, 1.09 mM NaH_2PO_4, and 1.47 mM KH_2PO_4, pH 7.4) (1:2 v/v) containing the peptide and IS immediately followed by vortexing (3–4 min). To determine recoveries, the proteins were precipitated immediately after adding the peptides to plasma/PBS (1:2 v/v) already containing IS. After vortexing, samples were centrifuged at 16,100 g at 4 °C for 10 min. This was followed by transferring 120 µL aliquots of the supernatant into 1.5-mL reaction vessels containing 10% aqueous TFA (3 µL). Further processing was carried out as described but slightly modified by using 70 µL MeCN/0.04% aqueous TFA (1:9 v/v) to take up the residues.[31] The studied incubation times were 1 h, 6 h, 24 h, 48 h and 72 h.

Samples were analyzed by analytical RP-HPLC using the system and conditions as previously described above (*Section 4.2.2.4 Analytical HPLC*) using the linear gradient: 0–14 min: MeCN/0.04% aqueous TFA 5:95-25:75, 14–15 min: 25:75-95:5, 15–19 min: 95:5 (isocratic). The obtained recoveries and the recovery ratios (peptide/internal standard) are summarized in Table A4.3 (see *Section 4.6 Appendix*). Data analysis was based on UV detection at 220 nm.

4.2.2.13 Induced fit docking (IFD) experiments

Geometries of the peptide ligands were prepared and energetically optimized using the LigPrep module (Maestro, Schrödinger LLC) to generate valid 3D models and charges. Both arginine residues and the carbamoyl-guanidine group within the

macrocycle were protonated, resulting in a formal charge of +3 for the ligands except for **4.6b** which had a charge of +4. A recently published Cryo-EM structure of the Y_4R in complex with PP and G_i (PDB ID: 7x9c) was used.[32] The G protein subunits *(alpha1, beta1, and gamma2)* were removed beforehand, and missing connections/loops *(between TM5 and TM6: Lys250 – break – Arg256)* were not filled in, to stay closer to the original crystal structure. The receptor was prepared using the standard procedures for the protein preparation wizard and workflow (Schrödinger LLC).

Using standard parameters, the ligands could not enter the binding site (Van-der-Waals scaling ≥ 0.70). Therefore, the Van-der-Waals-Scaling of the ligands and receptor were reduced. Reducing these parameters lowered the energetic barrier and allowed the ligands to enter the expected binding site more consistently. The final scaling factor used was 0.60 for both receptor and ligand during both docking stages *(single precision and extra precision)*. This approach resulted in docking poses (with the lowest scores) where the C-terminal tyrosine of the peptide ligands was positioned in or close to the orthosteric binding pocket except for **4.10b**, whose lowest score pose showed a location of the C-terminal Tyr outside the binding pocket.

4.3 Results and Discussion

4.3.1 Angiotensin-converting enzyme is responsible for degrading UR-AK86C (2.4)

To identify the enzyme(s) responsible for the proteolytic degradation of **2.4** in human plasma, the different degradative products were determined. Using LC-HRMS, analysis of the plasma samples revealed the presence of the cyclic tetrapeptide F1 as an N-terminal fragment and the amidated dipeptide F2 as a C-terminal fragment (Figure 4.3) among others. Based on their concentrations, the tetrapeptide F1 and the dipeptide F2 were identified as the major degradation products suggesting that the main proteolytic degradation of **2.4** occurs at the bond between Leu^4 and Arg^5. Furthermore, the investigations showed that the cyclic tetrapeptide F1 displays high stability, i.e. was not further degraded, being in agreement with the high proteolytic stability known for cyclic peptides.[33, 34] However, F1 is inactive in terms of Y_4R binding and activation since the amidated dipeptide in **2.4**, i.e. Arg-Tyr-NH_2, is crucial for receptor recognition.

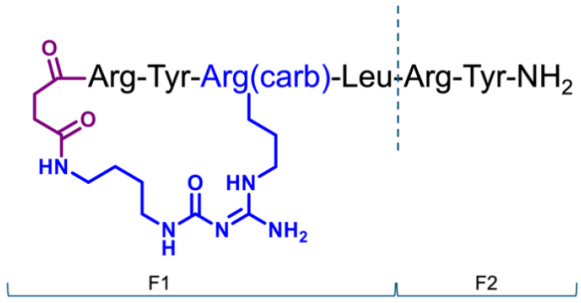

Arg(carb) = N^{ω}-carbamoylated arginine

Figure 4.3. Major enzymatic cleavage sites (dashed lines) of **2.4**, identified by the detection of fragments F1 and F2 by LC-HRMS analysis after incubation in human plasma/PBS 1:2 v/v.

To explore what type of peptidase is responsible for degrading **2.4**, its stability in plasma was investigated in the presence of various protease inhibitors. The protease inhibitors used were selected using the MEROPS peptidase database[35] and the Peptide Atlas[36]: Using MEROPS, peptidases described as potentially cleaving Leu-Arg bonds in peptides or proteins were identified, while Peptide Atlas was used to identify those known to be present in human blood plasma. This search yielded the serine endopeptidase matriptase (EC 3.4.21.109), the metalloprotease angiotensin converting enzyme (ACE) (EC 3.4.15.1), the cysteinyl proteases calpain-1/2/3 (EC 3.4.22.52/43/54) and metalloproteases such as carboxypeptidase U (plasma

carboxypeptidase B) (EC 3.4.17.20) or carboxypeptidase N (EC 3.4.17.3) as the most possible candidates. To investigate their putative activity on the degradation of the cyclic Y_4R ligands, **2.4** was incubated in human plasma in the absence and presence of inhibitors known to inhibit these enzymes (50 µM aprotinin to inhibit matriptase, 5 µM ramipril to inhibit ACE, 5 µM E-64 ((2*S*,3*S*)-3-(((*S*)-1-((4-guanidinobutyl)amino)-4-methyl-1-oxopentan-2-yl)carbamoyl)oxirane-2-carboxylic acid) to inhibit calpains and 20 µM 2-GEMSA (2-((2-guanidinoethyl)mercapto)succinic acid) for inhibition of carboxypeptidases) at 37 °C for 6 h. These studies showed that only ramipril inhibited the degradation of **2.4** (Figure 4.4), indicating that the dipeptidyl carboxypeptidase ACE is responsible for the observed enzymatic degradation (cleavage of the Leu^4-Arg^5 bond) of the studied peptides. It should be noted that ramipril, being a prodrug (ethyl ester) of the more active form ramiprilat, also represents a potent ACE inhibitor (pIC_{50} = 7.6).[37] Moreover, LC-HRMS analysis of the samples revealed that ramipril was in part hydrolyzed yielding ramiprilat (data not shown).

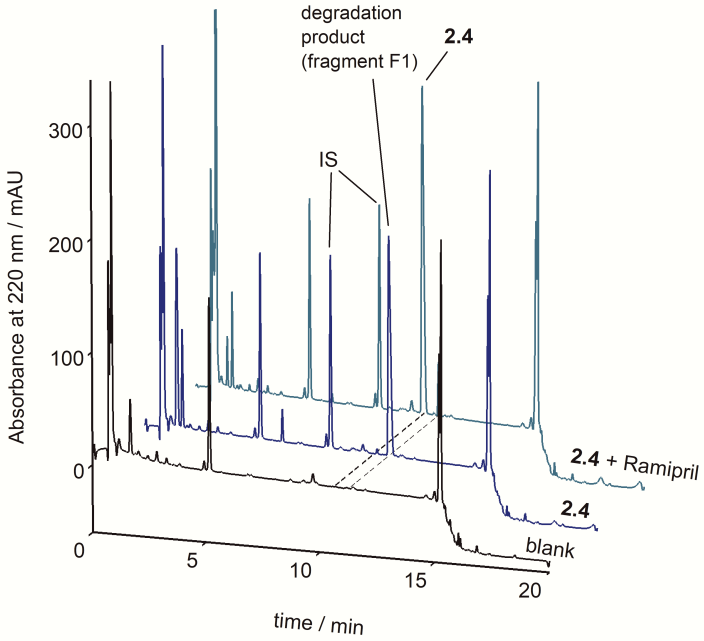

Figure 4.4. Chromatograms of the RP-HPLC analysis of **2.4** after incubation in human plasma/PBS (1:2 v/v) at 37 °C for 6 h. In the presence of the ACE inhibitor ramipril, which was partially converted to the more potent ACE inhibitor ramiprilat, the degradation of **2.4** was markedly inhibited, showing that it is a substrate of the dipeptidyl carboxypeptidase ACE. The initial concentration of the peptides in human plasma/PBS (1:2 v/v) was 100 µM. IS: internal standard.

4.3.2 Synthesized potential plasma stable analogs and their characterization

Following the finding that the Leu^4-Arg^5 bond is susceptible to ACE cleavage, several strategies were considered to improve the stability of this bond while considering the

effect of structural changes on the Y_4R binding affinity of the peptide. According to the location of the major proteolytic cleavage site in **2.4**, the structural modifications were focused on the exocyclic fragment (Leu^4-Arg^5-Tyr^6-NH_2) in **2.4**. The pursued approaches included N-methylation of the Leu^4-Arg^5 amide bond, replacement of Leu, Arg, and/or Tyr by natural or artificial amino acid analogs, and elongation of the peptide backbone by introducing β-homo amino acids. Other considered strategies were reducing the carboxylic group in the amide bond, replacing the Leu^4-Arg^5 bond with an azapeptide of Leu^4-Arg^5, or introducing peptoid analogs. However, these were not accomplished due to their incompatibility with solid phase peptide synthesis (SPPS) and/or their non-feasibility.

Compd.	Peptide sequence
2.4	cyclo[succinyl-Arg-Tyr-Arg(carb)]-Leu-Arg-Tyr-NH_2
4.2b	cyclo[succinyl-Arg-Tyr-Arg(carb)]-Leu-*N*(Me)-Arg-Tyr-NH_2
4.3b	cyclo[succinyl-Arg-Tyr-Arg(carb)]-Phe-Arg-Tyr-NH_2
4.4b	cyclo[succinyl-Arg-Tyr-Arg(carb)]-Gln-Arg-Tyr-NH_2
4.5b	cyclo[succinyl-Arg-Tyr-Arg(carb)]-Asn-Arg-Tyr-NH_2
4.6b	cyclo[succinyl-Arg-Tyr-Arg(carb)]-His-Arg-Tyr-NH_2
4.7b	cyclo[succinyl-Arg-Tyr-Arg(carb)]-Pro-Arg-Tyr-NH_2
4.8b	cyclo[succinyl-Arg-Tyr-Arg(carb)]-Tle-Arg-Tyr-NH_2
4.9b	cyclo[succinyl-Arg-Tyr-Arg(carb)]-Cpg-Arg-Tyr-NH_2
4.10b	cyclo[succinyl-Arg-Tyr-Arg(carb)]-allo-Ile-Arg-Tyr-NH_2
4.11b	cyclo[succinyl-Arg-Tyr-Arg(carb)]-Leu-β-homo-Arg-Tyr-NH_2
4.12b	cyclo[succinyl-Arg-Tyr-Arg(carb)]-Leu-Arg-β-homo-Tyr-NH_2
4.13b	cyclo[succinyl-Arg-Tyr-Arg(carb)]-Cpg-β-homo-Arg-Tyr-NH_2
4.14b	cyclo[succinyl-Arg-Tyr-Arg(carb)]-Cpg-β-homo-Arg-β-homo-Tyr-NH_2

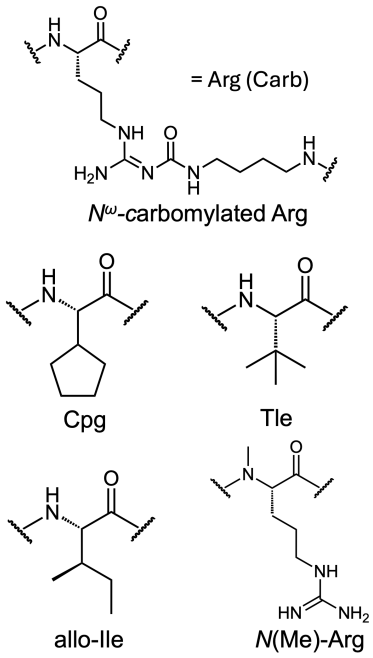

Figure 4.5. Peptide sequences of the synthesized analogs **4.2b−4.14b**. Amino acid replacements and insertions are highlighted in gray and blue, respectively.

In total, 13 analogs of **2.4** were synthesized by SPPS and subsequent cyclization in a solution phase (**4.2b–4.14b**; Figure 4.5). These peptides were characterized with respect to plasma stability, Y_4R binding affinity and selectivity, and Y_4R agonistic potencies and efficacies. IFD studies were also used to investigate the interaction of some of these analogs with Y_4R. In IFD studies, receptor side chains were allowed to be flexible, which facilitated ligand adjustment while optimizing its interactions within the binding pocket of the receptor.[38]

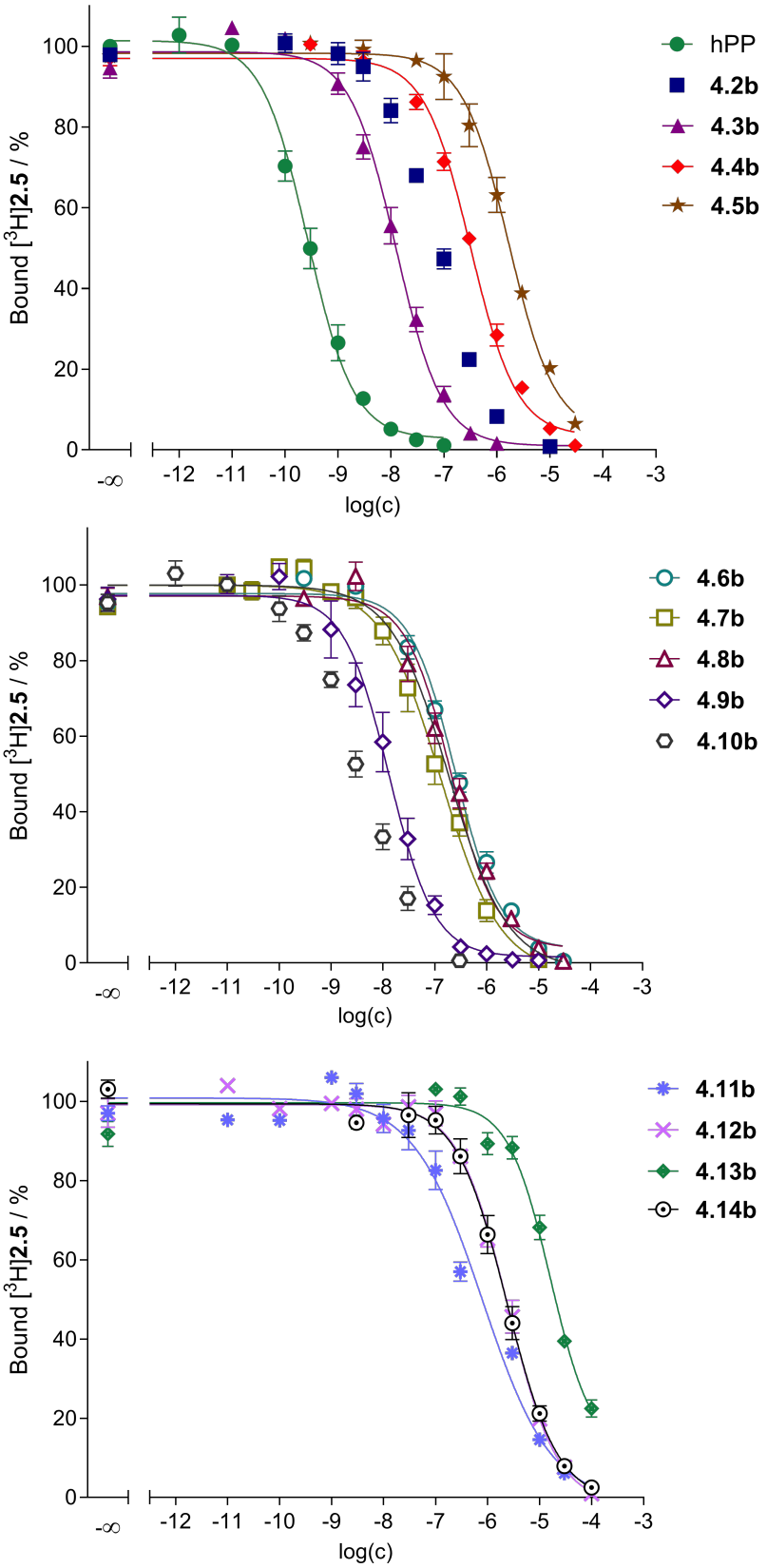

Figure 4.6. Radioligand displacement curves of **4.2b–4.14b** obtained from competition binding experiments at CHO-hY_4-G_{qi5}-mtAEQ cells with the radioligand [^{3}H]**2.5** (K_d = 0.11 nM, c = 0.25 nM). Data represent mean values ± SEM of at least three independent experiments, each performed in triplicate.

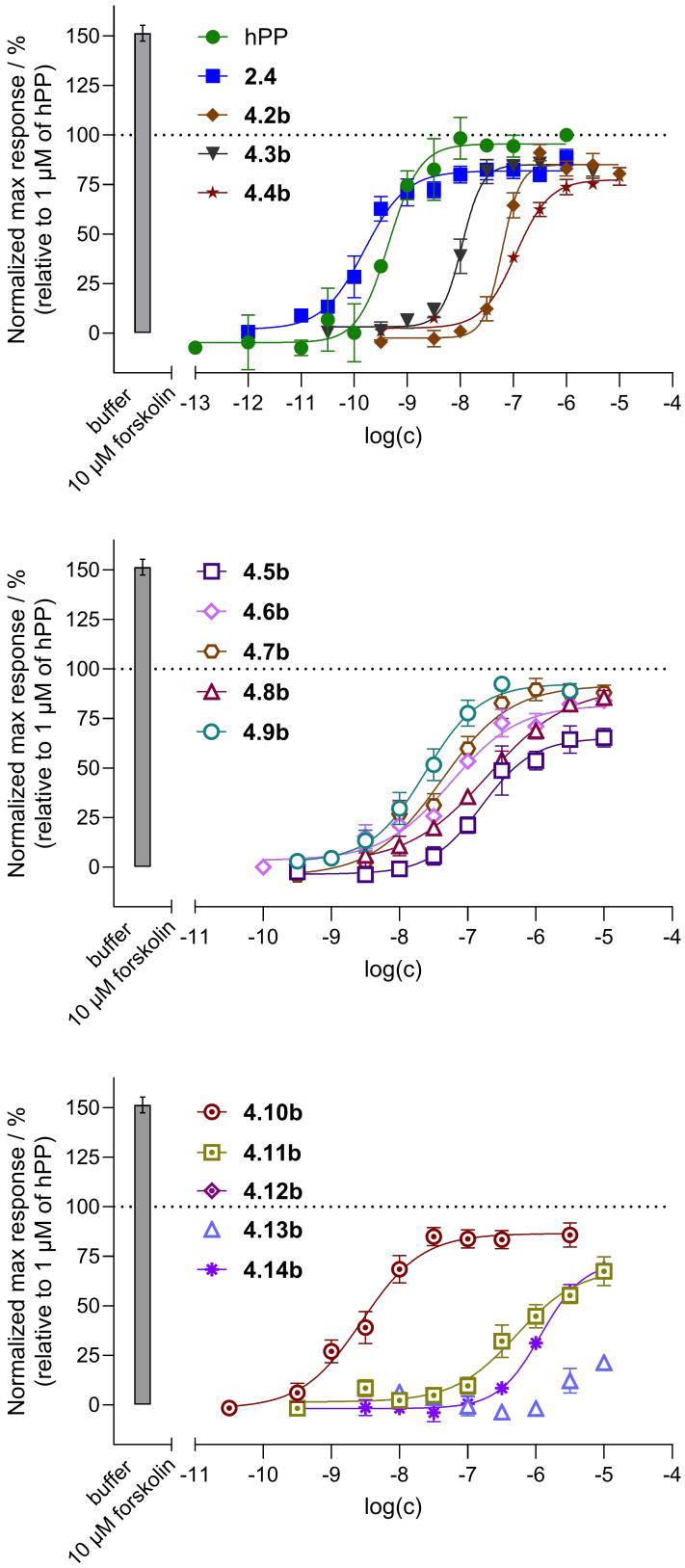

Figure 4.7. Concentration-response curves of hPP, peptides **2.4**, and **4.2b–4.14b**, obtained from a cAMP CAMYEN assay performed with live HEK293T-hY_4R-CAMYEN cells in agonist mode. To normalize the data, the effect elicited by 1 µM hPP was set to 100%. Presented are means ± SEM from at least three independent experiments, each performed in triplicate.

To investigate the stability of the analogs against enzymatic cleavage, the different peptides were incubated in human plasma at 37 °C up to 24 or 48 h, followed by precipitation of the plasma proteins and HPLC analysis (for recoveries see Table A4.3 in *Section 4.6 Appendix*). For the pharmacological characterization of **4.2b–4.14b**, Y_4R receptor affinities were determined in competition binding experiments at live CHO-hY_4-G_{qi5}-mtAEQ cells[24] using the described radioligand [^{3}H]**2.5** (K_d (hY_4R) = 0.11 nM).[29] Their selectivity was assessed through the determination of Y_1, Y_2, and Y_5 receptor binding data in previously used radioligand competition binding assays. In addition, the Y_4R potencies and efficacies of **4.2b–4.14b** were determined using the previously reported Y_4R cAMP CAMYEN assay[29] measuring the ability of the peptide to reduce the cAMP production induced by forskolin in live cells via their Y_4R activation. The overview of all the data is given in Tables 4.1 and 4.2. Radioligand displacement and concentration-response curves are shown in Figures 4.6 and 4.7.

With respect to the docking studies, a recently reported active conformation of the Y_4R cryo-EM structure (PDB ID: 7X9C) was used.[32] For the reference peptide **2.4**, the binding mode (pose) with interactions similar to what was reported by Konieczny *et al.*[16] was used to identify the important receptor and ligand residues involved in the Y_4R-**2.4** binding. All the various Y_4R-ligand interactions were considered, but with more attention on Tyr^6 interacting with residue Q222$^{5.46}$ and those close to it: E288$^{6.58}$ (interacting with Arg^5 of **2.4**), F284$^{6.54}$, N301$^{7.32}$, and Leu^4 fitting in a hydrophobic space surrounded by S178$^{4.64}$, A118$^{3.29}$, I179$^{3.30}$ and F174$^{4.60}$ (see Tables A4.4–A4.6 for a comprehensive overview of full interactions considered, *Section 4.6 Appendix*). For all ligands examined (**4.2b–4.14b**), binding modes exhibiting the lowest free energy (pose 1) were analyzed to identify residues with the highest probability of involvement in ligand-receptor interactions.

Table 4.1. Structures of peptide **2.4** and its analogs **4.2b–4.14b**, along with their stabilities in human plasma/PBS (1:2 v/v) at 37 °C.

Compd.	Structure	% Intact peptide in plasma[a] after the specified incubation times				Estimated $t_{1/2}$ [h][b]
		1 h	6 h	24 h	48 h	
2.4	X-Leu-Arg-Tyr-NH_2	85 ± 1[c]	3 ± 0.3[c]	n.d	n.d	1.9[c]
4.2b	X-Leu-N(Me)-Arg-Tyr-NH_2	> 99	> 99	> 99	> 99	> 72
4.3b	X-Phe-Arg-Tyr-NH_2	52 ± 2	< 1	< 1	n.d	1.0
4.4b	X = 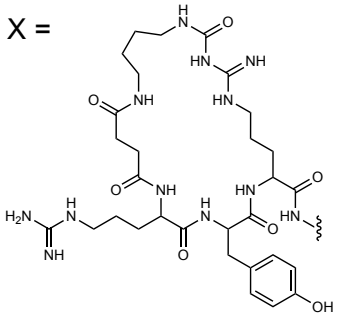 X-Gln-Arg-Tyr-NH_2	91 ± 3	23 ± 2	< 1	n.d	3.4
4.5b	X-Asn-Arg-Tyr-NH_2	81 ± 3	56 ± 3	22 ± 2	9 ± 1	5.9
4.6b	X-His-Arg-Tyr-NH_2	> 99	64 ± 1	21 ± 1	n.d	10.1
4.7b	X-Pro-Arg-Tyr-NH_2	95 ± 1	59 ± 1	3.1 ± 0.4	1.6 ± 0.1	7.8
4.8b	X-Tle-Arg-Tyr-NH_2	> 99	77 ± 5	45 ± 7	29 ± 3	13.8
4.9b	X-Cpg-Arg-Tyr-NH_2	> 99	80 ± 3	50 ± 3	27 ± 4	19.5
4.10b	X-allo-Leu-Arg-Tyr-NH_2	92 ± 2	64 ± 2	14 ± 1	n.d	9.9
4.11b	X-Leu-β-homo-Arg-Tyr-NH_2	> 99	98 ± 2	85 ± 1	83 ± 1	> 48
4.12b	X-Leu-Arg-β-homo-Tyr-NH_2	> 99	98 ± 3	81 ± 1	75 ± 1	> 48
4.13b	X-Cpg-β-homo-Arg-Tyr-NH_2	> 99	> 99	> 99	> 99	> 72
4.14b	X-Cpg-β Arg-β-homo-Tyr-NH_2	> 99	> 99	> 99	92 ± 0.3	> 72

[a]The initial concentration of the peptides in plasma/PBS (1:2 v/v) was 100 μM; presented are mean values ± SEM from three independent experiments (SEM not given if no decomposition was observed). [b]Determined by non-linear regression (two-parameter monoexponential decline) including t = 0 (100%); [c]Konieczny *et al.*[16]; n.d. = not determined.

Table 4.2. Y Receptor binding data of hPP, **2.4**, and **4.2b–4.14b** and their Y_4R agonistic (pEC_{50}, E_{max}) activities.

Compd.	hY_4R affinities (pK_i[a] ± SEM)	$Y_{1,2,5}R$ binding data			Selectivity towards Y_4R [ratio pK_i ($Y_{1,2,5}R$)/pK_i (Y_4R)]	Y_4R CAMYEN cAMP[g]	
		Y_1R[b]	Y_2R[c]	Y_5R[d]	$Y_1R/Y_2R/Y_5R$	pEC_{50} ± SEM	E_{max} ± SEM / %
hPP	10.08 ± 0.12	6.4[e]	< 5.5[e]	7.8[e]	< 6 / < 5 / < 8 [e]	9.35 ± 0.06	101± 1
2.4	10.13 ± 0.07	< 5.5[f]	< 5.0[f]	< 6.0[f]	< 4 / < 4 / < 4 [f]	9.82 ± 0.06	82± 4
4.2b	7.61 ± 0.03	< 5.5	< 5.5	< 5.5	< 7 / < 7 / < 7	7.23 ± 0.06	78 ± 10
4.3b	8.45 ± 0.08	5.64	< 6.0	< 6.0	< 6 / < 6 / < 7	8.05 ± 0.10	85 ± 3
4.4b	6.81 ± 0.14	< 5.5	< 5.5	< 5.5	< 8 / < 8 / < 8	7.05 ± 0.05	83 ± 4
4.5b	6.22 ± 0.06	< 5.5	< 5.5	< 5.5	< 8 / < 8 / < 8	6.74 ± 0.17	67 ± 5
4.6b	7.05 ± 0.06	< 5.5	< 5.5	< 5.5	< 7 / < 7 / < 7	7.29 ± 0.07	77 ± 9
4.7b	7.45 ± 0.14	< 5.5	< 5.5	< 6.0	< 7 / < 7 / < 8	7.34 ± 0.10	95 ± 4
4.8b	7.18 ± 0.10	< 5.5	< 5.5	< 5.5	< 7 / < 7 / < 7	6.61 ± 0.15	97 ± 6
4.9b	8.58 ± 0.13	< 5.5	< 5.5	< 6.0	< 6 / < 6 / < 6	7.60 ± 0.14	93 ± 2
4.10b	8.92 ± 0.07	< 5.5	< 5.5	< 6.0	< 6 / < 6 / < 6	8.66 ± 0.09	89 ± 4
4.11b	6.27 ± 0.06	5.72	< 5.5	6.17	< 8 / < 8 / < 9	6.18 ± 0.17	83 ± 6
4.12b	6.14 ± 0.06	< 5.5	< 5.5	< 6.0	< 8 / < 8 / < 9	6.38 ± 0.17	72 ± 8
4.13b	5.34 ± 0.01	< 5.5	< 5.5	< 6.0	< 9 / < 9 / < 10	n.d	21 ± 4
4.14b	6.16 ± 0.07	< 5.5	< 5.5	6.17	< 8 / < 8 / < 9	5.91 ± 0.02	73 ± 3

[a]Determined by competition binding at CHO-hY_4-G_{qi5}-mtAEQ cells using [^{3}H]**2.5** (K_d = 0.11 nM, c = 0.25 nM) as radioligand (*see* structure in Figure 2.2*, Chapter 2*).[29] [b]Determined by competition binding at SK-N-MC neuroblastoma cells using [^{3}H]UR-MK299 (K_d = 0.058 nM,[27] c = 0.075 nM) as radioligand (*see* structure in Figure A2.1*, Section 2.6 Appendix; Chapter 2*).[26] [c]Determined by competition binding with [^{3}H]propionyl-hPYY (K_d = 0.16 nM, c = 0.3 nM) at CHO-hY_2R cells (*see* structure in Figure A4.1*, Section 4.6 Appendix*).[27] [d]Determined by competition binding at HEC-1B-hY_5R cells using [^{3}H]propionyl-pNPY (K_d = 11 nM,[30] c = 5 nM) as radioligand (*see* structure in Figure A2.1*, Section 2.6 Appendix; Chapter 2*).[14] [e]Berlicki *et al.* (reported K_i values were converted to pK_i values)[39]; [f]Konieczny *et al.*[16]; [g]Agonistic potencies (pEC_{50}) and maximum efficacy (E_{max}) relative to the effect elicited by 1 µM hPP determined in a cAMP CAMYEN assay at HEK293T-CAMYEN-Y_4R cells. Data represent mean values from three or four independent experiments (SEM given for pK_i, pEC_{50}, and E_{max}). n.d.: not determined.

4.3.2.1 N^{α}-Methylation of the amide bond between Leu^4 and Arg^5 improves plasma stability

Methylation of amide bonds is one of the commonly used methods to improve the stability of peptides against enzymatic degradation while maintaining their biological activity. This strategy restricts the conformational flexibility of the peptide bonds and the side chains of residues adjacent to the bond, often making the bond resistant to proteolytic cleavage.[40, 41] With the findings showing that **2.4** is cleaved at the Leu^4-Arg^5 amide bond by ACE, a new analog (**4.2b**), with this amide bond methylated, was synthesized by replacing Arg^5 with N^{α}-methylated Arg during peptide synthesis.

As seen in Table 4.1, the plasma stability experiment performed with **4.2b** showed > 99% of intact peptide present after 48 h (even after 72 h, data not shown) of incubation. This finding, compared to that of the parent peptide **2.4**, where about 3% of intact peptide was found after 6 h, implies that the N^{α}-methylation of the Leu^4-Arg^5 amide bond drastically reduced the bond's susceptibility to ACE-mediated proteolysis. This was expected as N^{α}-methylation is known to improve metabolic stability through conformational control or steric hindrance.[40-42] However, binding studies at the Y_4R showed a decrease in affinity (pK_i = 7.61) of about 2.5 log units in comparison to **2.4** (pK_i = 10.18) (Table 4.2). A similar significant reduction in bioactivity was reported by Linde *et al*.[42] in a SAR study of N^{α}-methylated melanocortin peptides. These findings were attributed to the rigidization of the peptide bond by replacing the -NH with $-NCH_3$, which eliminates the partial double bond character of the C-N bond. This, in turn, promotes a *cis* conformation of the amide bond, thereby affecting the peptide backbone conformational flexibility as well as reducing the peptide bond's ability to form hydrogen bonds. This plays a crucial role in receptor interaction and enzyme recognition.

4.3.2.2 Replacing Leu^4 with selected amino acids improves plasma stability

Side chain modification is one of the easier approaches used to improve the plasma stability of peptides. This technique involves altering the enzyme recognition sites on the peptides, which could improve their plasma stability and preserve their bioactivity with fewer changes to their parent peptide structures.[40, 41] To apply this modification in developing plasma stable analogs of peptide **2.4**, an amino acid replacement strategy aimed at modifying the side chain of Leu^4 of the Leu^4-Arg^5 motif (cleaved by ACE) by replacing Leu^4 with both natural and artificial amino acids was used. It is important to note that a replacement of Arg^5 was not considered, as previous studies had shown

its importance for receptor recognition (a replacement usually leads to a loss in the analog's bioactivity).[13, 43]

In view of these, amino acids for the replacement of Leu^4 were first selected based on the similarity of their side chains (with emphasis on their size and their stereochemistry) to the targeted amino acids of the parent peptide. Some L-amino acids, such as Trp, Gly, and Ala, as well as D-amino acids, were excluded. This decision was based on previous findings by Konieczny *et al*.[13] and Kuhn *et al*.[43], which indicated that they significantly reduced the binding affinities of analogs of **2.4**. With regards to the hypothetically preferred analogs containing natural amino acid substitutions intended for synthesis, MEROPS, and Peptide Atlas databases were employed to eliminate candidates that could lead to an analog potentially susceptible to cleavage by ACE or other plasma enzymes.[16] Additionally, further exclusion of the preferred analogs designated for synthesis was carried out using IFD. For this, the differences in Y_4R interactions compared to **2.4** were used as parameters to assess the hypothetic analog with respect to its ability to bind to Y_4R.

As mentioned previously, MEROPS[35] was used to select Phe, Gln, Asn, His, and Pro as the natural amino acid replacements for Leu in the Leu^4-Arg^5 bond. Search results from MEROPS[35] and Peptide Atlas[36] predicted that the Xaa^4-Arg^5 bonds from the selected hypothetic analogs could not be cleaved by ACE but rather by antarease, a reprolysin from the venom of the Brazilian scorpion *Tityus serrulatus,* which does not exist in humans.[44] Furthermore, poses from the Y_4R IFD studies of these analogs were generally comparable to that of the reference peptide **2.4**, with only a few differences in their interactions with residues important for receptor binding (not shown). This consequently led to the synthesis of analogs **4.3b–4.7b** (for structures, see Figure 4.5 or Table 4.1).

With the exception of **4.5b** (Leu^4 replaced by Asn) and **4.6b** (Leu^4 replaced by His), these analogs yielded less than 2% intact peptide after 24 h of incubation in human plasma (Table 4.1). **4.5b** and **4.6b** gave 20-22% intact peptide after 24 h of incubation. Though surprising, the contradiction between this result and the prediction by MEROPS[35] could be due to stability information on these peptide bonds (Xaa^4-Arg^5) not yet included in the database. These results, however, could be attributed to the polarity of the side chains (Asn^4 in **4.5b**, His^4 in **4.6b**), which may result in different hydration/solvation shells before or during binding as well as their different steric

demand.[45] This could make it difficult for them to fit into the hydrophobic S_1 pocket of ACE, thereby improving the proteolytic stability.[46, 47] Notwithstanding, the increased stability of **4.5b** and **4.6b** could also be explained by the binding of the peptides to the enzyme, possibly inducing an enzyme conformation that decreases its activity.[48]

With respect to the analogs with cyclic side chains (**4.3b** and **4.6b**), the difference in stability could be attributed to the hydrophobicity of the enzyme's S_1 pocket, as well as the distinct hydrogen bond interactions of the cyclic side chains within this pocket, where stronger interactions are preferred.[46] While analog **4.3b** had a half-life < 1 h, it turned out to have the highest binding affinity to hY_4R (pK_i = 8.45) compared to the others (**4.4b–4.7b**) (Table 4.2). However, this was still more than 1.5 log unit lower compared to **2.4** (pK_i = 10.13) (Table 4.2). Careful examination of the docking poses of **4.3b–4.7b** in comparison to **2.4** suggests that the side chain of Leu^4 sits in a hydrophobic area formed by receptor residues $A118^{3.29}$, $F174^{4.60}$, $S178^{4.64}$ and $I179^{4.65}$ (Figure 4.8; Figure A4.2, Table A4.4–A4.6, *Section 4.6 Appendix*). This area appears not to tolerate polar groups and their interactions with the receptor residues. This is supported by the decrease in the determined pK_i values of **4.3b–4.7b** compared to **2.4**. As such, the high binding affinity of **4.3b** could be due to the hydrophobic side chain of Phe fitting in this hydrophobic area. On the contrary, for the other peptides, for example, **4.6b**, the weakly basic imidazole moiety in the side chain of histidine forms a hydrogen bond interaction with $S178^{4.64}$ in this area (not shown), which is incompatible with the binding mode preferred by the receptor (see Figure 4.8; Figure A4.2, Table A4.4–A4.6, *Section 4.6 Appendix*). In general, these findings suggest that Leu^4 is also crucial for binding, i.e., the interaction of the peptide with the respective hydrophobic space of Y_4R is also important for receptor recognition, just as Arg^5 and Tyr^6.

For analog **4.7b**, which had Pro replacing Leu^4, 59% of intact peptide remained after 6 h of incubation, signifying a notable increase in plasma stability compared to **2.4**. However, this increase in plasma stability was accompanied by a significant reduction in its binding affinity to the Y_4R (pK_i = 7.45). This was surprising because replacing Leu^4 with Pro^4 was expected to maintain or improve the binding affinity of **4.7b** as this makes the C-terminal tripeptide sequence of **4.7b** (Pro^4-Arg^5-Tyr^6-NH_2) identical to that of hPP (Pro^{34}-Arg^{35}-Tyr^{36}-NH_2). As shown in a cryoEM structural study of Y_4R, the binding of PP to Y_4R, compared to NPY and PYY, indicates that the presence of Pro^{34} restrains the flexibility of the C-terminal tripeptide sequence of PP, enabling it to

penetrate the Y_4R orthosteric binding pocket.[32] This allows the C-terminus of PP to interact with the receptor residues important for binding and activation. Likewise, IFD studies of **4.7b** to Y_4R imply that the presence of Pro^4 in the C-terminal tripeptide of **4.7b** also restricts its flexibility. However, this restriction, along with the rigidity from the macrocycle part of **4.7b**,[33, 49] prevents it from binding in the orthosteric binding pocket of Y_4R but rather above it (Figure A4.2C and Table A4.4–A4.6, *Section 4.6 Appendix*), resulting in the observed decrease in binding affinity.

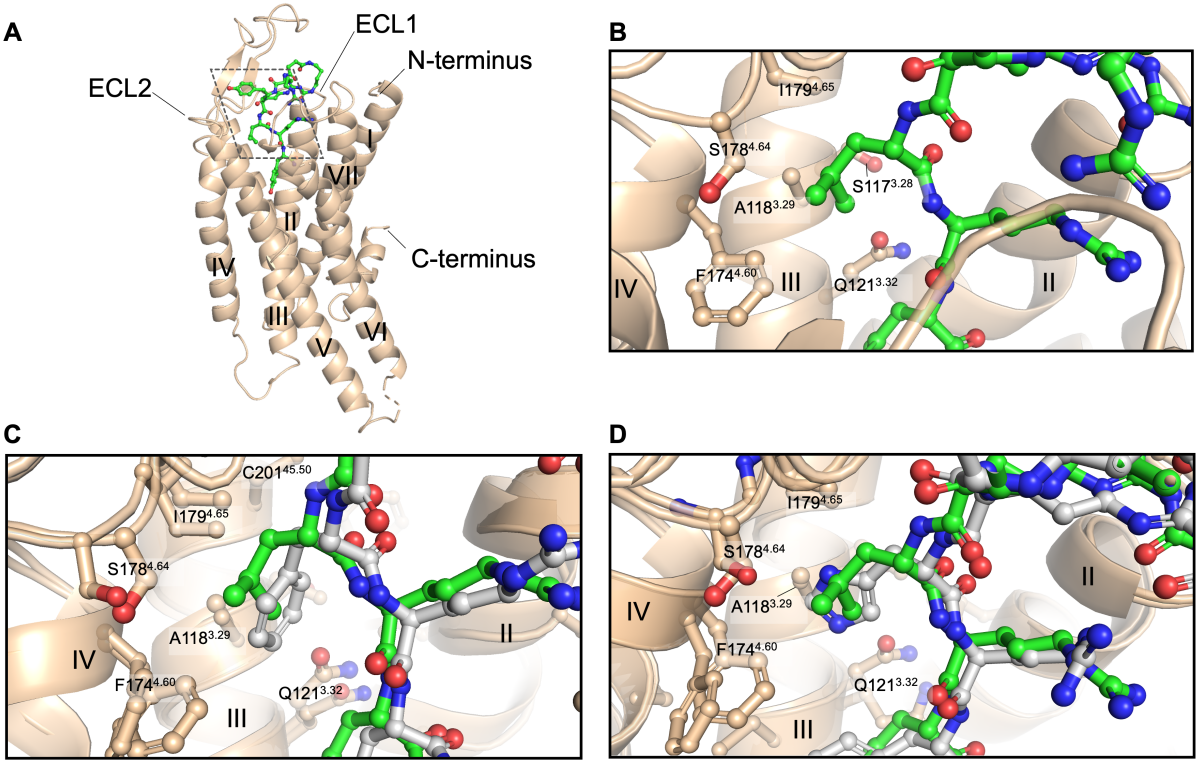

Figure 4.8. Binding poses of **2.4**, **4.3b**, and **4.6b** in the cryo-EM structure of hY_4R obtained from IFD studies. Images show the representative structure from the lowest free energy binding modes of (A) Y_4R-**2.4**, and the zoomed views of (B) Y_4R-**2.4**, (C) Y_4R-**2.4** compared to Y_4R-**4.3b**, and (D) Y_4R-**2.4** in comparison to Y_4R-**4.6b**. The zoomed views of the binding modes focus on the Leu^4 (**2.4**), Phe^4 (**4.3b**), and His^4 (**4.6b**) of the individual peptides in the hydrophobic space formed by receptor residues $A118^{3.29}$, $F174^{4.60}$, $S178^{4.64}$ and $I179^{4.65}$. Nitrogen and oxygen atoms are shown in blue and red, respectively. Carbon atoms of peptide **2.4** are shown in green, while those for **4.3b** and **4.6b** are in gray. Receptor residues interacting with the ligand are shown as beige sticks. Hydrogen bond contacts between the ligands and the receptor are not shown.

Given the results obtained for **4.3b-4.7b**, derivatives of **2.4** in which Leu^4 is replaced by the artificial amino acids *tert*-butyl-Gly, cyclopentyl-Gly, cyclohexyl-Ala, cyclopropyl-Ala, allo-Ile, or C^{α}-methyl-Leu were considered as potential candidates. Based on their IFD poses, *tert*-butyl-Gly (**4.8b**), cyclopentyl-Gly (**4.9b**), allo-Ile (**4.10b**), and C^{α}-methyl-Leu were selected for synthesis as the poses for both cyclohexyl-Ala and cyclopropyl-

Ala were deemed to be unsuitable, having significantly deviated from the interactions observed in the reference peptide **2.4** (not shown). Unfortunately, the synthesis of the analog with C^{α}-methyl-Leu in position 4 failed as the solid-phase synthesis of the linear precursor peptide yielded a very low amount of the product (yield < 2%). As a result, only the binding affinity of the linear precursor peptide was studied, which revealed a drastically reduced hY_4R binding affinity (pK_i = 5.03, not shown in the table) compared to **2.4**. Given the effect of the cyclization on Y_4R binding observed for the other analogs (increase in pK_i by 1-1.5 log units), it was assumed that the hY_4R binding affinity of the cyclized derivative would still be very low. Consequently, no further attempts were made for resynthesis.

For the analogs with *tert*-butyl-Gly (**4.8b**) and cyclopentyl-Gly (**4.9b**), plasma stability studies yielded about 50% of intact peptide after 24 h of incubation and about 30% after 48 h (estimated half-lives: 14 h (**4.8b**) and 20 h (**4.9b**); Table 4.1). With a pK_i of 8.58, peptide **4.9b** displayed a higher Y_4R binding affinity than **4.8b** (*cf.* Table 4.2). In contrast, analog **4.10b** (with allo-Ile) exhibited low plasma stability with about 14% intact peptide left after 24 h ($t_{1/2}$ ca. 9 h) but showed the highest binding affinity (pK_i = 8.92) among the synthesized peptides. The improvement in stability, along with a decrease in affinity of **4.10b** compared to that of parent peptide **2.4**, is most likely due to the different stereochemistry of the allo-Ile side chain affecting the binding mode of the peptide in the enzyme and receptor. This also may hold true for **4.8b** and **4.9b**. Overall, cyclopentyl-Gly (**4.9b**) appears to be the most effective at enhancing the peptide's resistance to ACE degradation. However, this notable improvement in plasma stability has a trade-off effect on its bioactivity.

4.3.2.3 Elongating the backbone using β-homo amino acids improves stability

Aiming for analogs of **2.4** with increased plasma stability, the backbone of **2.4** was elongated by introducing a methylene group close to the Leu^4-Arg^5 amide bond. By this, the amide bond is shifted a carbon atom away from the side chain where the methylene group is introduced, thus obstructing the recognition of the cleavage sites in the peptide by the protease. This, therefore, is expected to increase the stability of the peptide against proteolytic degradation.

Using this strategy, two different analogs of **2.4** were synthesized and characterized: analog **4.11b**, in which Arg^5 was replaced by β-homo-Arg, and analog **4.12b**, in which Tyr^6 was replaced by a β-homo-Tyr (*cf.* Figure 4.5). Results from their characterization

showed improved plasma stabilities but also reduced hY_4R binding affinities compared to **2.4**. In the case of **4.11b**, about 83% of intact peptide remained after 48 h of incubation in human plasma ($t_{1/2}$ > 48 h; Table 4.1). For analog **4.12b**, about 81% of intact peptide remained after 24 h of incubation and 75% after 48 h ($t_{1/2}$ > 48 h). Although their plasma stability half-lives were significantly higher than that of **2.4**, there were substantial reductions in Y_4R binding affinity (Table 4.2). A possible explanation could be the changes in the backbone conformation of the peptide in the receptor, impairing interactions necessary for Y_4R receptor binding. This was validated by the poses obtained in the docking studies (see *Section 4.6 Appendix*, Figure A4.3), which revealed that these peptides bind above the orthosteric binding pocket of Y_4R known for **2.4** binding, precluding the required interactions with the receptor's residues.

To further build on the improvement in plasma stability, two additional analogs were synthesized and characterized. These were analog **4.13b**, in which Leu^4 and Arg^5 were replaced by cyclopentyl-Gly and β-homo-Arg, respectively; and analog **4.14b**, in which Leu^4, Arg^5, and Tyr^6 were replaced by cyclopentyl-Gly, β-homo-Arg, and β-homo-Tyr respectively. These substitutions aimed to further improve the plasma stability of analogs **4.11b** and **4.12b**. The plasma stability studies showed that more than 99% of intact peptide remained for both **4.13b** and **4.14b** after 24 h of incubation (Table 4.1). Whereas for **4.13b**, 99% of intact peptide remained after 48 h of incubation, 92% of intact peptide remained for **4.14b.** Therefore, the half-lives of both analogs were > 48 h (Table 4.1), demonstrating that the structural changes present in **4.13b** and **4.14b** significantly improved plasma stability. Regarding the binding affinities of these analogs, replacement of Leu^4 in **4.11b** by cyclopentyl-Gly led to a further reduction in Y_4R affinity for the resulting analog **4.13b** (pK_i = 5.34), while for **4.14b**, replacement of Leu^4 and Arg^5 in **4.12b** by cyclopentyl-Gly and β-homo-Arg, respectively, had a negligible effect on Y_4R binding (pK_i = 6.14 vs. 6.16) (Table 4.2). In summary, these findings further confirm the significance of the amidated C-terminal dipeptide of **2.4** (Arg^5-Tyr^6-NH_2) for Y_4R recognition, meaning that little structural changes already have a high impact on Y_4R receptor binding.

4.3.2.4 Analogs **4.3b**, **4.9b**, and **4.10b** are selective towards Y_4R subtype

Y_4R selectivity was assessed for all peptides by studying their binding to Y_1, Y_2, and Y_5 receptors (Table 4.2). Due to the very low affinities of the investigated compounds at the Y_1, Y_2, and Y_5 receptors, pK_i values could not be determined in most cases. As

Y_4R selectivity decreases with decreasing Y_4R binding affinity, only the analogs **4.3b**, **4.9b,** and **4.10b**, displaying high Y_4R affinity ($pK_i > 8$), show pronounced Y_4R selectivity. On the contrary, the other peptides (**4.2b**, **4.3b**-**4.8b**, and **4.11b**–**4.14b**), exhibiting low to moderate Y_4R binding affinity, also show low Y_4R selectivity (Table 4.2).

4.3.2.5 Analogs **4.7b**, **4.8b**, and **4.9b** act as full agonists in the cAMP CAMYEN assay

All peptides were investigated in a previously described cAMP CAMYEN assay with respect to their Y_4R agonism using HEK293T-CAMYEN-hY_4R cells.[29] This assay was conducted by first pretreating the cells with forskolin to stimulate cAMP production by adenylyl cyclases, followed by the addition of the peptides (Y_4R agonists), resulting in an inhibition of cAMP production upon the activation of Y_4R coupled to G proteins of the $G_{i/o}$ subfamily.

As parent peptide **2.4**, showing full Y_4R agonism relative to the endogenous Y_4R agonist hPP, **4.7b**–**4.9b** also showed (nearly) full agonism ($E_{max} > 95\%$), but lower potencies (pEC_{50}) (Figure 4.7, Table 4.2). The other peptides (**4.2b–4.6b**, **4.10b–4.12b**, and **4.14b**) showed partial agonism. Interestingly, the curve for analog **4.13b** couldn't be fitted as its potency in the cAMP assay was very low ($pEC_{50} < 5.5$) precluding fitting of the data when using 10 µM as the highest concentration. This indicates that the replacement of Leu^4-Arg^5 by cyclopentyl-Gly and β-homo-Arg had the highest impact on agonistic potency. As seen in Table 4.2, the potencies of all the analogs were in accordance with their pK_i values except for **4.9b**, whose pK_i (8.58) differed from its pEC_{50} (7.60) by 1 log unit. Although the general agreement of the pEC_{50} values with the binding data can be explained by the equilibrium conditions achieved as a result of the more downstream measurement of amplified signals of cAMP in the CAMYEN assay[29], for **4.9b**, this discrepancy may be due to its interaction with the Y_4R residues compared to the **2.4**. This can be seen in the differences in the binding modes of **4.9b** compared to **2.4** (Figure 4.9). The docking studies show a shift of the **4.9b** in the binding pocket of Y_4R towards its transmembranes (TM) 5 and 6 compared to **2.4**, thus disrupting its interactions with Y_4R residues such as $His308^{7.39}$, $Leu281^{6.51}$ and Thr102 among others shown to be important for receptor activation by PP and **2.4** (see Table A4.4–A4.6 for overview of Y_4R-**4.9b** vs Y_4R-**2.4**).[16, 32, 50]

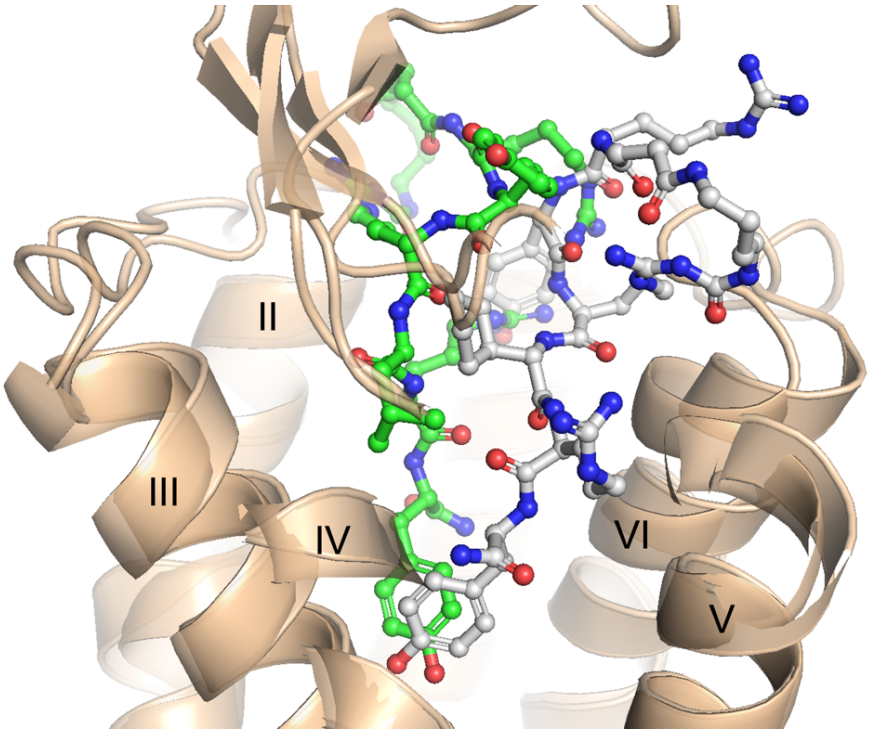

Figure 4.9. Binding modes of **2.4** in the hY_4R in comparison to **4.9b** obtained from IFD studies. Images show the representative structure from the lowest free energy binding modes where the binding of peptide **4.9b** binding is shifted towards the TM5 and TM6 of the receptor. Nitrogen and oxygen atoms are shown in blue and red, respectively. Carbon atoms of the peptide **2.4** are shown in green and for **4.9b** in gray. Hydrogen bond contacts between the ligands and the receptor are not shown.

4.4 Conclusion

Enzymatic degradation of potential therapeutic peptides in blood remains a major bottleneck in their use in therapies despite their remarkable pharmacological profiles. Proteolytic cleavage often reduces or results in a loss of bioactivity of the peptides. Similarly, enzymatic degradation of the potential therapeutic cyclic hexapeptide **2.4** in human plasma was shown to terminate its bioactivity.

By identifying the responsible enzyme (angiotensin-converting enzyme) as well as the amide bond that is hydrolyzed in the peptide (Leu^4-Arg^5), 13 different analogs of **2.4** were designed and synthesized with the aim of obtaining analogs with improved *in vitro* plasma stabilities and with similar or improved Y_4R affinity compared to **2.4**. Out of the 13 synthesized analogs, eight peptides (**4.3b**, **4.8b–4.14b**) exhibited a significantly improved plasma stability with more than 30% intact peptide remaining after 48 h of incubation in human plasma (half-lives ≥ 9 h). Considering these being significantly higher than **2.4** ($t_{1/2}$ = 1.9 h), their improved plasma stabilities, however, led to a drastically reduced Y_4R binding affinity and agonistic activity for analogs **4.9b–4.12b** (4–6 log units) and slight reduction for **4.3b** and **4.8b–4.10b** (1–2 log units), when compared to **2.4**.

Among these analogs, cyclic peptide **4.9b** (UR-AG27), containing the unnatural amino acid cyclopentyl-Gly instead of Leu^4 in **2.4**, emerged as the most promising analog. This is due to its high *in vitro* plasma stability ($t_{1/2}$ = 19.5 h), high Y_4R binding affinity (pK_i (Y_4R) = 8.64), its pronounced Y_4R selectivity (pK_i (Y_1R, Y_2R, Y_5R) < 6.5) and its high agonistic activity (pEC_{50} = 7.6) in comparison to the other synthesized analogs. It is important to note that under *in vivo* conditions, this plasma stability half-life of **4.9b** may be lower than 19 h due to other *in vivo* metabolic activities. Nonetheless, the Y_4R agonist **4.9b** represents a potential lead structure to further improve the plasma stability and bioactivity in addition to enhancing its permeability across lipid bilayers and the blood-brain barrier. This is particularly significant since Y_4R activity in the brain has been shown to induce satiety and reduce food intake in humans. To further improve the plasma stability, strategies such as replacing the proteolytic susceptible amide bond with amide bioisosteres could be explored. Some amide bioisosteres worth investigating include reverse amides, triazoles, tetrazoles, sulfonamides, urea, and thiourea, as they have been shown to reduce the proteolytic susceptibility of amide bonds in compounds with less or no effect on bioactivity.

4.5 References

(1) Purohit, K.; Reddy, N.; Sunna, A. Exploring the potential of bioactive peptides: from natural sources to therapeutics. *Int. J. Mol. Sci.* 2024, *25* (3). DOI: 10.3390/ijms25031391.

(2) Abid, M. S. R.; Mousavi, S.; Checco, J. W. Identifying receptors for neuropeptides and peptide hormones: challenges and recent progress. *ACS Chem. Biol.* 2021, *16* (2), 251-263. DOI: 10.1021/acschembio.0c00950.

(3) Mirabeau, O.; Perlas, E.; Severini, C.; Audero, E.; Gascuel, O.; Possenti, R.; Birney, E.; Rosenthal, N.; Gross, C. Identification of novel peptide hormones in the human proteome by hidden Markov model screening. *Genome Res.* 2007, *17* (3), 320-327. DOI: 10.1101/gr.5755407.

(4) Yosten, G. L.; Elrick, M. M.; Salvatori, A.; Stein, L. M.; Kolar, G. R.; Ren, J.; Corbett, J. A.; Samson, W. K. Understanding peptide biology: the discovery and characterization of the novel hormone, neuronostatin. *Peptides* 2015, *72*, 192-195. DOI: 10.1016/j.peptides.2015.05.011.

(5) Wang, L.; Wang, N.; Zhang, W.; Cheng, X.; Yan, Z.; Shao, G.; Wang, X.; Wang, R.; Fu, C. Therapeutic peptides: current applications and future directions. *Signal Transduct. Target Ther.* 2022, *7* (1), 48. DOI: 10.1038/s41392-022-00904-4.

(6) Low, K.; Roulin, A.; Kunz, S. A proopiomelanocortin-derived peptide sequence enhances plasma stability of peptide drugs. *FEBS Lett.* 2020, *594* (17), 2840-2866. DOI: 10.1002/1873-3468.13855.

(7) Li, J. B.; Asakawa, A.; Terashi, M.; Cheng, K.; Chaolu, H.; Zoshiki, T.; Ushikai, M.; Sheriff, S.; Balasubramaniam, A.; Inui, A. Regulatory effects of Y_4 receptor agonist (BVD-74D) on food intake. *Peptides* 2010, *31* (9), 1706-1710. DOI: 10.1016/j.peptides.2010.06.011.

(8) Zhang, L.; Bijker, M. S.; Herzog, H. The neuropeptide Y system: pathophysiological and therapeutic implications in obesity and cancer. *Pharmacol. Ther.* 2011, *131* (1), 91-113. DOI: 10.1016/j.pharmthera.2011.03.011.

(9) Balasubramaniam, A. Clinical potentials of neuropeptide Y family of hormones. *Am. J. Surg.* 2002, *183* (4), 430-434. DOI: 10.1016/s0002-9610(02)00803-6.

(10) Herzog, H. Neuropeptide Y and energy homeostasis: insights from Y receptor knockout models. *Eur. J. Pharmacol.* 2003, *480* (1-3), 21-29. DOI: 10.1016/j.ejphar.2003.08.089.

(11) Balasubramaniam, A.; Joshi, R.; Su, C.; Friend, L. A.; James, J. H. Neuropeptide Y (NPY) Y_2 receptor-selective agonist inhibits food intake and promotes fat metabolism in mice: combined anorectic effects of Y_2 and Y_4 receptor-selective agonists. *Peptides* 2007, *28* (2), 235-240. DOI: 10.1016/j.peptides.2006.08.041.

(12) Balasubramaniam, A.; Mullins, D. E.; Lin, S.; Zhai, W.; Tao, Z.; Dhawan, V. C.; Guzzi, M.; Knittel, J. J.; Slack, K.; Herzog, H.*; et al.* Neuropeptide Y (NPY) Y_4 receptor selective agonists based on NPY_{32-36}: development of an anorectic

Y_4 receptor selective agonist with picomolar affinity. *J. Med. Chem.* 2006, *49* (8), 2661-2665. DOI: 10.1021/jm050907d.

(13) Konieczny, A.; Braun, D.; Wifling, D.; Bernhardt, G.; Keller, M. Oligopeptides as neuropeptide Y Y_4 receptor ligands: identification of a high-affinity tetrapeptide agonist and a hexapeptide antagonist. *J. Med. Chem.* 2020, *63*, 8198-8215. DOI: 10.1021/acs.jmedchem.0c00426.

(14) Kuhn, K. K.; Ertl, T.; Dukorn, S.; Keller, M.; Bernhardt, G.; Reiser, O.; Buschauer, A. High affinity agonists of the neuropeptide Y (NPY) Y_4 receptor derived from the C-terminal pentapeptide of human pancreatic polypeptide (hPP): synthesis, stereochemical discrimination, and radiolabeling. *J. Med. Chem.* 2016, *59*, 6045-6058. DOI: 10.1021/acs.jmedchem.6b00309.

(15) Söll, R. M.; Dinger, M. C.; Lundell, I.; Larhammer, D.; Beck-Sickinger, A. G. Novel analogues of neuropeptide Y with a preference for the Y_1-receptor. *Eur. J. Biochem.* 2001, *268* (10), 2828-2837. DOI: 10.1046/j.1432-1327.2001.02161.x.

(16) Konieczny, A.; Conrad, M.; Ertl, F. J.; Gleixner, J.; Gattor, A. O.; Gratz, L.; Schmidt, M. F.; Neu, E.; Horn, A. H. C.; Wifling, D.*; et al.* N-terminus to arginine side-chain cyclization of linear peptidic neuropeptide Y Y_4 receptor ligands results in picomolar binding constants. *J. Med. Chem.* 2021, *64* (22), 16746-16769. DOI: 10.1021/acs.jmedchem.1c01574.

(17) Wu, H.; Huang, J. Optimization of protein and peptide drugs based on the mechanisms of kidney clearance. *Protein Pept. Lett.* 2018, *25* (6), 514-521. DOI: 10.2174/0929866525666180530122835.

(18) Di, L. Strategic approaches to optimizing peptide ADME properties. *AAPS J.* 2015, *17* (1), 134-143. DOI: 10.1208/s12248-014-9687-3.

(19) Al Musaimi, O.; Lombardi, L.; Williams, D. R.; Albericio, F. Strategies for improving peptide stability and delivery. *Pharmaceuticals (Basel)* 2022, *15* (10). DOI: 10.3390/ph15101283.

(20) Werle, M.; Bernkop-Schnurch, A. Strategies to improve plasma half life time of peptide and protein drugs. *Amino Acids* 2006, *30* (4), 351-367. DOI: 10.1007/s00726-005-0289-3.

(21) Kremsmayr, T.; Aljnabi, A.; Blanco-Canosa, J. B.; Tran, H. N. T.; Emidio, N. B.; Muttenthaler, M. On the utility of chemical strategies to improve peptide gut stability. *J. Med. Chem.* 2022, *65* (8), 6191-6206. DOI: 10.1021/acs.jmedchem.2c00094.

(22) Pernot, M.; Vanderesse, R.; Frochot, C.; Guillemin, F.; Barberi-Heyob, M. Stability of peptides and therapeutic success in cancer. *Expert Opin. Drug Metab. Toxicol.* 2011, *7* (7), 793-802. DOI: 10.1517/17425255.2011.574126.

(23) Keller, M.; Kuhn, K. K.; Einsiedel, J.; Hübner, H.; Biselli, S.; Mollereau, C.; Wifling, D.; Svobodová, J.; Bernhardt, G.; Cabrele, C.*; et al.* Mimicking of arginine by functionalized N^{ω}-carbamoylated arginine as a new broadly applicable approach to labeled bioactive peptides: high affinity angiotensin, neuropeptide Y, neuropeptide FF, and neurotensin receptor ligands as examples. *J. Med. Chem.* 2016, *59* (5), 1925-1945. DOI: 10.1021/acs.jmedchem.5b01495.

(24) Ziemek, R.; Schneider, E.; Kraus, A.; Cabrele, C.; Beck-Sickinger, A. G.; Bernhardt, G.; Buschauer, A. Determination of affinity and activity of ligands at the human neuropeptide Y Y_4 receptor by flow cytometry and aequorin luminescence. *J. Recept. Signal Transduct.* 2007, *27* (4), 217-233. DOI: 10.1080/10799890701505206.

(25) Moser, C.; Bernhardt, G.; Michel, J.; Schwarz, H.; Buschauer, A. Cloning and functional expression of the hNPY Y_5 receptor in human endometrial cancer (HEC-1B) cells. *Can. J. Physiol. Pharmacol.* 2000, *78* (2), 134-142.

(26) Keller, M.; Weiss, S.; Hutzler, C.; Kuhn, K. K.; Mollereau, C.; Dukorn, S.; Schindler, L.; Bernhardt, G.; König, B.; Buschauer, A. N^{ω}-Carbamoylation of the argininamide moiety: an avenue to insurmountable NPY Y_1 receptor antagonists and a radiolabeled selective high-affinity molecular tool ([^{3}H]UR-MK299) with extended residence time. *J. Med. Chem.* 2015, *58*, 8834-8849. DOI: 10.1021/acs.jmedchem.5b00925.

(27) Schettler, F.; Gattor, A. O.; Koch, P.; Keller, M. Characterization of [^{3}H]propionylated human peptide YY – a new probe for neuropeptide Y Y_2 receptor binding studies. *ACS Pharmacol. Transl. Sci.* 2025, *8* (3), 785-799. DOI: 10.1021/acsptsci.4c00666.

(28) Cheng, Y.; Prusoff, W. H. Relationship between the inhibition constant (K_1) and the concentration of inhibitor which causes 50 per cent inhibition (I_{50}) of an enzymatic reaction. *Biochem. Pharmacol.* 1973, *22* (23), 3099-3108. DOI: 10.1016/0006-2952(73)90196-2.

(29) Gleixner, J.; Gattor, A. O.; Humphrys, L. J.; Brunner, T.; Keller, M. [^{3}H]UR-JG102–A radiolabeled cyclic peptide with high affinity and excellent selectivity for the neuropeptide Y Y_4 receptor. *J. Med. Chem.* 2023, *66* (19), 13788-13808. DOI: 10.1021/acs.jmedchem.3c01224.

(30) Dukorn, S.; Littmann, T.; Keller, M.; Kuhn, K.; Cabrele, C.; Baumeister, P.; Bernhardt, G.; Buschauer, A. Fluorescence and radiolabeling of [Lys^4,$Nle^{17,30}$]hPP Yields Molecular Tools for the NPY Y_4 Receptor. *Bioconjug. Chem.* 2017, *28* (4), 1291-1304. DOI: 10.1021/acs.bioconjchem.7b00103.

(31) Pegoli, A.; Wifling, D.; Gruber, C. G.; She, X.; Hubner, H.; Bernhardt, G.; Gmeiner, P.; Keller, M. Conjugation of short peptides to Dibenzodiazepinone-type muscarinic acetylcholine receptor ligands determines M_2R selectivity. *J. Med. Chem.* 2019, *62* (11), 5358-5369. DOI: 10.1021/acs.jmedchem.8b01967.

(32) Tang, T.; Tan, Q.; Han, S.; Diemar, A.; Lobner, K.; Wang, H.; Schuss, C.; Behr, V.; Morl, K.; Wang, M.*; et al.* Receptor-specific recognition of NPY peptides revealed by structures of NPY receptors. *Sci. Adv.* 2022, *8* (18), eabm1232. DOI: 10.1126/sciadv.abm1232.

(33) Marsault, E.; Peterson, M. L. Macrocycles are great cycles: applications, opportunities, and challenges of synthetic macrocycles in drug discovery. *J. Med. Chem.* 2011, *54* (7), 1961-2004. DOI: 10.1021/jm1012374.

(34) Zorzi, A.; Deyle, K.; Heinis, C. Cyclic peptide therapeutics: past, present and future. *Curr. Opin. Chem. Biol.* 2017, *38*, 24-29. DOI: 10.1016/j.cbpa.2017.02.006.

(35) Rawlings, N. D.; Barrett, A. J.; Thomas, P. D.; Huang, X.; Bateman, A.; Finn, R. D. The MEROPS database of proteolytic enzymes, their substrates and inhibitors in 2017 and a comparison with peptidases in the PANTHER database. *Nucleic Acids Res.* 2018, *46* (D1), D624-D632. DOI: 10.1093/nar/gkx1134.

(36) Desiere, F.; Deutsch, E. W.; King, N. L.; Nesvizhskii, A. I.; Mallick, P.; Eng, J.; Chen, S.; Eddes, J.; Loevenich, S. N.; Aebersold, R. The PeptideAtlas project. *Nucleic Acids Res.* 2006, *34* (Database issue), D655-658. DOI: 10.1093/nar/gkj040.

(37) Metzger, H. M., R.; Sitter, C.; Stern, H.O. 2-[N-[(S)-1-ethoxycarbonyl-3-phenylpropyl]-L-alanyl]-(1S,3S,5S)-2-azabicyclo[3.3.0]octane-3-carboxylic acid (Hoe 498)--a new and highly effective angiotensin I converting enzyme inhibitor. *Arzneim.-Forsch.* 1984, *34(10b)*, 1402-1406.

(38) Miller, E.; Murphy, R.; Sindhikara, D.; Borrelli, K.; Grisewood, M.; Ranalli, F.; Dixon, S.; Jerome, S.; Boyles, N.; Day, T.*; et al.* A reliable and accurate solution to the induced fit docking problem for protein-ligand binding. *ChemRxiv* 2020. DOI: 10.26434/chemrxiv.11983845.v1 Europe PMC Preprints.

(39) Berlicki, L.; Kaske, M.; Gutierrez-Abad, R.; Bernhardt, G.; Illa, O.; Ortuno, R. M.; Cabrele, C.; Buschauer, A.; Reiser, O. Replacement of Thr^{32} and Gln^{34} in the C-terminal neuropeptide Y fragment 25-36 by cis-cyclobutane and cis-cyclopentane beta-amino acids shifts selectivity toward the Y_4 receptor. *J. Med. Chem.* 2013, *56* (21), 8422-8431. DOI: 10.1021/jm4008505.

(40) Barman, P.; Joshi, S.; Sharma, S.; Preet, S.; Sharma, S.; Saini, A. Strategic approaches to improvise peptide drugs as next generation therapeutics. *Int. J. Pept. Res. Ther.* 2023, *29* (4), 61. DOI: 10.1007/s10989-023-10524-3.

(41) Adessi, C.; Soto, C. Converting a peptide into a drug: strategies to improve stability and bioavailability. *Curr. Med. Chem.* 2002, *9* (9), 963-978. DOI: 10.2174/0929867024606731.

(42) Linde, Y.; Ovadia, O.; Safrai, E.; Xiang, Z.; Portillo, F. P.; Shalev, D. E.; Haskell-Luevano, C.; Hoffman, A.; Gilon, C. Structure-activity relationship and metabolic stability studies of backbone cyclization and N-methylation of melanocortin peptides. *Biopolymers* 2008, *90* (5), 671-682. DOI: 10.1002/bip.21057.

(43) Kuhn, K. K.; Littmann, T.; Dukorn, S.; Tanaka, M.; Keller, M.; Ozawa, T.; Bernhardt, G.; Buschauer, A. In search of NPY Y_4R antagonists: incorporation of carbamoylated arginine, aza-amino acids, or d-amino acids into oligopeptides derived from the C-termini of the endogenous agonists. *ACS Omega* 2017, *2* (7), 3616-3631. DOI: 10.1021/acsomega.7b00451.

(44) Ortiz, E.; Rendon-Anaya, M.; Rego, S. C.; Schwartz, E. F.; Possani, L. D. Antarease-like Zn-metalloproteases are ubiquitous in the venom of different scorpion genera. *Biochim. Biophys. Acta* 2014, *1840* (6), 1738-1746. DOI: 10.1016/j.bbagen.2013.12.012.

(45) Biedermannova, L.; Schneider, B. Structure of the ordered hydration of amino acids in proteins: analysis of crystal structures. *Acta Crystallogr. Sect. D. Biol. Crystallogr.* 2015, *71* (Pt 11), 2192-2202. DOI: 10.1107/S1399004715015679.

(46) Yu, D.; Wang, C.; Song, Y.; Zhu, J.; Zhang, X. Discovery of novel angiotensin-converting enzyme inhibitory peptides from *Todarodes pacificus* and their inhibitory mechanism: *in silico* and *in vitro* studies. *Int. J. Mol. Sci.* 2019, *20* (17). DOI: 10.3390/ijms20174159.

(47) Li, W.; Chen, W.; Ma, H.; Wu, D.; Zhang, Z.; Yang, Y. Structural characterization and angiotensin-converting enzyme (ACE) inhibitory mechanism of Stropharia rugosoannulata mushroom peptides prepared by ultrasound. *Ultrason. Sonochem.* 2022, *88*, 106074. DOI: 10.1016/j.ultsonch.2022.106074.

(48) Masuyer, G.; Schwager, S. L.; Sturrock, E. D.; Isaac, R. E.; Acharya, K. R. Molecular recognition and regulation of human angiotensin-I converting enzyme (ACE) activity by natural inhibitory peptides. *Sci. Rep.* 2012, *2*, 717. DOI: 10.1038/srep00717.

(49) Melnikov, S.; Mailliot, J.; Rigger, L.; Neuner, S.; Shin, B. S.; Yusupova, G.; Dever, T. E.; Micura, R.; Yusupov, M. Molecular insights into protein synthesis with proline residues. *EMBO Rep.* 2016, *17* (12), 1776-1784. DOI: 10.15252/embr.201642943.

(50) Schüß, C.; Behr, V.; Beck-Sickinger, A. G. Illuminating the neuropeptide Y_4 receptor and its ligand pancreatic polypeptide from a structural, functional, and therapeutic perspective. *Neuropeptides* 2024, *105*, 102416. DOI: 10.1016/j.npep.2024.102416.

4.6 Appendix

4.6.1 Figures A4.1–A4.3 and Table A4.1–A4.3

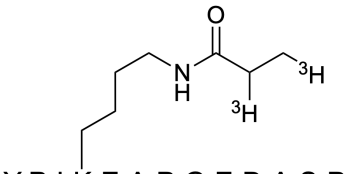

Y-P-I-K-E-A-P-G-E-D-A-S-P-
E-E-L-N-R-Y-Y-A-S-L-R-H-Y-
L-N-L-V-T-R-Q-R-Y-NH_2

[K^4-[^{3}H]propionyl]hPYY

Figure A4.1. Structure of the tritiated Y_2R radioligands [K^4-[^{3}H]propionyl]hPYY used in this study.

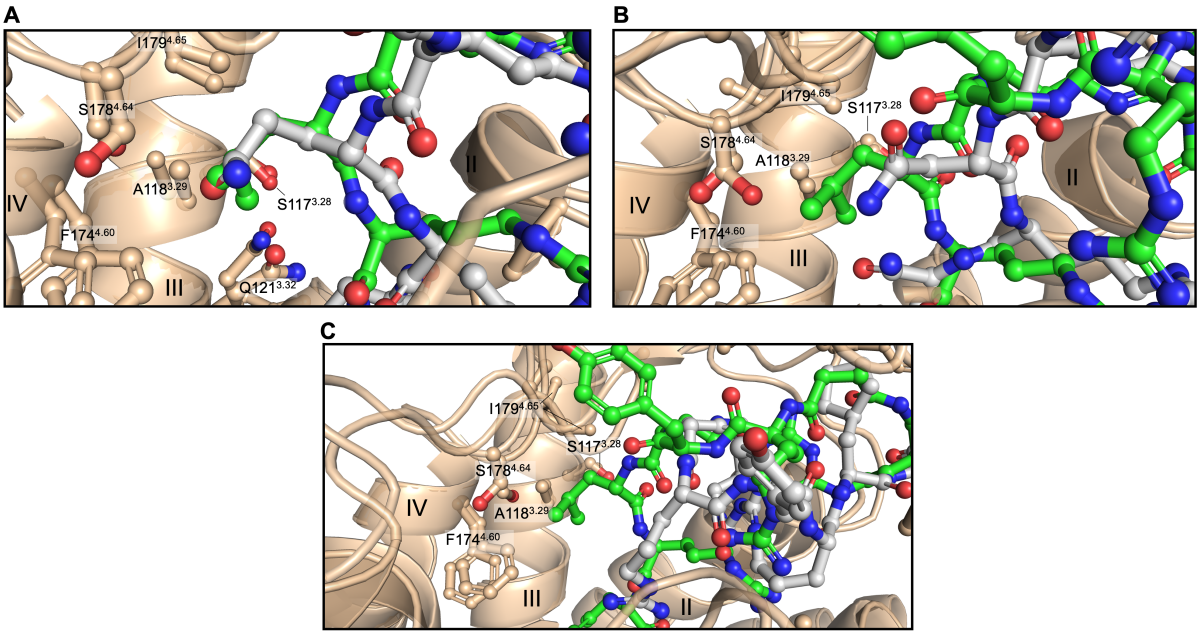

Figure A4.2. Binding poses of **2.4**, **4.4b**, **4.5b**, and **4.7b** in the hY_4R obtained from IFD studies. Images show the representative structure from the lowest free energy binding modes and zoomed views of (A) Y_4R-**2.4** compared to Y_4R-**4.4b**, (B) Y_4R-**2.4** compared to Y_4R-**4.7b**, and (C) Y_4R-**2.4** compared to Y_4R-**4.7b**. The zoomed views of the binding modes focus on the Leu^4 (**2.4**), Gln^4 (**4.4b**), Asn^4 (**4.5b**), and Pro^4 (**4.5b**) of the individual peptides in the hydrophobic space formed by receptor residues $A118^{3.29}$, $F174^{4.60}$, $S178^{4.64}$ and $I179^{4.65}$. Nitrogen and oxygen atoms are shown in blue and red, respectively. Carbon atoms of peptide **2.4** are shown in green, while those for **4.4b**, **4.5b**, and **4.7b** are in gray. Hydrogen bond contacts between the ligands and the receptor are not shown.

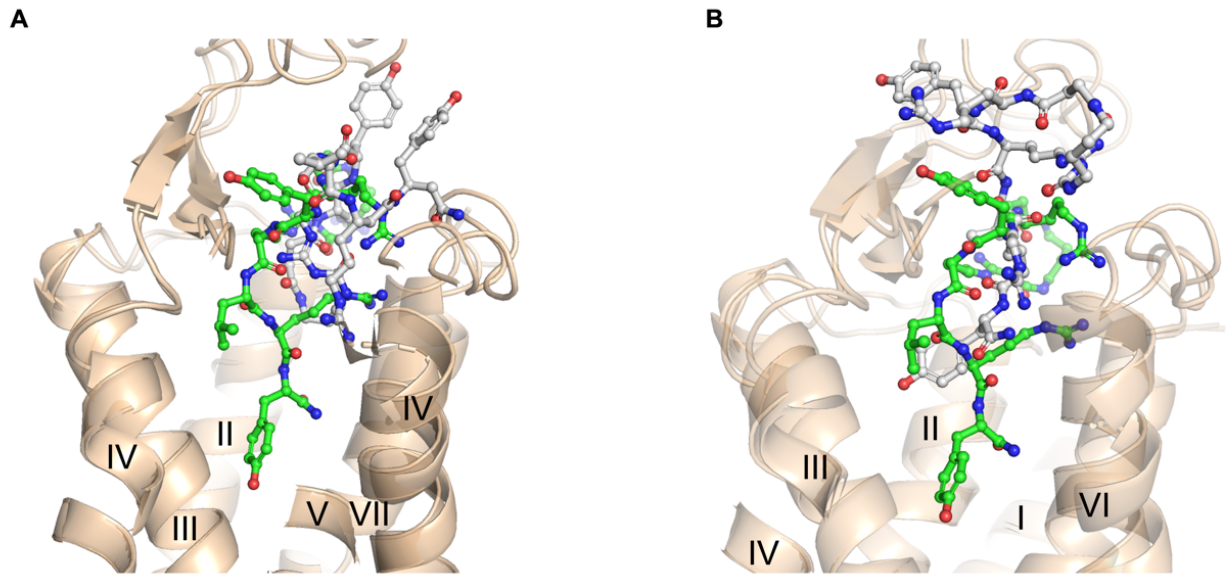

Figure A4.3. Binding poses of **2.4**, **4.11b**, and **4.12b** in a hY4R obtained from IFD studies. Images show the representative structure from the freest energy binding modes and interactions of A) Y_4R-**2.4** in comparison to Y_4R-**4.11b** and B) Y_4R-**2.4** in comparison to Y_4R-**4.12b**. Nitrogen and oxygen atoms are shown in blue and red, respectively. Carbon atoms of peptide **2.4**'s amino acids are shown in green, and **4.11b** and **4.12b** in gray.

Table A4.1. Analytical characterization of linear precursor peptides **4.2a–4.14a** for the synthesis of peptide **4.2b–4.14b.**

Linear precursor peptide	Peptide sequence	x-fold TFA	MW	Yield (%)	RP-HPLC purity (%) / t_R [min] / k	HRMS (ESI): m/z		
						calcd. for	calcd.	found
4.2a	Succinyl-Arg-Tyr-Arg(carb)-Leu-N(Me)-Arg-Tyr-NH_2	2	1153.36 + 228.05	8	> 95/9.8/11.9	$[M+2H]^{2+}$	577.3331	577.3333
4.3a	Succinyl-Arg-Tyr-Arg(carb)-Phe-Arg-Tyr-NH_2	4	1173.35 + 456.09	27	> 98/9.8/12.1	$[M+4H]^{4+}$	294.1624	294.1637
4.4a	Succinyl-Arg-Tyr-Arg(carb)-Gln-Arg-Tyr-NH_2	4	1154.30 + 456.09	34	> 96/5.7/6.6	$[M+4H]^{4+}$	289.4099	289.4111
4.5a	Succinyl-Arg-Tyr-Arg(carb)-Asn-Arg-Tyr-NH_2	4	1140.28 + 456.09	40	> 96/5.6/6.4	$[M+4H]^{4+}$	285.9060	285.9072
4.6a	Succinyl-Arg-Tyr-Arg(carb)-His-Arg-Tyr-NH_2	5	1163.31+ 570.10	33	> 96/5.3/6.13	$[M+4H]^{4+}$	291.6600	291.6612
4.7a	Succinyl-Arg-Tyr-Arg(carb)-Pro-Arg-Tyr-NH_2	4	1123.29 + 456.09	40	> 96/6.7/8.0	$[M+4H]^{4+}$	281.6584	281.6595
4.8a	Succinyl-Arg-Tyr-Arg(carb)-Tle-Arg-Tyr-NH_2	4	1139.33 + 456.09	35	> 96/8.1/9.8	$[M+4H]^{4+}$	285.6663	285.6674
4.9a	Succinyl-Arg-Tyr-Arg(carb)-Cpg-Arg-Tyr-NH_2	4	1151.34+ 456.09	14	> 97/9.5/11.7	$[M+4H]^{4+}$	288.6663	288.6677
4.10a	Succinyl-Arg-Tyr-Arg(carb)-allo-Leu-Arg-Tyr-NH_2	4	1139.33 + 342.06	26	> 93/8.2/9.7	$[M+3H]^{3+}$	380.5526	380.5537
4.11a	Succinyl-Arg-Tyr-Arg(carb)-Leu-β-homo-Arg-Tyr-NH_2	4	1153.36 + 456.09	46	> 96/8.2/9.9	$[M+4H]^{4+}$	289.1702	289.1712
4.12a	Succinyl-Arg-Tyr-Arg(carb)-Leu-Arg-β-homo-Tyr-NH_2	4	1153.36 + 456.09	50	> 96/8.4/10.2	$[M+4H]^{4+}$	289.1702	289.1712
4.13a	Succinyl-Arg-Tyr-Arg(carb)-Cpg-β-homo-Arg-Tyr-NH_2	4	1165.37+ 456.09	35	> 96/10.2/12.5	$[M+2H]^{2+}$	583.3331	583.3336
4.14a	Succinyl-Arg-Tyr-Arg(carb)-Cpg-β-homo-Arg-β-homo-Tyr-NH_2	4	1179.40 + 456.09	35	> 96/10.6/13.2	$[M+2H]^{2+}$	590.3409	590.3413

TFA- hydro-trifluoroacetate; MW- Molecular weight; HRMS-High Resolution Mass Spectrometry; m/z- mass/charge

Table A4.2. Overview of analytical data of cyclic peptides **4.4b–4.16b.**

Cmpd.	x-fold TFA	MW	Yield (%)	RP-HPLC purity (%) / t_R [min] / k	HRMS (ESI): m/z			NMR[a]
					calcd. for	calcd.	found	
4.2b	3	1135.34 + 342.07	82	> 96/10.9/13.2	$[M+2H]^{2+}$	568.3278	568.3289	^{1}H ^{1}H COSY
4.3b	3	1155.33 + 342.07	76	> 97/10.9/13.4	$[M+3H]^{3+}$	385.8772	385.8783	^{1}H ^{1}H COSY
4.4b	3	1136.29 + 342.07	41	> 97/7.4/8.7	$[M+3H]^{3+}$	379.5406	379.5415	^{1}H ^{1}H COSY
4.5b	3	1122.26 + 342.07	45	> 97/7.1/8.2	$[M+3H]^{3+}$	374.8687	374.8701	^{1}H ^{1}H COSY
4.6b	4	1145.30 + 456.09	53	> 97/6.8/8.0	$[M+3H]^{3+}$	382.5407	382.5411	^{1}H ^{1}H COSY
4.7b	3	1105.27 + 342.07	68	> 97/8.4/9.9	$[M+3H]^{3+}$	369.2053	369.2066	^{1}H ^{1}H COSY
4.8b	3	1121.32 + 342.07	80	> 97/9.9/12.1	$[M+3H]^{3+}$	374.5491	374.5500	^{1}H ^{1}H COSY
4.9b	3	1133.3 + 342.07	60	> 97/10.4/12.6	$[M+3H]^{3+}$	378.5491	378.5503	^{1}H ^{1}H COSY
4.10b	3	1121.32 + 342.07	82	> 97/8.9/10.7	$[M+3H]^{3+}$	374.5491	374.5503	^{1}H ^{1}H COSY
4.11b	3	1135.34 + 342.07	38	> 97/9.8/11.9	$[M+3H]^{3+}$	379.2210	379.2220	^{1}H ^{1}H COSY
4.12b	3	1135.34 + 342.07	50	> 97/10.5/12.8	$[M+3H]^{3+}$	379.2210	379.2221	^{1}H ^{1}H COSY
4.13b	3	1147.35 + 342.07	56	> 97/11.7/14.1	$[M+3H]^{3+}$	383.2210	383.2218	^{1}H ^{1}H COSY
4.14b	3	1161.38 + 342.07	69	> 97/11.9/14.4	$[M+3H]^{3+}$	387.8928	387.8936	^{1}H ^{1}H COSY

TFA-hydro-trifluoroacetate; MW- Molecular weight; HRMS-High Resolution Mass Spectrometry; m/z- mass/charge.

Table A4.3. Recoveries of peptides from human plasma/PBS (1:2 v/v) for two different concentrations (40 µM) and ratios of peptide recovery over recovery of internal standard (1-methyl-D-tryptophan).

Compounds	Peptide concentration 40 µM		
	Recovery peptide (%)[a]	Recovery D-Me-Trp (%)[b]	Ratio[b]
4.2b	76 61 80 65	92 81 95 91	0.82 0.75 0.84 0.71 (0.78 ± 0.03)
4.3b	64 67 54 58	102 95 83 83	0.63 0.71 0.65 0.70 (0.67 ± 0.02)
4.4b	57 44 59 78 49	92 81 95 90 91	0.62 0.54 0.63 0.86 0.54 (0.64 ± 0.07)
4.5b	44 51 55 60 46	87 94 105 86 78	0.51 0.52 0.55 0.70 0.59 (0.57 ± 0.03)
4.6b	57 52 61 52 57	81 91 103 89 84	0.70 0.57 0.59 0.58 0.68 (0.63 ± 0.03)
4.7b	24 56 84 77 85	34 82 117 109 117	0.71 0.68 0.72 0.71 0.73 (0.71 ± 0.01)
4.8b	68 62 67 63 62	81 91 103 89 84	0.84 0.68 0.66 0.71 0.74 (0.72 ± 0.03)

Table A4.3 continuation.

4.9b	69 59 64 60 64	81 91 103 89 84	0.84 0.65 0.63 0.68 0.76 (0.71 ± 0.04)
4.10b	65 51 69 88 56	92 81 95 90 91	0.71 0.63 0.73 0.98 0.61 (0.73 ± 0.07)
4.11b	25 60 89 81 90	34 82 117 109 117	0.73 0.72 0.76 0.74 0.77 (0.75 ± 0.01)
4.12b	25 58 87 78 87	34 82 117 109 117	0.74 0.71 0.74 0.72 0.74 (0.73 ± 0.01)
4.13b	70 76 77 79 81	91 100 101 97 99	0.76 0.76 0.77 0.82 0.83 (0.79 ± 0.02)
4.14b	82 76 52 76 80	100 94 69 95 96	0.82 0.81 0.75 0.79 0.83 (0.80 ± 0.02)

[a]Recoveries of peptides as well as internal standard 1-methyl-D-tryptophan from human plasma/PBS (1:2 v/v) using peptide concentrations of 40 μM and an internal standard concentration of 10 μM (five independent experiments). [b]Ratios of peptide recovery over recovery of 1-methyl-D-tryptophan calculated for individual experiments, as well as mean recovery ratios ± SEM. *Value not included in the mean.

Table A4.4. Overview of proposed relevant interactions between Y_4R residues and UR-AK86C (**2.4**) from IFD using cryo-EM structure of Y_4R.

Position in UR-AK86C (**2.4**)	Y_4R residues	Proposed relevant interactions
cyclo[succinyl-Arg^1-Tyr^2-Arg(carb, 4)^3] (*macrocycle$^{1-3}$*)	Asp105$^{2.68}$, Glu203, Glu288$^{6.58}$, Lys198, Asn301$^{7.32}$, Thr102, Glu298$^{7.28}$	Hydrogen bonding
	Ser204, Thr202, Val200, Phe184, Leu192, Phe194, Tyr401, Ile295	Non-hydrogen bonding Contacts
Leu^4	Cys201	Hydrogen bonding
	Ser178$^{4.64}$, Ile179	Non-hydrogen bonding Contacts
Arg^5	Asn301$^{7.32}$, Thr102, Glu288$^{6.58}$, Phe284$^{6.54}$, Gly300$^{7.31}$	Hydrogen bonding
Tyr^6-NH_2	Gln222$^{5.46}$, Asn285$^{6.55}$, His308$^{7.39}$	Hydrogen bonding
	Phe304$^{7.35}$, Leu281$^{6.51}$, Phe284$^{6.54}$, Val125$^{3.36}$, Cys132$^{3.43}$, Gln121$^{3.32}$	Non-hydrogen bonding Contacts

Table A4.5. Overview of proposed relevant hydrogen bonds interactions between Y_4R residues and the synthesized analogs in comparison with the proposed Y_4R-**2.4** interaction through IFD studies.

Y_4R residue	Synthesized Analogs of UR-AK86C (2.4)												
	4.2b	**4.3b**	**4.4b**	**4.5b**	**4.6b**	**4.7b**	**4.8b**	**4.9b**	**4.10b**	**4.11b**	**4.12b**	**4.13b**	**4.14b**
Thr102	n.d	+	+	-	+	-	+	-	n.d	-	-	n.d	n.d
Asp105$^{2.68}$	n.d	+	+	+	+	+	+	-	n.d	+	+	n.d	n.d
Lys198	n.d	+	-	-	-	-	-	-	n.d	+	-	n.d	n.d
Cys201	n.d	+	+	-	+	-	-	+	n.d	-	-	n.d	n.d
Glu203	n.d	+	+	+	+	+	+	+	n.d	+	+	n.d	n.d
Gln222$^{5.46}$	n.d	+	-	-	+	-	-	+	n.d	-	-	n.d	n.d
Phe284$^{6.54}$	n.d	-	-	-	-	-	-	-	n.d	-	+	n.d	n.d
Asn285$^{6.55}$	n.d	+	+	+	+	-	-	+	n.d	+	-	n.d	n.d
Glu288$^{6.58}$	n.d	+	+	+	+	+	+	+	n.d	+	+	n.d	n.d
Glu298$^{7.28}$	n.d	-	-	+	+	+	+	-	n.d	+	-	n.d	n.d
Gly300$^{7.31}$	n.d	-	-	+	-	-	-	+	n.d	+	-	n.d	n.d
Asn301$^{7.32}$,	n.d	+	+	+	+	+	+	+	n.d	+	+	n.d	n.d
His308$^{7.39}$	n.d	-	+	+	+	-	-	-	n.d	-	-	n.d	n.d

Table A4.6. Overview of proposed relevant non-hydrogen bonding contacts between Y_4R residues and the synthesized analogs in comparison with the proposed Y_4R-**2.4** interaction through IFD studies.

Y_4R residue	Synthesized Analogs of UR-AK86C (**2.4**)												
	4.2b	**4.3b**	**4.4b**	**4.5b**	**4.6b**	**4.7b**	**4.8b**	**4.9b**	**4.10b**	**4.11b**	**4.12b**	**4.13b**	**4.14b**
Gln121$^{3.32}$	n.d	+	+	+	+	-	+	+	n.d	+	-	n.d	n.d
Val125$^{3.36}$	n.d	+	+	-	-	-	-	+	n.d	-	-	n.d	n.d
Cys132$^{3.43}$	n.d	-	-	-	-	-	-	-	n.d	-	-	n.d	n.d
Ser178$^{4.64}$	n.d	-	+	-	+	-	-	+	n.d	-	-	n.d	n.d
Ile179	n.d	+	-	-	+	-	-	-	n.d	-	-	n.d	n.d
Phe184	n.d	+	+	+	+	+	-	-	n.d	-	-	n.d	n.d
Leu192	n.d	+	+	-	+	+	+	-	n.d	+	-	n.d	n.d
Phe194	n.d	+	-	-	-	-	+	-	n.d	-	+	n.d	n.d
Val200	n.d	+	+	-	+	+	+	-	n.d	+	+	n.d	n.d
Thr202	n.d	+	+	+	+	+	+	+	n.d	-	+	n.d	n.d
Ser204	n.d	+	-	+	+	-	-	-	n.d	-	+	n.d	n.d
Leu281$^{6.51}$	n.d	+	-	+	+	-	-	-	n.d	-	-	n.d	n.d
Phe284$^{6.54}$	n.d	-	-	-	-	-	-	-	n.d	-	+	n.d	n.d
Ile295	n.d	+	-	+	+	+	+	-	n.d	+	+	n.d	n.d
Phe 304$^{7.35}$	n.d	+	+	+	+	-	+	+	n.d	+	-	n.d	n.d
Tyr401	n.d	-	-	-	-	-	-	-	n.d	-	-	n.d	n.d

n.d – not determined

4.6.2 RP-HPLC chromatograms of peptides 4.2b–4.14b (Purity control)

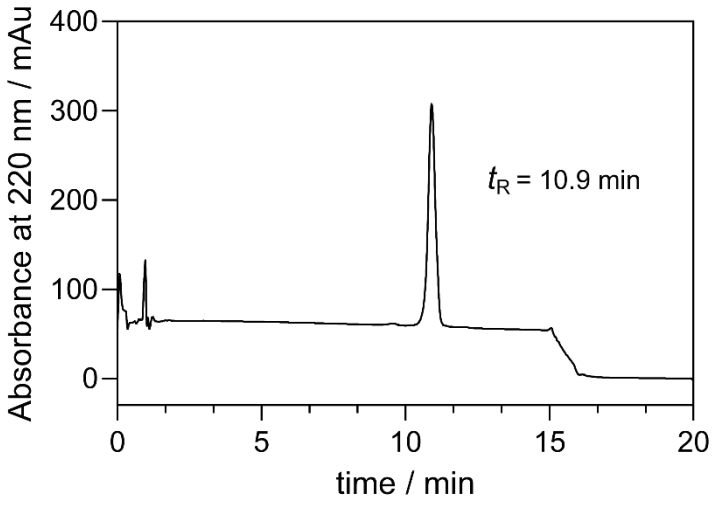

RP-HPLC analysis of peptide **4.2b**.

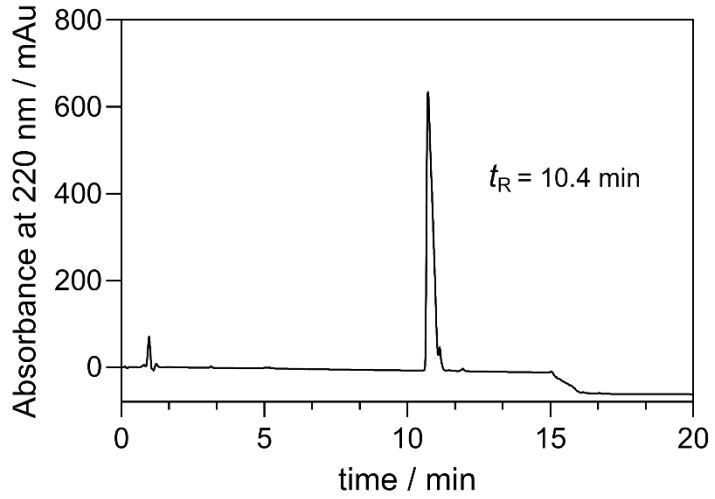

RP-HPLC analysis of peptide **4.3b**.

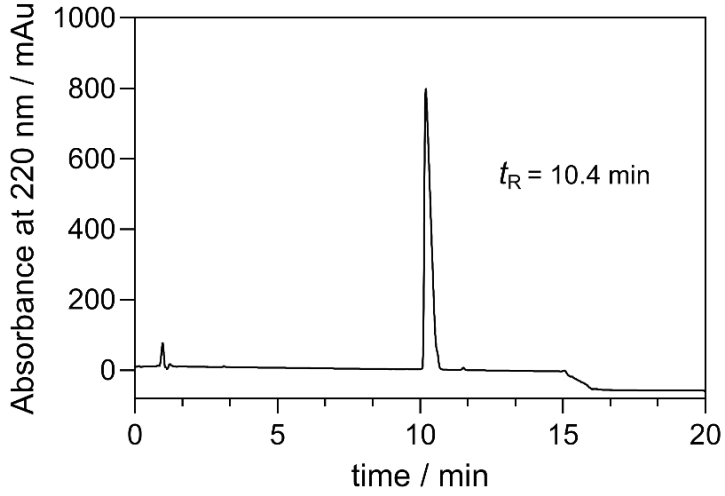

RP-HPLC analysis of peptide **4.4b**.

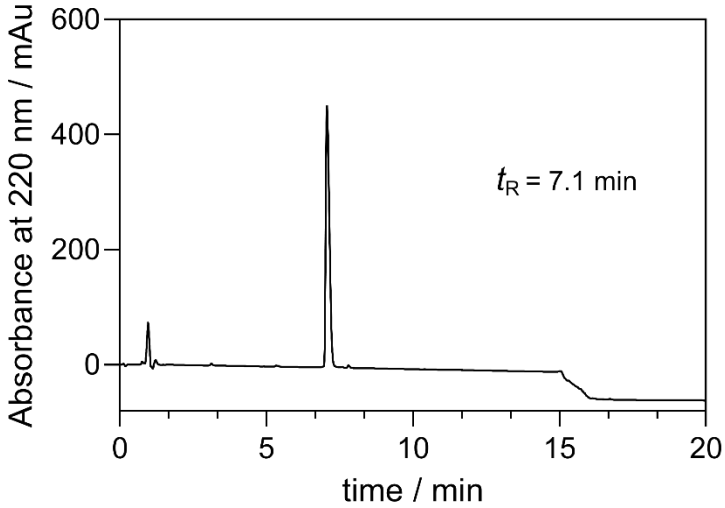

RP-HPLC analysis of peptide **4.5b**.

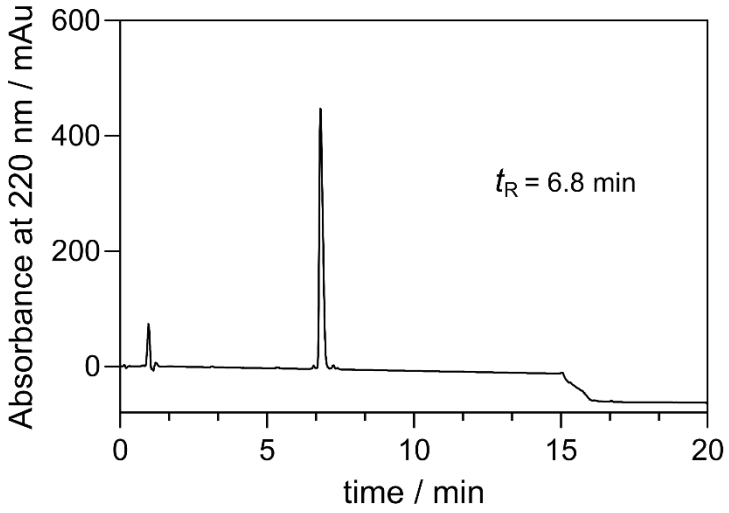

RP-HPLC analysis of peptide **4.6b**.

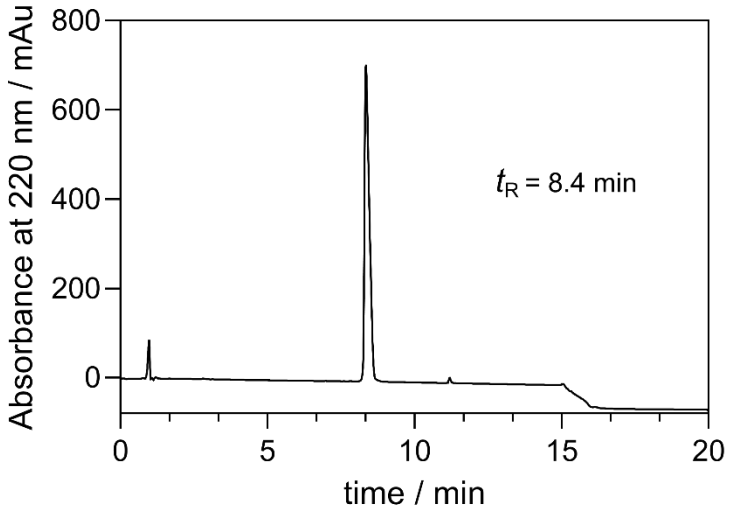

RP-HPLC analysis of peptide **4.7b**.

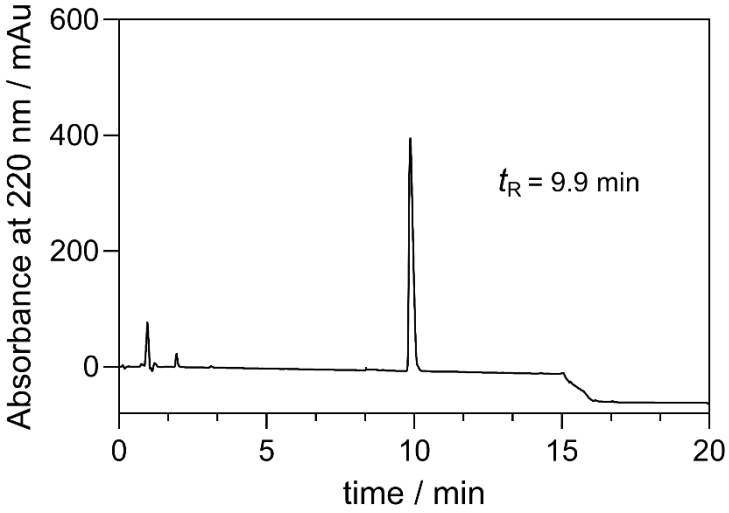

RP-HPLC analysis of peptide **4.8b**.

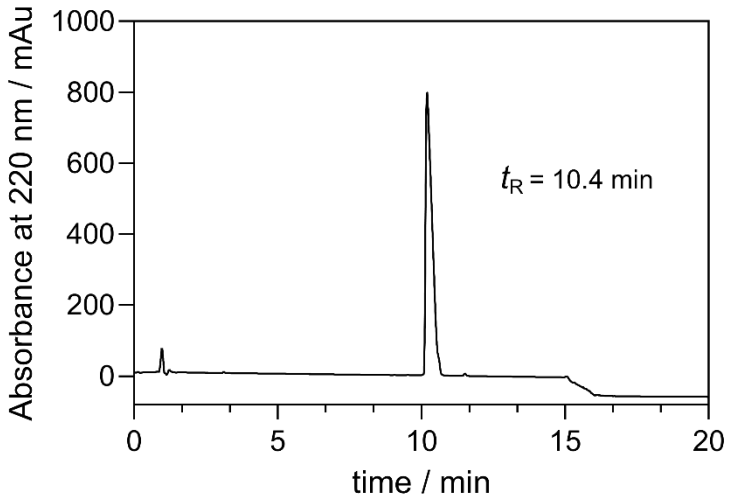

RP-HPLC analysis of peptide **4.9b**.

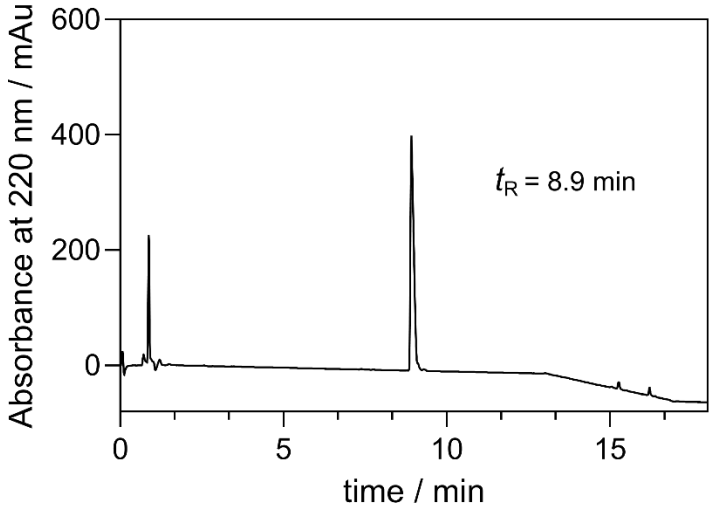

RP-HPLC analysis of peptide **4.10b**.

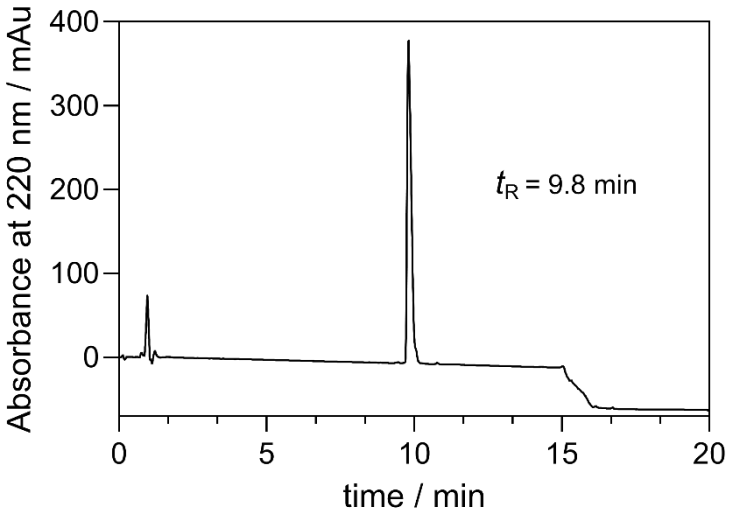

RP-HPLC analysis of peptide **4.11b**.

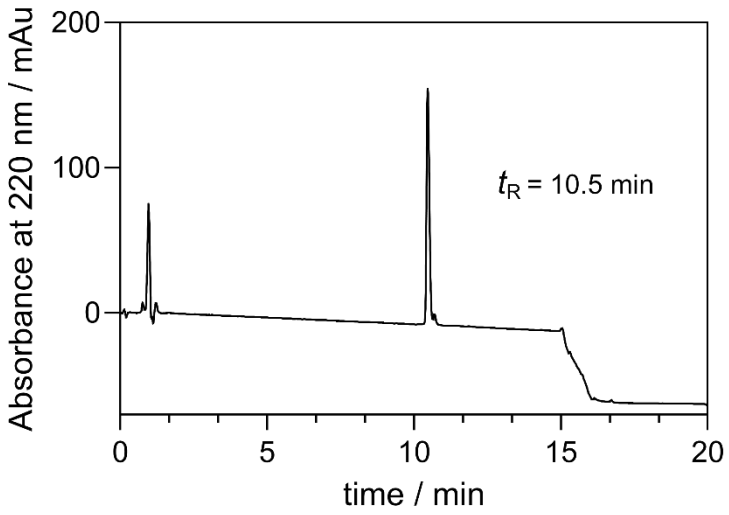

RP-HPLC analysis of peptide **4.12b**.

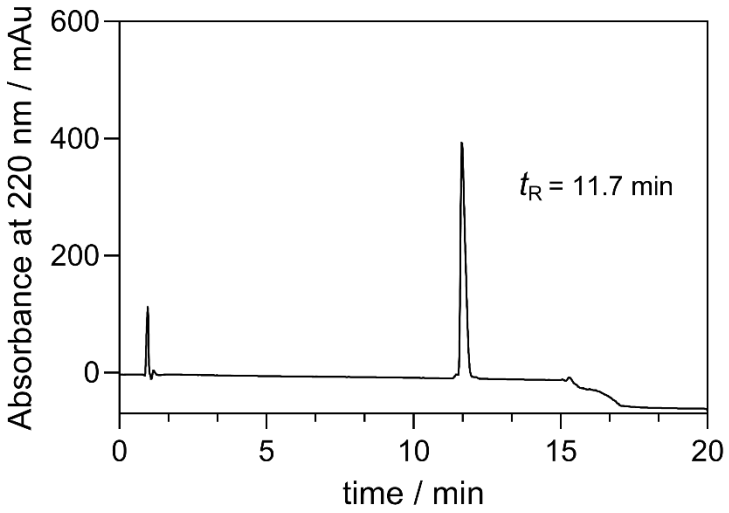

RP-HPLC analysis of peptide **4.13b**.

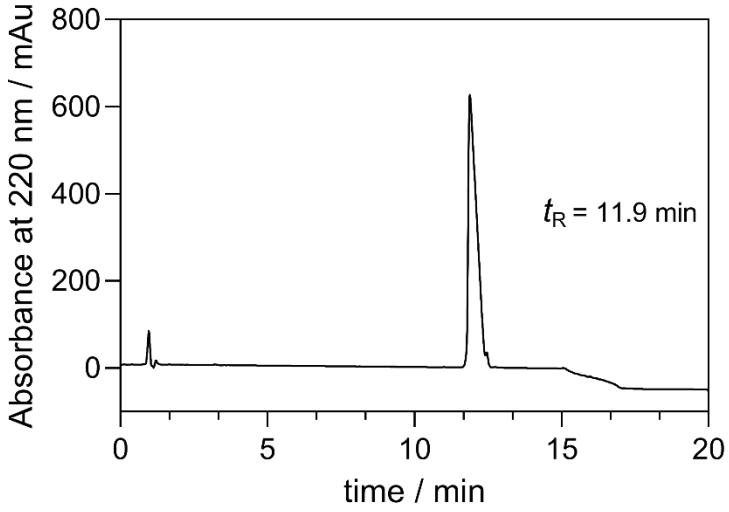

RP-HPLC analysis of peptide **4.14b**.

4.6.3 ^{1}H-NMR spectra of compounds 4.2b–4.14b in DMSO-d_6 and DMSO-d_6/D_2O

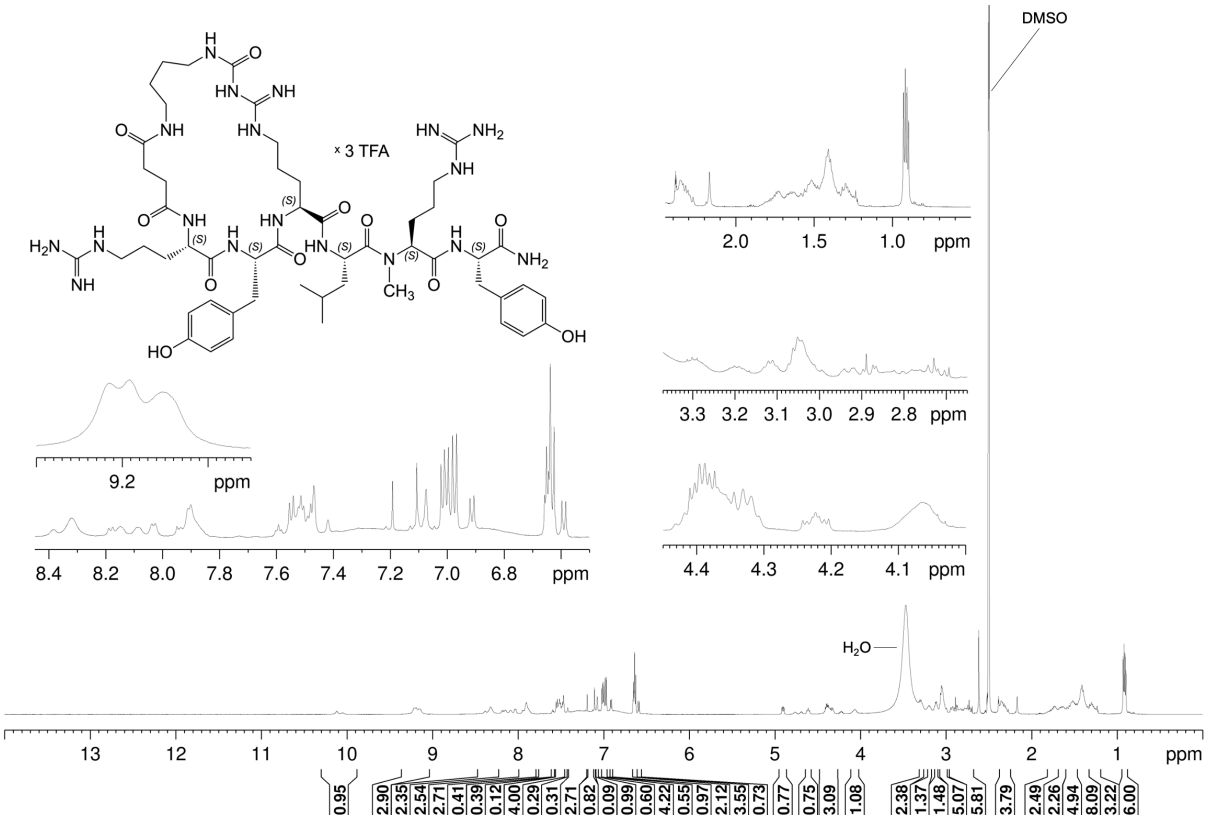

^{1}H-NMR spectrum (600 MHz, DMSO-d_6) of analog **4.2b**.

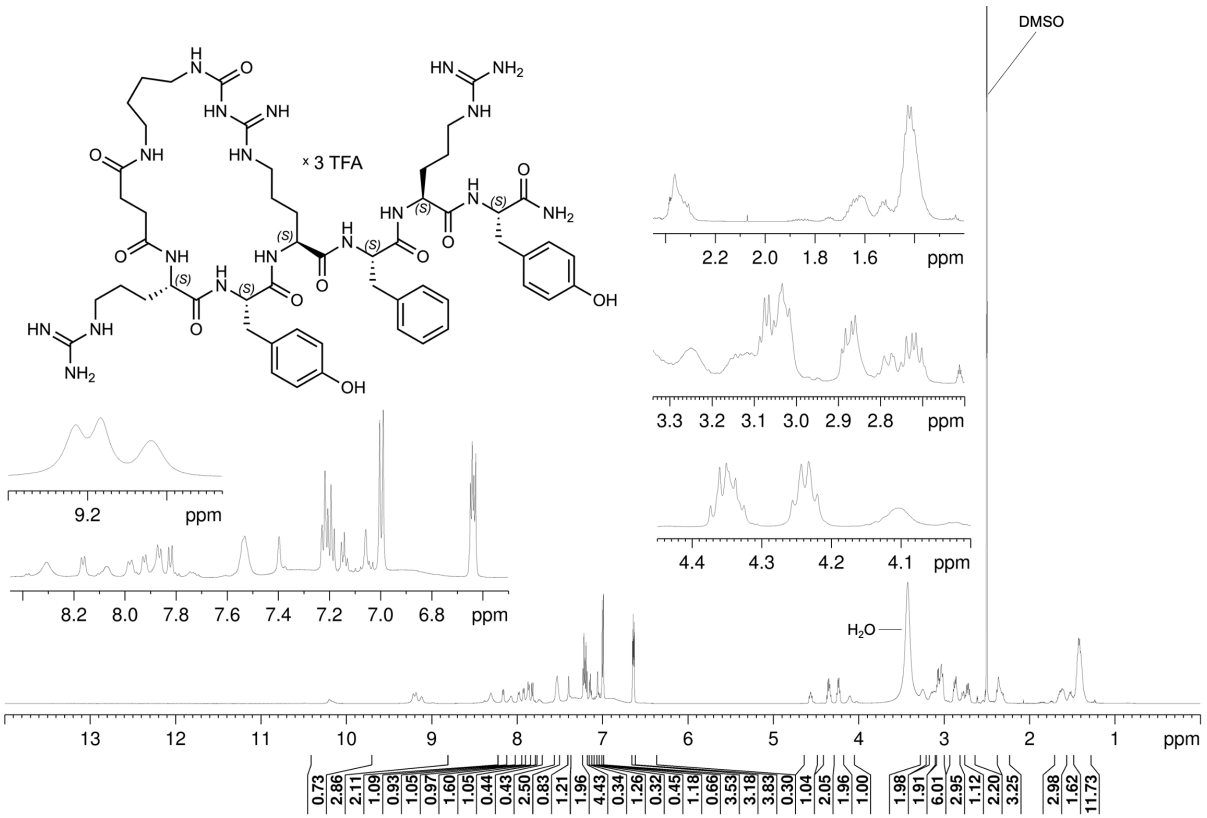

^{1}H-NMR spectrum (600 MHz, DMSO-d_6) of peptide **4.3b**.

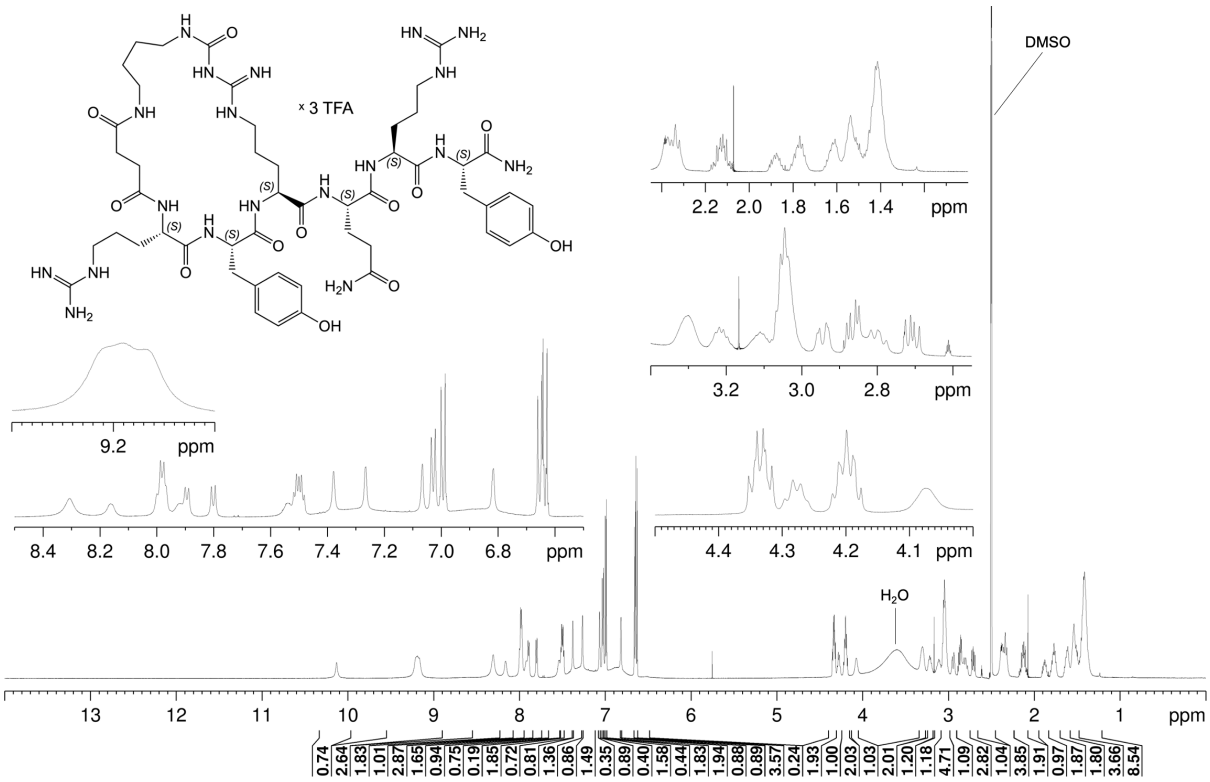

^{1}H-NMR spectrum (600 MHz, DMSO-d_6) of peptide **4.4b**.

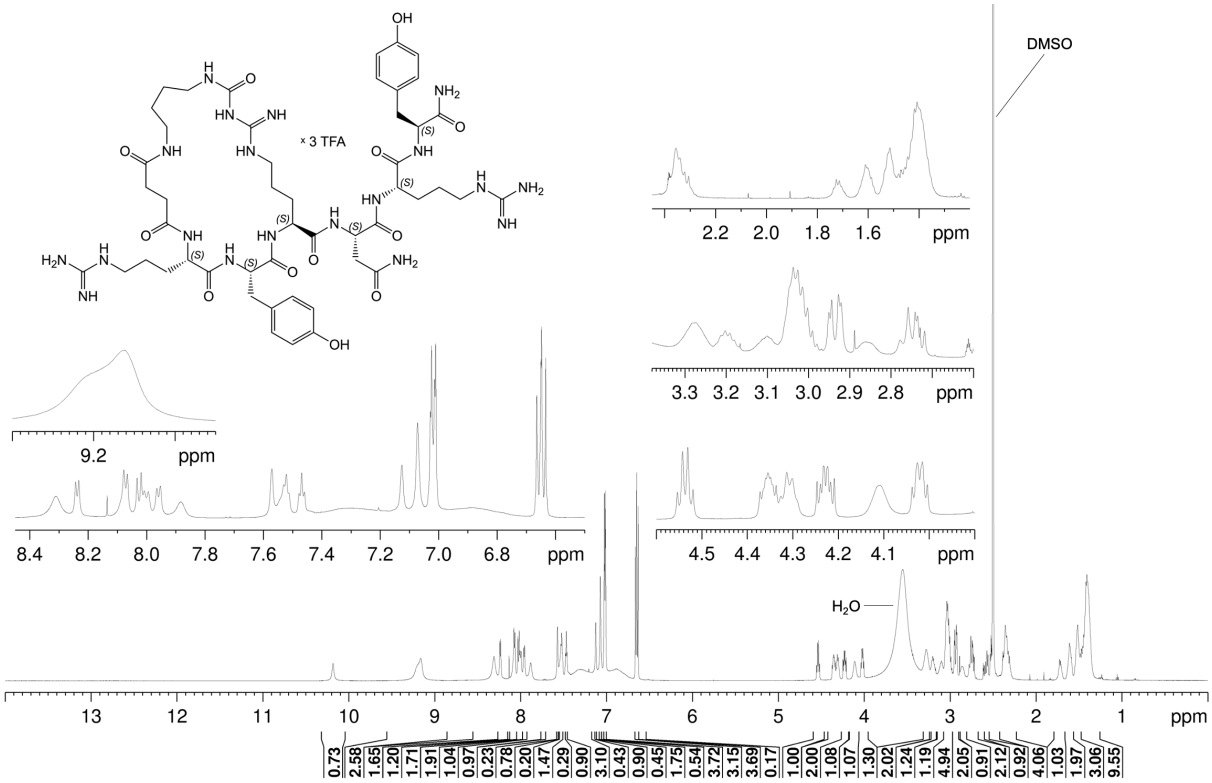

^{1}H-NMR spectrum (600 MHz, DMSO-d_6) of peptide **4.5b**.

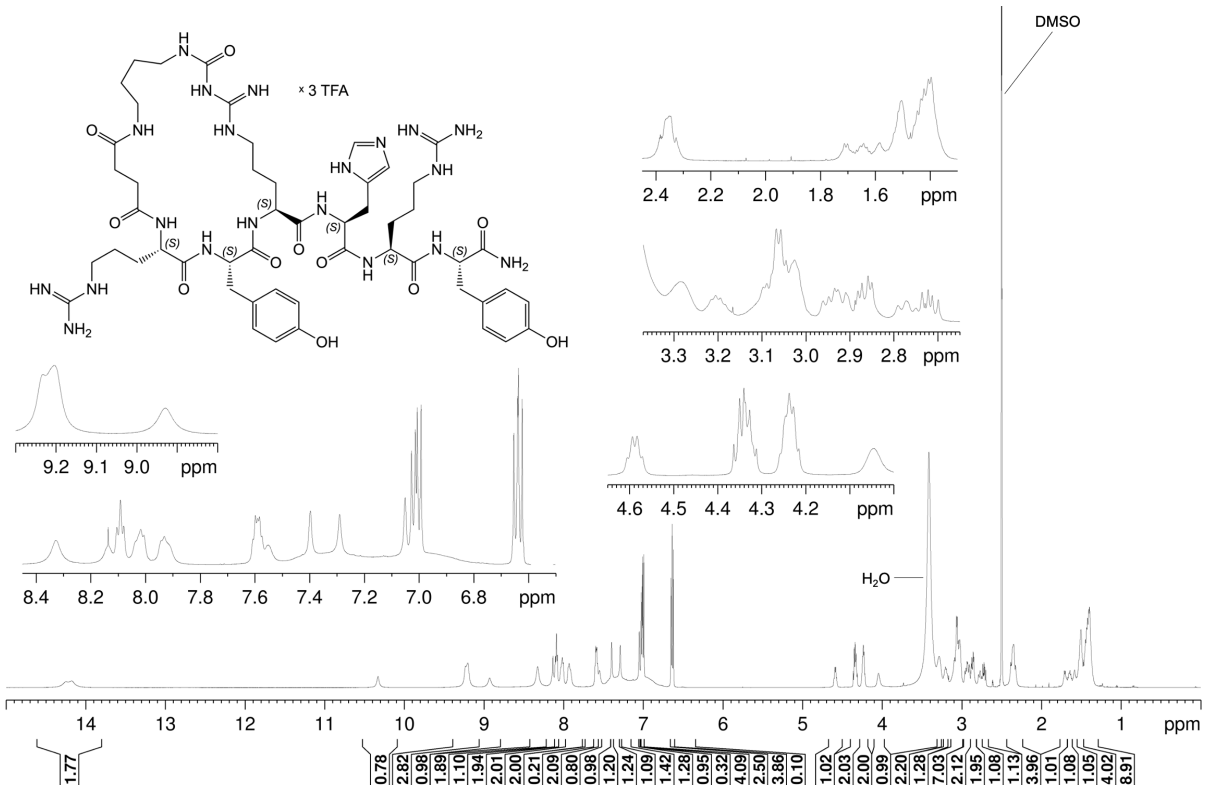

^{1}H-NMR spectrum (600 MHz, DMSO-d_6) of peptide **4.6b**.

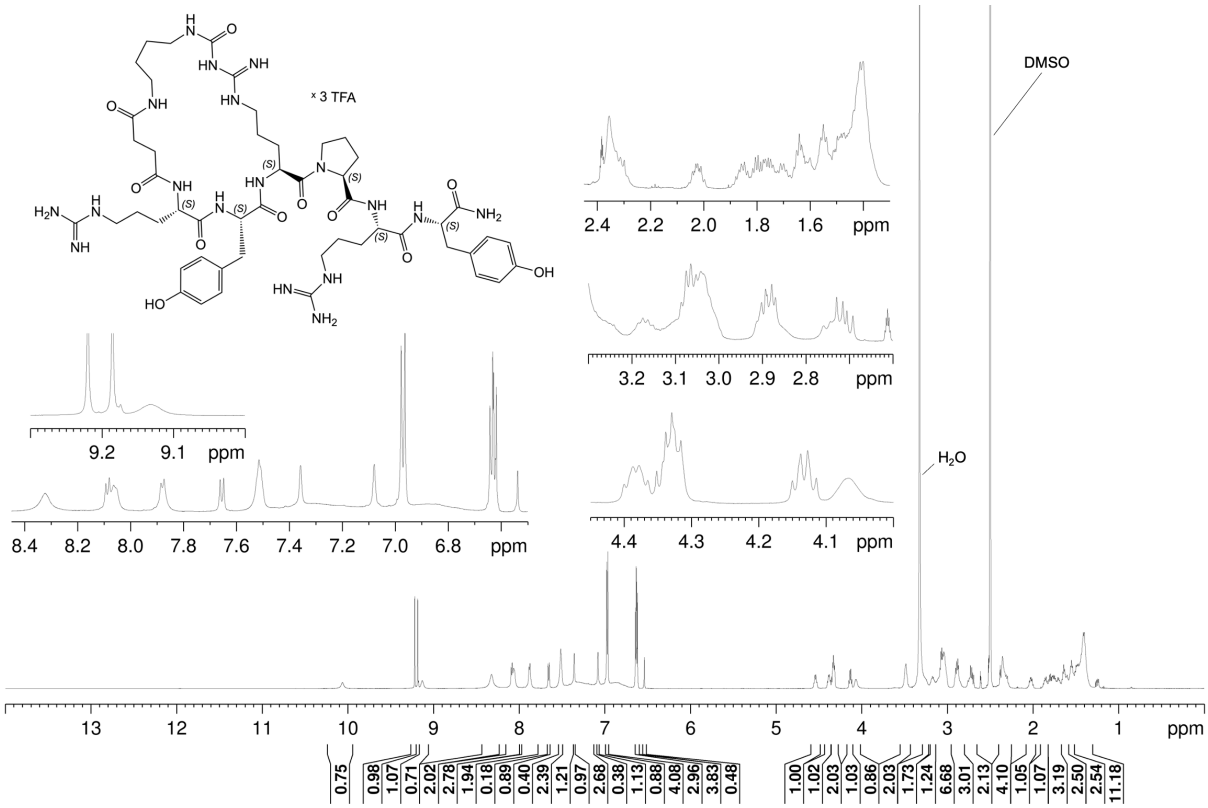

^{1}H-NMR spectrum (600 MHz, DMSO-d_6) of peptide **4.7b**.

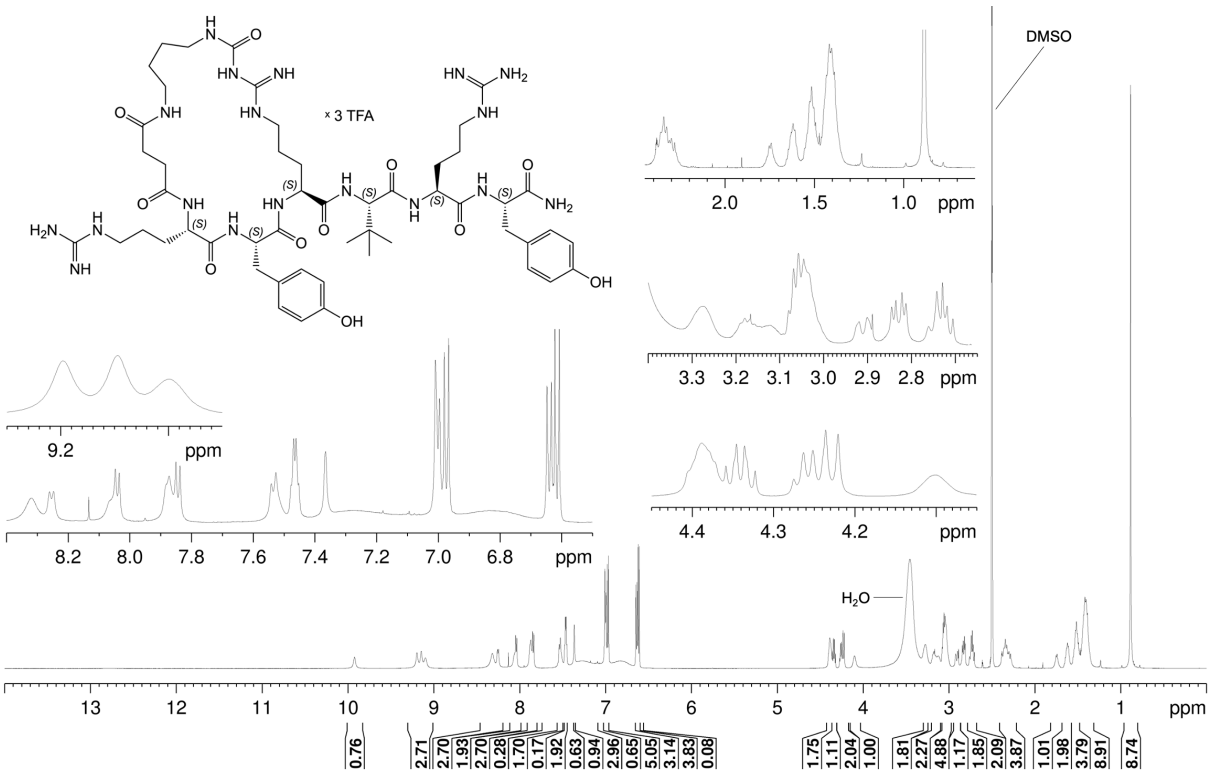

^{1}H-NMR spectrum (600 MHz, DMSO-d_6) of peptide **4.8b**.

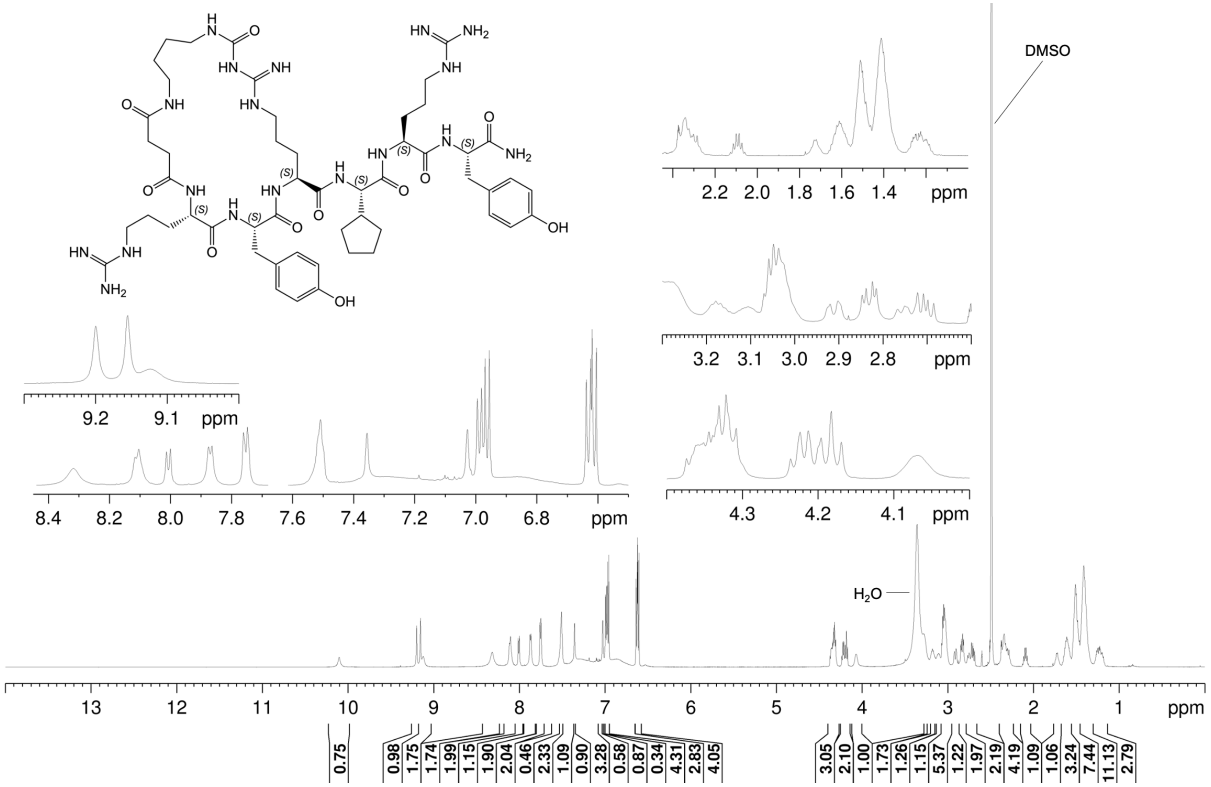

^{1}H-NMR spectrum (600 MHz, DMSO-d_6) of peptide **4.9b**.

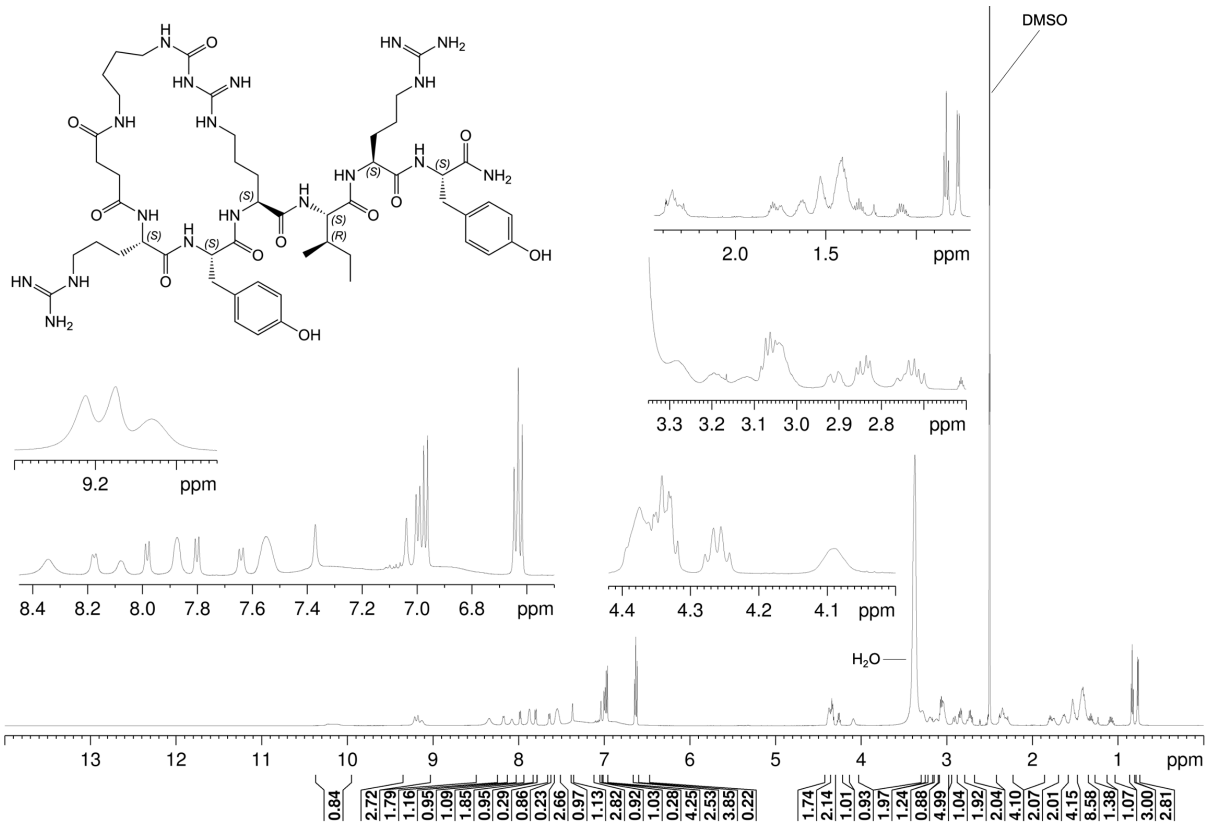

^{1}H-NMR spectrum (600 MHz, DMSO-d_6) of peptide **4.10b**.

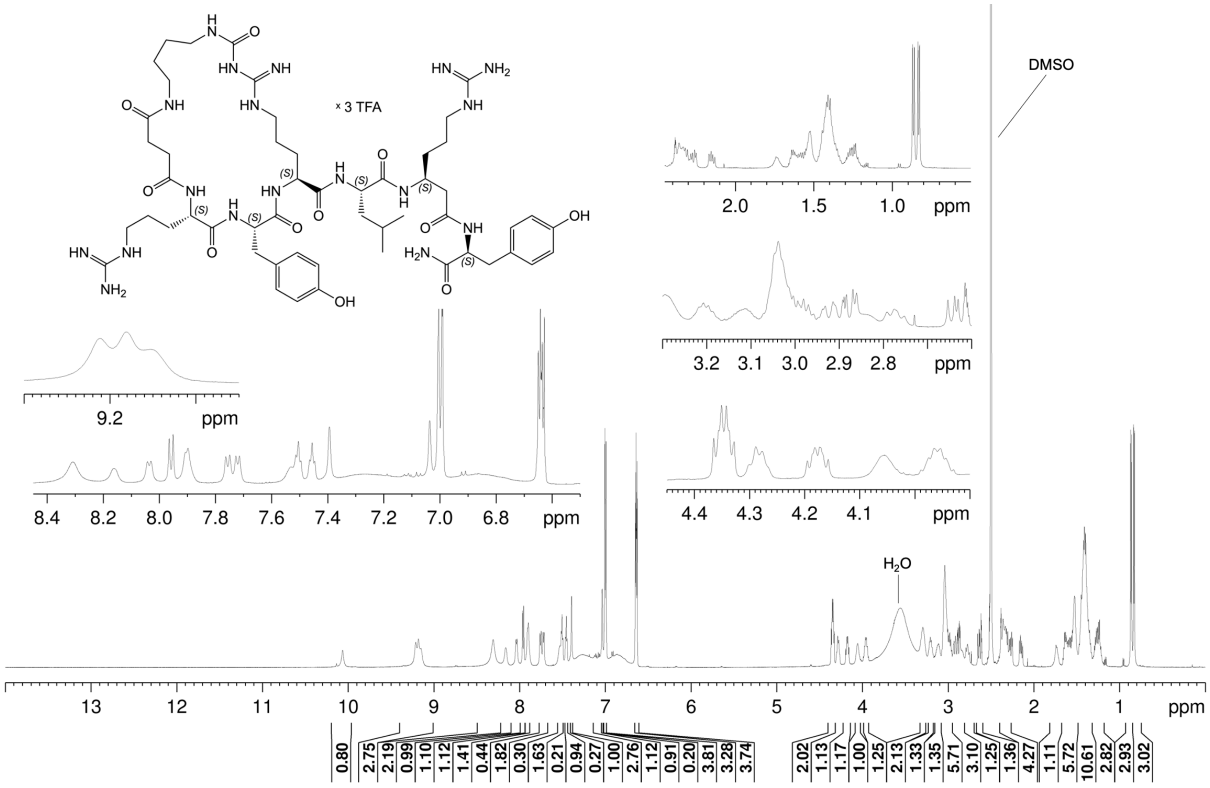

^{1}H-NMR spectrum (600 MHz, DMSO-d_6) of peptide **4.11b**.

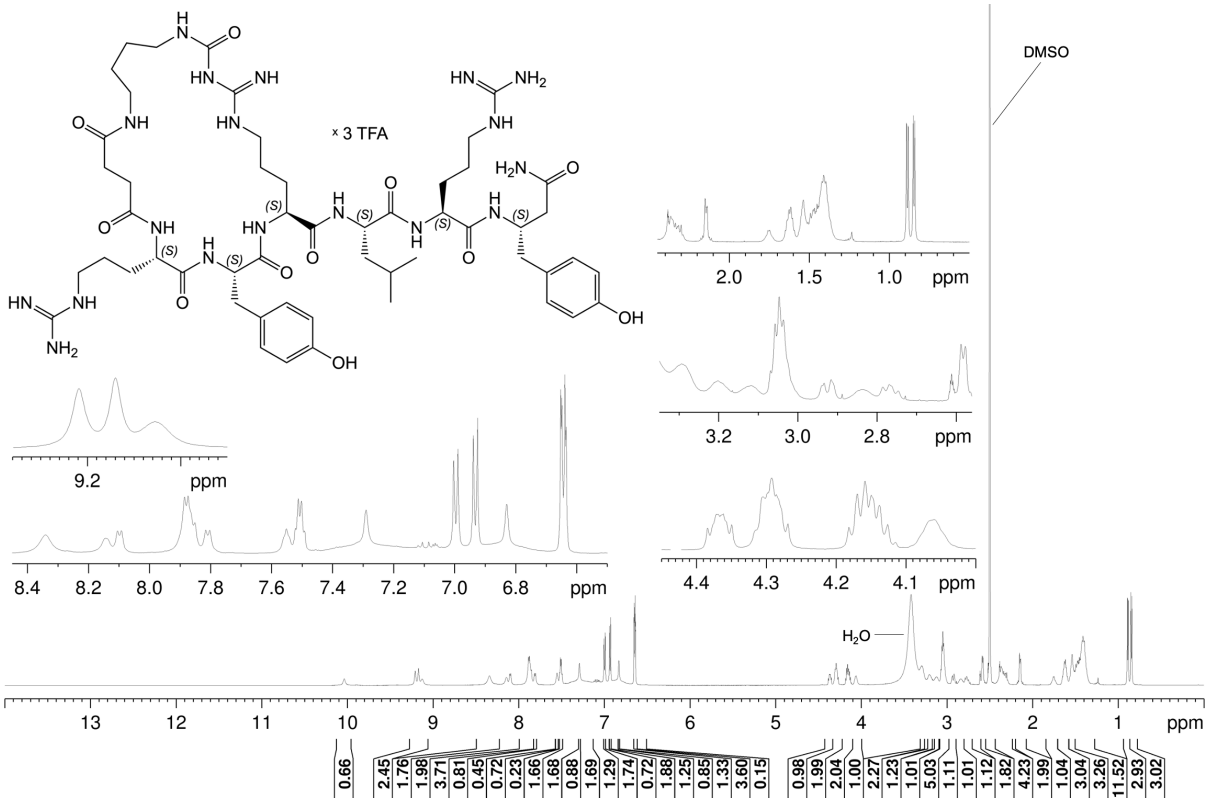

^{1}H-NMR spectrum (600 MHz, DMSO-d_6) of peptide **4.12b**.

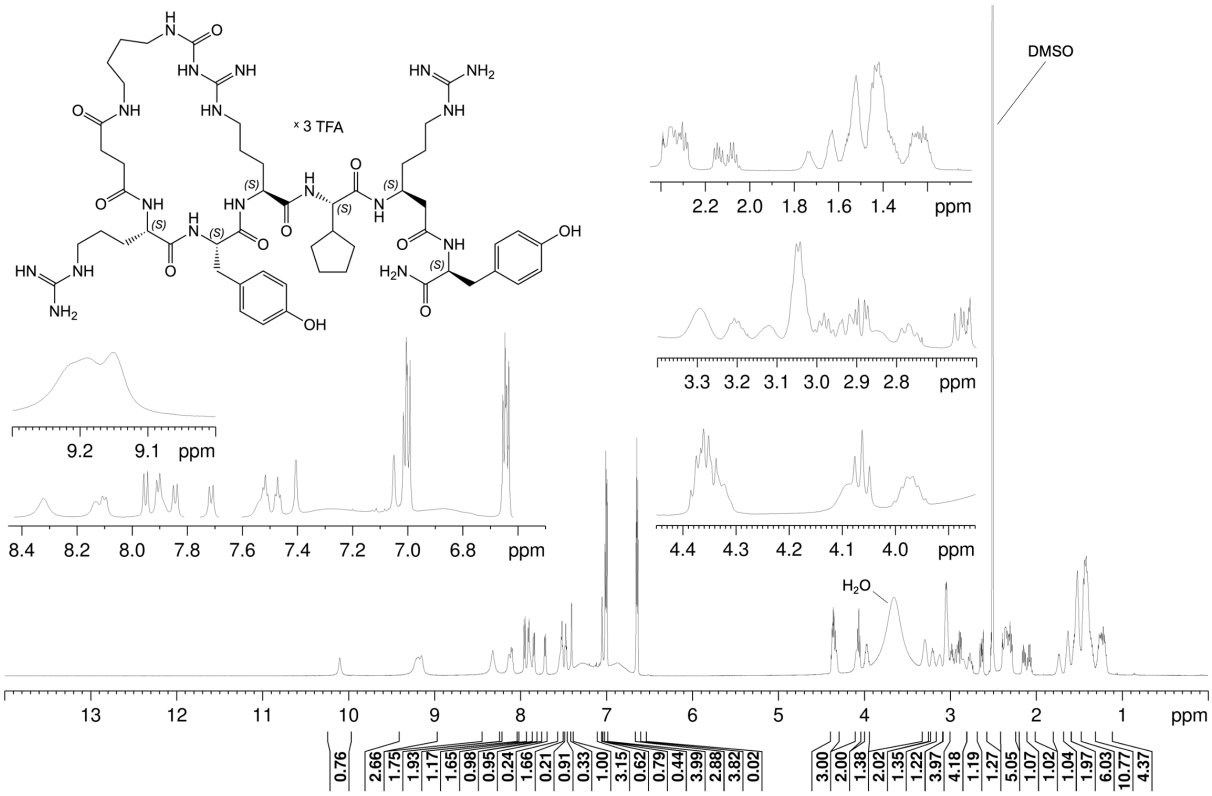

^{1}H-NMR spectrum (600 MHz, DMSO-d_6) of peptide **4.13b**.

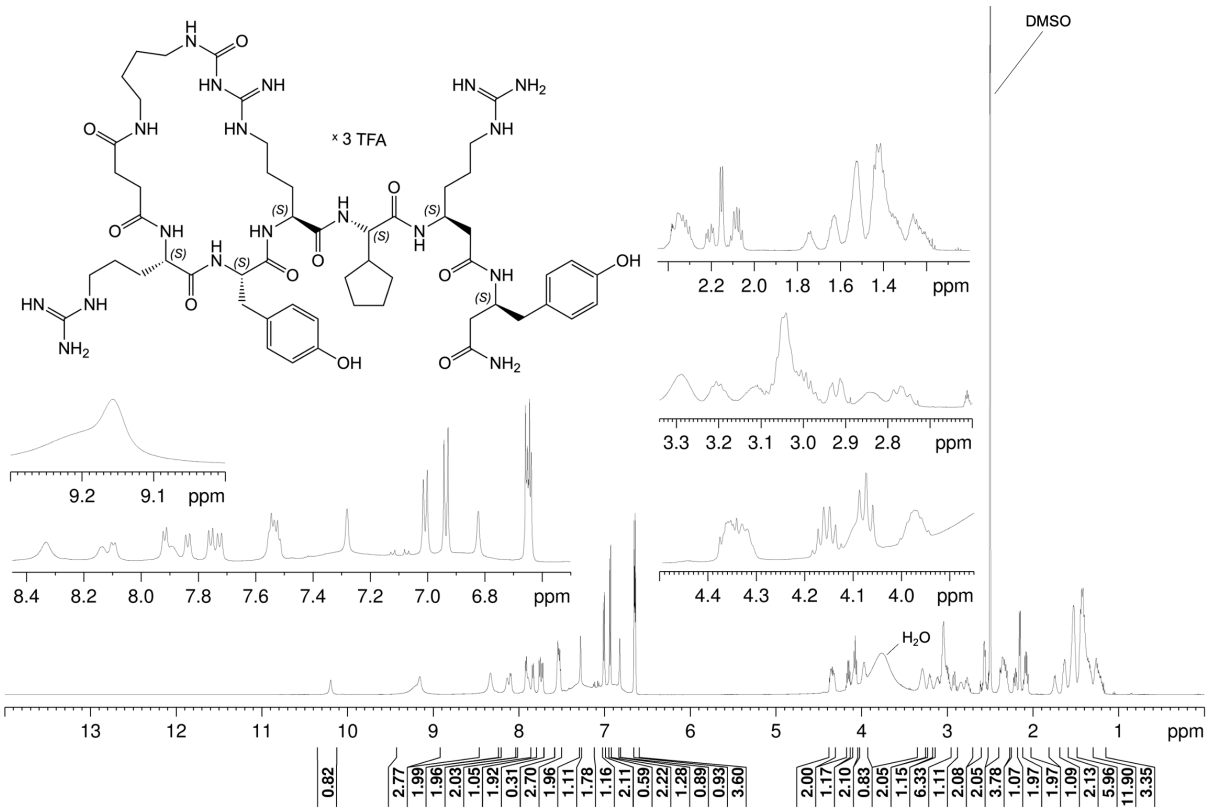

^{1}H-NMR spectrum (600 MHz, DMSO-d_6) of peptide **4.14b**.

Chapter 5

Design, Synthesis, and Characterization of UR-AK86C Derived Y_4R Agonists with Enhanced Lipophilicity

Note: In this chapter, the synthesis of the alkyne-functionalized arginine, the fluorescently labeled peptide UR-JG114, and the labeling of UR-AG15 with 3-azido-7-hydroxycoumarin to obtain UR-AG17 (**5.11**) were conducted by co-workers Thomas Brunner, Jakob Gleixner, and Fabian Ertl, respectively.

5.1 Introduction

The Y_4 receptor (Y_4R), a member of the neuropeptide Y (NPY) family, is associated with regulating important physiological functions such as feeding, energy homeostasis, gastrointestinal motility and secretion, circadian rhythm and is also involved in the pathophysiological condition of obesity.[1-4] With its role in these physiological processes, several rodent and human studies have highlighted its therapeutic potential in treating disorders that disrupt feeding, energy homeostasis, and gastrointestinal motility.[5-10]

The known expression regions of the NPY family of receptors are in both the CNS and peripheral tissues.[13] For Y_4R, several studies have confirmed its presence in human and rodent peripheral tissues, particularly in the intestines and pancreas, as well as in brain regions such as the hypothalamus, area postrema, and hippocampus.[2, 11-14] Despite these findings, it remains unclear how and where the observed physiological effects of the receptor's activity arise. Earlier studies by Adrian *et al*.[15] and Adrian *et al*.[16] have suggested that its endogenously preferred ligand, pancreatic polypeptide (PP), mostly produced in the pancreas, primarily acts in the intestine. This implies that the observed effects on feeding, energy homeostasis, and gastrointestinal motility and secretion originate from activities of the receptor in the peripheral tissues, mainly the intestine. On the contrary, a much later study by Whitcomb *et al.*[13], where radiolabeled PP was peripherally injected into mice, revealed the binding of PP to Y_4R in brain regions known to regulate feeding and energy homeostasis. Further studies on the physiological activities of Y_4R in the brain also showed significant involvement in the regulatory effects attributed to feeding.[17, 18] These findings also suggest that the physiological effects of Y_4R activation observed in both the CNS and peripheral tissues are complementary or synergistic.

Given that Y_4R is a potential therapeutic target in the treatment of feeding and energy homeostasis-related disorders/diseases, it is necessary to understand the origin of the regulatory effects in addition to the distal signaling processes. It is, therefore, of utmost importance to develop molecular tools that can be used to separately study the effects of Y_4R in the CNS and peripheral tissues. The CNS functions in a controlled microenvironment, which is protected from substances in the bloodstream through a tight monolayer of microvascular endothelial cells lining the cerebral capillaries penetrating the brain.[19] This layer forms a selective and semi-permeable barrier known

as the blood-brain barrier (BBB), which controls the influx or efflux of biological substances into and from the brain, only allowing a small fraction of these (about 3%) to permeate.[20] Accordingly, this study was mainly focused on developing analogs of the potent Y_4R cyclic hexapeptide agonist UR-AK86C (**2.4**) (Figure 4.1), with enhanced lipophilicities to facilitate their translocation across cell barriers such as the BBB, potentially improving their bioavailability. These analogs could then serve as molecular tools that can be used to investigate the possible additive or synergistic effect of the Y_4R in the brain.

5.2 Materials and Methods

5.2.1 Materials

The protected amino acids Fmoc-Tyr(tBu)-OH and Fmoc-Arg(Pbf)-OH were purchased from Carbolution Chemicals (St. Ingbert, Germany). Fmoc-Cpg-OH was obtained from BLD Pharma (Reinbek, Germany). *N*-methyl-2-pyrrolidinone (NMP) for peptide synthesis, and PyBOP were obtained from Iris Biotech (Marktredwitz, Germany). Fmoc-*N*-Me-Arg(Pbf)-OH, Fmoc-Leu-OH, 2-(1*H*-benzo[*d*][1,2,3]triazol-1-yl)-1,1,3,3-tetramethylisouronium (HBTU), Oxyma pure, *N,N'*-diisopropylcarbodiimide (DIC), Ramage amide resin (0.66 mmol/g), gradient grade MeOH for HPLC, and trifluoroacetic acid (TFA) were from Merck (Darmstadt, Germany). Hydroxybenzotriazole (HOBt) hydrate, succinic anhydride, and dichloromethane (CH_2Cl_2) were purchased from Acros Organics/Fisher Scientific (Nidderau, Germany). *N,N*-diisopropylethylamine (DIPEA), *tert*-butyl (3-aminopropyl)carbamate, and 5-((*tert*-butoxycarbonyl)amino)pentanoic acid were obtained from ABCR (Karlsruhe, Germany). Triisopropylsilane (TIPS), Dimethylformamide (DMF) for peptide synthesis, absolute EtOH, gradient grade acetonitrile (MeCN) for HPLC, forskolin, ramipril, and piperidine were from Sigma-Aldrich (Taufkirchen, Germany). MLN4760 was obtained from Bio-Techne GmbH (Wiesbaden, Germany), and ramiprilat was obtained according to the reported procedure[21] involving the hydrolysis of esters in compounds such as ramipril. Human pancreatic polypeptide (hPP) was from SynPeptide (Shanghai, China). The fluorescent dye 3-azido-7-hydroxycoumarin was purchased from TCI (Eschborn, Germany). The syntheses of UR-AK86C (**2.4**),[22] UR-JG114,[23] the azido functionalized dye Cy3B (**5.7**),[24] and [K^4-[^{3}H]propionyl]hPYY (molar activity: 3.44 TBq/mmol),[25] and [^{3}H]UR-JG102 (molar activity: 3.44 TBq/mmol)[26] were reported elsewhere. [^{3}H]UR-MK299 (molar activity: 3.885 TBq/mmol) was prepared according to a reported procedure.[27] [^{3}H]Propionyl-pNPY (molar activity: 1.39 TBq/mmol)[27] was prepared as previously reported but with minor modification as described by Müller *et al.*[28] Coelenterazine h was purchased from Biotrend (Cologne, Germany). Bacitracin and bovine serum albumin (BSA) were from Serva (Heidelberg, Germany). Fetal bovine serum (FBS) was purchased from Pan-Biotech (Aidenbach, Germany). Deuterated solvents were from Deutero (Kastellaun, Germany). Blood plasma was obtained by the collection of human blood from a healthy female donor in 5.5 mL heparinized plasma-monovettes followed by centrifugation at 1,200 g at 4 °C for

10 min. The supernatants were pooled in two 50 mL Falcon tubes and centrifuged again at 1,200 g at 4 °C for 10 min. The supernatant made of plasma was aliquoted and stored at −80 °C. Ultrapure water was used to prepare stock solutions, buffers, and eluents for HPLC. Polypropylene reaction vessels (1.5 and 2 mL) from Sarstedt (Nümbrecht, Germany) (in the following referred to as “reaction vessel”) were used to keep stock solutions and for the preparation of dilution series of the peptides.

5.2.2 Methods

Instruments and conditions used for mass spectrometry, NMR spectroscopy, and preparative HPLC were the same as described in Chapter 4.

5.2.2.1 Analytical HPLC

Analytical HPLC analysis was performed with a system from Agilent Technologies composed of a 1290 Infinity binary pump equipped with a degasser, a 1290 Infinity autosampler, a 1290 Infinity thermostatted column compartment, a 1260 Infinity UV/vis diode array detector, and a 1260 Infinity fluorescence detector. A Kinetex-XB C18, 2.6 µm, 100 × 3 mm (Phenomenex) RP column served as stationary phase at a flow rate of 0.6 mL/min. Detection was performed at 220 nm, and the oven temperature was 25 °C. Mixtures of MeCN (A) and 0.04% aqueous TFA (B) were used as mobile phase. The following linear gradients were applied: compound **5.5**: 0–30 min: MeCN/0.04% aqueous TFA 10:90-5:95, 40–41 min: 5:95-90:10, 41–50 min: 90:10 (isocratic); peptides **5.8a**, **5.8b**, **5.9a, 5.9b**, **5.10a**, **5.13a**, and **5.13b**: 0–14 min: A/B 5:95-25:75, 14–16 min: 25:75-95:5, 16–20 min: 95:5 (isocratic); peptides **5.10b**, **5.11**: 0–14 min: A/B 10:90-40:60, 14–16 min: 40:60-95:5, 16–20 min: 95:5 (isocratic); and peptide **5.12**: 0–14 min: A/B 20:80-40:60, 14–16 min: 40:60-95:5, 16–20 min: 95:5 (isocratic). The injection volume was 20 µL. Retention (capacity) factors k were calculated from the retention times t_R according to $k = (t_R - t_0)/t_0$ (t_0 = dead time).

5.2.2.2 General procedure for solid phase peptide synthesis (SPPS)

Peptides were synthesized either on Fmoc-Sieber-PS-resins or Ramage amide resins by the manual Fmoc strategy SPPS using DMF/NMP (8:2 v/v) as the solvent for the coupling reactions and the cleavage of Fmoc groups. 5 mL Injekt Solo (B. Braun, Melsungen, Germany) or NPRM-JECT (Henke Sass Wolf, Tuttlingen, Germany) syringes, equipped with polyethylene frits (pore size: 35 µm) (Roland Vetter Laborbedarf, Ammerbuch, Germany) were used as reaction vessels. DMF/NMP

(8:2 v/v) was used as a solvent for the coupling reactions and the cleavage of Fmoc groups. For synthesis using Fmoc-Sieber-PS-resin, initial Fmoc deprotection, and swelling were performed by treating the resin with 20% piperidine in the solvent at rt for 2 × 20 min. In the case of Ramage amide resin, the resin was first allowed to swell in solvent for 45 min at rt, followed by initial Fmoc deprotection with 20% piperidine in solvent (2 × 20 min at rt). For the synthesis of linear precursor peptides **5.8a**, **5.9a**, **5.10a**, and **5.13a**, the respective protected amino acids (Fmoc-aa) were used in 5-fold excess and preactivated with HBTU (4.9 equiv.)/HOBt (5 equiv.)/DIPEA (10 equiv.) in polypropylene reaction vessels for at least 5 min prior to addition to the resin (volume of the solvent: ca. 2.2 mL/mmol Fmoc-aa). In the case of standard (natural) Fmoc-aa, "double" coupling (2 × 45 min) was performed at 35 °C. Special building blocks **4.2**[29], **5.5**, and **5.6**[30] (Arginine derivatives; Figure 5.1) were used in 3-fold excess, preactivated with HBTU (2.95 equiv.)/HOBt (3 equiv.)/DIPEA (6 equiv.) (volume of the solvent: ca. 1.6 mL/mmol building block), and the reaction was performed at 35 °C for at least 4 h (maximum 18 h) for the first coupling followed by a second coupling using 3-fold excess and a pre-activation with Oxyma Pure (3 equiv.)/DIC (3 equiv.) also performed at 35 °C for at least 4 h. For the synthesis of **5.13a**, both protected amino acids and the special building blocks were used in 4-fold excess, preactivated with Oxyma Pure (4 equiv.)/DIC (4 equiv.), and a double coupling was performed using the same conditions. During the coupling reactions, syringes were shaken using a Multi Reax shaker (Heidolph, Schwabach, Germany) covered with a box, which was equipped with a thermostat-controlled heater. After coupling and Fmoc deprotection of the final amino acid, the resin-bound completely elongated peptide was treated with succinic anhydrate (10 equiv)/DIPEA (10 equiv) in the solvent at 35 °C for 30 min (see *Section 5.2.2.4* for the synthesis protocol of the respective linear peptides).

For synthesis using Sieber resins, the resin was washed with solvent (6 ×) and CH_2Cl_2 (treated with K_2CO_3) (4 ×) after this treatment, followed by cleavage of the resin with CH_2Cl_2/TFA (3:1 v/v) at rt (2 × 20 min, performed in the syringe). After the completion of cleavage, the liquid from the resin was collected, and the resin was washed three times with CH_2Cl_2/TFA (3:1 v/v). The washings were collected and combined with the cleavage liquid in a 100 mL round-bottom flask, where the volatiles were removed by rotary evaporation. The residue was dissolved in TFA/H_2O (95:5 v/v), and the mixture was stirred at rt for 3–5 h (for full side chain deprotection). With respect to syntheses

using Ramage amide resin, the resin was washed with solvent (6 ×) followed by treatment with TFA/TIPS/H_2O (95:2.5:2.5 v/v) at rt (2 × 30 min, performed in the syringe) to cleave peptides off the resin. The liquids from the cleavage were collected in a 100 mL round-bottom flask, and the resin was washed three times with the cleavage cocktail. The washings were added to the 100 mL round-bottom flask, and the combined mixture was directly stirred for at least 3–5 h.

After stirring, the volatiles were removed from the mixture by rotary evaporation, followed by the addition of 40–50 mL of water and lyophilization to obtain the crude peptide. The crude peptide was subsequently purified by preparative HPLC.

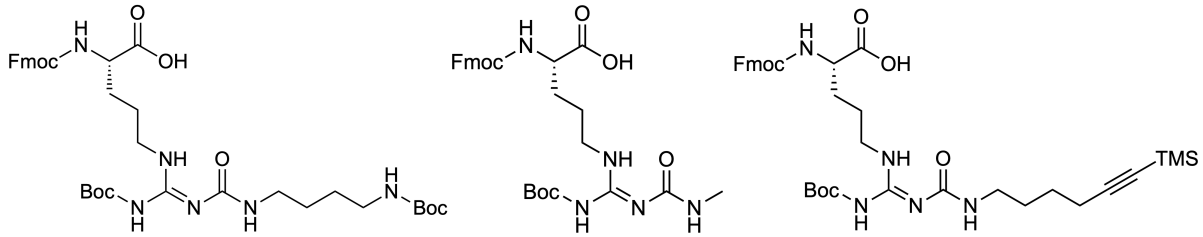

4.1 **5.5** **5.6**

Figure 5.1. Structures of the Fmoc and Boc, or the Fmoc, Boc, and TMS-protected N^{ω}-carbamoylated arginines **4.1**[29], **5.5**, and **5.6**[30], which were used in SPPS for the synthesis of linear precursor peptides.

5.2.2.3 Compound characterization

The synthesized amino acid building block **5.5** and its precursors **5.2** and **5.4** were characterized using ^{1}H-NMR and ^{13}C-NMR spectroscopy, HRMS, and RP-HPLC analysis. The linear precursor peptides **5.8a**, **5.9a**, **5.10a**, and **5.13a** were characterized by only HRMS, whereas the cyclic peptides **5.8b**, **5.9b**, and **5.13b** were characterized by ^{1}H-NMR and ^{1}H-COSY NMR spectroscopy, HRMS, and RP-HPLC analysis. Peptide **5.10b** and the fluorescently labeled peptides **5.11** and **5.12** were characterized by HRMS and RP-HPLC analysis**.** The purity of all final compounds, determined by RP-HPLC (220 nm), was ≥ 95%. Annotation concerning the ^{1}H-NMR spectra (solvent: DMSO-d_6) of the peptides: to allow integration of the signals interfering with the broad water signal at ca 3.5 ppm, ^{1}H-NMR spectra were additionally recorded in DMSO-d_6/D_2O (10:1 or 4:1 v/v). An overview of the analytical data can be seen in Table 5.1.

5.2.2.4 Synthesis protocols and analytical data

N-Boc-N'-Methylcarbamoyl-S-methylisothiourea (**5.2**). Triethylamine (8.0 mL, 57.3 mmol, 2.0 equiv.) and 2,5-dioxopyrrolidin-1-yl methylcarbamate (5.5 g, 28.6 mmol, 1.0 equiv.) were added to a stirred solution of *N*-Boc-*S*-methylisothiourea (4.9 g, 28.6 mmol, 1.0 equiv.) in MeCN (50 mL) and the resulting mixture was stirred at rt for 26 h. The solvent was removed under reduced pressure, and the remaining residue was subjected to column chromatography (SiO_2 (40-63 µm), CH_2Cl_2/MeOH 9:1 v/v) to yield **5.2** as a colorless oil (3.2 g, 12.8 mmol, 45%).

^{1}H-NMR (400 MHz, $CDCl_3$): δ (ppm) 1.47 (s, 9H), 2.28 (s, 3H), 2.82 (d, *J* = 5.1 Hz, 3H), 5.51 (br s, 1H), 12.27 (s, 1H). ^{13}C-NMR (101 MHz, $CDCl_3$): δ (ppm) 14.2, 26.7, 28.0, 82.6, 151.1, 162.6, 167.2 (three carbons). LC-HRMS (+ESI): *m*/*z* $[M+H]^+$ calcd. for $[C_9H_{18}N_3O_3S]^+$ 248.1063, found 248.1060. $C_9H_{17}N_3O_3S$ (247.31).

Benzyl (E)-N2-(((9H-fluoren-9-yl)methoxy)carbonyl)-Nω-(tert-butoxycarbonyl)-Nω'-(methylcarbamoyl)-L-argininate (**5.4**). $HgCl_2$ (2.1 g, 7.84 mmol, 1.5 equiv.), diisopropylethylamine (3.2 mL, 18.3 mmol, 3.5 equiv.), and **5.2** (1.3 g, 5.23 mmol, 1.0 equiv.) were added to a stirred solution of **3**[29] (2.9 g, 5.23 mmol, 1.0 equiv.) in CH_2Cl_2 (60 mL) and the mixture was stirred at rt for 1.5 h. The suspension was centrifuged, the supernatant was collected, and the pellet was washed with CH_2Cl_2 (3 x 20 mL, each followed by centrifugation). The organic phases were combined, and the solvent was removed under reduced pressure. The remaining residue was subjected to column chromatography (petroleum ether/ethyl acetate 4:1 to 3:2 v/v) to obtain **5.4** as a white crystalline solid (2.8 g, 83%).

^{1}H-NMR (400 MHz, DMSO–d_6) (two major rotamers with a ratio of approximately 1:1 were evident in the ^{1}H and ^{13}C NMR spectra): δ (ppm) 1.40 (s, 4H), 1.45 (s, 5H), 1.49–1.61 (m, 2H), 1.84–1.62 (m, 2H), 2.55 (d, *J* = 4.7 Hz, 1.5H), 2.62 (d, *J* = 4.3 Hz, 1.5H), 3.21–3.32 (m, 2H), 4.09–4.18 (m, 1H), 4.19–4.26 (m, 1H), 4.26–4.39 (m, 2H), 5.08–5.18 (m, 2H), 6.83 (q, *J* = 4.7 Hz, 0.5H), 7.27–7.36 (m, 7H), 7.37–7.46 (m, 2H), 7.68–7.75 (m, 2H), 7.84–7.94 (m, 3.5H), 8.07 (t, *J* = 5.9 Hz, 0.5H), 9.17 (t, *J* = 5.6 Hz, 0.5H), 11.15 (s, 0.5H), 12.50 (s, 0.5H). ^{13}C-NMR (101 MHz, DMSO-d_6): δ (ppm) 25.3 (0.5 carbons), 25.4 (0.5 carbons), 25.9 (0.5 carbons), 26.2 (0.5 carbons), 27.7 (1.5 carbons), 28.0, 28.1 (1.5 carbons), 39.4, 46.7, 53.8, 65.7, 65.9, 77.4 (0.5 carbons), 81.9 (0.5 carbons), 120.1 (2 carbons), 125.2 (2 carbons), 127.1

(2 carbons), 127.6 (2 carbons), 127.7 (2 carbons), 127.9, 128.3 (2 carbons), 135.9, 140.7 (2 carbons), 143.7, 143.8, 152.4 (0.5 carbons), 152.9 (0.5 carbons), 155.1 (0.5 carbons), 156.2 (0.5 carbons), 156.5 (0.5 carbons), 162.7 (0.5 carbons), 164.8 (0.5 carbons), 172.1 (0.5 carbons), 172.2 (0.5 carbons). LC-HRMS (+ESI): *m*/*z* $[M+H]^+$ calcd. for $[C_{35}H_{42}N_5O_7]^+$ 644.3079, found 644.3084. $C_{35}H_{41}N_5O_7$ (643.74).

(E)-N2-(((9H-Fluoren-9-yl)methoxy)carbonyl)-Nω-(tert-butoxycarbonyl)-Nω'-(methylcarbamoyl)-L-arginine (**5.5**). In a two-necked 100 mL round-bottom flask, under an atmosphere of argon, a 10% Pd/C catalyst (445 mg, 10 mol%) was added to a solution of **5.4** in 2-propanol (50 mL) and a slow stream of hydrogen gas was passed through a cannula into the vigorously stirred suspension at rt for 2.5 h. The suspension was centrifuged, the supernatant was collected and the pellet was washed with 2-propanol (100 mL, followed by centrifugation). The organic phases were combined, and the solvent was removed under reduced pressure (water bath temperature < 35 °C). The remaining residue was subjected to column chromatography (CH_2Cl_2/EtOH 49:1 to 93:7 v/v). The eluate containing the product was diluted with ethanol (15 mL) and concentrated to about 10 mL (water bath temperature < 35 °C). The residue was diluted with water (400 mL) and lyophilized, obtaining **5.5** as a white powder (1.4 g, 60%).

^{1}H-NMR (400 MHz, DMSO-d_6) (two major rotamers with a ratio of approximately 1:1 were evident in the ^{1}H and ^{13}C NMR spectra): δ (ppm) 1.40 (s, 4H), 1.45 (s, 5H), 1.49–1.68 (m, 3H), 1.68–1.80 (m, 1H), 2.54 (d, *J* = 4.6 Hz, 1.5H), 2.60 (d, *J* = 4.3 Hz, 1.5H), 3.21–3.32 (m, 2H), 3.89–4.02 (m, 1H), 4.18–4.26 (m, 1H), 4.25–4.35 (m, 2H), 6.77–6.93 (m, 0.5H), 7.28–7.37 (m, 2H), 7.36–7.45 (m, 2H), 7.56–7.67 (m, 1H), 7.68–7.76 (m, 2H), 7.83–7.94 (m, 2.5H), 7.99–8.12 (m, 0.5H), 9.16 (t, *J* = 4.8 Hz, 0.5H), 11.14 (s, 0.5H), 12.10 (br s, 0.5H, interfering with the previous and next listed signal), 12.48 (s, 0.5H). Note: 0.5 exchangeable protons (NH, OH) were not apparent. ^{13}C-NMR (101 MHz, DMSO): δ (ppm) 25.6 (0.5 carbons), 25.6 (0.5 carbons), 25.9 (0.5 carbons), 26.2 (0.5 carbons), 27.7 (1.5 carbons), 28.1 (1.5 carbons), 28.4, 39.6, 46.7, 53.8, 65.6, 77.4 (0.5 carbons), 81.9 (0.5 carbons), 120.1 (2 carbons), 125.3 (2 carbons), 127.1 (2 carbons), 127.6 (2 carbons), 140.7 (2 carbons), 143.8, 143.9, 152.4 (0.5 carbons), 152.9 (0.5 carbons), 155.1 (0.5 carbons), 156.1, 156.5 (0.5 carbons), 162.7 (0.5 carbons), 164.9 (0.5 carbons), 173.8 (0.5 carbons), 173.9

(0.5 carbons). LC-HRMS (+ESI): *m*/*z* $[M+H]^+$ calcd. for $[C_{28}H_{36}N_5O_7]^+$ 554.2609, found 554.2614. RP-HPLC (220 nm): > 96% (t_R = 11.0 min, *k* = 13.3) $C_{28}H_{35}N_5O_7$ (553.62).

(13S,16S,19S)-1-amino-13-(((S)-1-(((S)-1-(((S)-1-amino-3-(4-hydroxyphenyl)-1-oxopropan-2-yl)amino)-5-guanidino-1-oxopentan-2-yl)amino)-4-methyl-1-oxopentan-2-yl)carbamoyl)-16-(4-hydroxybenzyl)-8-imino-19-(3-((E)-2-(methylcarbamoyl)guanidino)propyl)-6,15,18,21-tetraoxo-5,7,9,14,17,20-hexaazatetracosan-24-oic acid tetrakis(hydrotrifluoroacetate) (**5.8a**). Peptide **5.8a** was synthesized on a Ramage amide resin (100 mg of Fmoc-Ramage amide resin, 0.66 mmol/g) according to the general procedure. After coupling of the last amino acid and subsequent Fmoc deprotection, the resin was treated with a solution of succinic anhydride (66 mg, 0.660 mmol) and DIPEA (115 µL, 0.66 mmol) in DMF/NMP 8:2 v/v (500 µL) at 35 °C for 30 min. The resin was washed with DMF/NMP 8:2 v/v (6 ×), followed by cleavage off the resin and deprotection according to the general procedure. Purification by preparative HPLC (gradient: 0–30 min MeCN/0.1% aqueous TFA 10:90-35:65, t_R = 6 min) yielded **5.8a** as a white fluffy solid (13.2 mg, 12%). LC-HRMS (+ESI): *m/z* $[M+4H]^{4+}$ calcd. for $[C_{53}H_{89}N_{19}O_{13}]^{4+}$ 299.9216, found: 299.9228. RP-HPLC (220 nm): > 97% (t_R = 9.6 min, *k* = 11.7). $C_{53}H_{85}N_{19}O_{13} \cdot C_8H_4F_{12}O_8$ (1196.38 + 456.09).

(9S,12S,15S)-N-((S)-1-(((S)-1-(((S)-1-amino-3-(4-hydroxyphenyl)-1-oxopropan-2-yl)amino)-5-guanidino-1-oxopentan-2-yl)amino)-4-methyl-1-oxopentan-2-yl)-12-(4-hydroxybenzyl)-4-imino-15-(3-((E)-2-(methylcarbamoyl)guanidino)propyl)-2,11,14,17,20-pentaoxo-1,3,5,10,13,16,21-heptaazacyclopentacosane-9-carboxamide tris(hydrotrifluoroacetate) (**5.8b**). The linear precursor peptide **5.8a** (7.9 mg, 4.79 µmol), HOBt (3.7 mg, 0.024 mmol) and DIPEA (8.4 µL, 0.048 mmol) were dissolved in DMF/NMP 8:2 v/v (500 µL) in a round-bottom flask. Under stirring, a solution of PyBOP (12.5 mg, 0.024 mmol) in DMF/NMP 8:2 v/v (500 µL) was added and the mixture was stirred at rt overnight. 0.1% aqueous TFA (30 mL) was added followed by freeze-drying and purification by preparative HPLC (gradient: 0–30 min MeCN/0.1% aqueous TFA 10:90-35:65, t_R = 20 min) to yield **5.8b** as a white fluffy solid (3.8 mg, 52%).

^{1}H-NMR (600 MHz, DMSO-d_6): δ (ppm) 0.76–0.86 (m, 3H), 0.86–0.95 (m, 3H), 1.30–1.50 (m, 11H), 1.50–1.58 (m, 4H), 1.58–1.70 (m,3H), 1.70–1.82 (m, 1H), 2.27–2.41 (m, 4H), 2.63–2.81 (m, 5H), 2.81–2.97 (m, 3H), 3.01–3.09 (m, 3H), 3.10–3.14 (m, 1H),

3.19 (br s, 3H), 3.26–3.30 (br s, 2H), 4.07 (br s, 1H), 4.17–4.23 (m, 1H), 4.25–4.34 (m, 3H), 4.34–4.41 (m, 1H), 6.43–7.14 (br s, 2H, interfering with the next three listed signals), 6.61–6.65 (m, 4H), 6.96–7.02 (m, 4H), 7.06 (s, 1H), 7.14–7.70 (br s, 2H, interfering with the next two listed signals), 7.35–7.41 (m, 2H), 7.48–7.60 (m, 2H), 7.70–7.78 (m, 1H), 7.78–7.85 (m, 1H), 7.85–7.94 (m, 2H), 7.94–8.03 (m, 1H), 8.03–8.11 (s, 1H), 8.15 (m, 1H), 8.21–8.74(m, 4H), 8.95 (s, 1H), 9.05–9.38 (m, 3H), 10.06 (br s, 2H). LC-HRMS (+ESI): *m/z* $[M+3H]^{3+}$ calcd. for $[C_{53}H_{86}N_{19}O_{12}]^{3+}$ 393.5562, found: 393.5572. RP-HPLC (220 nm): > 97% (t_R = 11.0 min, *k* = 13.3). $C_{53}H_{83}N_{19}O_{12} \cdot C_6H_3F_9O_6$ (1178.37+ 342.07).

(10S,13S,16S,19S,22S,E)-5-amino-10-(((S)-1-amino-3-(4-hydroxyphenyl)-1-oxopropan-2-yl)carbamoyl)-16-(3-(3-((4-aminobutyl)carbamoyl)guanidino)propyl)-19-(4-hydroxybenzyl)-13-isobutyl-22-(3-((E)-2-(methylcarbamoyl)guanidino)propyl)-3,12,15,18,21,24-hexaoxo-2,4,6,11,14,17,20,23-octaazaheptacos-4-en-27-oic acid tetrakis(hydrotrifluoroacetate) (**5.9a**). Peptide **5.9a** was synthesized on a Ramage amide resin (100 mg of Fmoc-Ramage amide resin, 0.66 mmol/g) according to the general procedure. After coupling of the last amino acid and subsequent Fmoc deprotection, the resin was treated with a solution of succinic anhydride (66.0 mg, 0.66 mmol) and DIPEA (115 µL, 0.66 mmol) in DMF/NMP 8:2 v/v (500 µL) at 35 °C for 30 min. The resin was washed with DMF/NMP 8:2 v/v (6 ×), followed by cleavage off the resin and deprotection according to the general procedure. Purification by preparative HPLC (gradient: 0–30 min MeCN/0.1% aqueous TFA 10:90-35:65, t_R = 19 min) yielded **5.9a** as a white fluffy solid (15 mg, 13%). LC-HRMS (+ESI): *m/z* $[M+4H]^{4+}$ calcd. for $[C_{55}H_{92}N_{20}O_{14}]^{4+}$ 314.1770, found: 314.1780. RP-HPLC (220 nm): > 97% (t_R = 10.3 min, *k* = 12.5). $C_{55}H_{88}N_{20}O_{14} \cdot C_8H_4F_{12}O_8$ (1253.44 + 456.09).

(9S,12S,15S)-N-((10S,13S,E)-5-amino-10-(((S)-1-amino-3-(4-hydroxyphenyl)-1-oxopropan-2-yl)carbamoyl)-15-methyl-3,12-dioxo-2,4,6,11-tetraazahexadec-4-en-13-yl)-12-(4-hydroxybenzyl)-4-imino-15-(3-((E)-2-(methylcarbamoyl)guanidino)propyl)-2,11,14,17,20-pentaoxo-1,3,5,10,13,16,21-heptaazacyclopentacosane-9-carboxamide tris(hydrotrifluoroacetate) (**5.9b**). The linear precursor peptide **5.9a** (4.8 mg, 2.81 µmol), HOBt (2.1 mg, 0.014 mmol), and DIPEA (4.8 µL, 0.028 mmol) were dissolved in DMF/NMP 8:2 v/v (500 µL) in a round-bottom flask. Under stirring, a solution of PyBOP (7.2 mg, 0.014 mmol) in DMF/NMP 8:2 v/v (500 µL) was added, and the mixture was stirred at rt overnight. 0.1% aqueous TFA (30 mL) was added

followed by freeze-drying and purification by preparative HPLC (gradient: 0–30 min MeCN/0.1% aqueous TFA 10:90-35:65, t_R = 23 min) to yield **5.9b** as a white powder (3.5 mg, 80%).

^{1}H-NMR (600 MHz, DMSO-d_6): δ (ppm) 0.80–0.86 (m, 3H), 0.86–0.90 (m, 3H), 1.30–1.51 (m, 11H), 1.51–1.58 (m, 4H), 1.58–1.70 (m, 3H), 1.74 (m, 1H), 2.22–2.41 (m, 4H), 2.63–2.81 (m, 8H), 2.81–2.96 (m, 3H), 2.97–3.07 (m, 2H), 3.09–3.22 (m, 6H), 3.26–3.27 (m, 1H), 4.07 (br s, 1H), 4.17–4.25 (m, 3H), 4.25–4.34 (m, 3H), 4.34–4.43 (m, 1H), 6.60–6.65 (m, 4H), 6.96–7.01 (m, 4H), 7.06 (s, 1H), 7.35 (s, 2H), 7.52 (s, 1H), 7.74–7.77 (m, 1H), 7.80–7.85 (m, 1H), 7.85 (s, 2H), 7.94–8.01 (m, 1H), 8.04–8.11 (m, 1H), 8.11–8.19 (m, 1H), 8.19–9.75 (m, 6H), 8.94 (s, 2H), 9.05–9.34 (m, 3H), 9.99 (br s, 2H). LC–HRMS (+ESI): *m/z* $[M+3H]^{3+}$ calcd. for $[C_{55}H_{89}N_{20}O_{13}]^{3+}$ 412.5634, found: 412.5640. RP-HPLC (220 nm): > 97% (t_R = 11.6 min, k = 14.2). $C_{55}H_{86}N_{20}O_{13} \cdot C_6H_3F_9O_6$ (1235.42 + 342.07).

(10S,13S,16S,19S,22S,E)-5-amino-10-(((S)-1-amino-3-(4-hydroxyphenyl)-1-oxopropan-2-yl)carbamoyl)-16-(3-(3-((4-aminobutyl)carbamoyl)guanidino)propyl)-22-(3-((E)-2-(hex-5-yn-1-ylcarbamoyl)guanidino)propyl)-19-(4-hydroxybenzyl)-13-isobutyl-3,12,15,18,21,24-hexaoxo-2,4,6,11,14,17,20,23-octaazaheptacos-4-en-27-oic acid tetrakis(hydrotrifluoroacetate) (**5.10a**). Peptide **5.10a** was synthesized on a Ramage amide resin (183 mg of Fmoc-Sieber Amide resin, 0.61 mmol/g) according to the general procedure. After coupling of the last amino acid and subsequent Fmoc deprotection, the resin was treated with a solution of succinic anhydride (112 mg, 1.16 mmol) and DIPEA (194.4 µL, 1.16 mmol) in DMF/NMP 8:2 v/v (500 µL) at 35 °C for 30 min. The resin was washed with DMF/NMP 8:2 v/v (6 ×) and CH_2Cl_2 (3 ×), followed by cleavage off the resin and deprotection according to the general procedure. Purification by preparative HPLC (gradient: 0−30 min: MeCN/0.1% aqueous TFA 15:85-40:60, t_R = 18 min) yielded **5.10a** as a white fluffy solid (14.6 mg, 7%). LC-HRMS (+ESI): *m/z* $[M+4H]^{4+}$ calcd. for $[C_{60}H_{98}N_{20}O_{14}]^{4+}$ 330.6887 found: 330.6896. RP-HPLC (220 nm): > 97% (t_R = 13 min, k = 16.4). $C_{60}H_{94}N_{20}O_{14} \cdot C_8H_4F_{12}O_8$ (1319.54 + 456.09).

(9S,12S,15S)-N-((10S,13S,E)-5-amino-10-(((S)-1-amino-3-(4-hydroxyphenyl)-1-oxopropan-2-yl)carbamoyl)-15-methyl-3,12-dioxo-2,4,6,11-tetraazahexadec-4-en-13-yl)-15-(3-((E)-2-(hex-5-yn-1-ylcarbamoyl)guanidino)propyl)-12-(4-hydroxybenzyl)-4-imino-2,11,14,17,20-pentaoxo-1,3,5,10,13,16,21-heptaazacyclopentacosane-9-

carboxamide tris(hydrotrifluoroacetate) (**5.10b**). The linear precursor peptide **5.10a** (9.3 mg, 5.24 µmol), HOBt (4.0 mg, 0.026 mmol) and DIPEA (9.3 µL, 5.2 µmol) were dissolved in DMF/NMP 8:2 v/v (500 µL) in a round-bottom flask. Under stirring, a solution of PyBOP (13.6 mg, 0.026 mmol) in DMF/NMP 8:2 v/v (500 µL) was added and the mixture was stirred at rt overnight. 0.1% aqueous TFA (30 mL) was added followed by freeze-drying and purification by preparative HPLC (gradient: 0–30 min MeCN/0.1% aqueous TFA 15:85-40:60, t_R = 20 min) to yield **5.10b** as a white fluffy solid (3.4 mg, 40%). LC-HRMS (+ESI): *m/z* $[M+3H]^{3+}$ calcd. for $[C_{60}H_{95}N_{20}O_{14}]^{3+}$ 434.5790, found: 434.5802. RP-HPLC (220 nm): > 97% (t_R = 8.4 min, k = 9.9). $C_{60}H_{92}N_{20}O_{13} \cdot C_6H_3F_9O_6$ (1301.52 + 342.07).

(9S,12S,15S)-15-(3-((E)-2-((4-(1-(5-(8-Sulfonato-5,5,27,27-tetramethyl-16-oxa-20-aza12-azoniaheptacyclo[15.11.0.03,15.04,12.06,11.020,28.021,26]-octacosa-1(28),2,4(12),6(11),7,9,21(26),22,24-nonaen-24-yl)-3-pent-4ynyl-amidopropyl)-1H-1,2,3-triazol-4-yl)butyl)carbamoyl)guanidino)propyl)-N-((10S,13S,E)-5-amino-10-(((S)-1-amino-3-(4-hydroxyphenyl)-1-oxopropan-2-yl)carbamoyl)-15-methyl-3,12-dioxo-2,4,6,11-tetraazahexadec-4-en-13-yl)-12-(4-hydroxybenzyl)-4-imino-2,11,14,17,20-pentaoxo-1,3,5,10,13,16,21-heptaazacyclopentacosane-9-carboxamide tetrakis(hydrotrifluoroacetate) (**5.11**). Peptide **5.10b** (1.1 mg, 0.69 µmol) was dissolved in PBS (25 µL), and a solution of **5.7** (1.1 mg, 1.04 µmol) in DMSO (50 µL) was added. A solution of $CuSO_4 \cdot 5H_2O$ (0.35 mg, 1.39 µmol) in NMP/PBS 1:1 v/v (60 µL) (note: $CuSO_4$ was first dissolved in 25 µL of PBS and then 25 µL of NMP were added) and a solution of sodium ascorbate (0.55 mg, 2.77 µmol) in PBS (25 µL) were added. After stirring at rt in the dark for 3 h, the mixture was diluted with 1 mL of 0.1% aqueous TFA/MeCN 85:15 v/v, and the product was isolated by preparative HPLC (gradient: 0−30 min: MeCN/0.1% aqueous TFA 15:85-40:60, t_R = 28 min). Lyophilization of the eluate afforded **5.11** as a purple fluffy solid (0.62 mg, 37%). LC-HRMS (+ESI): m/z $[M+4H]^{4+}$ calcd for $[C_{97}H_{136}N_{26}O_{18}S]^{4+}$ 496.5063, found: 496.5077. RP-HPLC (220 nm): > 95% (t_R = 9.8 min, k = 11.5). $C_{97}H_{132}N_{26}O_{18}S \cdot C_8H_4F_{12}O_8$ (1982.35 + 456.09).

(9S,12S,15S)-N-((10S,13S,E)-5-amino-10-(((S)-1-amino-3-(4-hydroxyphenyl)-1-oxopropan-2-yl)carbamoyl)-15-methyl-3,12-dioxo-2,4,6,11-tetraazahexadec-4-en-13-yl)-15-(3-((E)-2-((4-(1-(7-hydroxy-2-oxo-2H-chromen-3-yl)-1H-1,2,3-triazol-4-yl)butyl)carbamoyl)guanidino)propyl)-12-(4-hydroxybenzyl)-4-imino-2,11,14,17,20-

pentaoxo-1,3,5,10,13,16,21-heptaazacyclopentacosane-9-carboxamide tetrakis(hydrotrifluoroacetate) (**5.12**)**.** Peptide **5.10b** (1.2 mg, 0.73 µmol) was dissolved in PBS (75 µL), and a solution of 3-azido-7-hydroxycoumarin (0.23 mg, 1.13 µmol) in DMSO (50 µL) was added. A solution of $CuSO_4 \cdot 5H_2O$ (0.38 mg, 1.50 µmol) in NMP/PBS 1:1 v/v (60 µL) (note: $CuSO_4$ was first dissolved in 25 µL of PBS and then 25 µL of NMP were added) and a solution of sodium ascorbate (0.60 mg, 3.01 µmol) in PBS (25 µL) were added. After stirring at rt in the dark for 3 h, the mixture was diluted with 900 µL of 0.1% aqueous TFA/MeCN 85:15 v/v and the product was isolated by preparative HPLC (gradient: 0−40 min: MeCN/0.1% aqueous TFA 15:85−45:55, t_R = 23 min). Lyophilization of the eluate afforded **5.12** as a green fluffy solid (0.15 mg, 11%). LC-HRMS (+ESI): m/z $[M+3H]^{3+}$ calcd for $[C_{69}H_{100}N_{23}O_{16}]^{3+}$ 502.2567, found: 502.2576. RP-HPLC (220 nm): > 99% (t_R = 6.5 min, k = 7.2). $C_{69}H_{97}N_{23}O_{16} \cdot C_6H_3F_9O_6$ (1504.68 + 342.07).

(10S,13S,16S,19S,22S,Z)-5-amino-10-(((S)-1-amino-3-(4-hydroxyphenyl)-1-oxopropan-2-yl)carbamoyl)-16-(3-(3-((4-aminobutyl)carbamoyl)guanidino)propyl)-13-cyclopentyl-19-(4-hydroxybenzyl)-22-(3-((E)-2-(methylcarbamoyl)guanidino)propyl)-3,12,15,18,21,24-hexaoxo-2,4,6,11,14,17,20,23-octaazaheptacos-4-en-27-oic acid tetrakis(hydrotrifluoroacetate) (**5.13a**). Peptide **5.13a** was synthesized on a Ramage aamide resin (100 mg of Fmoc-Ramage amide resin, 0.66 mmol/g) according to the general procedure. After coupling of the last amino acid and subsequent Fmoc deprotection, the resin was treated with a solution of succinic anhydride (66 mg, 0.66 mmol) and DIPEA (115 µL, 0.66 mmol) in DMF/NMP 8:2 v/v (500 µL) at 35 °C for 30 min. The resin was washed with DMF/NMP 8:2 v/v (6 ×), followed by cleavage off the resin and deprotection according to the general procedure. Purification by preparative HPLC (gradient: 0–30 min MeCN/0.1% aqueous TFA 10:90-35:65, t_R = 15 min) yielded **5.13a** as a white fluffy solid (51 mg, 45%). LC-HRMS (+ESI): *m/z* $[M+4H]^{4+}$ calcd. for $[C_{56}H_{82}N_{20}O_{14}]^{4+}$ 317.1770, found: 317.1788. RP-HPLC (220 nm): > 97% (t_R = 10.0 min, k = 12.2). $C_{56}H_{88}N_{20}O_{14} \cdot C_8H_4F_{12}O_8$ (1265.45 + 456.09).

(9S,12S,15S)-N-((10S,13S,Z)-5-amino-10-(((S)-1-amino-3-(4-hydroxyphenyl)-1-oxopropan-2-yl)carbamoyl)-13-cyclopentyl-3,12-dioxo-2,4,6,11-tetraazatridec-4-en-13-yl)-12-(4-hydroxybenzyl)-4-imino-15-(3-((E)-2-(methylcarbamoyl)guanidino)propyl)-2,11,14,17,20-pentaoxo-1,3,5,10,13,16,21-heptaazacyclopentacosane-9-carboxamide tris(hydrotrifluoroacetate) (**5.13b**)**.** The

linear precursor peptide **5.13a** (14.6 mg, 8.45 µmol), HOBt (6.5 mg, 0.042 mmol) and DIPEA (14.7 µL, 0.085 mmol) were dissolved in DMF/NMP 8:2 v/v (500 µL) in a round-bottom flask. Under stirring, a solution of PyBOP (22 mg, 0.042 mmol) in DMF/NMP 8:2 v/v (500 µL) was added and the mixture was stirred at rt overnight. 0.1% aqueous TFA (30 mL) was added followed by freeze-drying and purification by preparative HPLC (gradient: 0–30 min MeCN/0.1% aqueous TFA 10:90-35:65, t_R = 17 min) to yield **5.13b** as a white powder (4.4 mg, 33%).

^{1}H-NMR (600 MHz, DMSO-*d*$_6$): δ (ppm) 1.04–1.31 (m, 3H), 1.32–1.47 (m, 10H), 1.47–1.57 (s, 9H), 1.57–1.88 (m, 5H), 2.03–2.19 (m, 1H), 2.20–2.42 (m, 4H), 2.62–2.80 (s, 8H), 2.80–3.11 (m, 5H), 3.12–3.22 (m, 6H), 4.10 (br s, 1H), 4.19 (t, *J* = 7.97 Hz, 1H), 4.22–4.29 (m, 1H), 4.29–4.52 (m, 3H), 6.59–6.71 (m, 4H), 6.92–7.03 (m, 4H), 7.05 (s, 1H), 7.27–7.46 (m, 3H), 7.53 (br s, 1H), 7.68–7.83 (d, 2H), 7.83–7.95 (m, 2H), 7.95–8.06 (s, 1H), 8.06–8.19 (d, 2H), 8.19–8.35 (s, 2H), 8.35–8.65 (s, 3H), 8.94 (s, 2H), 9.10 (s, 1H), 9.15 (s, 1H), 9.19 (s, 1H), 10.00 (br s, 2H). LC-HRMS (ESI): *m/z* $[M+3H]^{3+}$ calcd. for $[C_{56}H_{89}N_{20}O_{13}]^{3+}$ 416.5634, found: 416.5645. RP-HPLC (220 nm): > 97% (t_R = 11.3 min, *k* = 13.8). $C_{56}H_{86}N_{20}O_{13} \cdot C_6H_3F_9O_6$ (1250.45 + 342.07).

5.2.2.5 Circular dichroism

Circular dichroism (CD) spectra of the different peptides were acquired in a J-815 spectropolarimeter (Jasco, Japan) at 25 °C in the 190–260 nm wavelength range, with a bandwidth of 1 nm and a scan speed of 50 nm/min, using a 0.1 cm quartz cell. Samples containing 50 µM peptide solutions were prepared in a 50 µM aqueous HCl. The final spectra for each peptide were the average of three consecutive scans per sample after the subtraction of buffer baselines. Results were expressed as mean residue ellipticity ($[\theta]_{MRW}$) (deg × cm^{-2} × dmol^{-1}), as follows:

$$[\theta]_{MRW} = \frac{\theta_{Obs} \times MRW}{10dc} \qquad \text{(equation 1)}$$

where θ_{obs} is the observed ellipticity in degrees, MRW is the mean residue weight, d is the cell path length and c is the peptide molar concentration.

5.2.2.6 Distribution coefficients ($logD_{7.4}$ value) determination (lipophilicity)

The distribution coefficients $logD_{7.4}$ of peptides **2.4**, **4.2b**, **4.9b**, **5.8b**, **5.9b**, and **5.13b** were determined using two different procedures (A and B). The mixture for analysis

was prepared by adding 600 µL of a 300 µM solution of the peptide in PBS (pH 7.4; aqueous phase) to 600 µL of n-octanol (organic phase) in a 1.5 mL polypropylene reaction vessel and vortexed for 3 mins.

For procedure A, 300 µL of the mixture was immediately transferred into a 0.3 mL HPLC vial (article number LP1190932; Merz Brothers GmbH, Haid, Austria) with a screw cap equipped with a septum (article number 5182-0717; Agilent) and vortexed again for 1 min. The mixture was allowed to sit for 5 min to enable the separation of the two phases (with the upper layer being the organic phase and the lower layer being the aqueous phase). Using syringes (1 mL Henke-ject, Ref. 4010-200V0, Henke Sass Wolf) equipped with injection needles (0.70 × 30 mm BL/LB, B. Braun), 100–150 µL aliquots of each phase were carefully taken (ensuring the needles were not contaminated by the other phase) and transferred into 1.5 mL reaction vessels for further processing. To obtain a sample of the aqueous phase, the HPLC vial was held upside down for about a minute, and approximately 100–120 µL of the aqueous phase were taken and collected into a reaction vessel for further processing.

With respect to procedure B, the remaining mixture in the reaction vessel (300 µL) was allowed to sit for 5 min to enable the separation of the two phases. A 200 µL pipette was used to remove 70-120 µL of the different phases. For the organic phase, the pipette was used to directly transfer the upper layer of the separated mixture into a reaction vessel for further processing while ensuring the pipette tips were not contaminated by the other phase. To obtain the aqueous phase (lower layer), the tube was tilted, and 70–100 µL of this phase was removed without touching the remaining organic phase. The sample was then transferred into a reaction vessel for further processing.

The obtained samples were processed as follows: a 50 µL aliquot of the aqueous phase was directly transferred into an HPLC vial (Merz Brothers GmbH) with a screw cap equipped with a septum (Agilent) and subjected to RP-HPLC analysis using the system and conditions detailed in *Section 5.2.2.1*. For the organic phase, a 50 µL aliquot was transferred into a 1.5 mL reaction vessel, lyophilized, and the residue was dissolved in 50 µL PBS, followed by its transfer into an HPLC vial (Merz Brothers GmbH) with a screw cap equipped with a septum (Agilent) for RP-HPLC analysis using the system and conditions detailed in *Section 5.2.2.1*. The injection volume was 20 µL. The area under the curves (AUC) obtained from the HPLC chromatogram was

transformed to a distribution coefficient $logD_{7.4}$ according to the formula $logD_{7.4} = log(AUC_{octanol}/AUC_{aqueous})$, where $AUC_{octanol}$ is the area under the curve values obtained for the n-octanol phase sample of a peptide, and $AUC_{aqueous}$ is the area under the curve values obtained for the aqueous phase sample of the same peptide.

5.2.2.7 Cell culture

Cells were cultured in T75 or T175 flasks (Sarstedt, Nümbrecht, Germany) in a humidified atmosphere (95% air, 5% CO_2) at 37 °C. SK-N-MC neuroblastoma cells (obtained from the American Type Culture Collection, ATCC HTB-10) were maintained in EMEM supplemented with 5% FCS. CHO-hY_2R cells (obtained from PerkinElmer, Rodgau, Germany) were cultured in Ham's F-12 supplemented with 10% FBS and G418 (400 µg/mL). CHO-hY_4-G_{qi5}-mtAEQ cells[31] were cultured in HAM's F-12 supplemented with 10% FBS, hygromycin (400 µg/mL), zeocin (250 µg/mL), and G418 (400 µg/mL). HEC-1B-hY_5 cells[32] were maintained in EMEM supplemented with 5% FBS and G418 (400 µg/mL). Human cerebral microvascular endothelial cells (HBEC- 5i, ATCC CRL-3245) obtained from the Miguel Castanho Lab (iMM) were cultured as a monolayer on 0.1% gelatin solution (Gibco, United States) coated T-flasks in 1:1 mixture of DMEM and HAM's F-12 (DMEM:F12 (1:1)) medium (Sigma, Taufkirchen, Germany) supplemented with 10% FBS, 1% penicillin/streptomycin antibiotic solution (Sigma, Taufkirchen, Germany), and 1% endothelial growth supplement (ECGS) (Cell Application Inc., California, United States), according to the manufacturer's instructions. The neuroblastoma cells SH-SY5Y (ATCC CRL-2266) were cultured as a monolayer using a 1:1 mixture of EMEM and HAM's F-12 (EMEM:F12 (1:1)) medium supplemented with 10% FBS and 1% penicillin/streptomycin antibiotic solution according to the manufacturer's instructions.

5.2.2.8 Buffers and media used for binding and functional assays.

Buffer II (used for binding experiments at the Y_1R, Y_2R, and Y_5R): an isotonic sodium-containing HEPES buffer (150 mM NaCl, 10 mM HEPES, 25 mM $NaHCO_3$, 2.5 mM $CaCl_2$, 5 mM KCl, pH 7.4) supplemented with 1% BSA and 0.1 mg/mL bacitracin. *DPBS* (used for binding studies at Y_4R): Dulbecco's phosphate-buffered saline with calcium and magnesium (1.8 mM $CaCl_2$, 2.68 mM KCl, 1.47 mM KH_2PO_4, 3.98 mM $MgSO_4$, 137 mM NaCl, 8.06 mM Na_2HPO_4, pH 7.4) supplemented with 1% BSA and

0.1 mg/mL bacitracin. L-15 medium (used for the CAMYEN assays): Leibovitz's L-15 medium (140 mM NaCl, 1.3 mM $CaCl_2$, 1 mM $MgCl_2$, various amino acids and vitamins, pH 7.4) without phenol red supplemented with 10 mM HEPES and 5% FBS. DMEM:F12 (1:1) medium without phenol red was used for the cell viability assay, *in vitro* BBB assay, BBB integrity assay, and HBEC-5i stability experiments.

5.2.2.9 Radioligand binding assays

Y_1R Binding. Competition binding experiments at Y_1R-expressing SK-N-MC neuroblastoma cells were performed in *buffer II* as described previously using the radioligand [^{3}H]UR-MK299 (K_d = 0.058 nM,[25] used concentration: 0.075 nM) (see structure in Figure A2.1, *Section 2.6 Appendix; Chapter 2*).[27] Experiments were performed in triplicate and due to low radioligand displacement, no curve fitting was performed for the studied compounds.

Y_2R Binding. Competition binding experiments at CHO-hY_2R cells were performed in *buffer II* as previously reported, using the radioligand [K^4-[^{3}H]propionyl]hPYY (K_d = 0.16 nM; concentration used: 0.3 nM) (see structure in Figure A4.1, *Section 4.6 Appendix; Chapter 4*).[25] Experiments were performed in triplicate, and due to low radioligand displacement, no curve fitting was applied for the studied compounds.

Y_4R Binding. Y_4R competition binding studies with [^{3}H]**2.5** (see structure in Figure 2.2; *Chapter 2*) were performed with suspensions of intact CHO-hY_4-G_{qi5}-mtAEQ cells[31] in *DPBS,* as described by Gleixner *et al*.[26] Each experiment was carried out in triplicate. Total binding data (dpm) from radioligand competition binding experiments (including total binding in the absence of competitor) were plotted against log(concentration competitor) and analyzed by a four-parameter logistic equation (log(inhibitor) vs. response-variable slope, GraphPad Prism 10, GraphPad Software, San Diego, California, United States) followed by normalization (100% = 'top' of the four-parameter logistic fit, 0% = unspecifically bound radioligand) and analysis of the normalized data by a four-parameter logistic equation. pIC_{50} and IC_{50} values from individual experiments were converted to pK_i and K_i values according to the Cheng-Prusoff equation.[33]

Y_5R Binding. Competition binding experiments at HEC-1B-hY_5R cells[32] were performed in *buffer II* using the radioligand [^{3}H]propionyl-pNPY (K_d = 11 nM,[34] used concentration: 5 nM) (see structure in Figure A2.1, *Section 2.6 Appendix; Chapter 2*).[35]

Experiments were performed in triplicate. Due to low radioligand displacement, no curve fitting was performed for the studied compounds.

5.2.2.10 Y_4R cAMP CAMYEN-assay

The assay was performed with HEK293T-CAMYEN-hY_4R cells in agonist mode, as reported.[26] Experiments were performed in triplicate. Data were analyzed as reported using GraphPad Prism 10 (GraphPad Software): raw BRET ratios were determined by dividing the acceptor fluorescence (520–580 nm) by the donor luminescence (< 470 nm). Baseline-corrected relative cAMP responses were calculated by dividing data by the buffer control (with no forskolin). The area under the curve for the 60 min read was taken for each agonist concentration and was normalized to the response of 1 µM hPP (100%) and the effect of 10 µM forskolin in the absence of agonist (0%). The normalized responses were plotted against log[Y_4R agonist], and concentration-response curves were generated using the four-parameter logistic equation (GraphPad Prism 10) to obtain pEC_{50} values. Efficacies E_{max} correspond to the upper plateaus of the normalized concentration-response curves.

5.2.2.11 *In vitro* human plasma stability assay

The stabilities of the peptides in human heparinized plasma were investigated in triplicate at 37 °C using a modified method described by Pegoli *et al*.[36] 1-Methyl-D-tryptophane (Sigma) was used as internal standard (IS) (note: as the purity of 1-methyl-D-tryptophane was < 95%, it was repurified by preparative HPLC to give a purity of > 99%, data not shown). For the plasma stability and recovery determination, the peptide concentration used was 40 µM. In contrast to the method described by Pegoli *et al*.,[36] for protein precipitation, 93 µL of ice-cold EtOH/MeCN (50:50 v/v) were added to 46 µL aliquots of plasma/PBS (136.9 mM NaCl, 2.68 mM KCl, 5.62 mM Na_2HPO_4, 1.09 mM NaH_2PO4, and 1.47 mM KH_2PO4, pH 7.4) 1:2 v/v containing the peptide and IS immediately followed by vortexing (3–4 min). To determine recoveries, the proteins were precipitated immediately after adding the peptides to plasma/PBS (1:2 v/v) already containing IS. After vortexing, samples were centrifuged at 16,100 g at 4 °C for 10 min. This was followed by transferring 120 µL aliquots of the supernatant into 1.5 mL reaction vessels containing 10% aqueous TFA (3 µL). Further processing was carried out as described but slightly modified by using 70 µL MeCN/0.04%

aqueous TFA (1:9 v/v) to take up the residues.[36] The studied incubation times were 1 h, 6 h, 24 h, and 48 h.

Samples were analyzed by analytical RP-HPLC using the system and conditions as described under the *Section 5.2.2.1* (purity controls) but applying a different linear gradient: 0–14 min: MeCN/0.04% aqueous TFA 5:95-25:75, 14–15 min: 25:75-95:5, 15–19 min: 95:5 (isocratic). The obtained recoveries and the recovery ratios (peptide/internal standard) are summarized in Table A5.2 (See *Section 5.6 Appendix*). Data analysis was based on UV detection at 220 nm.

5.2.2.12 Cell viability assay

The cytotoxic effect of the peptides to be studied in translocation studies on HBEC-5i cells was determined using CellTiter-Blue® Cell Viability Assay, as described by Cavaco *et al*.[37] A day prior to the assay, 100 µL of both HBEC-5i and SH-SY5Y cell suspensions containing 150,000 cells/mL were seeded into the wells of solid black 96-well flat-bottom microplates (Corning Life Sciences, Durham, United States) and incubated for 24 h. On the day of the experiment, the culture medium was aspirated, and the cells were washed two times with PBS. 100 µL of peptide serial dilutions (concentrations ranging between 0.01 and 100 µM) in DMEM:F12 (1:1) medium without phenol red (assay medium) were added to each well, after which the plate was incubated for 24 h in a humidified atmosphere of 5% CO_2 at 37 °C. After incubation, cells were washed two times with PBS, and 100 µL of a diluted solution of CellTiter-Blue® Reagent (0.2X) prepared in assay medium was added to each well and incubated for 3 h. The fluorescence intensity was measured at an excitation of 560 nm and maximum emission at 590 nm using a Varioskan™ LUX multimode microplate reader with excitation and emission monochromators (spectral bandwidths of 5 nm (excitation slit) and 12 nm (emission slit)) (Thermo Fisher, Massachusetts, United States). Assay medium and 1% Triton X-100-containing medium were used as positive controls (100% cell viability) and negative controls (0% cell viability), respectively, whereas 1–30 µM of HCl serially diluted in assay medium were used as vehicle controls. Cell viability (%) was determined using the following equation:

$$\text{Cell Viability (\%)} = \frac{F_s - F_{nc}}{F_{pc} - F_{nc}} \times 100 \qquad \text{(equation 2)}$$

F_s is the fluorescence intensity of a sample, F_{nc} is the fluorescence intensity for negative controls, and F_{pc} is the fluorescence intensity for positive controls.

Cell viability (%) were plotted against log(concentration of peptide) and analyzed by a four-parameter logistic equation (log(inhibitor) vs. response-variable slope, GraphPad Prism 10, GraphPad Software) to obtain IC_{50} values. Experiments were performed on different days using independently grown cell cultures.

5.2.2.13 Metabolic stability of peptide in the presence of HBEC-5i cells

Prior to the investigation of the peptides in the translocation assay using HBEC-5i cells, the stability of the peptides in the presence of HBEC-5i cells was studied. HBEC-5i cells were grown until 80–90% confluence in a T75 culture flask. The cells were carefully harvested with trypsin-EDTA (Gibco/Thermo Fisher, Massachusetts, United States) and centrifuged at 300 g at rt for 5 min. After discarding the supernatant, the cells were resuspended in culture medium to densities between 40,000–80,000 cells/mL. 200 µL of the cell suspension were seeded into each 0.1% gelatin solution wells of 24-well tissue culture plates (Sarstedt, Nümbrecht, Germany) and cultured between 7–25 days. The culture medium was changed every 2-3 days until the day of the experiment. On the day of the experiment, the cells were washed twice with 200 µL of PBS and once with 200 µL of assay medium. The peptides to be studied were diluted in assay medium to a final concentration of 10 and 50 µM, and 300 µL were added to the cells and incubated for 24 h. At time points 1 h, 6 h (or 17 h), and 24 h of incubation, 50 µL of the cell medium were collected for analytical RP-HPLC analysis. Prior to the analysis, the collected samples were centrifuged at 16,100 g at 4 °C for 10 min to condense cell debris at the bottom of the Eppendorf tube. 35 µL of the resulting supernatants were then loaded into HPLC vials for analysis. Samples were analyzed by RP-HPLC using the system and conditions described in *Section 5.2.2.1*.

5.2.2.14 *In vitro* BBB Translocation Studies

Translocation Assays were used to study the translocation of the fluorescently labeled peptides and non-labeled peptides as described elsewhere[37] with some modifications. Herein, 200 µL of HBEC-5i cell suspension containing 40,000 cells/mL were seeded into each 0.1% gelatin solution coated tissue culture inserts or transwell (transparent polyester (PET) membrane with 1.0 µm pores; Cat. No. 353104, Corning Life

Science) sitting the wells of a 24-well plate (support companion plate with lid; Cat. No. 353504, Corning Life Science) containing 500 µL of culture medium. The adhered cells were cultured for 21–25 days to create an *in vitro* BBB model, with the inside compartment of the insert serving as the apical side of the cell while the well the insert sits in along with its outside part serves as the basolateral side of the cell. During the 21–25 days of culturing, the culture medium was changed every 2-3 days, and the barrier integrity of the growing cell monolayers on the inserts was determined every 6-7 days for the culture designated for the evaluation of non-labeled peptides by RP-HPLC. After 21–25 days of culture, cells were washed twice with 150 µL PBS and once with 200 µL of assay medium, followed by the transfer of the inserts into a new 24-well plate. The peptides to be studied were diluted in assay medium to a final concentration of 0.1, 1.0, and 10 µM (fluorescently labeled peptides **5.11** and **5.12**), 10 µM (non-labeled peptides **5.8b** and **5.9b**), or 50 µM (non-labeled peptides **4.2b**, **4.9b** and **5.13b**). 200 µL of this solution was added to the inserts (apical side), whereas 500 µL of the assay medium was added to the wells (basolateral side) of the 24-well plates, followed by incubation for 24 h at 37 ºC. For the experiments aimed at studying the non-labeled peptides, 30 µL aliquots were collected from both the apical and basolateral sides after 1 and 24 h of incubation to quantify the amount of peptide translocated. All experiments were performed in triplicate and on different days using independently grown cell cultures. The same procedure was used for translocation studies of peptides in the presence of serum but with minor modifications. In these studies, an assay medium containing 5% FBS was used for the assay.

Evaluation of fluorescence emission. The translocation of fluorescently labeled peptides was determined by fluorescence emission. After 24 h incubation, samples from the apical and basolateral sides were collected and analyzed. Fluorescence was measured using a Varioskan™ LUX multimode microplate reader (Thermo Fisher) equipped with excitation and emission monochromators (λ_{ex} = 560 nm, λ_{em} = 590 nm; spectral bandwidths of 5 nm (excitation slit) and 12 nm (emission slit)). The percentage (%) of translocation was calculated using the following equation:

$$\text{Translocation (\%)} = \frac{(\text{df} \times F_i) - F_{cells}}{F_{peptide} - F_{medium}} \times 100 \qquad \text{(equation 3)}$$

F_i is the fluorescence intensity recovered from the basolateral side, F_{cells} is the fluorescence intensity recovered from cells without peptide incubation, $F_{peptide}$ is the fluorescence intensity of total peptide initially added to the transwell apical side, and F_{medium} is the fluorescence intensity of DMEM:F12 medium without phenol red. F_i is multiplied by a dilution factor (df) of 2.5 based on the volumes of assay medium in the basolateral (500 µL) and apical (200 µL) side to obtain the actual concentration of the peptide detected.

Evaluation of translocated peptides by RP-HPLC. The translocation of non-labeled peptides was determined by the calculation of the respective area under the curve (AUC) in the RP-HPLC chromatograms. Samples collected from the apical and basolateral side after 1 h and 24 h of incubation were analyzed by RP-HPLC using the system and conditions as described in *Section 5.2.2.1*. The percentage (%) of translocation was calculated using the following equation:

$$\text{Translocation (\%)} = \frac{\text{df} \times AUC_i}{AUC_{peptide}} \times 100 \qquad \text{(equation 4)}$$

AUC_i is the AUC of peptide recovered in the basolateral side and $AUC_{peptide}$ is the AUC of total peptide initially added to the transwell apical side. AUC_i is multiplied by a dilution factor (df) of 2.5 based on the volumes of assay medium in the basolateral (500 µL) and apical (200 µL) side to obtain the actual concentration of the peptide detected.

5.2.2.15 *In vitro* Integrity Assay

In vitro integrity assays were performed a day prior to and immediately after the translocation studies. To determine the cell layers' barrier integrity, the cells were washed two times with PBS and once with the assay medium, DMEM:F12 medium without phenol (200 µL). 200 µL of a solution of fluorescein isothiocyanate- dextran with a MW of 4 kDa (FD4) (Sigma-Aldrich, Missouri, United States) in assay medium at a concentration of 46 µg/mL was added to the apical side and incubated for 2 h. Samples were collected from the apical and basolateral side, and fluorescence intensity was measured at an excitation of 485 nm and maximum emission at 530 nm using a Varioskan™ LUX multimode microplate reader with excitation and emission monochromators (spectral bandwidths of 5 nm (excitation slit) and 12 nm (emission

slit)) (Thermo Fisher). The percentage of FD4 recovered was determined using the following equation:

$$\text{FD4 Permeability (\%)} = \frac{(\text{df} \times F_{\text{sample}}) - F_{\text{cells}}}{F_{\text{FD4}} - F_{\text{medium}}} \times 100 \qquad \text{(equation 5)}$$

F_{sample} is the fluorescence intensity recovered, F_{cells} is the fluorescence intensity recovered from cells without FD4 incubation, F_{FD4} is the fluorescence intensity of total FD4 initially added to the transwell apical side, and F_{medium} is the fluorescence intensity of assay medium. F_{i} is multiplied by a dilution factor (df) of 2.5 based on the volumes of assay medium in the basolateral (500 µL) and apical (200 µL) side. The barrier's integrity is indirectly proportional to the percentage of FD4 recovered and was calculated using this equation:

$$\text{Barrier Integrity(\%)} = 100\% - \text{FD4 Permeability (\%)} \qquad \text{(equation 6)}$$

An overview of the average barrier integrity can be seen in Table A5.2 (*Section 5.6 Appendix*).

5.2.2.16 Statistical Analysis

For the *in vitro* HBEC-5i modification, translocation, and barrier integrity studies, quantitative data were processed using Excel 2013 (Microsoft, Washington, United States) and the GraphPad Prism 10 (GraphPad Software). Means and standard errors are shown in the figures and tables. Pairwise significances for translocation studies were calculated using one-way ANOVA followed by Tukey’s multiple comparison test.

5.3 Results and Discussions

5.3.1 Design and synthesis of UR-AK86C (2.4) derivatives 5.8b, 5.9b, 5.11, and 5.12

The blood-brain barrier (BBB), a semi-permeable barrier surrounding the CNS, plays a vital regulatory role in controlling the influx and efflux of small organic compounds, such as drugs, into and out of the brain.[20] While the BBB typically excludes about 98% of small molecules and all macromolecular therapeutics, studies have shown that small lipid-soluble drugs with molecular weights between 400 and 600 Da can cross the BBB to some extent.[38, 39] This is evident in the enhanced BBB penetration of the kinase inhibitor Crizotinib following its conjugation to a lipophilic fluoroethyl moiety.[40] However, it is well established that this conjugation also affects the bioactivity and physicochemical properties of the pharmacophore.[39]

A commonly employed strategy to improve the lipophilicity of molecules while minimally impacting their bioactivity is N- or O-methylation.[41, 42] As such, to design and synthesize BBB-permeable derivatives of the parent peptide **2.4**, methylation in different positions on **2.4** was considered. A widely used methylation approach known to improve lipophilicity and cell membrane penetration in peptides is the methylation of their backbone amide bonds (N-methylation).[42] However, findings from Chapter 4 and a previous study by Kuhn *et al*.[43], revealed that modifying the peptide backbone of this compound of **2.4** significantly reduces its binding affinity (up to 3 log units of pK_i). Therefore, a different strategy was pursued. This involved replacing the two strong basic guanidinium moieties present in **2.4** with weakly basic groups only partially protonated at pH 7.4, as this should result in obtaining analogs with higher lipophilicity (i.e., increased logD values). As carbamoylated guanidines, exhibiting a pK_a of ca. 8,[44] fulfill this criterium and have been reported to serve as a bioisosteric substitute of guanidine groups in arginine side chains of bioactive peptides,[29] Arg^1 and Arg^5 in **2.4** (Figure 4.1) were replaced by a methyl-carbamoylated Arg derived from using **5.5** as building block during synthesis.

The synthesis of **5.5**, containing a methyl-carbamoyl group at N^{ω}, was performed according to the reported preparation of N^{ω}-carbamoylated arginines (see Scheme 5.1).[29, 43] Using **5.5** as a building block, peptides **5.8b**, with only Arg^1 replaced by the modified arginine derived from **5.5**, and **5.9b**, with its Arg^1 and Arg^5 replaced, were synthesized. Additionally, another derivative (**5.10b**) was prepared with its Arg^1 and

Arg[5] replaced by an alkyne-functionalized Arg (derived from **5.6**)[30] and a methyl-carbamoylated Arg (derived from **5.5**), respectively. This modification, as recently reported by Gleixner *et al*.,[26] allowed for the coupling of lipophilic, azide-functionalized fluorescent dyes to the alkyne-functionalized Arg at position 1 through click chemistry (CuAAC reaction). The coupling of the fluorescent dye had almost no effect on the compound's bioactivity.

Considering that the coupling of small molecules or peptides with fluorescent dyes can significantly alter their physicochemical and pharmacological properties,[45, 46] **5.7**, a high molecular weight dye, and 3-Azido-7-hydroxycoumarin, a low molecular weight dye (structures shown in Figure 5.2), were selected to be coupled to **5.10b**. This was aimed at providing a basis for comparing the effect of the molecular weight of the dyes on the characteristics of the analogs to be studied. Accordingly, congeners **5.11** and **5.12**, fluorescently labeled with **5.7** and 3-azido-7-hydroxycoumarin, respectively, were synthesized (Scheme 5.2).

All these compounds were characterized and subsequently tested in translocation assays. Based on the results (which will be later discussed), an additional lipophilic analog, **5.13b**, was synthesized using the reported **4.9b** as a lead structure (*cf*. *Chapter 4*), characterized, and evaluated in translocation assays (See Table 5.1 and Figure 5.3 for the analytical and structural overview of all synthesized peptides, respectively).

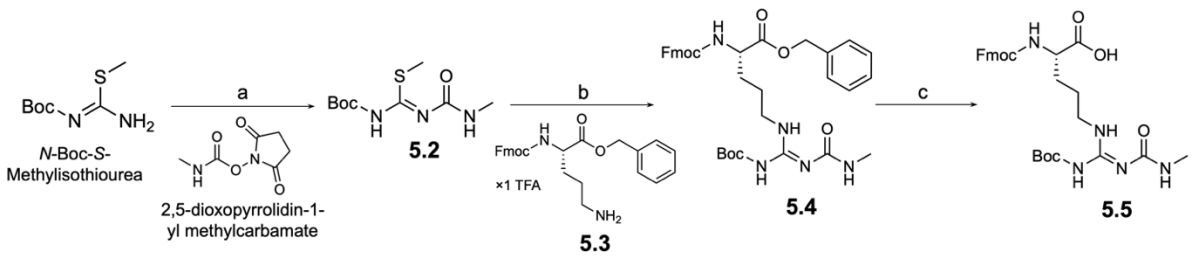

Scheme 5.1. Synthesis scheme of methyl-carbamoylated arginine building block **5.5**. Reagents and conditions: (a) NEt_3, MeCN, rt, 26 h, 45%; (b) $HgCl_2$, DIPEA, dichloromethane, rt, 1.5 h, 83%; (c) 10% Pd/C, H_2, 2-propanol, rt, 2.5 h, 60%.

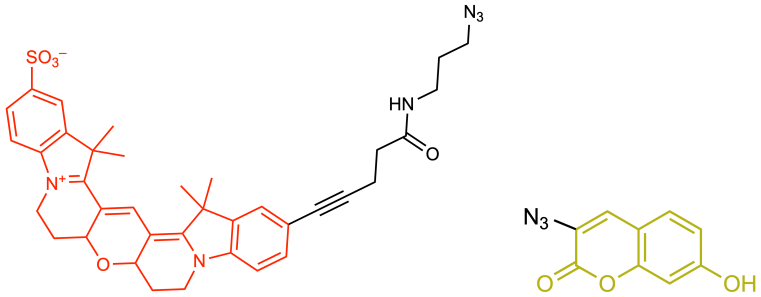

5.7, Azido functionalized Cy3B

3-Azido-7-hydroxycoumarin

Figure 5.2. Structures of the azido functionalized dyes **5.7** and 3-Azido-7-hydroxycoumarin.

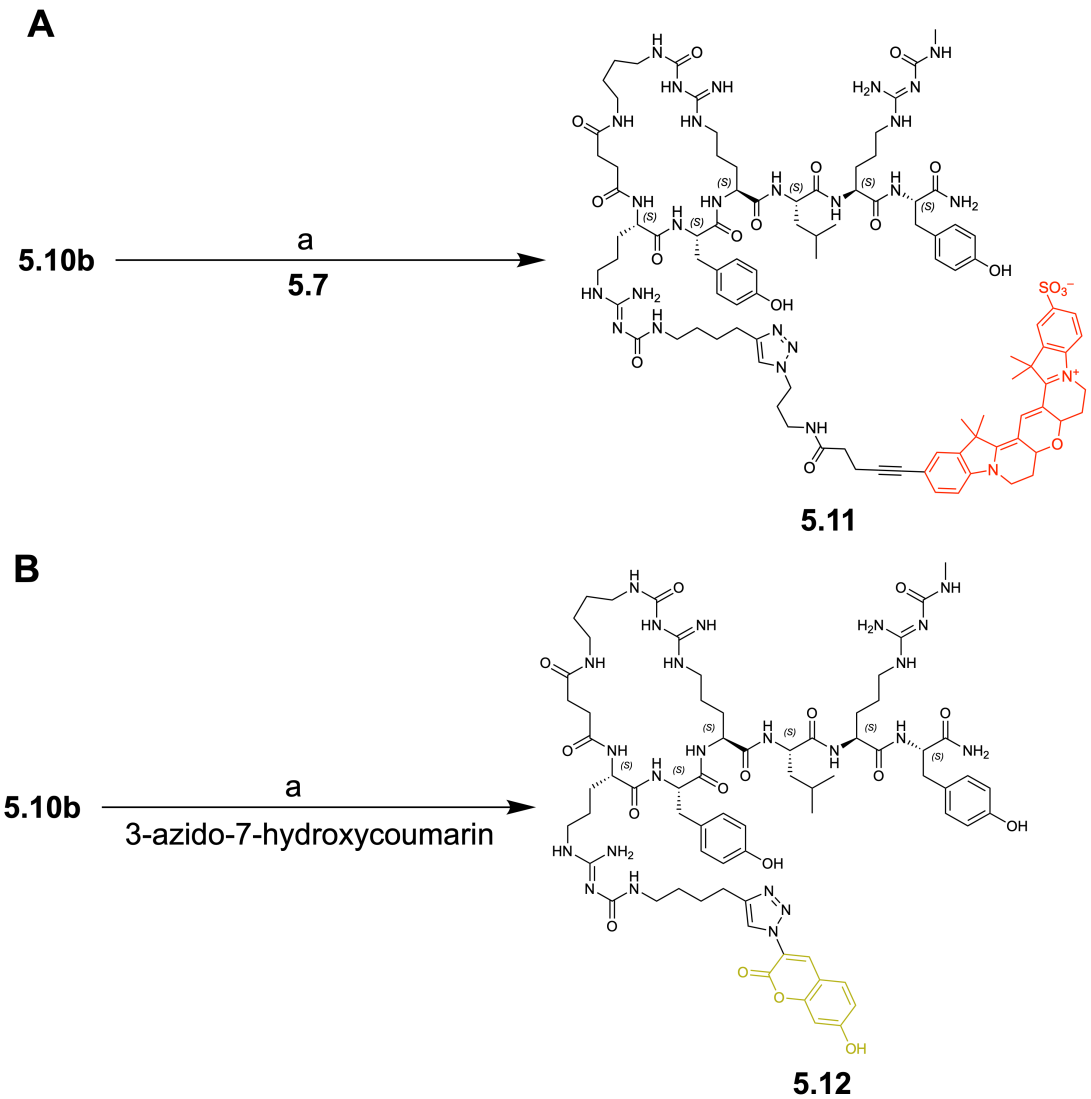

Scheme 5.2. Synthesis of the fluorescently labeled peptides **5.11** and **5.12** obtained by CuAAC reaction of alkyne-functionalized analog **5.10b** to (A) **5.7** and (B) 3-azido-7-hydroxycoumarin. Reagents and conditions: (a) $CuSO_4$, sodium ascorbate, NMP/PBS 1:1 v/v, rt, 2 h, 35% (**5.11**), 11% (**5.12**).

Cmpd.	Peptide sequence
2.4	cyclo[succinyl-Arg-Tyr-Arg(carb)]-Leu-Arg-Tyr-NH_2
4.2b	cyclo[succinyl-Arg-Tyr-Arg(carb)]-Leu-*N*(Me)-Arg-Tyr-NH_2
4.9b	cyclo[succinyl-Arg-Tyr-Arg(carb)]-Cpg-Arg-Tyr-NH_2
5.8b	cyclo[succinyl-Arg(methyl-carb)-Tyr-Arg(carb)]-Leu-Arg-Tyr-NH_2
5.9b	cyclo[succinyl-Arg(methyl-carb)-Tyr-Arg(carb)]-Leu-Arg(methyl-carb)-Tyr-NH_2
5.10b	cyclo[succinyl-Arg(alkyne functionalized)-Tyr-Arg(carb)]-Leu-Arg(methyl-carb)-Tyr-NH_2
5.11	cyclo[succinyl-Arg(alkyne with Cy3B)-Tyr-Arg(carb)]-Leu-Arg(methyl-carb)-Tyr-NH_2
5.12	cyclo[succinyl-Arg(alkyne with Coumarin)-Tyr-Arg(carb)]-Leu-Arg(methyl-carb)-Tyr-NH_2
5.13b	cyclo[succinyl-Arg(methyl-carb)-Tyr-Arg(carb)]-Cpg-Arg(methyl-carb)-Tyr-NH_2

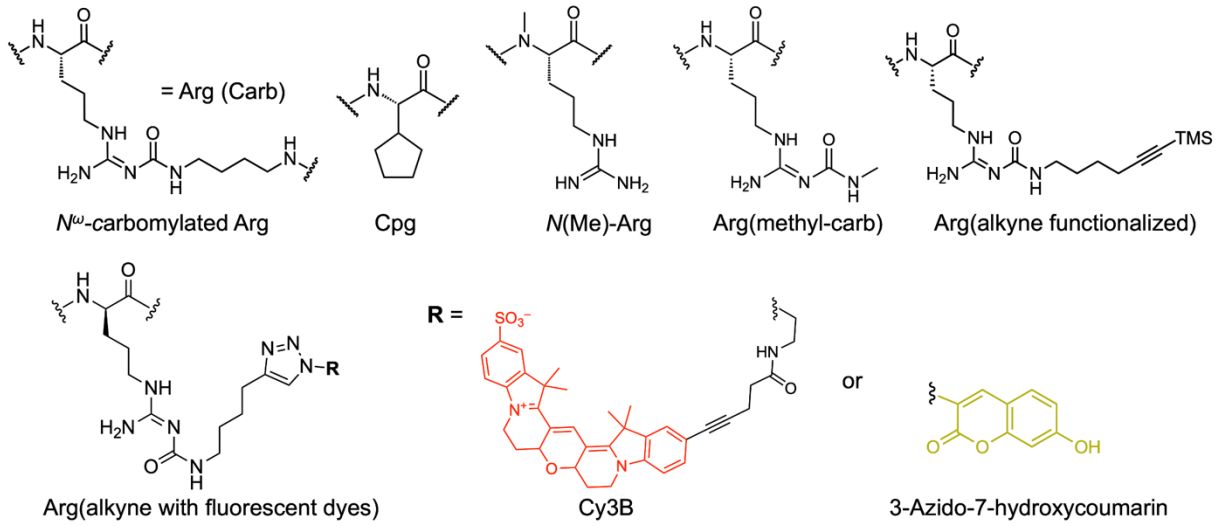

Figure 5.3. Peptide sequences of the synthesized analogs of **2.4** (**4.2b**, **4.9b**, **5.8b–5.10b**, **5.11**–**5.12**). Amino acid replacements and insertions are highlighted in blue, red, and gray, respectively.

Table 5.1. Overview of analytical data of linear precursor peptides **5.8a**–**5.10a** and **5.13b**, as well as the cyclic peptides **5.8b**–**5.10b**, **5.11**, **5.12**, and **5.13b**.

Cpd.	x-fold TFA	MW	Yield (%)	RP-HPLC purity (%) / t_R [min] / k	HRMS (+ESI): m/z			NMR[a]
					calcd. for	calcd.	found	
5.8a	4	1196.38 +456.09	12	> 97/9.6/11.7[a]	$[M+4H]^{4+}$	299.9216	299.9228	^{1}H ^{1}H COSY
5.8b	3	1178.37 +342.07	52	> 97/11.0/13.3[a]	$[M+3H]^{3+}$	393.5562	393.5572	^{1}H ^{1}H COSY
5.9a	4	1253.44 +456.09	13	>97/10.3/12.5[a]	$[M+4H]^{4+}$	314.1770	314.1780	^{1}H ^{1}H COSY
5.9b	3	1235.42 +342.07	80	>97/11.6/14.2[a]	$[M+3H]^{3+}$	412.5634	412.5645	^{1}H ^{1}H COSY
5.10a	3	1319.54 +456.09	7	> 97/13/16.4[a]	$[M+4H]^{4+}$	330.6887	330.6896	^{1}H ^{1}H COSY
5.10b	3	1301.52 +342.07	40	> 97/8.4/9.9[b]	$[M+3H]^{3+}$	434.5790	434.5802	^{1}H ^{1}H COSY
5.11	4	1982.35 +456.09	37	> 95/9.8/13.0[b]	$[M+3H]^{4+}$	496.5063	496.5077	^{1}H ^{1}H COSY
5.12	3	1504.68 +342.07	11	> 99/6.5/7.2[c]	$[M+3H]^{3+}$	502.2567	502.2576	^{1}H ^{1}H COSY
5.13a	3	1265.45 +456.09	45	> 97/10.0/12.2[a]	$[M+4H]^{4+}$	317.1770	317.1788	^{1}H ^{1}H COSY
5.13b	3	1250.45 +342.07	33	> 97/11.3/13.8[a]	$[M+3H]^{3+}$	416.5634	416.5645	^{1}H ^{1}H COSY

[a]*k* was determined using RP-HPLC linear gradient 0–14 min: MeCN/0.04% aqueous TFA 5:95-25:75, 14–15 min: 25:75-95:5, 15–19 min: 95:5 (isocratic); [b]*k* was determined using RP-HPLC linear gradient 0–14 min: MeCN/0.04% aqueous TFA 10:90-40:60, 14–15 min: 40:60-95:5, 15–19 min: 95:5 (isocratic); [c]*k* was determined using RP-HPLC linear gradient 0–14 min: MeCN/0.04% aqueous TFA 20:80-40:60, 14–15 min: 40:60-95:5, 15–19 min: 95:5 (isocratic).

5.3.2 Characterization of the synthesized analogs of UR-AK86C (2.4)

The characterization of all synthesized analogs of **2.4** was aimed at assessing their secondary structure using circular dichroism, evaluating their binding affinities to human Y_4R through radioligand binding assays, determining their Y_4R potency in cAMP assays and analyzing their cytotoxicity against HBEC-5i and SH-SHY5 cell lines at concentrations ranging from 0.1 to 30 µM. A comprehensive overview of the results from the characterization of the analogs is provided below (Figures 5.4–5.7 and Table 5.2). It is important to note that the yields of analogs **5.11** and **5.12** were very low; therefore, they were not studied in the YR binding and cAMP assays, as well as in the $logD_{7.4}$ and plasma stability studies. As expected for small cyclic peptides, the synthesized analogs **5.8b**, **5.9b**, **5.10b**, **5.11**, and **5.12**, along with the parent peptide **2.4**, exhibited a random coil secondary structure.

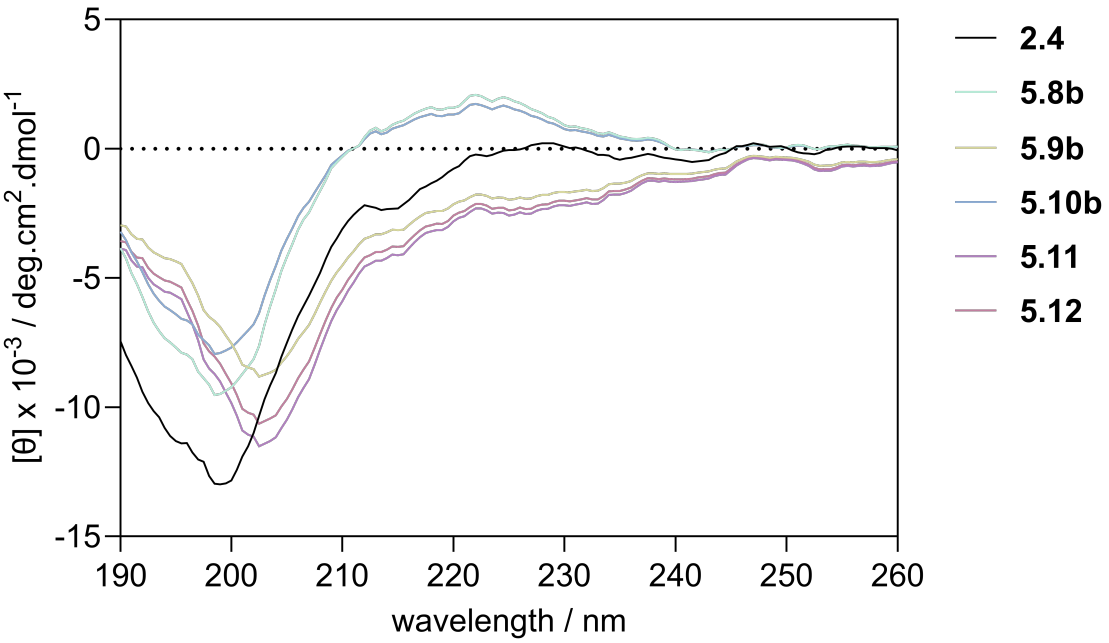

Figure 5.4. CD spectra of **2.4** and analogs **5.8b**, **5.9b**, **5.10b**, **5.11** and **5.12**. Spectra of peptides dissolved in a 50 µM aqueous HCl to a concentration of 50 µM were recorded at 25 °C across a wavelength range of 190–260 nm using a 0.1 cm quartz cell.

5.3.2.1 Replacing Arg^1 and Arg^5 in **2.4** with methyl-carbamoylated Arg improved lipophilicity

As mentioned earlier, enhancing the lipophilicity of bioactive compounds, such as peptides, potentially improves their penetration across cell membranes and cell barriers, such as the blood-brain barrier (BBB). Thus, the lipophilicity of a compound is generally used as a measure of its ability to cross cell membranes or barriers. In this study, the lipophilicities of the synthesized peptide analogs were assessed by determining their logD values at a pH of 7.4 ($logD_{7.4}$).

The lipophilicities of the peptides, which are directly proportional to their $logD_{7.4}$ values, were initially evaluated using an indirect RP-HPLC method,[47, 48] where a compound's retention factor, *k*, is correlated to a calibration curve derived from standards with known logD values and their retention factors to estimate its logD value. Using phosphate buffer (pH = 7) and MeCN as mobile phase, chromatograms from the HPLC runs displayed very broad sample peaks (up to approximately 5 mins peak width; data not shown), making it challenging to estimate their retention factor and, hence, their *logD* values. As a consequence, the Shake-Flask method, which is based on the concentration ratio of a compound separated between non-aqueous and aqueous phases in the equilibrium, was used to determine the $logD_{7.4}$ values for **2.4**

and its analogs **4.2b**, **4.9b**, **5.8b**, **5.9b**, and **5.13b**. No $logD_{7.4}$ values were determined for analogs **5.10b**, **5.11**, and **5.12** because all stocks or solids had been used up at the time of these experiments. Results from the study of **4.2b**, **4.9b**, **5.8b**, and **2.4** revealed no significant differences for **4.2b**, **4.9b**, and **5.8b** when compared to **2.4**. In contrast, analogs **5.9b** and **5.13b** exhibited significantly increased $logD_{7.4}$ (about 0.8 log units; $P < 0.005$) compared to **2.4** (Table 5.2). These enhanced lipophilicities were also evident in the longer retention times (or higher retention factors, *k*) in RP-HPLC analysis of the peptides at pH = 4, as more lipophilic compounds typically take longer to elute (see Table 5.1). This increase in lipophilicity ($logD_{7.4}$) can be attributed to the reduced pK_a of the methyl-carbamoylated Arg at positions 1 and 5 of the peptides, resulting in an increase in the amount of the more lipophilic peptide species with reduced protonation (cationic net charge → 0) at pH of 7.[46, 49, 50] For analog **5.8b**, where the guanidinium group of Arg^1 is replaced by a methyl-carbamoylated guanidinium moiety, the negligible impact of this moiety on **5.8b**'s lipophilicity may stem from the compensating effect of the remaining strong basic guanidinium group of Arg^5 on the protonation state of the peptide. With lipophilic compounds shown to have longer retention times, analog **5.10b**, and its congeners **5.11** and **5.12** could also be inferred to show increased lipophilicities as its linear precursor **5.10a** exhibited a longer retention time compared to **2.4** (see Table 5.1). This could even be higher for **5.11** and **5.12** as they are coupled to fluorescent dyes known to have high logD values.

With regards to the Y_4R binding affinities of the synthesized analogs of **2.4**, analogs **5.8b**–**5.10b** exhibited about 0.4–1 log units decrease in pK_i (pK_i = 9.38, 9.75, and 8.85, respectively) compared to the parent peptide **2.4** (pK_i = 10.13) (Table 5.2 and Figure 5.5). Analogs **5.11** and **5.12**, although not determined (very low yields obtained after synthesis), are also likely to display reduced binding affinities since their precursor **5.10b** shows a lower binding affinity compared to the others. Analogs **5.8b**–**5.10b** also exhibited significant selectivity towards the human Y_4R (Table 5.2) with analogs **5.8b** and **5.9b** activating the hY_4R in the cAMP assay with potencies (pEC_{50}) of 9.11 to 9.37 and efficacies (E_{max}) of 93% and 95%, respectively. These findings suggest that the structural modifications (replacement of Arg^1 and Arg^5 by carbamoylated arginines) were well tolerated with respect to Y_4R binding and agonism.

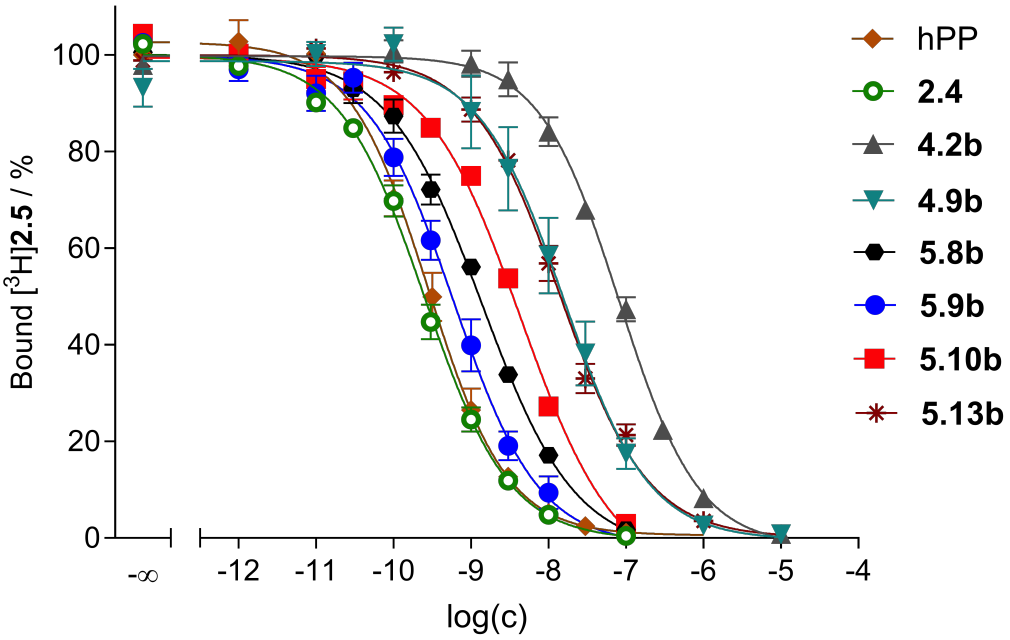

Figure 5.5 Radioligand displacement curves of hPP, **2.4**, **4.2b**, **4.9b**, **5.8b**, **5.9b**, **5.10b**, and **5.13b** obtained from competition binding experiments with the radioligand [^{3}H]UR-JG102 at CHO-hY_4-G_{qi5}-mtAEQ cells (K_d = 0.11 nM, c = 0.25 nM). Data represent mean values ± SEM of at least three independent experiments performed in triplicate.

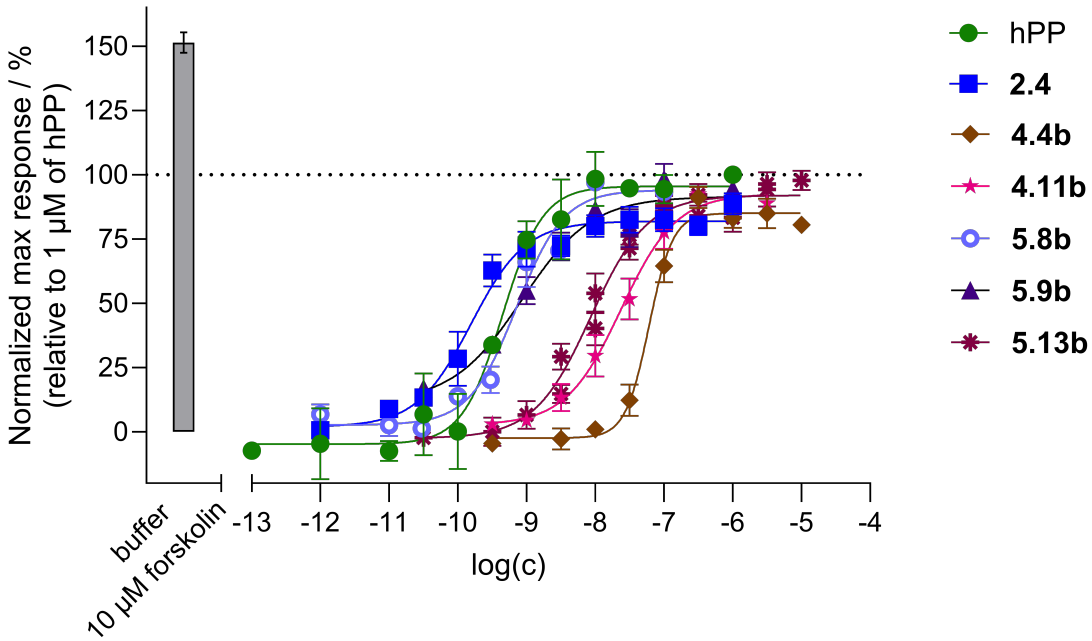

Figure 5.6. Concentration-response curves of peptides hPP, **2.4**, **4.2b**, **4.9b**, **5.8b**, **5.9b**, **5.10b**, and **5.13b** obtained from a cAMP CAMYEN assay performed with live HEK293T-CAMYEN-hY_4R cells in agonist mode. The effect elicited by 1 µM hPP was set to 100% to normalize the data. Presented are means ± SEM from at least three independent experiments, each performed in at least triplicate.

Table 5.2. The determined $logD_{7.4}$ values (lipophilicity), Y receptor binding affinities, and Y_4R agonistic potencies of peptide **2.4** and analog **4.2b**, **4.9b**, **5.8b**, **5.9b**, **5.10b**, and **5.13b**.

Compd.	$logD_{7.4}$	hY_4R Affinity (pK_i[a] ± SEM)	YR binding			Y_4R CAMYEN cAMP[h]	
			Y_1R[b]	Y_2R[c]	Y_5R[d]	pEC_{50} ± SEM	E_{max} ± SEM(%)
hPP	n.d	10.08 ± 0.12	6.4[e]	< 5.5[e]	7.8[e]	9.35 ± 0.06	101± 1
2.4	-2.90±0.08	10.13 ± 0.07[f]	< 5.5[g]	< 5.0[g]	< 6.0[g]	9.82 ± 0.06	82± 4
4.2b	-3.02±0.05	7.62 ± 0.03	< 5.5	< 5.5	< 5.5	7.23 ± 0.06	78 ± 10
4.9b	-2.92±0.08	8.60 ± 0.13	< 5.5	< 5.5	< 6.0	7.60 ± 0.14	93 ± 2
5.8b	-2.95±0.14	9.38 ± 0.06	< 5.5	< 5.5	< 5.5	9.11 ± 0.14	93 ± 2
5.9b	-2.27±0.05**	9.75 ± 0.10	< 5.5	< 5.5	< 5.5	9.37 ± 0.05	95 ± 10
5.10b	n.d	8.97 ± 0.06	< 5.5	n.d	< 6	n.d	n.d
5.13b	-2.26±0.04**	8.37 ± 0.07	< 5.5	< 5.5	< 6.0	8.66 ± 0.09	89 ± 4

[a]Determined by competition binding at CHO-hY_4-G_{qi5}-mtAEQ cells using [^{3}H]**2.5** (K_d = 0.11 nM, c = 0.25 nM) as radioligand (see structure in Figure 2.2, *Chapter 2*).[26] [b]Determined by competition binding at SK-N-MC neuroblastoma cells using [^{3}H]UR-MK299 (K_d = 0.058 nM,[25, 26] c = 0.075 nM) as radioligand (see structure in Figure A2.1, *Section 2.6 Appendix; Chapter 2*).[27] [c]Determined by competition binding with [K^4-[^{3}H]propionyl]-hPYY (K_d = 0.16 nM, c = 0.3 nM) at CHO-hY_2R cells (see structure of radioligand in Figure A4.1, *Section 4.6 Appendix; Chapter 4*).[25] [d]Determined by competition binding at HEC-1B-hY_5R cells using [^{3}H]propionyl-pNPY (K_d = 11 nM,[34] c = 5 nM) as radioligand (see structure in Figure A2.1, *Section 2.6 Appendix; Chapter 2*).[35] [e]Berlicki et al. (reported K_i values were converted to pK_i values)[51]; [f]Gleixner *et al.*[26]; [g]Konieczny *et al.*[22]; [h]Agonistic potencies (pEC_{50}/EC_{50}) and maximum efficacy (E_{max}) relative to the effect elicited by 1 µM hPP determined in a cAMP CAMYEN assay at HEK293T-CAMYEN-Y_4R cells. Data represent mean values from *at least* three independent experiments (SEM given for pK_i, pEC_{50}, and E_{max}). **means are significantly different compared to that of **2.4** with P < 0.005 (One-way ANOVA Tukey's multiple comparison test). n.d.: not determined.

5.3.2.2 Analogs of **2.4** are non-cytotoxic to neuronal and brain endothelial cells

An essential aspect of evaluating the therapeutic potential of a bioactive peptide designed to penetrate the brain is determining its cytotoxicity on relevant CNS tissue cells. Thus, the cytotoxicity of the synthesized analogs was examined on SH-SY5Y and HBEC-5i cells, (which serve as models for neuronal cells and BBB endothelial cells, respectively)[52, 53] using the CellTiter-Blue® Cell Viability Assay. This cell viability assay is based on the ability of living cells to metabolically convert the redox dye, resazurin, into the fluorescent resorufin, after 24 h incubation with a test compound.

The cytotoxic effects of analogs **5.8b**, **5.9b**, **5.10b**, **5.11**, and **5.12** were investigated at concentrations ranging from 0.01 to 30 µM. Results from the study indicated a high viability rate (> 99%) for both SH-SY5Y and HBEC-5i cells following their treatments with the peptides at these concentrations (Figure 5.7). Furthermore, treatment of HBEC-5i cells with these peptides at concentrations up to 100 µM also showed no signs of cytotoxicity (see *Section 5.6 Appendix*, Figure A5.1). These findings suggest

that the potential translocation of these peptides across the artificial BBB is unlikely to impact the viability of the endothelial cells used in the translocation study, as well as these cell types or neurons *in vivo*.

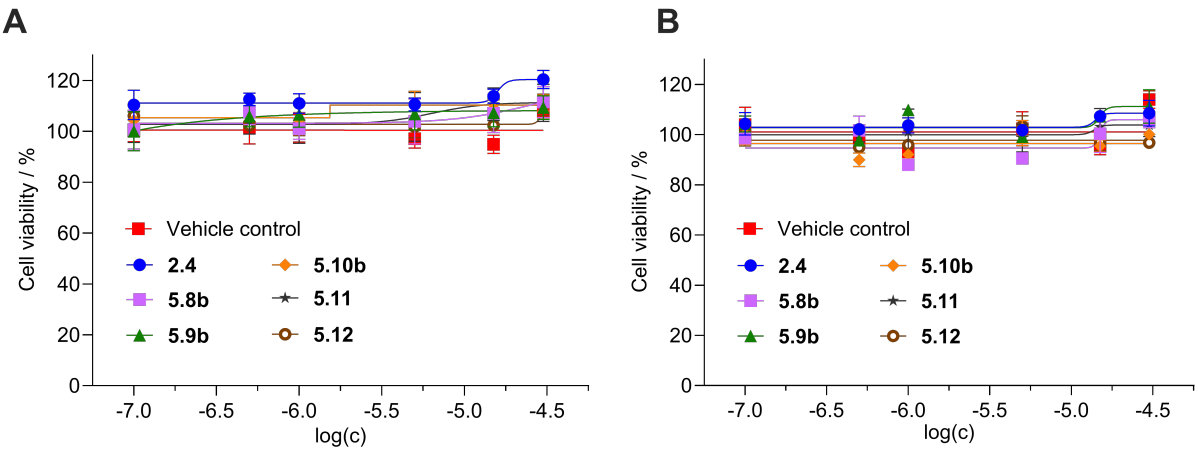

Figure 5.7. *In vitro* cytotoxicity of peptides **2.4**, **5.8b**, **5.9b**, **5.10b**, **5.11**, and **5.12** studied with (A) HBEC-5i and (B) SH-SY5Y cells using the CellTiter-Blue® Cell Viability Assay kit. Cell counts of 15,000 cells per well of HBEC-5i and SH-SY5Y were incubated (24 h, 37 °C) with various concentrations of peptides (range from 0.01–30 µM). Vehicle control: 0.01–100 µM of aqueous solution of HCl in assay medium. Data represent mean values ± SEM of at least three independent experiments performed in triplicate.

5.3.2.3 Peptides **5.11**, and **5.12** are not translocated but rather degraded or modified

Several endogenous processes, including passive diffusion, cell migration, adsorptive-mediated transcytosis (AMT), carrier- or receptor-mediated transcytosis, facilitate the transport of peptides and therapeutics across the blood-brain barrier (BBB). Among these, the more passive adsorptive-mediated transcytosis is a well-known mechanism used by cells to transport most peptides across the BBB.[54-58] This means of translocation is time and concentration-dependent and may also be affected by the presence of serum, as it has been demonstrated to decrease the penetration of peptides into the brain.[59] For this study, the fluorescently labeled peptides (**5.11** and **5.12**) were examined in translocation assays with or without the presence of heat-inactivated serum in the assay medium, whereas the non-labeled peptides (**5.8b** and **5.9b**) were only studied in assay medium without serum due to its known negative impact on the quality of results from the HPLC analysis of serum-containing samples.[60-62]

For the fluorescently labeled peptides, concentrations of 0.1 µM, 1 µM, and 10 µM were used to investigate the impact of concentration on the peptides' translocation since they could easily be detected using the plate reader. At first glance, initial results

from the study of peptides **5.11** and **5.12** revealed significant translocation (> 30%) of the peptides across the BBB model with barrier integrity ≥ 89% (see Figure 5.8 and Table A5.2) in both serum and non-serum conditions. The results also indicated that higher concentrations of the peptide improved translocation, regardless of the presence of serum. However, the results show that serum significantly improved the apparent peptide translocation only at a concentration of 1 μM for peptide **5.11**. Validation of these results (specifically for peptide **5.11** at 10 μM) through HPLC analysis of samples from the basolateral side revealed low amounts of the intact peptide and high amounts of a degradation or modification product in the basolateral compartment (see Figure 5.9 and Figure A5.2).

In the case of the non-labeled peptides, the peptides were studied at a concentration of 10 μM due to the challenges that may arise from the RP-HPLC detection (at UV wavelength of 220 nm) at low concentrations. The choice of this concentration was based on the easy detection of 5–10 μM solutions of these peptides in 0.1% aqueous TFA at a UV wavelength of 220 nm in the RP-HPLC run. However, in the translocation studies of analogs **5.8b** and **5.9b**, no peptides were detected in the samples from the basolateral side during HPLC analysis, precluding the estimation of the amount of peptide translocated. This suggests that the studied peptides were either degraded, not translocated, or that the amount translocated was very low and as such, was diluted in the basolateral side, making it undetectable in the HPLC analysis.

To further investigate possible degradation of the peptides, HBEC-5i cells were incubated with the peptides under study in a metabolic stability assay. Specifically, peptides **2.4**, **5.8b**, **5.9b**, and a fluorescently labeled peptide, UR-JG114, which is structurally similar to peptide **5.11** (see *Section 5.6 Appendix* for the structure, Figure A5.3), were examined. UR-JG114 was selected as a representative of the fluorescently labeled peptides as stocks of **5.11** and **5.12** were no longer available. The results, presented in Table 5.3, showed significant degradation or modification of the peptides, with less than 6% of intact peptides remaining in the medium after 24 h of incubation.

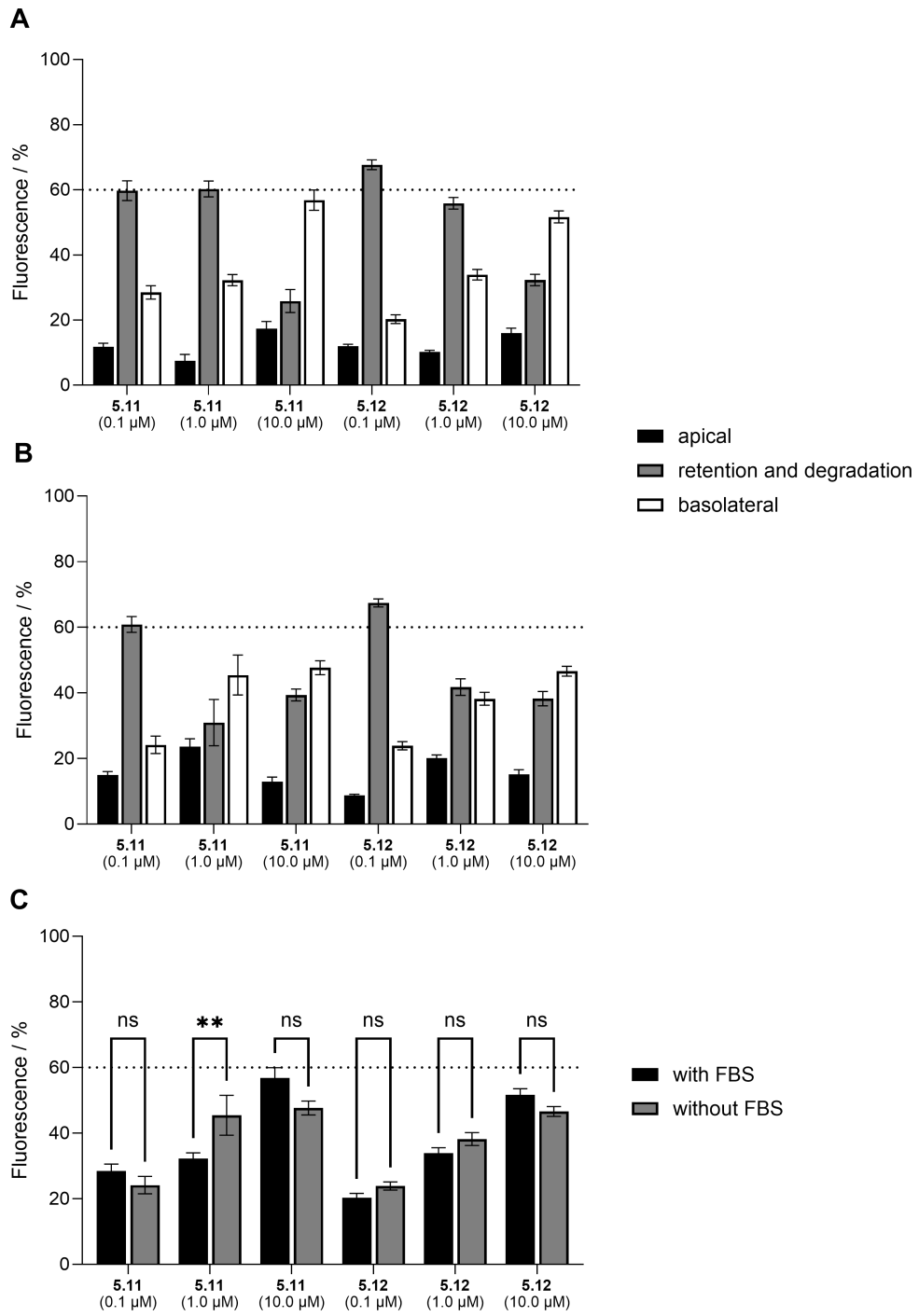

Figure 5.8. Percentage of fluorescently labeled peptide analogs **5.11** and **5.12** apparently translocated across the HBEC-5i cells in the *in vitro* BBB model. Graphs represent percent amount of **5.11** and **5.12** at concentrations 0.1 µM, 1 µM, and 10 µM fluorescently detected in the apical side and basolateral side in the (A) absence and (B) presence of serum after 24 h of incubation. Retention is calculated by subtracting amounts detected in both the apical and basolateral sides from 100% to represent the percent amount of peptides either adsorbed to the filter, attachment factor (0.1% gelatin), or internalized by the cells. (C) Statistical comparison of the translocation of **5.11** and **5.12** in assay medium with or without serum. The values were obtained from three independent experiments. ns indicates non-significant with $P > 0.05$ and **significant with $P < 0.005$ (one-way ANOVA multiple comparison).

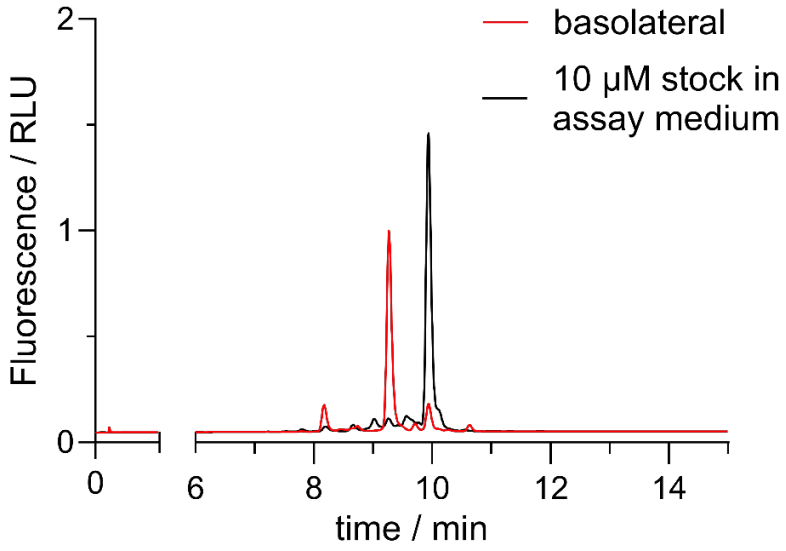

Figure 5.9. Chromatograms from the RP-HPLC analysis of samples obtained from the assay stock of **5.11** (10 µM) and the basolateral side in translocation assays. Fluorescence was measured in relative light units (RLU) at λ_{ex} = 560 nm, λ_{em} = 590 nm. The HPLC gradient used is described in *Section 5.2.2.1*.

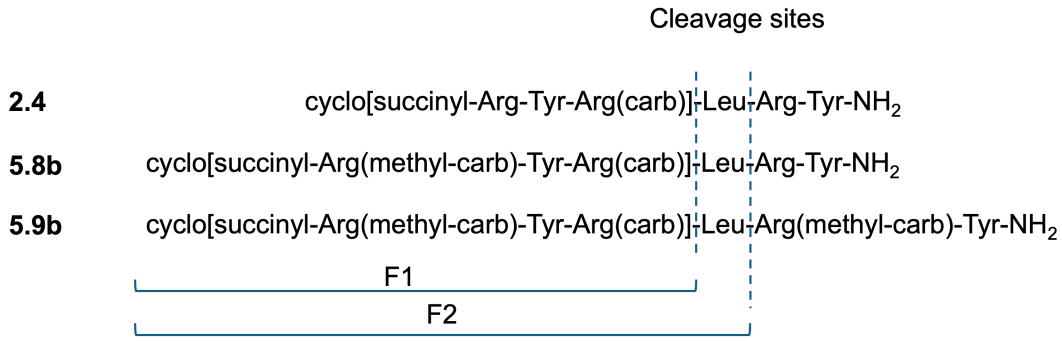

Figure 5.10. Fragments of **2.4**, **5.8b**, and **5.9b** (F1 and F2) identified by LC-HRMS analysis after 24 h incubation with HBEC-5i cells. Dashed lines represent possible cleavage sites.

For the non-labeled peptides, a cyclic tetrapeptide (fragment F2 in Figure 5.10) and a cyclic tripeptide (fragment F1 in Figure 5.10) were identified as degradation products in HPLC analysis (Figure 5.11) of samples of the assay medium and later confirmed by LC-MS analysis (data not shown). However, for UR-JG114, identifying the potential structures of the degradation products based on LC-MS analysis proved to be difficult. Although these findings clearly show that the peptides under study are undergoing degradation in the presence of HBEC-5i cells, the rate and amount of degradation observed were directly linked to cell density prior to its use in the assays (data not shown).

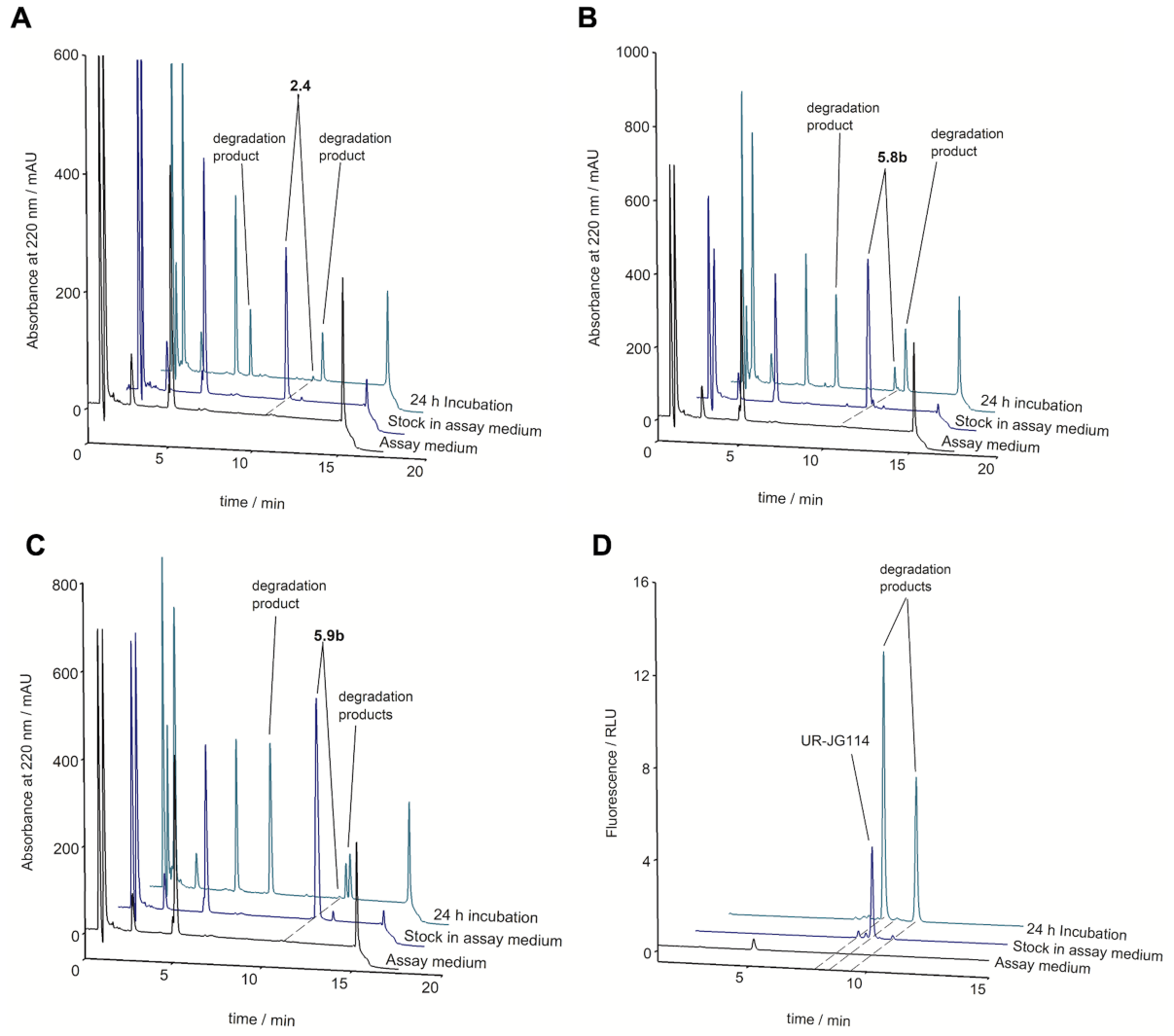

Figure 5.11. RP-HPLC chromatograms of peptides (A) **2.4**, (B) **5.8b**, (C) **5.9b**, and (D) UR-JG114 obtained from the metabolic stability assays in the presence of HBEC-5i. Chromatograms are from the assay medium, stock solutions of the peptides, and samples collected after 24 h incubation with HBEC-5i cells at 37 °C. The RP-HPLC shows the degradation of peptides in comparison to the assay medium (negative control) and their respective stock solution (positive control). These degradation products linked to the peaks were confirmed in LC-MS analysis (data not shown). The initial concentrations of the peptides used were 10 µM (UR-JG114), 50 µM (**2.4**), and 100 µM (**5.8b**, **5.9b**). Fluorescence was measured in relative light units (RLU) at λ_{ex} = 560 nm, λ_{em} = 590 nm

Table 5.3. The metabolic stabilities of peptide **2.4** and its analogs **4.2b**, **4.9b**, **5.8b**, **5.9b**, **5.10b**, **5.11**, **5.12**, **5.13b** and UR-JG114 after incubation with HBEC-5i cells (37°C) and their estimated half-lives in human plasma (plasma/PBS (1:2 v/v)) (37°C).

Peptide	% Intact peptide in assay medium[a] after the specified incubation times		Estimated $t_{1/2}$ [h][b] in human plasma
	1 h	24 h	
2.4	81	2	1.9[c]
4.2b	> 99	> 99	> 72
4.9b	97	60	19.5
5.8b	93	6	n.d
5.9b	89	5	n.d
5.10b	n.d	n.d	n.d
5.11	n.d	n.d	n.d
5.12	n.d	n.d	n.d
5.13b	96	56	33
UR-JG114	88	2	n.d

[a]The initial concentration of the peptides incubated with the HBEC-5i was 100 μM; presented are mean values ± SEM from at least two independent experiments (SEM not given if no decomposition was observed). [b]Determined by non-linear regression (two-parameter monoexponential decline) including t = 0 (100%).

5.3.3 Synthesis, characterization, and translocation studies of analog 5.13b

Considering the similarities between the degradation products identified by LC-MS and those identified in the plasma stability studies of **2.4** reported by Konieczny *et al.*[22], the degradation of the peptides was hypothesized to be a result of an exopeptidase activity, presumably, the angiotensin-converting enzyme since it is also expressed in many endothelial cells.[63] Consequently, plasma-stable derivatives of **2.4** (*Chapter 4*) with moderate to high binding affinities and potency were evaluated in the HBEC-5i cells metabolic stability assay, from which UR-AG27 (**4.9b**) (see Figure 5.3 for structure) was selected as the lead structure for creating a metabolic stable analog with improved lipophilicity. This new analog, **5.13b**, was synthesized by replacing the Arg residues in positions 1 and 5 of **4.9b** with a methyl-carbamoylated Arg, similar to the design and synthesis of **5.9b**. Analog **5.13b** was then characterized by determining its YR binding affinity, agonism, and stability in plasma and in the presence of HBEC-5i cells. With its sequence similarity to the previously studied analog **5.9b**, **5.13b** was assumed to exhibit a random coil secondary structure and remain non-toxic to both

HBEC-5i and SH-SY5Y cells; hence, its structural characteristics and cytotoxicity were not assessed.

In comparison to **2.4**, there was a significant increase in lipophilicity (ca. 0.8 log unit increase; $P < 0.005$) accompanied by a reduction in Y_4R binding affinity (ca. 1.8 log units lower) and potency with respect to the cAMP assay (about 1 log unit lower) (Table 5.2 and Figures 5.5–5.6). However, analog **5.13b** showed a similar Y_4R affinity (pK_i = 8.4 vs 8.6) and selectivity (pK_i (Y_1R, Y_2R, Y_5R) < 6) to the lead structure **4.9b** when compared. Additionally, this analog (**5.13b**) also exhibited improved potency (pEC_{50} = 7.6 vs 8.5) and lipophilicity ($logD_{7.4}$ = 2.92 vs 2.26) (Table 5.2). Regarding its stability, analog **5.13b** was also found to be stable in human plasma with a half-life of about 33 h and about 56% of intact peptide remaining after 24 h of incubation with HBEC-5i cells (Table 5.3). These findings were also similar to that of **4.9b**, indicating that the replacement of Arg^1 and Arg^5 in **4.9b** with methyl-carbamoylated Arg did not have a negative impact on the pharmacological and chemical properties of its analog **5.13b**.

5.3.3.1 The enhanced lipophilicity of analog **5.13b** had no impact on its translocation

Given that analog **5.13b** exhibits increased lipophilicity, peptides **4.2b**, **4.9b**, and **5.13b** were investigated in a translocation assay to evaluate how this increase influences the peptide's movement across the HBEC-5i BBB model. To accurately determine the amount of intact peptide being apparently translocated across the BBB model, a baseline was adopted to account for potential paracellular leakages due to its imperfect barrier integrity (% Integrity = 90-100%). A strict baseline twice the average amount of FD4 detected in the basolateral samples from the *in vivo* integrity assays (conducted before and after the translocation assay) was used.

As shown in Figure 5.12, about 25% of intact **4.2b** was detected in samples from the basolateral side of the model. In contrast, less than 2% of **4.9b** and its analog **5.13b** were detected in the basolateral samples. With a baseline of about 19%, 19%, and 16% established for the **4.2b**, **4.9b**, and analog **5.13b**, respectively, it can be inferred that about 8% of intact **4.2b** were translocated across the cells after 24 h, whereas for **4.9b** and **5.13b**, none were translocated across the cells. The results also show that a large amount of the peptide is either retained in the cells, adsorbed to the filter, or possibly degraded over time. It is worth mentioning that an average of 31% (**4.2b**),

44% (**4.9b**), and 40% (**5.13b**) of the peptides in the initial solution were estimated to have been adsorbed to the filter of the insert (determined in insert controls without cells).

Considering that analog **5.13b** and its lead structure **4.9b** were not successfully translocated across the BBB model, these results suggest that enhancing lipophilicity by increasing the less protonated species of the peptide known to be more lipophilic at physiological pH (in the case of **5.13b**) does not necessarily improve its translocation as hypothesized. Although **4.2b** and **4.9b** share some similarities in their structure and lipophilicity, the significant amounts of **4.2b** translocated across the BBB model, in contrast to **4.9b** (and **5.13b**), could be attributed to its high metabolic stability in the presence of HBEC-5i cells since the effect of the lipophilicity and the structure-related cationic net charge of the peptide **4.2b** and **4.9b** are similar. This was evident from the negligible detection of intact **5.13b** and the appearance of new peaks, which are likely degradation products of the peptides, observed in the HPLC analysis of **5.13b** samples taken from both the apical and basolateral sides after 1 h and 24 h of incubation (see *Section 5.6 Appendix*; Figure A5.4 shows an example of HPLC chromatograms for **5.13b**). LC-MS analysis of the samples from the apical and basolateral sides confirmed the presence of degradation products that can be linked to the new peaks seen in the HPLC analysis when compared to their respective stock solution (data not shown).

Based on these findings, further metabolic stability studies in the presence of HBEC-5i cells and translocation studies using **4.6b** (a more hydrophilic analog of **2.4**) and **4.9b** were conducted. Given the similarities in the degradation products identified in the plasma stability studies of **2.4** and the known expression of ACE by brain endothelial cells,[22, 63] **4.6b** was co-incubated with the potent ACE inhibitors, ramipril, and its metabolic active form, ramiprilat. Results from this assay generally showed no significant inhibitory effects on the peptide's degradation (Figure A5.5 and A5.6). To rule out the possible involvement of ACE-2, a variant of ACE not inhibited by ramipril or ramiprilat and known to be expressed by HBEC-5i cells,[64, 65] another assay using MLN4760, a potent ACE-2 inhibitor, was conducted. Similarly, no inhibitory effect of MLN4760 was observed (not shown), suggesting there could be other peptidases responsible for the observed degradation. Accordingly, no significant increase in

translocated peptides was observed when **4.6b** and **4.9b** were co-incubated with the inhibitors during the translocation studies (Figure A5.6).

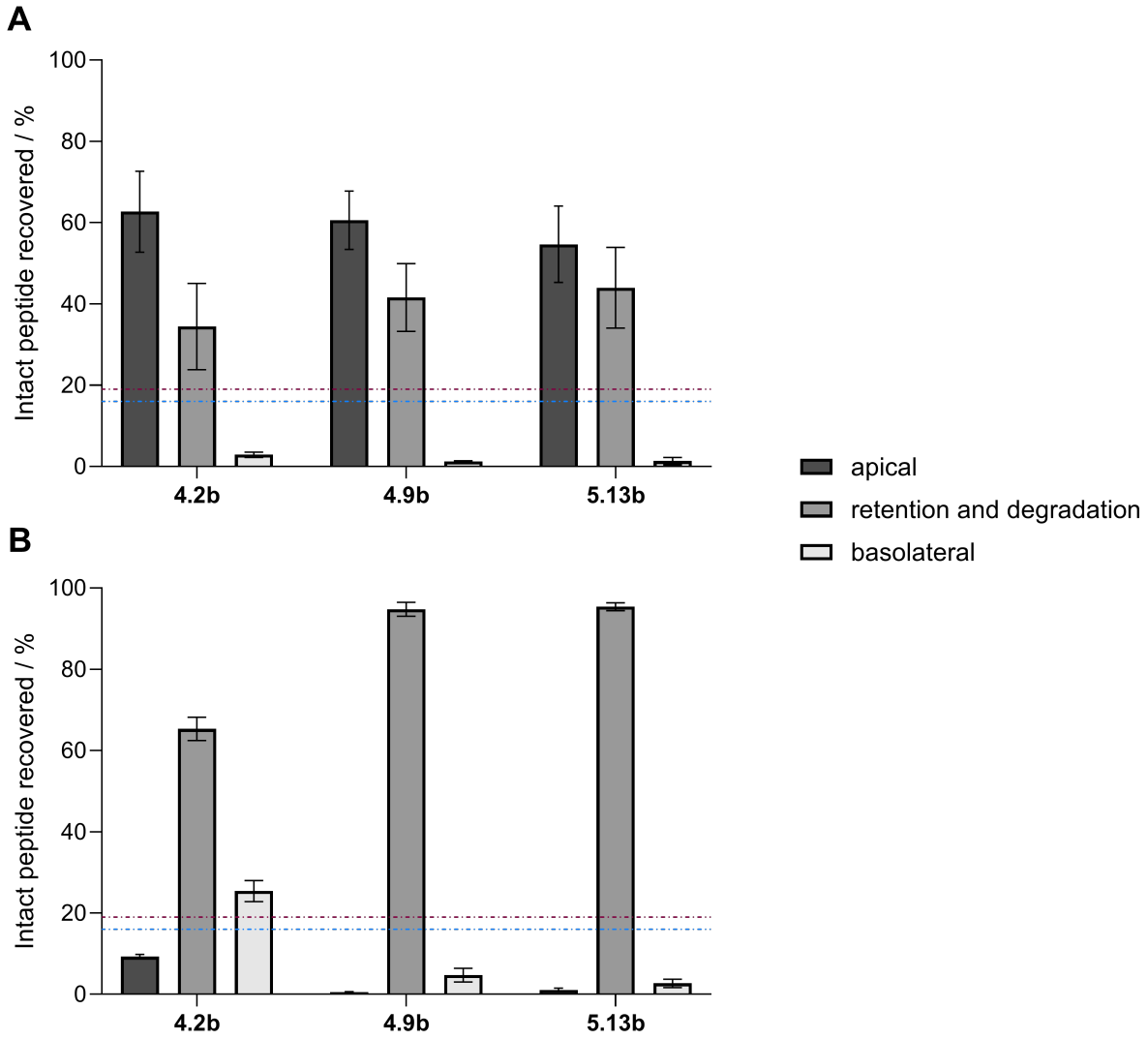

Figure 5.12. Translocation of peptide analogs **4.2b**, **4.9b,** and **5.13b** across the HBEC-5i cells in the *in vitro* BBB model in the absence of serum. The graphs show percental amounts of the peptides detected in samples taken from the apical and basolateral side after (A) 1 h and (B) 24 h of incubation using a concentration of 50 µM. Retention and degradation is calculated by subtracting amounts detected in both the apical and basolateral sides from 100% to represent the percent amount of peptides either adsorbed to the filter, attachment factor (0.1% gelatin) or internalized by the cells. The values were obtained from at least three independent experiments (mean ± SEM). Dashed lines represent the baseline set for peptide **4.2b** at 19% (red). For **4.9b** and **5.13b**, baselines are set to 19% (red) and 16% (blue) respectively.

5.4 Conclusion

The expression of neuropeptide Y_4R in both the CNS and peripheral tissues and its therapeutic potential for various feeding-related disorders, notably obesity, highlights the need for targeted drug development. While it is less cumbersome to develop drugs targeting the receptor in the peripheral tissues, getting these drugs to be bioavailable and act on the receptors in the CNS poses a significant challenge due to the blood-brain barrier (BBB).

Efforts to synthesize analogs of parent peptide **2.4** (**5.8b**, **5.9b**, **5.11**, and **5.12**) via methyl-carbamoylation of guanidinium groups of the Arg residues and fluorescence labeling were aimed at obtaining analogs with enhanced lipophilicity in order to potentially improve their ability to cross membranes and cell barriers such as the BBB. Although these synthesized analogs exhibited high affinity and potency for Y_4R, they were degraded by HBEC-5i cells (used in the *in vitro* BBB model) after 24 h of incubation. A new lipophilic analog, **5.13b** (with two methyl-carbamoylated Arg in positions 1 and 5), was developed using plasma-stable **4.9b** as a lead structure. Although **5.13b**, aside from its high Y_4R binding affinity, displayed increased lipophilicity with high stability in plasma and in the presence of the HBEC-5i cells, it was degraded in the translocation studies. The degradation products from all these analogs, although similar to that in plasma, were shown not to be a result of ACE or its variant ACE-2 activity on the peptide. However, the less lipophilic **4.2b**, which exhibits very high stability in plasma and in the presence of the HBEC-5i cells, was successfully translocated (ca. 8%) across the HBEC-5i BBB model, suggesting the metabolic stability of the peptide is an important factor for its translocation.

Taken together, these findings suggest that although methyl-carbamoylation of Arg may enhance a peptide's lipophilicity, it might not necessarily improve its translocation across membranes, as its metabolic stability, if low, will rather lead to its degradation. These findings point to **4.2b** as a promising lead structure for developing lipophilic and translocatable analogs with high metabolic stability. Some potential analogs of **4.2b** could be derived by replacing the guanidine groups of the arginines in positions 1 and 5 of **4.2b** with methyl-carbamoylguanidine moieties, as shown in this study. Other potential analogs could be derived from the conjugation of **4.2b** with short cell-penetrating peptides at their N-terminus, since attaching even large moieties at the N-terminus of derivatives of **2.4** has been shown to have a negligible impact on their

bioactivity. These potential metabolic-stable and translocatable analogs with increased lipophilicities could aid in the study of the synergistic or combined effects of Y_4R in both the CNS and peripheral tissues.

5.5 References

(1) Sainsbury, A.; Shi, Y. C.; Zhang, L.; Aljanova, A.; Lin, Z.; Nguyen, A. D.; Herzog, H.; Lin, S. Y_4 receptors and pancreatic polypeptide regulate food intake via hypothalamic orexin and brain-derived neurotropic factor dependent pathways. *Neuropeptides* 2010, *44* (3), 261-268. DOI: 10.1016/j.npep.2010.01.001.

(2) Schüß, C.; Behr, V.; Beck-Sickinger, A. G. Illuminating the neuropeptide Y_4 receptor and its ligand pancreatic polypeptide from a structural, functional, and therapeutic perspective. *Neuropeptides* 2024, *105*, 102416. DOI: 10.1016/j.npep.2024.102416.

(3) Schmidt, P. T.; Naslund, E.; Gryback, P.; Jacobsson, H.; Holst, J. J.; Hilsted, L.; Hellstrom, P. M. A role for pancreatic polypeptide in the regulation of gastric emptying and short-term metabolic control. *J. Clin. Endocrinol. Metab.* 2005, *90* (9), 5241-5246. DOI: 10.1210/jc.2004-2089.

(4) Asakawa, A.; Inui, A.; Yuzuriha, H.; Ueno, N.; Katsuura, G.; Fujimiya, M.; Fujino, M. A.; Niijima, A.; Meguid, M. M.; Kasuga, M. Characterization of the effects of pancreatic polypeptide in the regulation of energy balance. *Gastroenterology* 2003, *124* (5), 1325-1336. DOI: 10.1016/s0016-5085(03)00216-6.

(5) Vona-Davis, L. C.; McFadden, D. W. NPY family of hormones: clinical relevance and potential use in gastrointestinal disease. *Curr. Top. Med. Chem.* 2007, *7* (17), 1710-1720. DOI: 10.2174/156802607782340966.

(6) Kamiji, M. M.; Inui, A. NPY Y_2 and Y_4 receptors selective ligands: promising anti-obesity drugs? *Curr. Top. Med. Chem.* 2007, *7* (17), 1734-1742. DOI: 10.2174/156802607782340957.

(7) Okumura, T.; Pappas, T. N.; Taylor, I. L. Pancreatic polypeptide microinjection into the dorsal motor nucleus inhibits pancreatic secretion in rats. *Gastroenterology* 1995, *108* (5), 1517-1525. DOI: 10.1016/0016-5085(95)90702-5.

(8) Zhang, L.; Riepler, S. J.; Turner, N.; Enriquez, R. F.; Lee, I. C.; Baldock, P. A.; Herzog, H.; Sainsbury, A. Y_2 and Y_4 receptor signaling synergistically act on energy expenditure and physical activity. *Am. J. Physiol. Regul. Integr. Comp. Physiol.* 2010, *299* (6), R1618-1628. DOI: 10.1152/ajpregu.00345.2010.

(9) Zipf, W. B.; O'Dorisio, T. M.; Berntson, G. G. Short-term infusion of pancreatic polypeptide: effect on children with Prader-Willi syndrome. *Am. J. Clin. Nutr.* 1990, *51* (2), 162-166. DOI: 10.1093/ajcn/51.2.162.

(10) Batterham, R. L.; Le Roux, C. W.; Cohen, M. A.; Park, A. J.; Ellis, S. M.; Patterson, M.; Frost, G. S.; Ghatei, M. A.; Bloom, S. R. Pancreatic polypeptide reduces appetite and food intake in humans. *J. Clin. Endocrinol. Metab.* 2003, *88* (8), 3989-3992. DOI: 10.1210/jc.2003-030630.

(11) Dumont, Y.; Jacques, D.; Bouchard, P.; Quirion, R. Species differences in the expression and distribution of the neuropeptide Y Y_1, Y_2, Y_4, and Y_5 receptors in rodents, guinea pig, and primates brains. *J. Comp. Neurol.* 1998, *402* (3), 372-384.

(12) Larsen, P. J.; Kristensen, P. The neuropeptide Y Y_4 receptor is highly expressed in neurones of the rat dorsal vagal complex. *Brain Res. Mol.* 1997, *48* (1), 1-6. DOI: 10.1016/s0169-328x(97)00069-7.

(13) Whitcomb, D. C.; Taylor, I. L.; Vigna, S. R. Characterization of saturable binding sites for circulating pancreatic polypeptide in rat brain. *Am. J. Physiol.* 1990, *259* (4 Pt 1), G687-691. DOI: 10.1152/ajpgi.1990.259.4.G687.

(14) Dumont, Y.; Moyse, E.; Fournier, A.; Quirion, R. Distribution of peripherally injected peptide YY ([^{125}I]PYY_{3-36}) and pancreatic polypeptide ([^{125}I]hPP) in the CNS: enrichment in the area postrema. *J. Mol. Neurosci.* 2007, *33* (3), 294-304. DOI: 10.1007/s12031-007-9007-9.

(15) Adrian, T. E.; Besterman, H. S.; Mallinson, C. N.; Greenberg, G. R.; Bloom, S. R. Inhibition of secretin stimulated pancreatic secretion by pancreatic polypeptide. *Gut* 1979, *20* (1), 37-40. DOI: 10.1136/gut.20.1.37.

(16) Adrian, T. E.; Bloom, S. R.; Bryant, M. G.; Polak, J. M.; Heitz, P. H.; Barnes, A. J. Distribution and release of human pancreatic polypeptide. *Gut* 1976, *17* (12), 940-944. DOI: 10.1136/gut.17.12.940.

(17) Asakawa, A.; Inui, A.; Ueno, N.; Fujimiya, M.; Fujino, M. A.; Kasuga, M. Mouse pancreatic polypeptide modulates food intake, while not influencing anxiety in mice. *Peptides* 1999, *20* (12), 1445-1448. DOI: 10.1016/s0196-9781(99)00155-2.

(18) Campbell, R. E.; Smith, M. S.; Allen, S. E.; Grayson, B. E.; Ffrench-Mullen, J. M.; Grove, K. L. Orexin neurons express a functional pancreatic polypeptide Y_4 receptor. *J. Neurosci.* 2003, *23* (4), 1487-1497. DOI: 10.1523/JNEUROSCI.23-04-01487.2003.

(19) Pardridge, W. M. The blood-brain barrier: bottleneck in brain drug development. *NeuroRx* 2005, *2* (1), 3-14. DOI: 10.1602/neurorx.2.1.3.

(20) Kadry, H.; Noorani, B.; Cucullo, L. A blood-brain barrier overview on structure, function, impairment, and biomarkers of integrity. *Fluids Barriers CNS* 2020, *17* (1), 69. DOI: 10.1186/s12987-020-00230-3.

(21) Ruble, J. C.; Vandeveer, H. G.; Navarro, A. Large scale synthesis of enantiomerically pure (S)-3-(4-Bromophenyl) butanoic acid. *Org. Synth.* 2003, *95*, 328-344.

(22) Konieczny, A.; Conrad, M.; Ertl, F. J.; Gleixner, J.; Gattor, A. O.; Grätz, L.; Schmidt, M. F.; Neu, E.; Horn, A. H. C.; Wifling, D.*; et al.* N-Terminus to arginine side-chain cyclization of linear peptidic neuropeptide Y Y_4 receptor ligands results in picomolar binding constants. *J. Med. Chem.* 2021, *64* (22), 16746-16769. DOI: 10.1021/acs.jmedchem.1c01574.

(23) Gleixner, J.; Kopanchuk, S.; Gratz, L.; Tahk, M. J.; Laasfeld, T.; Veiksina, S.; Horing, C.; Gattor, A. O.; Humphrys, L. J.; Muller, C.*; et al.* Illuminating neuropeptide Y Y_4 receptor binding: fluorescent cyclic peptides with subnanomolar binding affinity as novel molecular tools. *ACS Pharmacol. Transl. Sci.* 2024, *7* (4), 1142-1168. DOI: 10.1021/acsptsci.4c00013.

(24) Ertl, F. J.; Kopanchuk, S.; Dijon, N. C.; Veiksina, S.; Tahk, M. J.; Laasfeld, T.; Schettler, F.; Gattor, A. O.; Hubner, H.; Archipowa, N.*; et al.* Dually labeled neurotensin NTS_1R ligands for probing radiochemical and fluorescence-based

binding assays. *J. Med. Chem.* 2024, *67* (18), 16664-16691. DOI: 10.1021/acs.jmedchem.4c01470.

(25) Schettler, F.; Gattor, A. O.; Koch, P.; Keller, M. Characterization of [^{3}H]propionylated human peptide YY – a new probe for neuropeptide Y Y_2 receptor binding studies. *ACS Pharmacol. Transl. Sci.* 2025, *8* (3), 785-799. DOI: 10.1021/acsptsci.4c00666.

(26) Gleixner, J.; Gattor, A. O.; Humphrys, L. J.; Brunner, T.; Keller, M. [^{3}H]UR-JG102–A radiolabeled cyclic peptide with high affinity and excellent selectivity for the neuropeptide Y Y_4 receptor. *J. Med. Chem.* 2023, *66* (19), 13788-13808. DOI: 10.1021/acs.jmedchem.3c01224.

(27) Keller, M.; Weiss, S.; Hutzler, C.; Kuhn, K. K.; Mollereau, C.; Dukorn, S.; Schindler, L.; Bernhardt, G.; König, B.; Buschauer, A. N^{ω}-Carbamoylation of the argininamide moiety: an avenue to insurmountable NPY Y_1 receptor antagonists and a radiolabeled selective high-affinity molecular tool ([^{3}H]UR-MK299) with extended residence time. *J. Med. Chem.* 2015, *58*, 8834-8849. DOI: 10.1021/acs.jmedchem.5b00925.

(28) Müller, C.; Gleixner, J.; Tahk, M.-J.; Kopanchuk, S.; Laasfeld, T.; Weinhart, M.; Schollmeyer, D.; Betschart, M. U.; Lüdeke, S.; Koch, P.*; et al.* Structure-based design of high-affinity fluorescent probes for the neuropeptide Y Y_1 receptor. *J. Med. Chem.* 2022, *65* (6), 4832-4853. DOI: 10.1021/acs.jmedchem.1c02033.

(29) Keller, M.; Kuhn, K. K.; Einsiedel, J.; Hubner, H.; Biselli, S.; Mollereau, C.; Wifling, D.; Svobodova, J.; Bernhardt, G.; Cabrele, C.*; et al.* Mimicking of arginine by functionalized N^{ω}-Carbamoylated arginine as a new broadly applicable approach to labeled bioactive peptides: high affinity angiotensin, neuropeptide Y, neuropeptide FF, and neurotensin receptor ligands as examples. *J. Med. Chem.* 2016, *59* (5), 1925-1945. DOI: 10.1021/acs.jmedchem.5b01495.

(30) Spinnler, K.; von Kruchten, L.; Konieczny, A.; Schindler, L.; Bernhardt, G.; Keller, M. An alkyne-functionalized arginine for solid-phase synthesis enabling "Bioorthogonal" peptide conjugation. *ACS Med. Chem. Lett.* 2020, *11* (3), 334-339. DOI: 10.1021/acsmedchemlett.9b00388.

(31) Ziemek, R.; Schneider, E.; Kraus, A.; Cabrele, C.; Beck-Sickinger, A. G.; Bernhardt, G.; Buschauer, A. Determination of affinity and activity of ligands at the human neuropeptide Y Y_4 receptor by flow cytometry and aequorin luminescence. *J. Recept. Signal Transduct.* 2007, *27*, 217-233. DOI: 10.1080/10799890701505206.

(32) Moser, C.; Bernhardt, G.; Michel, J.; Schwarz, H.; Buschauer, A. Cloning and functional expression of the hNPY Y_5 receptor in human endometrial cancer (HEC-1B) cells. *Can. J. Physiol. Pharmacol.* 2000, *78* (2), 134-142. DOI: 10.1139/y99-125 %M 10737676.

(33) Cheng, Y.; Prusoff, W. H. Relationship between the inhibition constant (K_1) and the concentration of inhibitor which causes 50 per cent inhibition (I_{50}) of an enzymatic reaction. *Biochem. Pharmacol.* 1973, *22* (23), 3099-3108. DOI: 10.1016/0006-2952(73)90196-2.

(34) Dukorn, S.; Littmann, T.; Keller, M.; Kuhn, K.; Cabrele, C.; Baumeister, P.; Bernhardt, G.; Buschauer, A. Fluorescence- and radiolabeling of [Lys^4,Nle^{17},^{30}]hPP yields molecular tools for the NPY Y_4 receptor. *Bioconjug. Chem.* 2017, *28*, 1291-1304. DOI: 10.1021/acs.bioconjchem.7b00103.

(35) Kuhn, K. K.; Ertl, T.; Dukorn, S.; Keller, M.; Bernhardt, G.; Reiser, O.; Buschauer, A. High affinity agonists of the neuropeptide Y (NPY) Y_4 receptor derived from the C-terminal pentapeptide of human pancreatic polypeptide (hPP): synthesis, stereochemical discrimination, and radiolabeling. *J. Med. Chem.* 2016, *59*, 6045-6058. DOI: 10.1021/acs.jmedchem.6b00309.

(36) Pegoli, A.; Wifling, D.; Gruber, C. G.; She, X.; Hubner, H.; Bernhardt, G.; Gmeiner, P.; Keller, M. Conjugation of short peptides to dibenzodiazepinone-type muscarinic acetylcholine receptor ligands determines M_2R selectivity. *J. Med. Chem.* 2019, *62* (11), 5358-5369. DOI: 10.1021/acs.jmedchem.8b01967.

(37) Cavaco, M.; Perez-Peinado, C.; Valle, J.; Silva, R. D. M.; Correia, J. D. G.; Andreu, D.; Castanho, M.; Neves, V. To what extent do fluorophores bias the biological activity of peptides? A practical approach using membrane-aactive peptides as models. *Front. Bioeng. Biotechnol.* 2020, *8*, 552035. DOI: 10.3389/fbioe.2020.552035.

(38) Wu, D.; Chen, Q.; Chen, X.; Han, F.; Chen, Z.; Wang, Y. The blood-brain barrier: structure, regulation, and drug delivery. *Signal Transduct. Target Ther.* 2023, *8* (1), 217. DOI: 10.1038/s41392-023-01481-w.

(39) Banks, W. A. Characteristics of compounds that cross the blood-brain barrier. *BMC Neurol.* 2009, *9 Suppl 1* (Suppl 1), S3. DOI: 10.1186/1471-2377-9-S1-S3.

(40) Shaw, A. T.; Yasothan, U.; Kirkpatrick, P. Crizotinib. *Nat. Rev. Drug Discov.* 2011, *10* (12), 897-898. DOI: 10.1038/nrd3600.

(41) Md Abdur Rauf, S.; Arvidsson, P. I.; Albericio, F.; Govender, T.; Maguire, G. E.; Kruger, H. G.; Honarparvar, B. The effect of N-methylation of amino acids (Ac-X-OMe) on solubility and conformation: a DFT study. *Org. Biomol. Chem.* 2015, *13* (39), 9993-10006. DOI: 10.1039/c5ob01565k.

(42) Ritchie, T. J.; Macdonald, S. J. F.; Pickett, S. D. Insights into the impact of N- and O-methylation on aqueous solubility and lipophilicity using matched molecular pair analysis. *MedChemComm* 2015, *6* (10), 1787-1797, 10.1039/C5MD00309A. DOI: 10.1039/C5MD00309A.

(43) Kuhn, K. K.; Littmann, T.; Dukorn, S.; Tanaka, M.; Keller, M.; Ozawa, T.; Bernhardt, G.; Buschauer, A. In search of NPY Y_4R antagonists: incorporation of carbamoylated arginine, aza-amino acids, or d-amino acids into oligopeptides derived from the C-termini of the endogenous agonists. *ACS Omega* 2017, *2*, 3616-3631. DOI: 10.1021/acsomega.7b00451.

(44) Biselli, S.; Bresinsky, M.; Tropmann, K.; Forster, L.; Honisch, C.; Buschauer, A.; Bernhardt, G.; Pockes, S. Pharmacological characterization of a new series of carbamoylguanidines reveals potent agonism at the H_2R and D_3R. *Eur. J. Med. Chem.* 2021, *214*, 113190. DOI: 10.1016/j.ejmech.2021.113190.

(45) Szeto, H. H.; Schiller, P. W.; Zhao, K.; Luo, G. Fluorescent dyes alter intracellular targeting and function of cell-penetrating tetrapeptides. *FASEB J.* 2005, *19* (1), 118-120. DOI: 10.1096/fj.04-1982fje.

(46) Takakura, H.; Sato, H.; Nakajima, K.; Suzuki, M.; Ogawa, M. *In vitro* and *in vivo* cell uptake of a cell-penetrating peptide conjugated with fluorescent dyes having different chemical properties. *Cancers (Basel)* 2021, *13* (9). DOI: 10.3390/cancers13092245.

(47) Valko, K. L. Lipophilicity and biomimetic properties measured by HPLC to support drug discovery. *J. Pharm. Biomed. Anal.* 2016, *130*, 35-54. DOI: 10.1016/j.jpba.2016.04.009.

(48) Kovacevic, S.; Karadzic Banjac, M.; Anojcic, J.; Podunavac-Kuzmanovic, S.; Jevric, L.; Nikolic, A.; Savic, M.; Kuzminac, I. Chemometrics of anisotropic lipophilicity of anticancer androstane derivatives determined by reversed-phase ultra high performance liquid chromatography with polar aprotic and protic modifiers. *J. Chromatogr. A* 2022, *1673*, 463197. DOI: 10.1016/j.chroma.2022.463197.

(49) Pergande, M. R.; Cologna, S. M. Isoelectric point separations of peptides and proteins. *Proteomes* 2017, *5* (1). DOI: 10.3390/proteomes5010004.

(50) Kumar, S. CHAPTER 14 - Local anesthetics. In *Anesthesia Secrets (Fourth Edition)*, Duke, J. Ed.; Mosby, 2011; pp 105-111.

(51) Berlicki, L.; Kaske, M.; Gutierrez-Abad, R.; Bernhardt, G.; Illa, O.; Ortuno, R. M.; Cabrele, C.; Buschauer, A.; Reiser, O. Replacement of Thr^{32} and Gln^{34} in the C-terminal neuropeptide Y fragment 25-36 by cis-cyclobutane and cis-cyclopentane beta-amino acids shifts selectivity toward the Y_4 receptor. *J. Med. Chem.* 2013, *56* (21), 8422-8431. DOI: 10.1021/jm4008505.

(52) Puech, C.; Hodin, S.; Forest, V.; He, Z.; Mismetti, P.; Delavenne, X.; Perek, N. Assessment of HBEC-5i endothelial cell line cultivated in astrocyte conditioned medium as a human blood-brain barrier model for ABC drug transport studies. *Int. J. Pharm.* 2018, *551* (1), 281-289. DOI: 10.1016/j.ijpharm.2018.09.040.

(53) Hoffmann, L. F.; Martins, A.; Majolo, F.; Contini, V.; Laufer, S.; Goettert, M. I. Neural regeneration research model to be explored: SH-SY5Y human neuroblastoma cells. *Neural Regen. Res.* 2023, *18* (6), 1265-1266. DOI: 10.4103/1673-5374.358621.

(54) Blades, R.; Ittner, L. M.; Tietz, O. Peptides for trans-blood-brain barrier delivery. *J. Label. Compd. Radiopharm.* 2023, *66* (9), 237-248. DOI: 10.1002/jlcr.4023.

(55) Egleton, R. D.; Davis, T. P. Development of neuropeptide drugs that cross the blood-brain barrier. *NeuroRx* 2005, *2* (1), 44-53. DOI: 10.1602/neurorx.2.1.44.

(56) Palian, M. M.; Boguslavsky, V. I.; O'Brien, D. F.; Polt, R. Glycopeptide-membrane interactions: glycosyl enkephalin analogues adopt turn conformations by NMR and CD in amphipathic media. *J. Am. Chem. Soc.* 2003, *125* (19), 5823-5831. DOI: 10.1021/ja0268635.

(57) Bickel, U.; Yoshikawa, T.; Pardridge, W. M. Delivery of peptides and proteins through the blood-brain barrier. *Adv. Drug Deliv. Rev.* 2001, *46* (1-3), 247-279. DOI: 10.1016/s0169-409x(00)00139-3.

(58) Di Pisa, M.; Chassaing, G.; Swiecicki, J. M. Translocation mechanism(s) of cell-penetrating peptides: biophysical studies using artificial membrane bilayers. *Biochemistry* 2015, *54* (2), 194-207. DOI: 10.1021/bi501392n.

(59) Triguero, D.; Buciak, J. L.; Pardridge, W. M. Cationization of immunoglobulin G results in enhanced organ uptake of the protein after intravenous administration in rats and primate. *J. Pharmacol. Exp. Ther.* 1991, *258* (1), 186-192.

(60) Taylor, P. J. Matrix effects: the achilles heel of quantitative high-performance liquid chromatography-electrospray-tandem mass spectrometry. *Clin. Biochem.* 2005, *38* (4), 328-334. DOI: 10.1016/j.clinbiochem.2004.11.007.

(61) Panuwet, P.; Hunter, R. E., Jr.; D'Souza, P. E.; Chen, X.; Radford, S. A.; Cohen, J. R.; Marder, M. E.; Kartavenka, K.; Ryan, P. B.; Barr, D. B. Biological matrix effects in quantitative tandem mass spectrometry-based analytical methods: advancing biomonitoring. *Crit. Rev. Anal. Chem.* 2016, *46* (2), 93-105. DOI: 10.1080/10408347.2014.980775.

(62) Mostafavi, S. A.; Tahvilian, R.; Dehghani Poudeh, M.; Rafeepour, Z. A simple sample preparation with HPLC-UV method for estimation of clomipramine from plasma. *Iran J. Pharm. Res.* 2010, *9* (3), 243-250.

(63) Coates, D. The angiotensin converting enzyme (ACE). *Int. J. Biochem. Cell Biol.* 2003, *35* (6), 769-773. DOI: 10.1016/s1357-2725(02)00309-6.

(64) Puech, C.; Hodin, S.; Forest, V.; He, Z.; Mismetti, P.; Delavenne, X.; Perek, N. Assessment of HBEC-5i endothelial cell line cultivated in astrocyte conditioned medium as a human blood-brain barrier model for ABC drug transport studies. *Int. J. Pharm.* 2018, *551* (1-2), 281-289. DOI: 10.1016/j.ijpharm.2018.09.040.

(65) Lindskog, C.; Mear, L.; Virhammar, J.; Fallmar, D.; Kumlien, E.; Hesselager, G.; Casar-Borota, O.; Rostami, E. Protein expression profile of ACE2 in the normal and COVID-19-affected human brain. *J. Proteome Res.* 2022, *21* (9), 2137-2145. DOI: 10.1021/acs.jproteome.2c00184.

5.6 Appendix

5.6.1 Figures A5.1–A5.6 and Table A5.1–A5.2

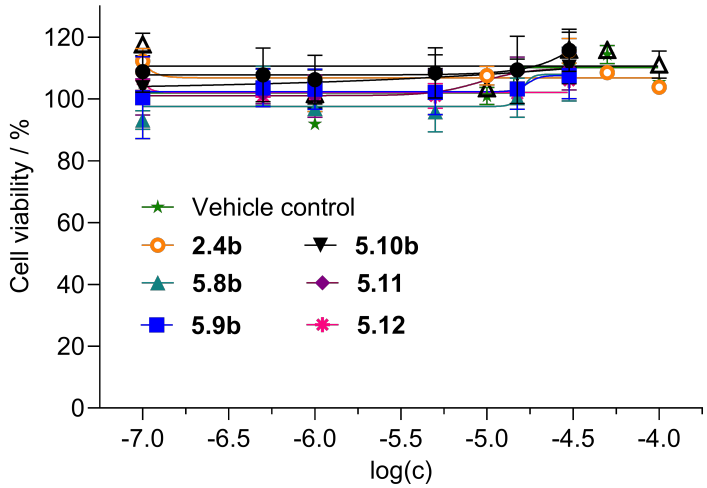

Figure A5.1. *In vitro* cytotoxicity of peptides **2.4**, **5.8b**, **5.9b**, **5.10b**, **5.11**, **and 5.12** studied with HBEC-5i cells using the CellTiter-Blue® Cell Viability Assay kit. Cell counts of 15,000 cells per well of HBEC-5i were incubated (24 h, 37 °C) with various concentrations of peptides (range from 0.01–100 µM). Vehicle control: 0.01–100 µM of aqueous solution of HCl in assay medium

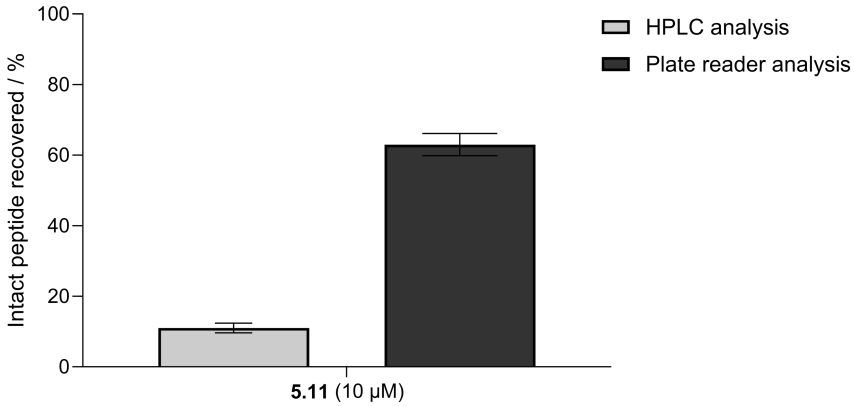

Figure A5.2. Difference in the amount of intact peptide **5.11** translocated across HBEC-5i cells in the translocation studies using the detection from HPLC and microplate reader (λ_{ex} = 560 nm, λ_{em} = 590 nm)

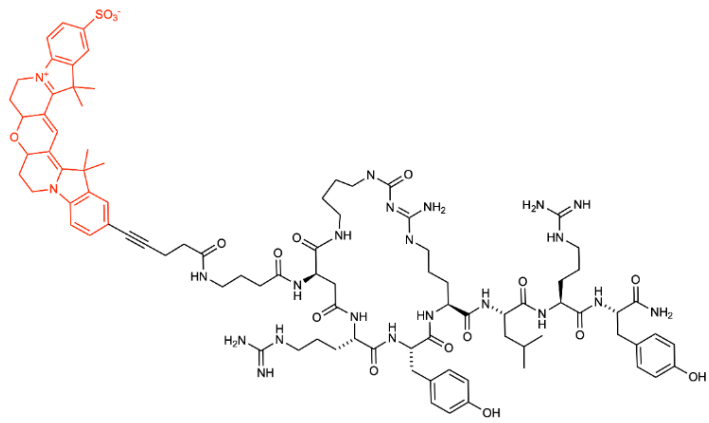

Figure A5.3. Structure of UR-JG114[23] (pK_i (hY_4R) = 9.71 ± 0.09)

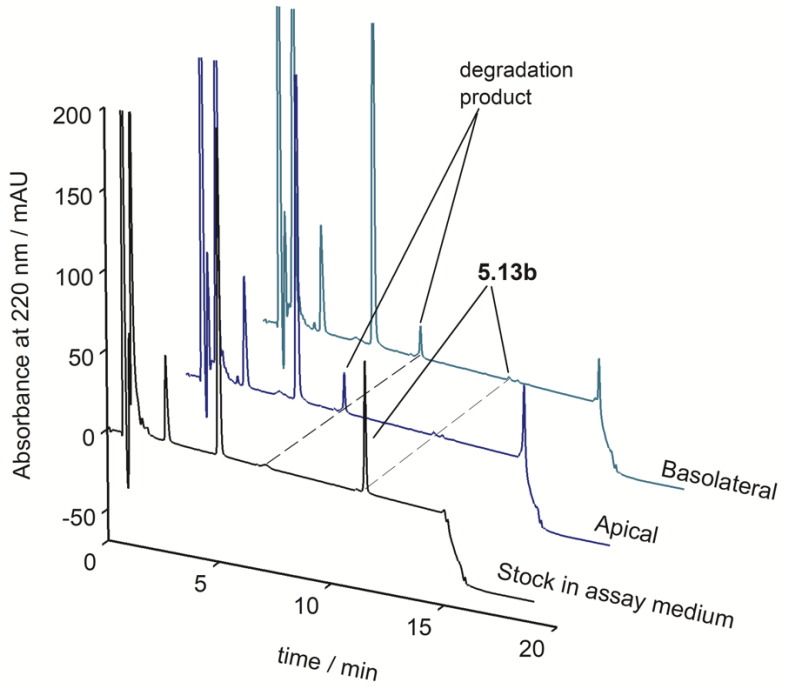

Figure A5.4. RP-HPLC chromatograms obtained from the translocation study of peptide analog **5.13b**. The chromatograms include data from the stock solution of the peptide, and samples collected from the apical and basolateral sides of the *in vitro* HBEC-5i BBB model after 24 h of incubation. RP-HPLC analysis reveals the complete degradation of **5.13b** within 24 h as also indicated by the detection of degradation products through LC-MS analysis (data not shown). The initial concentration of the peptide used was 50 µM.

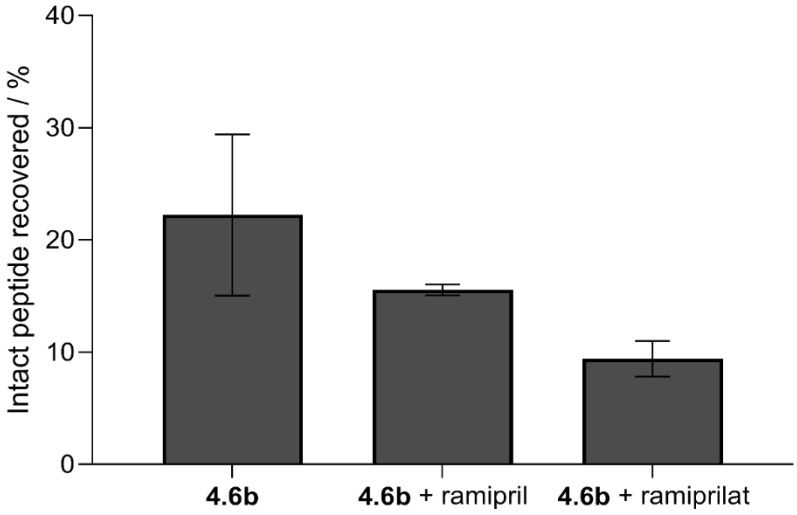

Figure A5.5. Percental amount of intact **4.6b** detected in samples from the metabolic stability study of peptides in the presence of HBEC-5i and ACE inhibitors by HPLC. The presence of the ACE inhibitor ramipril or ramiprilat did not inhibit the degradation of the peptide. Data from two to three independent experiments performed in triplicate.

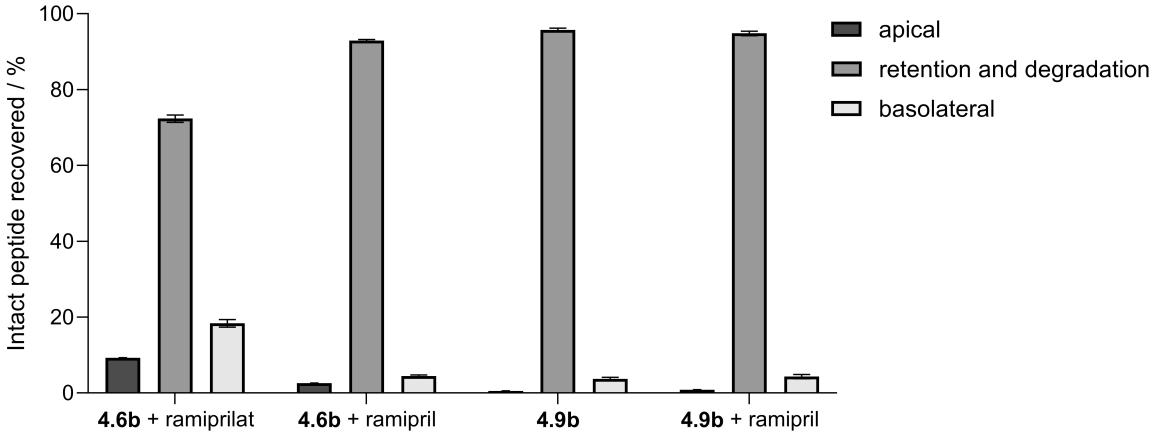

Figure A5.6. Percental amount of intact peptides recovered from the translocation studies of **4.9b** and **4.6b** in the absence and presence of the ACE inhibitor ramipril. Retention is calculated by subtracting amounts detected in both the apical and basolateral sides from 100% to represent the percent amount of peptides either adsorbed to the filter, attachment factor (0.1% gelatin) or internalized by the cells. Data from one to two independent experiments performed in triplicate.

Table A5.1. Recoveries of peptides from human plasma/PBS (1:2 v/v) at a concentration of 40 μM and ratios of peptide recovery over recovery of internal standard (1-methyl-D-tryptophan).

Compd.	Peptide concentration 40 μM		
	Recovery peptide (%)[a]	Recovery D-Me-Trp (%)[b]	Ratio[b]
5.13b	31	34	0.92
	69	82	0.83
	104	117	0.89
	96	109	0.88
	106	117	0.91
			(0.89 ± 0.02)

[a]Recovery of peptide **5.13b** and internal standard, 1-methyl-D-tryptophan from human plasma/PBS (1:2 v/v) using peptide concentrations of 40 μM and an internal standard concentration of 10 μM (five independent experiments). [b]Ratios of peptide recovery over recovery of internal standard calculated for individual experiments (mean recovery ratios ± SEM).

Table A5.2. Average percent barrier integrities of cell models used in the translocation studies of peptides **5.8b**, **5.9b**, **5.11**, **5.12**, **4.2b**, **4.9b**, and **5.13b**.

Compd.	Average percent FD4 detected in basolateral side (%)	Average barrier integrity (%)	
		before assay	after assay
5.8b	-	-	-
5.9b	-	-	-
5.11 (no FBS)	12	-	89
5.11 (FBS)	10	-	90
5.12 (no FBS)	11	-	89
5.12 (FBS)	11	-	90
4.2b	9.4[#]	91	90
4.9b	9.4[#]	90	91
5.13b	8.1[#]	93	91

[#]Determined from the average percent of FD4 detected in barrier integrity assays before and after the translocation assays

5.6.2 RP-HPLC chromatograms of peptides 5.8b, 5.9b, 5.10b, 5.11, 5.12, and 5.13b (Purity control)

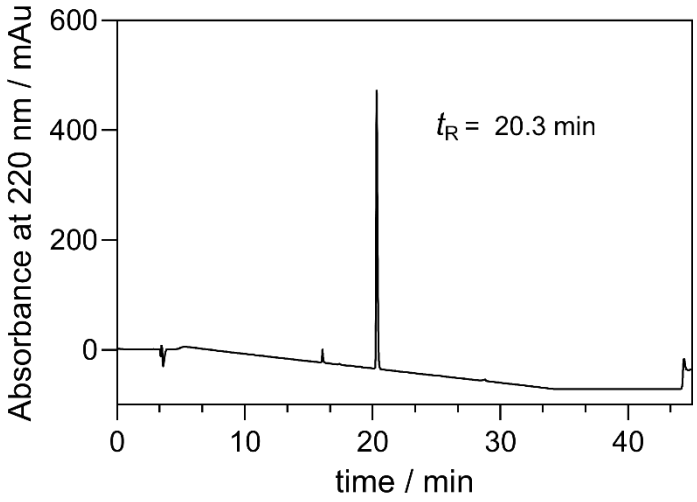

RP-HPLC analysis of peptide **5.5**.

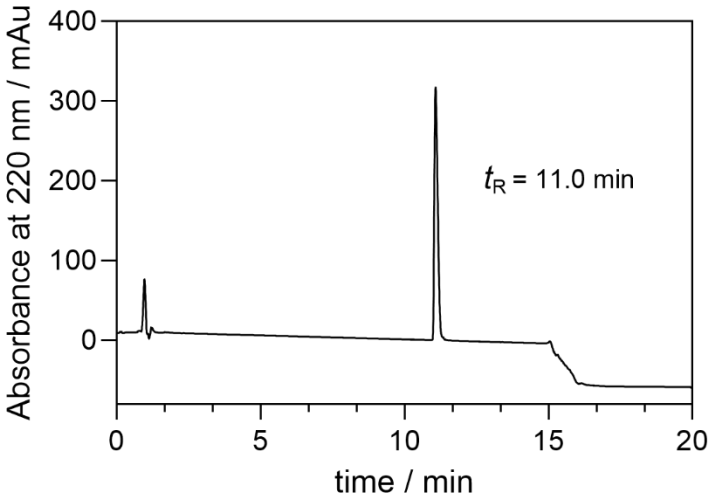

RP-HPLC analysis of peptide **5.8b**.

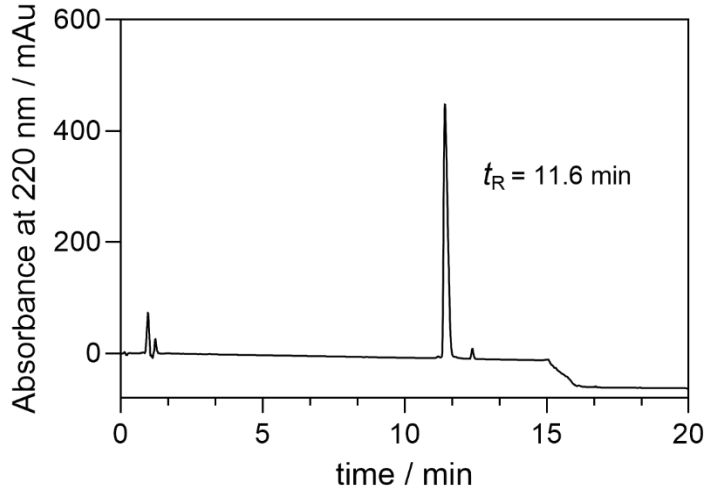

RP-HPLC analysis of peptide **5.9b**.

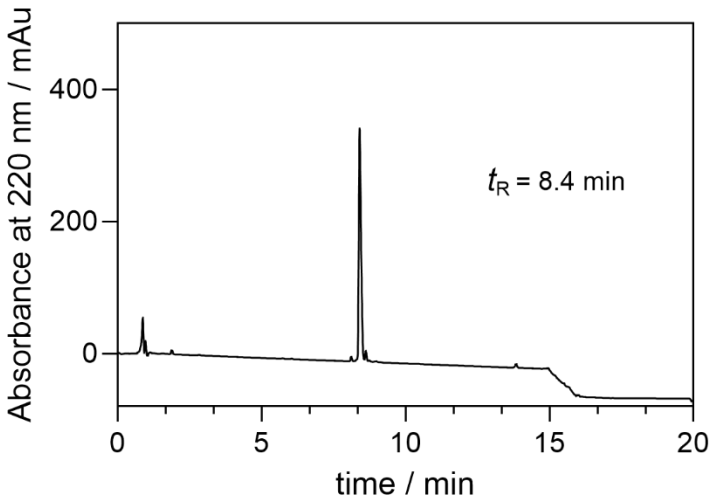

RP-HPLC analysis of peptide **5.10b**.

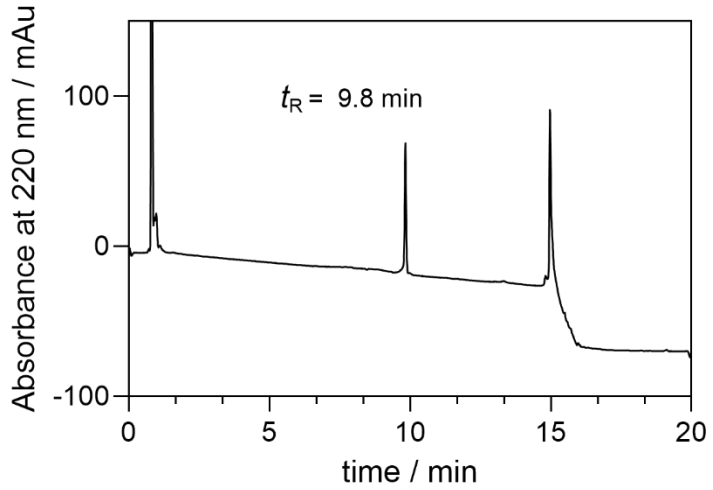

RP-HPLC analysis of peptide **5.11**.

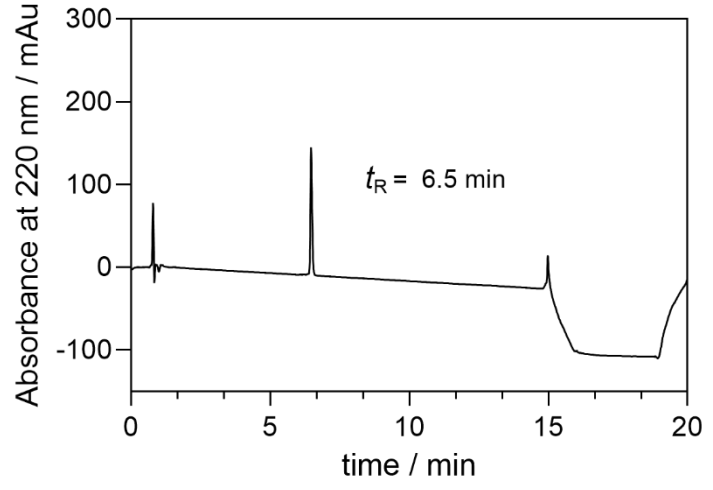

RP-HPLC analysis of peptide **5.12**.

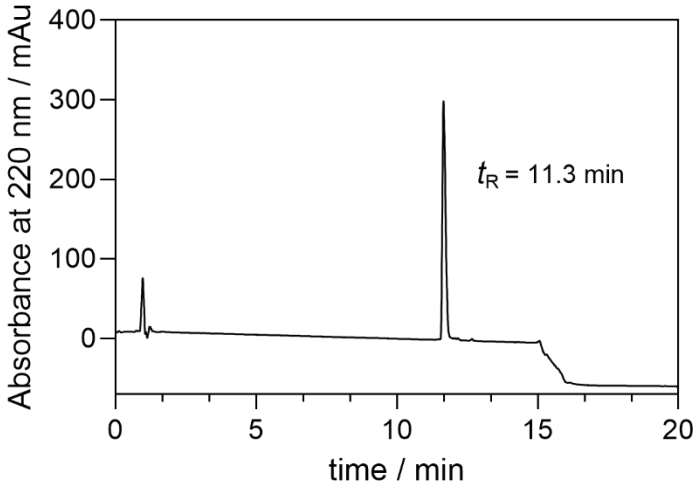

RP-HPLC analysis of peptide **5.13b**.

5.6.3 ^{1}H-NMR spectra of compound 5.5, peptides 5.8b, 5.9b, and 5.13b and ^{13}C-NMR spectrum of compound 5.5

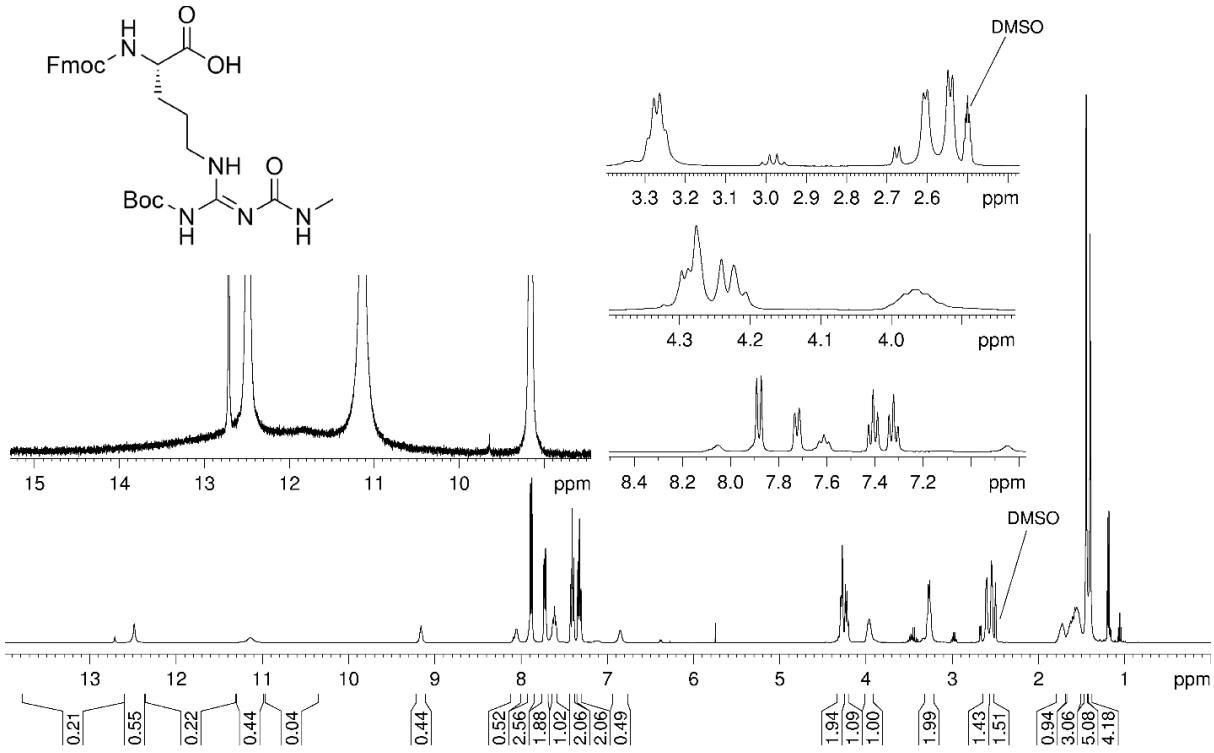

^{1}H-NMR spectrum (400 MHz, DMSO-d_6) of peptide **5.5**.

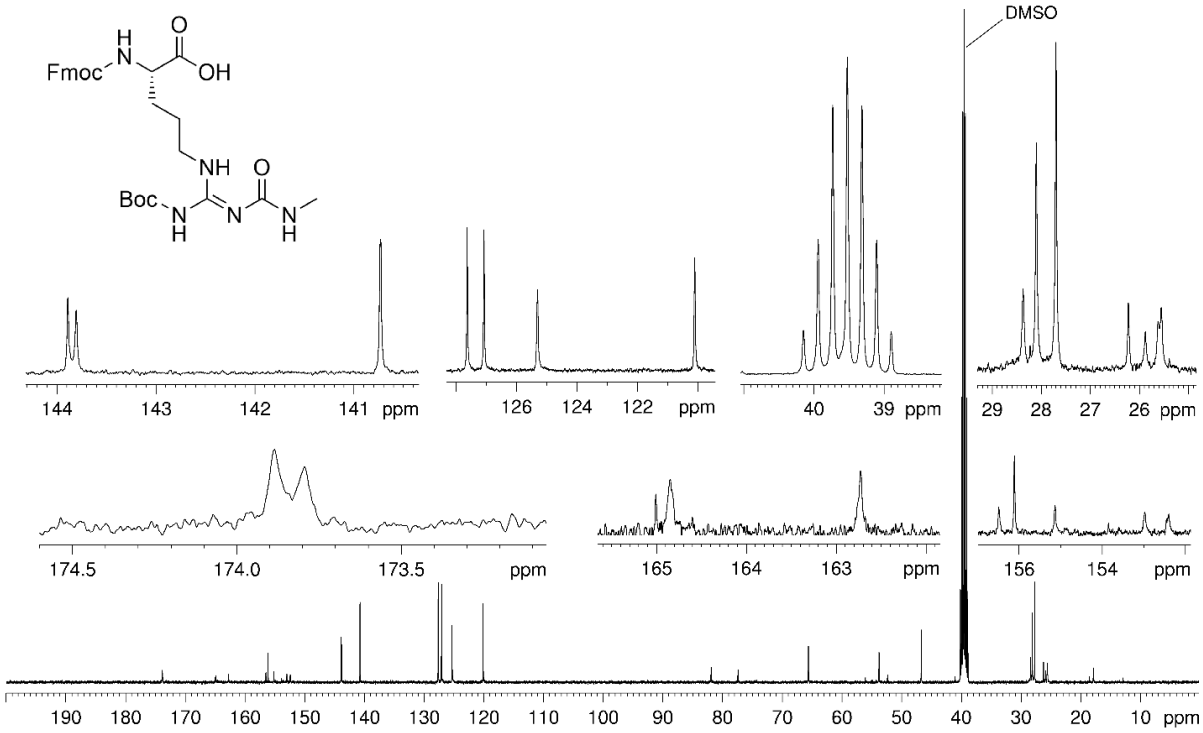

^{13}C-NMR spectrum (150 MHz, DMSO-d_6) of peptide **5.5**.

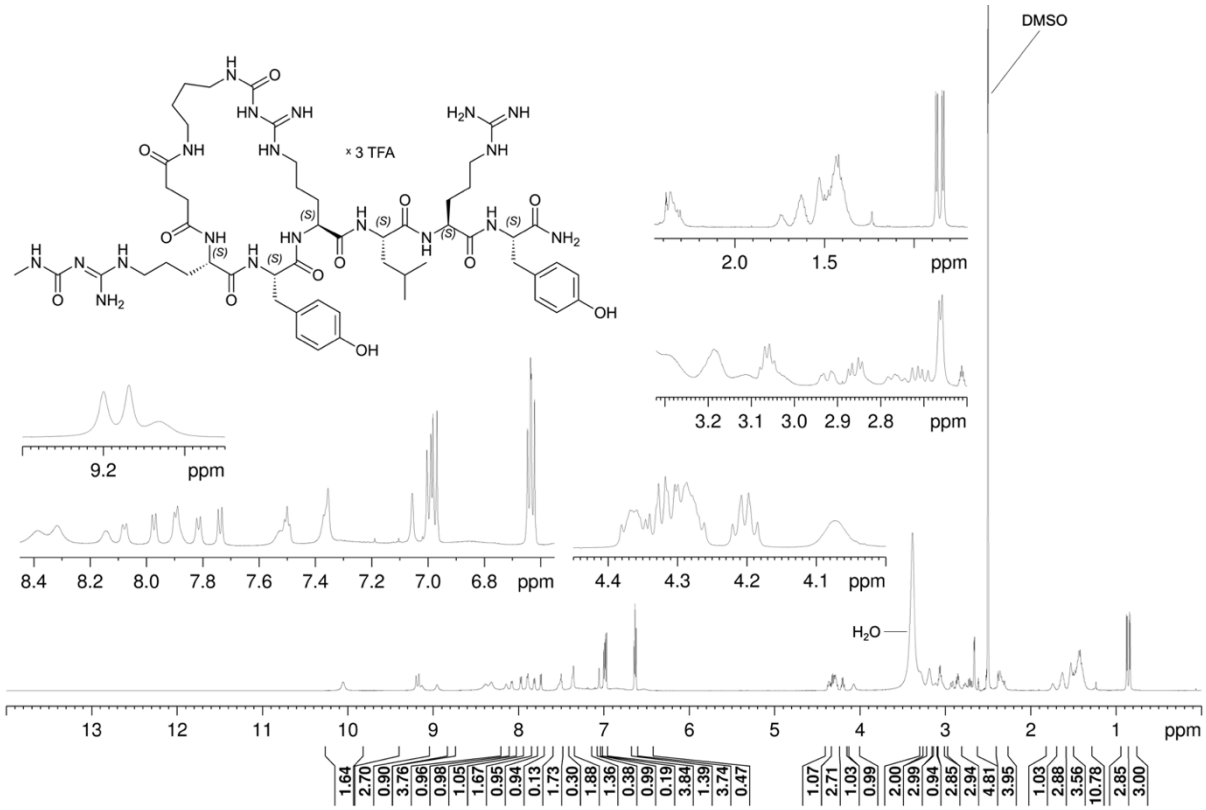

^{1}H-NMR spectrum (600 MHz, DMSO-d_6) of peptide **5.8b**.

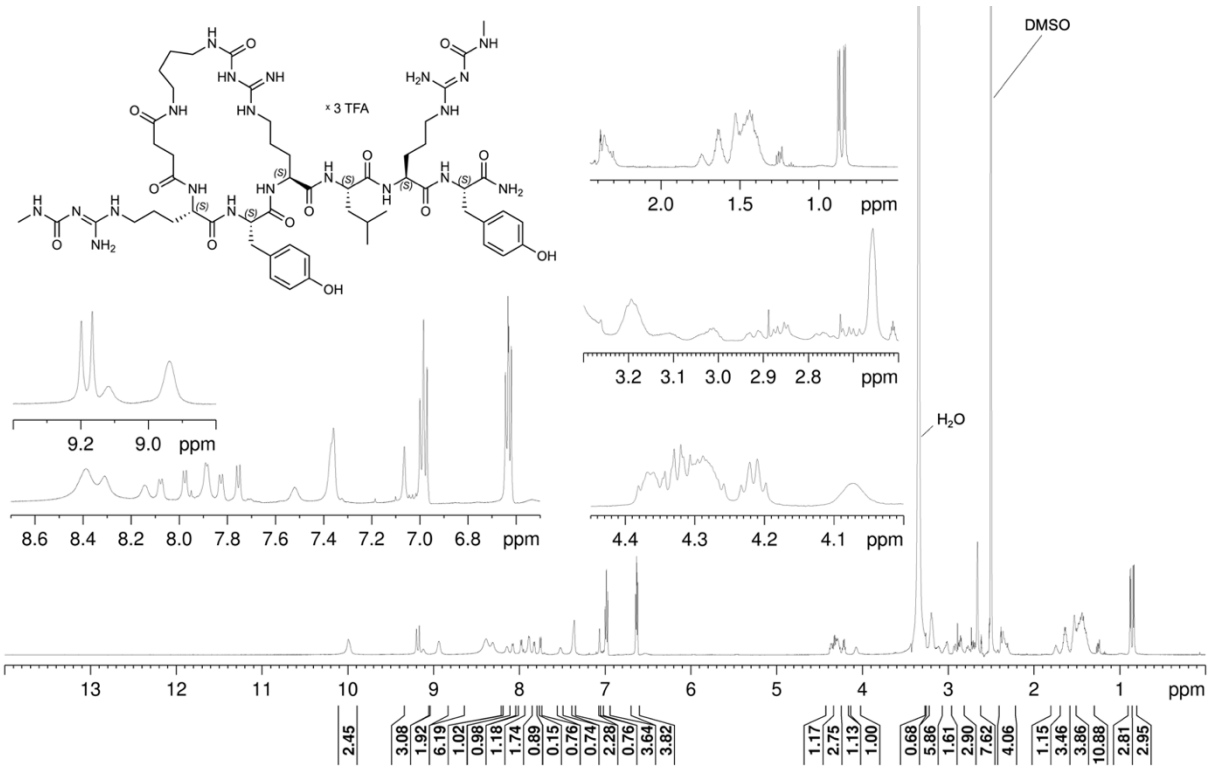

^{1}H-NMR spectrum (600 MHz, DMSO-d_6) of peptide **5.9b**.

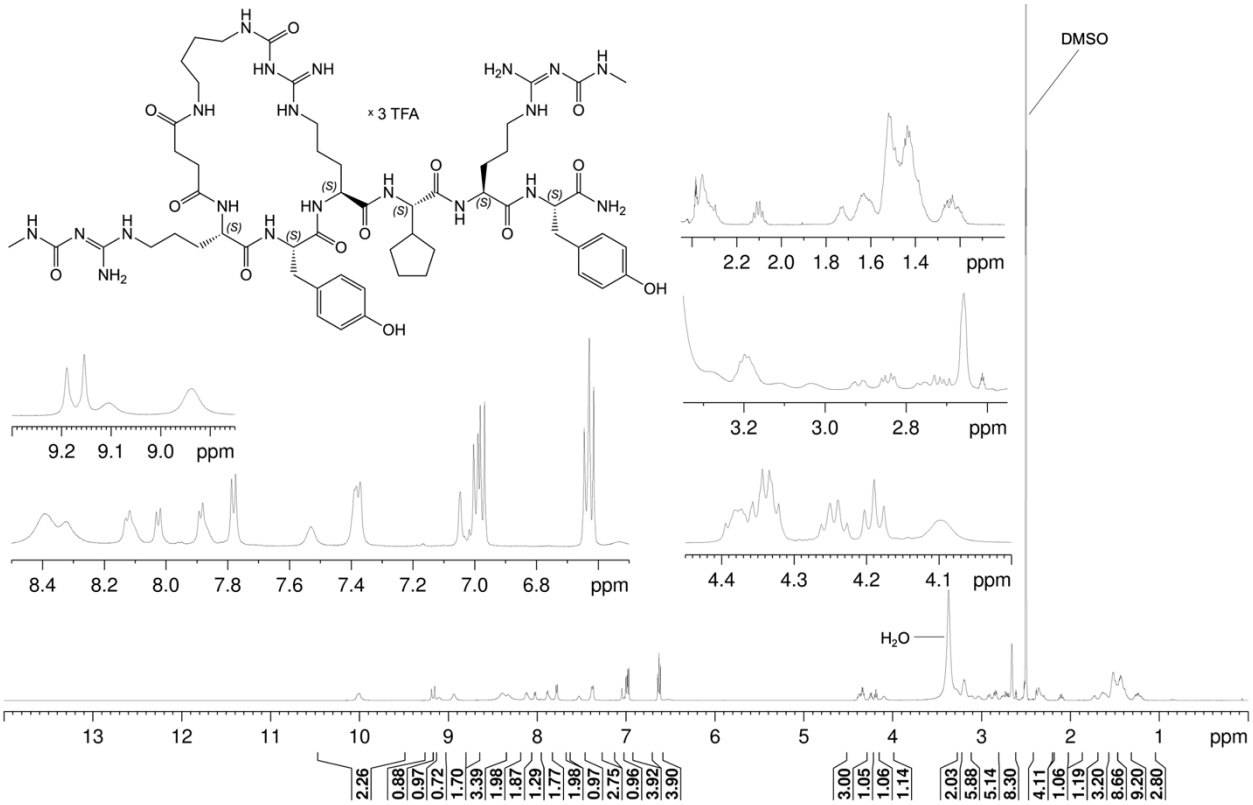

^{1}H-NMR spectrum (600 MHz, DMSO-d_6) of peptide **5.13b**.

Chapter 6

YR Binding Profiles of Endogenous Ligands

Note: In this chapter, the synthesis of the radioligand [K^5-[^{3}H]propionyl]His-PYY was performed by Franziska Schettler and Prof. Dr. Max Keller, and the determination of Y_2R binding in sodium-containing buffer was conducted by Franziska Schettler.

6.1 Introduction

The human neuropeptide Y (NPY) receptors (YRs) and their endogenous ligands are abundant in mammals' CNS and peripheral tissues. Their abundance in humans can be linked to their involvement in important physiological activities such as regulating anxiety, food intake, inflammation, cardiovascular activities, circadian rhythm, and gastrointestinal motility.[1-3] This class A family of G-protein coupled receptors, consisting of the Y_1R, Y_2R, Y_4R, and Y_5R subtypes in humans, forms a multi-receptor or multi-ligand system with the endogenous ligands NPY, peptide YY (PYY), and pancreatic polypeptide (PP) largely due to the sequence similarities between the ligands themselves and the YR subtypes (see Figure 1.1).[4] This situation complicates the design and development of ligands (particularly agonists) selectively targeting an individual YR subtype.

While the endogenous ligands NPY, PYY, and PP generally bind and activate the different YR subtypes, they usually exhibit varying receptor binding affinities. To date, iodinated, tritiated, or fluorescence labeled analogs of NPY, PYY, or PP and tritiated antagonists have been used to determine YR-ligand binding affinities. Noteworthy, various conditions (sodium-free buffers (mostly hypotonic) vs. isotonic sodium-containing buffers) have been used for YR binding assays. Radioligand binding studies at the Y_1R and Y_2R have been generally conducted using both sodium-free and sodium-containing buffers. By contrast, Y_4R binding assays, until recently, have been primarily performed in hypotonic sodium-free buffers. On the other hand, sodium-containing buffers have been almost exclusively used for Y_5R binding studies. A summary of the assay conditions and the most often used radioligands is provided in Table 6.1.

Using different buffers with varying sodium concentrations for the determination of YR-ligand binding affinities can lead to discrepancies in the determined binding data. Assay conditions using buffers containing sodium at physiological concentrations (130–175 mM) tend to produce lower binding affinities of agonists (compared to sodium-free conditions), including radiolabeled agonists, since sodium acts as a negative allosteric modulator for numerous class A GPCRs like YRs.[5-8] This effect is clearly observed in Y_4R binding, where the presence of sodium in binding assays, compared to sodium-free conditions, leads to a decrease in the agonist's binding affinity by a factor of more than 10.[7, 9, 10] This might be the reason why sodium-free

buffers have been used for radioligand binding studies at YRs; a higher radioligand affinity implies lower radioligand concentrations in the experiment, which in turn means lower consumption of radioligand and lower unspecific binding.

Table 6.1. Binding assay conditions (sodium-free vs. sodium-containing buffer) and radioligands commonly used for binding studies at YRs.

YR subtype	Species	Buffer used	Commonly used radioligands	References
Y_1R	human rat	both sodium-free and containing buffer	[^{125}I]PYY, [^{3}H]propionyl-NPY [^{125}I][Leu^{31},Pro^{34}]NPY	Gerald *et al.*[12], Söll *et al.*[13], Krause *et al.*[14], Loh *et al.*[15], Lundell *et al.*[16]
Y_2R	human rat	both sodium-free and sodium-containing	[^{125}I]PYY, [^{3}H]propionyl-NPY [^{125}I]NPY, [^{125}I]PYY_{3-36}	Gerald *et al.*[12], Krause *et al.*[14], Söll *et al.*[13], Rose *et al.*[17], Dumont *et. al.*[18]
Y_4R	human rat mouse	mostly sodium-free	[^{125}I]PP, [^{125}I]PYY	Walker *et al.*[19], Berglund *et al.*[20], Söll *et al.*[13], Balasubramaniam *et al.*[21], Yan *et al.*[22], Eriksson *et al.*[23]
Y_5R	human rat	mostly sodium-containing	[^{3}H]propionyl-NPY, [^{125}I]pPYY, [^{125}I][hPP_{1-17},Ala^{31},Aib^{32}]NPY, [^{125}I][cPP_{1-7},NPY_{19-23},Ala^{31}, Aib^{32},Gln^{34}]hPP	Söll *et al.*[13], Borowsky *et al.*[24], Dumont *et al*.[25], Dumont *et al*.[26]

As the use of sodium-free buffers does not mimic physiological-like conditions, receptor-ligand binding affinities should generally be determined in buffers containing sodium at physiological concentrations. For this reason, we recently introduced the tritium-labeled radioligands [^{3}H]**2.5** ([^{3}H]UR-JG102)[10] (see structure in Figure 2.2; *Chapter 2*) and [K^{4}-[^{3}H]propionyl]hPYY[11] (see structures Figure A4.1, *Section 4.6 Appendix; Chapter 4*), which represents useful probes for binding studies in sodium-containing buffers at the Y_4R and Y_2R, respectively.

In order to create a comprehensive overview of YR binding profiles of the endogenous agonists NPY, PYY, and PP, including the comparison of sodium-free buffers with sodium-containing buffers (which mimics physiological-like conditions), we determined the binding affinities of pNPY, hNPY, hPYY, and hPP for the different human YR subtypes in a sodium-free buffer and in a buffer with physiological levels of sodium (130–175 mM Na^{+}). Additionally, at least one standard antagonist was

included for each receptor subtype. All competition binding assays were performed with intact cells stably expressing human YRs using well-characterized tritiated radioligands (Y_1R, Y_2R, Y_4R) and one newly prepared tritium-labeled radioligand (Y_5R). As pNPY, containing, in contrast to hNPY, no oxidation-prone methionine, is more frequently used than hNPY for pharmacological investigations, it was also included in the study. Functional characterization of the endogenous peptides NPY, PYY, and PP was not included in the present study since it is well-known that these peptides act as full agonists and functional assays have generally been performed in sodium-containing buffers.

6.2 Materials and Methods

6.2.1 Materials

Acetonitrile (MeCN) (HPLC gradient grade) was from VWR (Ismaning, Germany). Leibovitz's L-15 (L-15) without phenol red was purchased from Thermo Fisher Scientific GmbH (Nidderau, Germany). The peptides hPP, pNPY, hNPY, hPYY, and His-hPYY were purchased from Synpeptide (Shanghai, China). Bacitracin and bovine serum albumin (BSA) were obtained from Serva (Heidelberg, Germany). Glycine, dimethyl sulfoxide (DMSO), penicillin, streptomycin, geneticin (G418), L-glutamine, forskolin, trypsin, and HAM´s F-12 medium were obtained from Sigma-Aldrich (Taufkirchen, Germany). Zeocin and hygromycin B were obtained from InvivoGen (Toulouse, France). The Y_2R antagonists BIIE0246 and JNJ31020028 were obtained from Boehringer Ingelheim (Ingelheim, Germany) and Cayman Chemical (Ann Arbor, USA), respectively. The Y_5R antagonist CGP71683A was obtained from BLD Pharmatech GmbH (Reinbek, Germany). Succinimidyl [^{3}H]propionate (molar activity: 3.44 TBq/mmol) was purchased from Novandi (Södertälje, Sweden). The syntheses of the Y_1R antagonist BIBP3226,[27] the Y_1R antagonist BIBO3304,[28] [^{3}H]**2.5** ([^{3}H]UR-JG102)[10] (molar activity: 3.44 TBq/mmol), [^{3}H]UR-MK299[11] (molar activity: 3.885 TBq/mmol), and [K^4-[^{3}H]propionyl]hPYY[11] (molar activity: 3.44 TBq/mmol) were described previously. Succinimidyl propionate[29] and the Y_4R antagonist UR-MK188,[30] were synthesized according to reported procedures. Ultrapure water was used to prepare stock solutions, buffers, and eluents for HPLC. Polypropylene reaction vessels (1.5 and 2 mL) from Sarstedt (Nümbrecht, Germany) (in the following referred to as "reaction vessel") were used to keep stock solutions. For the preparation of dilution series of the peptides, siliconized (Sigmacote, Sigma) polypropylene reaction vessels were used.

6.2.2 Methods

6.2.2.1 Mass spectrometry

High-resolution mass spectrometry (HRMS) was performed with an Agilent 6540 UHD accurate-mass Q-TOF LC/MS system coupled to an Agilent 1290 analytical HPLC system (Agilent Technologies, Santa Clara, CA) using an ESI source and the following LC method: column: Luna Omega C18, 1.6 µm, 50 × 2.1 mm (Phenomenex, Aschaffenburg, Germany), column temperature: 40 °C, solvent/linear gradient:

0−4 min: 0.1% aqueous HCOOH/MeCN supplemented with 0.1% HCOOH 95:5−2:98, 4−5 min: 2:98, flow: 0.6 mL/min.

6.2.2.2 Preparative HPLC

Preparative HPLC was performed with a system from Knauer (Berlin, Germany) consisting of two K-1800 pumps and a K-2001 detector. A Gemini NX-C18, 5 µm, 250 mm × 21 mm (Phenomenex) was used as reversed-phase (RP) column at a flow rate of 20 mL/min using mixtures of 0.1% aqueous TFA and MeCN as the mobile phase. A detection wavelength of 220 nm was used throughout. Collected fractions were lyophilized using a Scanvac CoolSafe 100-9 freeze dryer (Labogene, Allerød, Denmark) equipped with a RZ 6 rotary vane vacuum pump (Vacuubrand, Wertheim, Germany).

6.2.2.3 Analytical HPLC

Analytical HPLC analysis was performed with an 1100 series system from Agilent Technologies composed of a degasser (G1379A), a binary pump (G1312A), a variable wavelength detector (G1314A), a thermostatted column compartment (G1316A), and an autosampler (G1329A). Detection was performed at 220 nm, and the oven temperature was 30 °C.

For the analysis of reaction mixtures and purity controls, a Kinetex-XB C18 100A, 5 µm, 250 × 4.6 mm (Phenomenex) served as the stationary phase at a flow rate of 0.8 mL/min. Mixtures of 0.05% aqueous TFA (A) and MeCN (B) were used as the mobile phase. The following linear gradient was applied: 0–30 min: A/B 90:10-5:95, 30–40 min: 5:95 (isocratic). The injection volume was 80 µL. Retention (capacity) factors k were calculated from the retention times t_R according to $k = (t_R - t_0)/t_0$ (t_0 = dead time, 2.6 min for the system, column and flow rate mentioned above).

For the analysis of samples from stability studies with [K^5-propionyl]His-hPYY (**6.1**) in PBS, a Gemini-NX C18, 100A, 5 µm, 250 × 4.6 mm (Phenomenex) served as stationary phase at a flow rate of 0.8 mL/min. Mixtures of 0.25% aqueous TFA (C) and 0.175% TFA in MeCN (D) were used as mobile phases. The following linear gradient was applied: 0–25 min: C/D 90:10-5:95, 25-32 min: 5:95 (isocratic). The injection volume was 40 µL.

6.2.2.4 Synthesis protocols and analytical data

Synthesis of His-Tyr-Pro-Ile-Nε-propionyl-Lys-Pro-Glu-Ala-Pro-Gly-Glu-Asp-Ala-Ser-Pro-Glu-Glu-Leu-Asn-Arg-Tyr-Tyr-Ala-Ser-Leu-Arg-His-Tyr-Leu-Asn-Leu-Val-Thr-Arg-Gln-Arg-Tyr-amide ([K^5-propionyl]His-hPYY) heptakis(hydrotrifluoroacetate) (**6.1**)**.** The reaction was carried out in a 2 mL polypropylene reaction vessel. A solution of *N*-succinimidyl propionate (0.31 mg, 1.81 µmol) in anhydrous DMF (7.6 µL) was added in two portions (3.8 µL + 3.8 µL with a time lag of 2 min) to a stirred solution of His-hPYY (7.9 mg, 1.50 µmol) and DIPEA (3.6 µL, 21.1 µmol) in DMF/NMP/H_2O 6:2.5:1.5 (200 µL). The mixture was stirred at rt for 2 h. 10% aqueous TFA (17 µL) was added, followed by isolation of the product by preparative HPLC (gradient: 0–30 min: 0.1% aqueous TFA/MeCN 90:10-60:40, t_R = 23 min) yielding **6.1** as a white fluffy solid (1.3 mg, 17%) (note: the number of seven TFA^- counter ions corresponds to the number of seven basic groups in the peptide; the correlation of the number of basic groups with the number of TFA^- counter ions was recently verified for [K^4-propionyl]hPYY hexakis(hydrotrifluoroacetate) by ^{19}F-NMR spectroscopy[11]). HRMS (ESI): *m/z* $[M+4H]^{4+}$ calcd. for $[C_{203}H_{310}N_{58}O_{59}]^{4+}$ 1126.5771, found: 1126.5781. RP-HPLC (220 nm): 98% (t_R = 12.7 min, k = 3.9). $C_{203}H_{306}N_{58}O_{59} \cdot C_{14}H_7F_{21}O_{14}$ (4503.03 + 798.14).

[K^5-[^{3}H]propionyl]His-hPYY ([^{3}H]**6.1**)*.* The radioligand [K^5-[^{3}H]propionyl]His-hPYY ([^{3}H]**6.1**; see structure in Figure A6.1, *Section 6.6 Appendix*) was prepared following a reported procedure for synthesizing [^{3}H]propionylated neurotensin receptor ligands and was modified as required.[31] A solution of succinimidyl [^{3}H]propionate (molar activity: 3.44 TBq/mmol; Novandi, Södertälje, Sweden) (77.7 MBq, 1.05 mL, 22.6 nmol) in n-heptane/EtOAc 3:2 v/v was transferred from the delivered ampoule into a 1.5 mL polypropylene reaction vessel with screw cap, and the solvent was removed in a vacuum concentrator (rt, ca. 45 min). A solution of the precursor His-hPYY (0.29 mg, 56.8 nmol) and DIPEA (1.0 µL, 5.73 µmol) in DMF/NMP/H_2O 6:2.5:1.5 v/v (35 µL) was added, immediately followed by vortexing. Subsequently, the vessel was shaken at rt for 2.5 h. The mixture was acidified by the addition of 2% aqueous TFA (30 µL), followed by the addition of 0.05% aqueous TFA (200 µL) and MeCN/0.05% aqueous TFA 1:9 v/v (150 µL). The resulting solution was directly injected into the HPLC system (no filtration). [^{3}H]**6.1** was isolated using an HPLC system from Waters (Eschborn, Germany) consisting of two pumps 510, a pump

control module, a manual injector (loop size: 200 µL), a 486 UV/vis detector, and a Flow-one Beta series A-500 radiodetector (Packard, Meriden, USA) (the latter was disconnected during the purification process, i.e. fractions containing [^{3}H]**6.1** were collected based on UV detection). A Luna C18(2) column (3 µm, 150 mm × 4.6 mm, Phenomenex, Aschaffenburg, Germany) was used as a stationary phase at a flow rate of 0.8 mL/min. Mixtures of MeCN supplemented with 0.04% TFA (A) and 0.05% aqueous TFA (B) were used as mobile phase. The following linear gradient was applied: 0–20 min: A/B 20:80-34:66, 20–22 min: 34:66-95:5, 22–30 min: 95:5 (isocratic). Four runs were conducted (for a representative chromatogram, see Figure A6.4, *Section 6.6 Appendix*). All fractions containing [^{3}H]**6.1** (t_R = 20.2 min) were collected and combined in a 2 mL polypropylene reaction vessel with a screw cap. The volume of the combined eluates was reduced by evaporation in a vacuum concentrator to approximately 350 µL. EtOH (35 µL) and a mixture of EtOH/water 1:9 v/v (420 µL) were added, resulting in a mixing ratio of EtOH/aqueous solvent 1:9 v/v and a total volume of 800 µL (preliminary stock solution). To determine the radiochemical purity and to prove the identity of [^{3}H]**6.1**, 5 µL of the preliminary stock solution were added to 100 µL of a 20 µM solution of [K^5-propionyl]His-hPYY (**6.1**) in MeCN/0.05% aqueous TFA 1.5:8.5 v/v, affording the sample to be analyzed using the aforementioned HPLC system, column and solvents (injection volume: 100 µL). The following linear gradient was applied: 0–20 min: A/B 15:85-42:58, 20–30 min: 42:58-95:5, 30–38 min: 95:5 (isocratic). The radiochemical purity was > 99% (t_R = 17.2 min). To quantify the activity of [^{3}H]**6.1** and to determine the molar concentration, 2 × 2 µL of the preliminary stock solution were added to 998 µL of DMSO/H_2O 3:7 v/v and 4 × 10 µL of these dilutions were counted in 3 mL of liquid scintillator (Rotiscint Eco Plus, Carl Roth, Karlsruhe, Germany) with a Tri-Carb 3100TR liquid scintillation counter (PerkinElmer). The activity concentration was adjusted to 11.10 MBq/mL by adding EtOH/H_2O 1:9 v/v (56.2 µL), resulting in a final concentration of 3.23 µM and a total volume of 847.2 µL. Radiochemical yield: 9.40 MBq (0.25 mCi), 12.7%. Molar activity: As the supplier of the labeling reagent succinimidyl [^{3}H]propionate (Novandi, Södertälje, Sweden) provides a precisely determined molar activity and due to [^{3}H]**6.1** bears exactly one tritiated propionyl residue originating from the labeling reagent, the molar activities of [^{3}H]**6.1** was defined to be equal to the molar activity of the labeling reagent, amounting to 3.44 TBq/mmol (it is assumed that under the mild reaction conditions the carbon-tritium bonds remained intact). The molar activity of the labeling

reagent succinimidyl [^{3}H]propionate was determined by LC-MS analysis. Co-injection of “cold” succinimidyl propionate allowed the quantification of the incorporated tritium (Novandi, Södertälje, Sweden).

6.2.2.5 Cell Culture

Cells were cultured in T75 or T175 flasks (Sarstedt, Nümbrecht, Germany) in a humidified atmosphere (95% air, 5% CO_2) at 37 °C. SK-N-MC neuroblastoma cells (obtained from the American Type Culture Collection, ATCC HTB-10) were maintained in EMEM supplemented with 5% FBS. CHO-hY_2R cells (obtained from PerkinElmer, Rodgau, Germany) were cultured in Ham’s F-12 supplemented with 5% FBS and G418 (400 µg/mL). CHO-hY_4-Gq_{i5}-mtAEQ cells[32] were cultured in HAM’s F-12 supplemented with 10% FBS, hygromycin (400 µg/mL), zeocin (250 µg/mL), and G418 (400 µg/mL). HEC-1B-hY_5 cells[33] were maintained in EMEM supplemented with 5% FBS and G418 (400 µg/mL).

6.2.2.6 Buffers and media used for binding assays

Buffer Ia (used for binding experiments at the Y_4R, sodium-free conditions): a hypotonic sodium-free 4-(2-hydroxyethyl)-1-piperazineethanesulfonic acid (HEPES) buffer (25 mM HEPES, 2.5 mM $CaCl_2$, 1 mM $MgCl_2$, pH 7.4) supplemented with 1% BSA (Serva, Heidelberg, Germany) and 0.1 mg/mL bacitracin (Serva). *Buffer Ib* (used for binding experiments at the Y_1R, Y_2R, and Y_5R, sodium-free conditions): *buffer Ia* additionally supplemented with 0.3 M glycine (Sigma-Aldrich, Steinheim, Germany). *Buffer II* (used for binding experiments at the Y_1R, Y_2R, and Y_5R in the presence of sodium): an isotonic sodium-containing HEPES buffer (10 mM HEPES, 150 mM NaCl, 25 mM $NaHCO_3$, 2.5 mM $CaCl_2$, 5 mM KCl, pH 7.4) supplemented with 1% BSA. *DPBS* (used for binding studies at the Y_4R in the presence of sodium): Dulbecco’s phosphate-buffered saline with calcium and magnesium (1.8 mM $CaCl_2$, 2.68 mM KCl, 1.47 mM KH_2PO_4, 3.98 mM $MgSO_4$, 137 mM NaCl, 8.06 mM Na_2HPO_4, pH 7.4) supplemented with 1% BSA and 0.1 mg/mL bacitracin. *L-15* (used for the impedance assay): Leibovitz’s L-15 medium without phenol-red (140 mM NaCl, 1.3 mM $CaCl_2$, 1 mM $MgCl_2$, various amino acids and vitamins, pH 7.4, Thermo Fischer Scientific, Nidderau, Germany).

6.2.2.7 Radioligand binding assays

All radioligand binding assays were performed with whole Y receptor-expressing cells at 23 ± 2 °C. The radioligands used for Y_1, Y_2, and Y_4 receptor binding assays were previously characterized (for K_d values, see Table A6.1, *Section 6.6 Appendix*), except for Y_1R binding of the tritiated Y_1R ligand [^{3}H]UR-MK299 (see structure in Figure A4.1, *Section 4.6 Appendix*; *Chapter 4*) in sodium-free buffer. For Y_5R binding studies, a new radioligand ([^{3}H]**6.1**), which was characterized by saturation binding prior to the competition binding assays, was used. All experiments were performed in triplicate.

For all binding experiments, the same filtration procedure for separating free radioligand from cell-bound radioligand and for measuring the activity of the latter was used: after completed incubation, cells were collected on GF/C filter mats (0.26 mm; Whatman, Maidstone, UK) (pretreated with 0.3% polyethylenimine for 30 min) using an in-house manufactured harvester for 96-well plates (precision mechanic workshop of the University of Regensburg, Regensburg, Germany), and the wells of the plate and the cells on the filter mat were immediately washed twice with ice-cold PBS (200 µL). Filter pieces for each well were punched out and transferred into flexible 96-well sample plates (Part no. 1450-401; PerkinElmer, Rodgau, Germany) followed by the addition of Rotiscint Routine (Carl Roth, Karlsruhe, Germany) (200 µL). The plates were sealed with a transparent sealing tape (Greiner Bio-One EASYseal, part no. 676001; Greiner Bio-One, Frickenhausen, Germany) and shaken in the dark for at least three hours before measurement. Radioactivity (dpm) was measured with a MicroBeta2 plate counter equipped with six pairs of photomultiplier tubes (PerkinElmer, Rodgau, Germany).

Y_1R binding. Competition binding assays at Y_1R-expressing SK-N-MC neuroblastoma cells in sodium-containing *buffer II*, using [^{3}H]UR-MK299 as radioligand, were performed as previously described with the minor modification of using a radioligand concentration of 0.075 nM instead of 0.15 nM.[29] Y_1R binding assays with [^{3}H]UR-MK299 in sodium-free *buffer Ib* were performed with suspended SK-N-MC cells. Cell suspensions were prepared as follows: cells were grown in T175 flasks to reach a confluency of 80-90% on the day of the experiment. The culture medium was removed, and the adherent cells were washed twice with *buffer Ib* (in this case, the buffer was not supplemented with BSA and bacitracin). Subsequently, the cells were covered with BSA- and bacitracin-free *buffer Ib* and scraped off the flask, followed by centrifugation

at 300 g at rt for 5 min. The supernatant was discarded, and the cells were resuspended in *buffer Ib* at a density of 200,000-500,000 cells/mL. To determine the K_d value of [^{3}H]UR-MK299 for these conditions, saturation binding experiments were performed prior to competition binding assays.

Saturation binding with [^{3}H]UR-MK299 in buffer Ib. The wells of a flexible 96-well sample plate (Part no. 1450-401; PerkinElmer) were prefilled with freshly prepared cell suspension (160 µL) followed by the addition of 20 µL of *buffer Ib* (determination of total binding) or 20 µL of a 10-fold concentrated solution (compared to the final concentration) of BIBO3304 in *buffer Ib* (determination of unspecific binding; the final concentration of BIBO3304 was 1000-fold higher than the radioligand concentration), and the addition of 20 µL of a 10-fold concentrated (compared to the final concentration) solution of [^{3}H]UR-MK299 in *buffer Ib*. Samples were incubated under shaking for 2 h followed by cell harvesting and further processing as described afore. Specific binding data, obtained by subtracting triplicate radioactivity (dpm) mean values of unspecific binding from triplicate radioactivity (dpm) mean values of total binding, were plotted against the free radioligand concentration and analyzed by a two-parameter equation describing hyperbolic single site binding (one-site, specific binding, GraphPad Prism 5) to obtain K_d values (*cf*. Table A6.1, *Section 6.6 Appendix*). The free concentration of [^{3}H]UR-MK299 (nM) was calculated by subtracting the amount of specifically bound [^{3}H]UR-MK299 (nM) (calculated from specifically bound radioligand in dpm, the molar activity, and the volume per well) from the total concentration of [^{3}H]UR-MK299.

Competition binding assay with [^{3}H]UR-MK299 in buffer Ib. The wells of a flexible 96-well sample plates (Part no. 1450-401; PerkinElmer) were prefilled with freshly prepared cell suspension (160 µL). 20 µL of a 10-fold concentrated (relative to the final concentration) solution of the compound of interest in *buffer Ib*, and 20 µL of a 5 nM solution of [^{3}H]UR-MK299 in *buffer Ib* were added (final radioligand concentration: 0.5 nM). To determine total binding in the absence of a competitor, 20 µL of *buffer Ib* were added, followed by the addition of 20 µL of the aforementioned radioligand solution. To determine unspecific binding, 20 µL of a 5 µM solution of BIBO3304 in *buffer Ib* (final concentration: 0.5 µM) and 20 µL of the aforementioned radioligand solution were added. Samples were incubated under shaking for 2 h followed by cell harvesting and further processing as described afore.

Total binding data from competition binding experiments (dpm, including total binding in the absence of competitor) were plotted against log(concentration competitor) and analyzed by a four-parameter logistic equation (log(inhibitor) vs. response-variable slope, GraphPad Prism 5, GraphPad Software, San Diego, CA, USA) followed by normalization (100% = 'top' of the four-parameter logistic fit, 0% = unspecifically bound radioligand) and analysis of the normalized data by a four-parameter logistic equation. Individual IC_{50} values were converted to K_i values according to the Cheng-Prusoff equation[34] followed by the conversion of individual K_i values to pK_i values and calculation of mean pK_i values.

Y_2R binding. Competition binding experiments in sodium-containing *buffer II* were performed as reported using suspended CHO-hY_2R cells and the radioligand [K^4-[^{3}H]propionyl]hPYY (K_d = 0.16 nM, c = 0.4 nM).[11] Unspecific binding was determined in the presence of BIIE0246 and JNJ31020028 (at a concentration of 800 nM each). Data were processed as described under *Y_1R binding*. Competition binding experiments in sodium-free *buffer Ib* were performed at suspended CHO-hY_2R cells with the radioligand [K^4-[^{3}H]propionyl]hPYY (K_d = 0.078 nM c = 0.12 nM) according to a reported procedure, but the *buffer Ib* was used instead of *buffer Ia*.[11] Unspecific binding was determined in the presence of BIIE0246 and JNJ31020028 (240 nM each). Prior to the competition binding studies, the K_d value of [K^4-[^{3}H]propionyl]hPYY was determined by saturation binding at CHO-hY_2R cells in *buffer Ib* following the reported procedure for saturation binding experiments with [K^4-[^{3}H]propionyl]hPYY[11] with the following modifications: *buffer Ib* was used instead of *buffer Ia* and unspecific binding was determined in the presence of BIIE0246 and JNJ31020028 each at a concentration of 800 nM. Data were processed as described under *Y_1R binding* yielding an average K_d of 0.078 nM (*cf*. Table A6.1, *Section 6.6 Appendix*).

Y_4R binding. Competition binding experiments were performed in *buffer Ia* and *DPBS* as reported using CHO-hY_4-G_{qi5}-mtAEQ cells[32] and the radioligand [^{3}H]**2.5** (*buffer Ia*: K_d = 0.012 nM, concentration: 0.030 nM; *buffer II*: K_d = 0.11 nM, concentration: 0.25 nM).[10] Data were processed as described under *Y_1R binding*.

Y_5R binding. Binding studies at Y_5R were performed with adherent HEC-1B-hY_5R cells.[33] Competition bind experiments in sodium-containing *buffer II* were performed in white 96-well plates with transparent flat bottom (Catalog no. 732-3740, VWR, Ismaning, Germany) as previously described, but [K^4-[^{3}H]propionyl]hPYY was used as

radioligand instead of [K^4-[^{3}H]propionyl]pNPY and Ultima Gold™ (PerkinElmer) was used as scintillator instead of Optiphase Supermix (PerkinElmer).[35] Prior to the conduction of competition binding experiments, the K_d value of [K^4-[^{3}H]propionyl]hPYY was determined by saturation binding under the same assay conditions (unspecific binding was determined in the presence of 4 µM CGP71683A, the incubation time was 2 h). Data were processed as described above for saturation binding experiments with [^{3}H]UR-MK299 at SK-N-MC cells in *buffer Ib*. The obtained K_d value amounted to 9.5 ± 1.5 nM (mean value ± SEM from 4 independent determinations performed in triplicate; for a representative saturation binding curve, see Figure A6.6; *Section 6.6 Appendix*).

For competition binding experiments, a final concentration of 10 nM of [K^4-[^{3}H]propionyl]hPYY was used. Unspecific binding was determined in the presence of 2 µM CGP71683A. Data were processed as described under *Y_1R binding*.

For Y_5R binding studies in sodium-free *buffer Ib*, the radioligand [^{3}H]**6.1** was used because it showed more favorable binding characteristics (lower K_d value and higher reproducibility) in this buffer than [K^4-[^{3}H]propionyl]hPYY. The binding experiments in *buffer Ib* were performed in transparent 24-well plates (Catalog no. 662160, Greiner Bio-One GmbH, Frickenhausen, Germany) because this resulted in a markedly higher ratio of total over unspecific binding compared to experiments performed in white 96-well plates with transparent bottom (data of the latter are not shown). Cells were seeded in the plates one day prior to the experiment. On the day of the experiment, with cells at a confluence of 80-100%, the culture medium was aspirated, and the cells were washed with PBS (500 µL), followed by pre-filling the wells with 160 µL of *buffer Ib*. For saturation binding experiments, 20 µL of *buffer Ib* (determination of total binding) or 20 µL of an 80 µM solution of CGP71683A (final concentration: 8 µM) in *buffer Ib* (determination of unspecific binding), and 20 µL of a 10-fold concentrated (compared to the final concentration) solution of [^{3}H]**6.1** in *buffer Ib* were added. In the case of competition binding experiments, 20 µL of a 10-fold concentrated (compared to the final concentration) solution of the compound of interest in *buffer Ib*, and 20 µL of a 150 nM solution of [^{3}H]**6.1** in *buffer Ib* (final concentration: 15 nM) were added. To determine total binding in the absence of a competitor, 20 µL of *buffer Ib* were added followed by the addition of 20 µL of the aforementioned radioligand solution. To determine unspecific binding, 20 µL of a 30 µM solution of CGP71683A in *buffer Ib*

(final concentration: 3 µM) and 20 µL of the aforementioned radioligand solution were added.

Samples were incubated under shaking for 2 h. The binding buffer was aspirated, the cells were washed twice with ice-cold PBS (2 × 200 µL), and lysis solution (urea (8 M), acetic acid (3 M) and Triton-X-100 (1%) in water) (200 µL) was added. The plates were shaken at rt for 30 min and the lysis solutions were transferred into 6 mL scintillation vials filled with 3 mL of liquid scintillator (Rotiszint Routine; Carl Roth, Karlsruhe, Germany). Radioactivity (dpm) was measured with a Beckman LS6500 liquid scintillation counter. Data from saturation and competition binding experiments were processed as described under *Y_1R binding*.

6.2.2.8 Impedance assay

To perform impedance measurements, 96-well electrode arrays with circular gold-film electrodes (SP-96 CardioExcyte Sensor Plates, electrode diameter 0.6 mm, growth area: 34 mm^2) were first sterilized in argon plasma (Argon Plasma Cleaner PDC 002, Harrick Plasma, Ithaca, US) for 30 seconds and subsequently pre-incubated with 50 µL HAM´s F-12 medium for 2 h. The medium from a T75 flask with CHO-hY_4-G_{qi5}-mtAEQ cells[32] of confluency 80-90% was aspirated, and a cell suspension in HAM´s F-12 of density 340,000 cells/mL was prepared. 100 µL of the cell suspension were added to each well, approximately resulting in a cell density of 100,000 cells per cm^2). The cells were allowed to sediment for 15 minutes, after which the plates were placed in the incubator for 48 h, with a medium exchange after 24 h.

On the day of the experiment, the culture medium was aspirated, and the cells were washed with *L-15*. Each well was filled with 50 µL of *L-15* to record a stable impedance baseline at 12 kHz. The impedance was measured inside the CardioExcyte 96 tabletop incubator/measurement chamber (Nanion Technologies Inc., Munich, Germany), designed for 96-well electrode arrays. It was coupled to a heating and ventilation system as well as a gas mixer (ibidi GmbH, Gräfelfing, Germany) to maintain 37 °C, 0% CO_2, and 80% humidity.

Cells were then pre-stimulated with forskolin (50 µL/well, dissolved in *L-15*) at a final concentration of 0.4 µM. The test ligands (hPP and UR-MK188) were diluted to obtain two times the final concentrations in *L-15*, which contained 0.4 µM forskolin. 100 µL of this solution were added to each well after the forskolin pre-stimulation signal was

stable. For the assay controls, 0.2 µM of hPP (yielding a final concentration of 0.1 µM) and a solution of 0.01% (v/v) DMSO were added as positive and vehicle control, respectively. All experiments were conducted in *L-15* medium and in triplicate. Data were collected using the software SpectraControl (Nanion Technologies Inc., Munich, Germany), which also allowed setting the measurement frequency of the AC to 12 kHz with a non-invasive driving voltage of 40 mV. The data acquired was first baseline corrected by subtracting the baseline measurements from the agonist stimulation measurement. The area under the curves (AUC) of observation time between 1200–2400 s of the baseline-corrected data were then calculated using GraphPad Prism 10. The resulting AUCs were normalized (100% = AUC obtained from 100 nM hPP, 0% = AUC obtained by vehicle addition (basal effect), GraphPad Prism 10). The normalized responses were then plotted against log (concentration of agonist), and the data were fitted using a four-parameter logistic equation (log(agonist) vs response – variable slope, GraphPad Prism 10) to obtain pEC_{50} values, which were converted to EC_{50} values.

6.2.2.9 Statistical Significance

For the applied statistical tests (Welch t-test, GraphPad Prism 10), the significance level was set to $P \leq 0.05$.

6.2.2.10 Calculation of propagated errors

Propagated errors (applying to specifically bound radioligand calculated from saturation binding data) were calculated as described elsewhere.[10]

6.3 Results and Discussion

For the purpose of this study, tritium-labeled radioligands were used to determine the binding affinities of the various endogenous agonists as well as reported antagonists to the human YR subtypes Y_1R, Y_2R, Y_4R, and Y_5R. Typically, iodinated (I-125) peptidic radioligands are used for YR binding studies. However, as iodinated derivatives of NPY, PYY or PP, unlike tritium-labeled analogs, have several disadvantages, such as the different radiolabeled species obtained by iodination,[36] adverse effect on the physicochemical properties of the ligand,[37] and their lower stability,[38] the recently reported tritium-labeled high-affinity radioligands [^{3}H]UR-MK299[29] (Y_1R), [K^4-[^{3}H]propionyl]hPYY[11] (Y_2R), and [^{3}H]**2.5** (Y_4R) were used in the present study. The radioligands [K^4-[^{3}H]propionyl]hPYY and [^{3}H]**2.5** were developed with the purpose of establishing Y_2R and Y_4R binding assays, respectively, using a sodium-containing buffer and a tritium-labeled radioligand.[10, 11] Since a tritium-labeled radioligand with high affinity (K_d < 10 nM) is still lacking for the Y_5 subtype, a newly synthesized tritiated hPYY derivative, [K^5-[^{3}H]propionyl]His-hPYY ([^{3}H]**6.1**), was used to determine Y_5R binding in sodium-free buffer while [K^4-[^{3}H]propionyl]hPYY was used for Y_5R binding studies in sodium-containing buffer.

All binding assays were performed using whole cells to better mimic physiological conditions as compared to the use of cell membranes or homogenates. For Y_1R binding studies, human SK-N-MC neuroblastoma cells, a canonical cell line endogenously expressing moderate levels of Y_1R,[39] were used. In the case of Y_2R, Y_4R, and Y_5R, stably transfected cell lines expressing human variants of these receptors were used (CHO-hY_2R cells (PerkinElmer), CHO-hY_4-G_{qi5}-mtAEQ cells[32], and HEC-1B-hY_5R cells[33]). The competition binding curves originating from the binding studies at the four YR subtypes are presented in Figure 6.1.

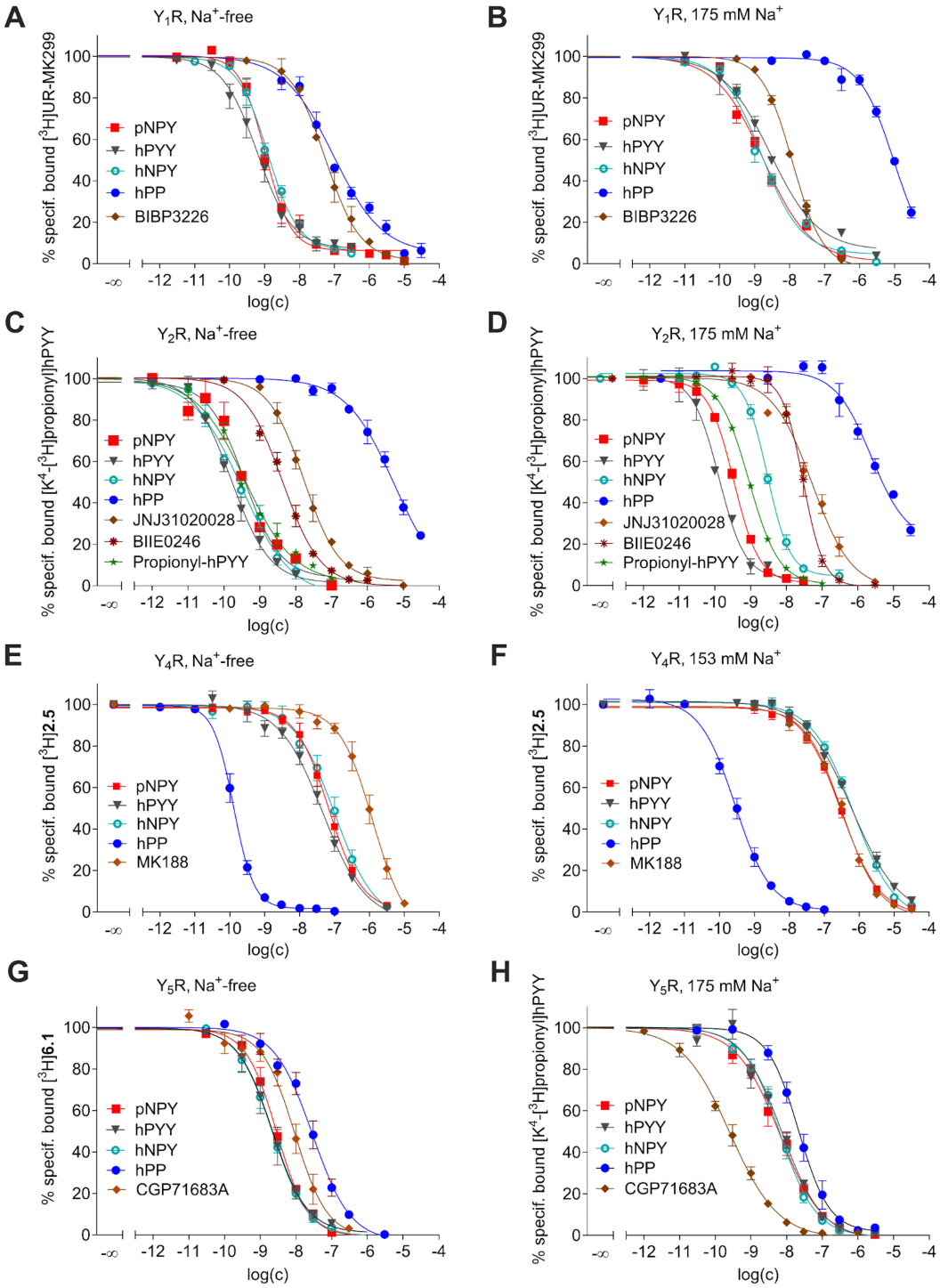

Figure 6.1. Radioligand displacement curves obtained from competition binding experiments at the different YR subtypes performed in sodium-free (*buffer Ia* or *buffer Ib*) and sodium-containing buffer (*II* or *DPBS*). Used cells, radioligands and buffers: (A) SK-N-MC cells, [^{3}H]UR-MK299 (*buffer Ib*, K_d = 0.41 nM, c = 0.5 nM; *buffer II*, K_d = 0.058 nM, c = 0.075 nM). (B) CHO-hY$_2$R cells, [K^4-[^{3}H]propionyl]hPYY (*buffer Ib*, K_d = 0.078 nM, c = 0.12 nM; *buffer II*, K_d = 0.16 nM, c = 0.4 nM). (C) CHO-hY$_4$-G$_{qi5}$-mtAEQ cells, [^{3}H]**2.5** ([^{3}H]UR-JG102) (*buffer Ia*, K_d = 0.012 nM, c = 0.03 nM; *DPBS*, K_d = 0.11 nM, c = 0.25 nM). (D) HEC-1B-hY$_5$R cells, [K^5-[^{3}H]propionyl]His-hPYY ([^{3}H]**6.1**) (*buffer Ib*, K_d = 20 nM, c = 15 nM), [K^4-[^{3}H]propionyl]hPYY (*buffer II*, K_d = 9.5 nM, c = 10 nM). Data represent mean values ± SEM of at least three independent experiments performed in triplicate.

Table 6.2. YR binding affinities of the endogenous agonists pNPY, hNPY, hPYY, and hPP determined in sodium-containing and sodium-free buffer.

Compd.		pK_i ± SEM or *pIC_{50}*							
		hY_1R		hY_2R		hY_4R		hY_5R	
		with Na^+	Na^+-free	with Na^+	Na^+-free	with Na^+	Na^+-free	with Na^+	Na^+-free
pNPY	determined	##9.12±0.07	9.29±0.12	##10.01±0.04	9.90±0.09	##7.02±0.07**	7.72±0.10**	##8.55±0.11	8.80±0.06
	literature	#10.18[12] ##10.92[13] ##*8.59*[40](r)	10.07[41] 9.22[42]	##9.92[13] #9.07[12] ##*10.40*[43] ##*9.40*[40](r)	9.68-39[44] 9.10[45] 9.40[46]	##*6.42*[40](r) ##8.22[23]	9.70[13] 6.55[45]	##8.79[13](r) #8.85[24] ##7.96[9] ##*8.40*[40](r)	7.82[9] 8.82[42]
hNPY	determined	##9.16±0.08	9.26±0.06	##9.11±0.08*	9.89±0.13*	##6.66±0.07**	7.56±0.12**	##8.52±0.10*	8.92±0.08*
	literature	#10.06[12, 47]	9.30[21] 9.74[41] *9.40*[48] 9.74-39	#9.27[12]	9.60 9.70[21]	#8.68[47]	8.01[16] 7.92[44]	#*8.53*[49]	8.66[21](rh)
hPYY	determined	##8.91±0.08	9.56±0.13	##10.40±0.04	10.16±0.13	##6.69±0.07***	7.89±0.04***	##8.43±0.06	8.94±0.17
	literature	#9.77[12, 47] ##*8.72*[40](r)	9.85[41]	#9.47[12] ##*10.0*[40](r)	9.85[41] ##*7.51*[40](r)	#9.06[47]	8.84[16] 9.03[50] 9.51[44]	#9.0[24]	##*8.52*[40](r)
hPP	determined	##5.42±0.03**	7.43±0.08**	##6.19±0.07	5.83±0.12	##10.06±0.11	10.44±0.07	##7.96±0.12	7.79±0.12
	literature	#7.10[12, 47] ##6.36[35] ##< 5.5[9] ##*6.44*[40](r)	7.72[41] 9.30[21] 6.36[45]	#< 6.0[12] ##*<6.0*[40](r)	6.0[41] < 5.5[45] < 5.5[35] <5.5[9]	#10.29[50] #10.25[47] ##8.85[9] ##10.41[23]	10.86[16] 10.10[21] 9.35[9]	##7.96[51] #8.85[24] ##7.77[35] ##*8.68*[40](r)	7.77[45] 7.70[9]

#10-30 mM of Na^+ is contained in the binding buffer. ##100–175 mM of Na^+ is contained in the binding buffer. r-pK_i values were obtained at rat YR, rh-pK_i values were obtained at rat-human chimeric YR. Mean values ± SEM (pK_i) were obtained from at least three independent experiments performed in triplicate. Data reported as IC_{50} or K_i were converted to pIC_{50} or pK_i. *, **, ***Mean pK_i values (Na^+-free buffer compared to Na^+-containing buffer) are significantly different with *P < 0.05, **P < 0.005 or ***P < 0.0005 (Welch t-test). n.a.: not available.

Table 6.3. YR binding affinities of the antagonists BIBP3226 (Y_1R), JNJ31020028 (Y_2R), BIIE0246 (Y_2R), UR-MK188 (Y_4R) and CGP71683A (Y_5R) determined in sodium-containing and sodium-free buffer.

Compd.		pK_i ± SEM or *pIC_{50}*							
		hY_1R		hY_2R		hY_4R		hY_5R	
		with Na^+	Na^+-free	with Na^+	Na^+-free	with Na^+	Na^+-free	with Na^+	Na^+-free
BIBP3226	determined	##8.28±0.03	7.56±0.15	-	-	-	-	-	-
	literature	##8.82[28, 52] ##8.89[28] ##*8.19*[53] ##*7.97*[53]	8.92[54]	-	-	-	-	-	-
JNJ31020028	determined	-	-	##7.87±0.09	8.17±0.14	-	-	-	-
	literature	-	-	##*8.07*[55]	n.a.		-	-	-
BIIE0246	determined	-	-	8.07±0.09*	8.76±0.08*	-	-	-	-
	literature	-	-	##*8.48*[43] ##*7.92*[55]	7.77[56]	-	-	-	-
UR-MK188	determined	-	-	-	-	##7.00±0.06*	6.47±0.13*	-	-
	literature	-	-	-	-	##6.62[9]	6.53[9]	-	-
CGP71683A	determined	-	-	-	-	-	-	##9.89±0.08**	8.31±0.14**
	literature	-	-	-	-	-	-	##9.52[26](r) ##8.80[9]	8.72[9]

#10-30mM of Na^+ is contained in the binding buffer ##100–175 mM of Na^+ is contained in the binding buffer. r-indicates pK_i values were obtained at rat Y receptor, Mean values ± SEM (pK_i) were obtained from at least three independent experiments performed in triplicate. Data reported as IC_{50} or pK_i values were converted to pIC_{50} or pK_i. *, **Mean pK_i values (Na^+-free buffer compared to Na^+-containing buffer) are significantly different with *P < 0.05, **P < 0.005 or (Welch t-test). n.a.: not available.

6.3.1 Y_1R Binding

Binding studies at Y_1R in sodium-containing buffer (*buffer II*) were performed with [^{3}H]UR-MK299 according to the reported procedure.[29] For the sodium-free conditions, [^{3}H]UR-MK299 was first characterized in *buffer Ib* by saturation binding, yielding a K_d of 0.41 nM (Figure A6.6A, Table A6.1; *Section 6.6 Appendix*) before it was used in competition binding experiments.

Y_1R binding of NPY, hNPY, and pNPY showed similar affinities in both types of buffer (Table 6.2, Figure 6.1A-B). Likewise, when comparing the sodium-free and sodium-containing conditions, binding of both hNPY and pNPY to Y_1R was not significantly different ($P > 0.05$). In contrast, hPYY showed a slightly higher affinity in sodium-free buffer compared to sodium-containing buffer (ca. 0.6 log units, $P < 0.05$). In the case of hPP, the difference in the binding affinity was even more pronounced (ca. 2 log units, Table 6.2) ($P < 0.005$). When comparing the determined binding data of the endogenous ligands with reported Y_1R binding affinities, the discrepancies were generally more pronounced for the sodium-containing buffers compared to the sodium-free conditions. The Y_1R antagonist BIBP3226 exhibited a lower Y_1R binding affinity (ca. 0.7 log units, $P < 0.05$) in *buffer Ib* (Na^+ free) than in *buffer II* (175 mM Na^+), suggesting that the antagonist under study may prefer the inactive Y_1R conformation, which is stabilized in the presence of sodium.[5, 8] Nonetheless, the pK_i of 8.82 obtained for BIBP3226 in *buffer II* was in agreement with reported binding data (difference ≤ 0.6 log unit, Table 3). For the sodium-free conditions, there is only one reported pK_i for BIBP3226, which is more than 1 log unit higher than the one determined in this study.

6.3.2 Y_2R Binding

Binding studies at Y_2R in sodium-containing *buffer II* were conducted with [K^4-[^{3}H]propionyl]hPYY according to the reported procedure.[11] For the determinations under sodium-free conditions, the reported procedure was slightly modified by supplementing the *buffer Ia* with 0.3 M glycine (*buffer Ib*) to obtain an isosmotic solution.[9] Therefore, [K^4-[^{3}H]propionyl]hPYY was characterized in *buffer Ib* by saturation binding, yielding a K_d of 0.078 nM (Figure A6.6B, Table A6.1; *Section 6.6 Appendix*) before it was used in competition binding experiments. The K_d value of 0.078 nM was similar to the reported K_d of 0.067 nM determined in the hypotonic sodium- and glycine-free buffer.[11]

With the exception of hNPY, all peptides under study showed similar Y_2R binding affinities in *buffer II* and *buffer Ib* ($P > 0.05$) (Table 6.2, Figure 6.1C-D). In the case of hNPY, the pK_i value determined in *buffer Ib* was about 0.8 log units higher than the pK_i resulting from the binding studies performed in *buffer II*. All the determined pK_i values, except for that of hPYY determined in sodium-containing buffer, were in accordance with those reported in literature. For hPYY, a difference of ca. 1 log unit was observed (Table 6.2), which could be attributed to the assay conditions used, specifically the concentration of sodium used in the assay buffer (20 mM vs 175 mM).

With respect to the binding of the Y_2R antagonists (structures shown in Figure A6.2, *Section 6.6 Appendix*), JNJ31020028 showed similar binding affinities in the used buffers. In the case of BIIE0246, the observed difference in the pK_i values of 0.7 log units (pK_i *buffer II* = 8.07, pK_i *buffer Ib* = 8.76, $P < 0.05$) indicates that this antagonist may prefer the active receptor conformation, contrary to what was proposed for the Y_1R antagonist BIBP3226 (Table 3). Generally, the pK_i values of JNJ31020028 and BIIE0246 obtained under sodium conditions were in line with reported data. Concerning the sodium-free conditions, the reported pK_i of BIIE0246 is approximately one order of magnitude lower than the pK_i determined in this study, whereas in the case of JNJ31020028, there are no reported Y_2R binding data determined in sodium-free buffer. To note, the discrepancy between the reported pK_i of BIIE0246 (Na^+-free buffer) and the determined pK_i could be explained by the unfavorable binding characteristics of the radioligand used by Pluym *et al*.[56], which shows a high K_d of 67 nM and incomplete dissociation.

6.3.3 Y_4R Binding

Binding studies at Y_4R were performed with [^{3}H]**2.5** using reported procedures for the sodium-free and sodium-containing buffer (*buffer Ia* and *DPBS,* respectively).[10] The peptides pNPY, hNPY, and hPYY showed similar Y_4R binding affinities in sodium-containing buffer (pK_i = 6.66–7.02), as well as in sodium-free buffer (pK_i = 7.5–7.89) (Table 6.2, Figure 6.1E–F). The differences in Y_4R binding between the two buffers were significant for each of these peptides (pK_i *DPBS* < pK_i *buffer Ia*; $P < 0.01$, < 0.01 and < 0.005, respectively). Additionally, the pK_i values of pNPY, hNPY, and hPYY determined in sodium-containing buffer in the present study were markedly lower than reported pK_i values (up to 2 log units, Table 6.2). For sodium-free conditions, the determined pK_i of pNPY falls within the range of the reported data, whereas for hNPY

and hPYY, the determined pK_i was 0.5–1 log units lower compared to reported data (Table 6.2).

Regarding the Y_4R binding affinities of hPP, the determined pK_i values were in accordance with reported binding data for both sodium-free and sodium-containing buffers. The increase in Y_4R binding of hPP in the absence of sodium was less pronounced (no significant difference in the pK_i values determined in *buffer Ia* and *DPBS*) compared to pNPY, hNPY, and hPYY. Similar to the latter, recently reported small oligopeptides acting as Y_4R agonists also showed a pronounced increase in Y_4R binding affinity in the absence of sodium (up to 25-fold).[10]

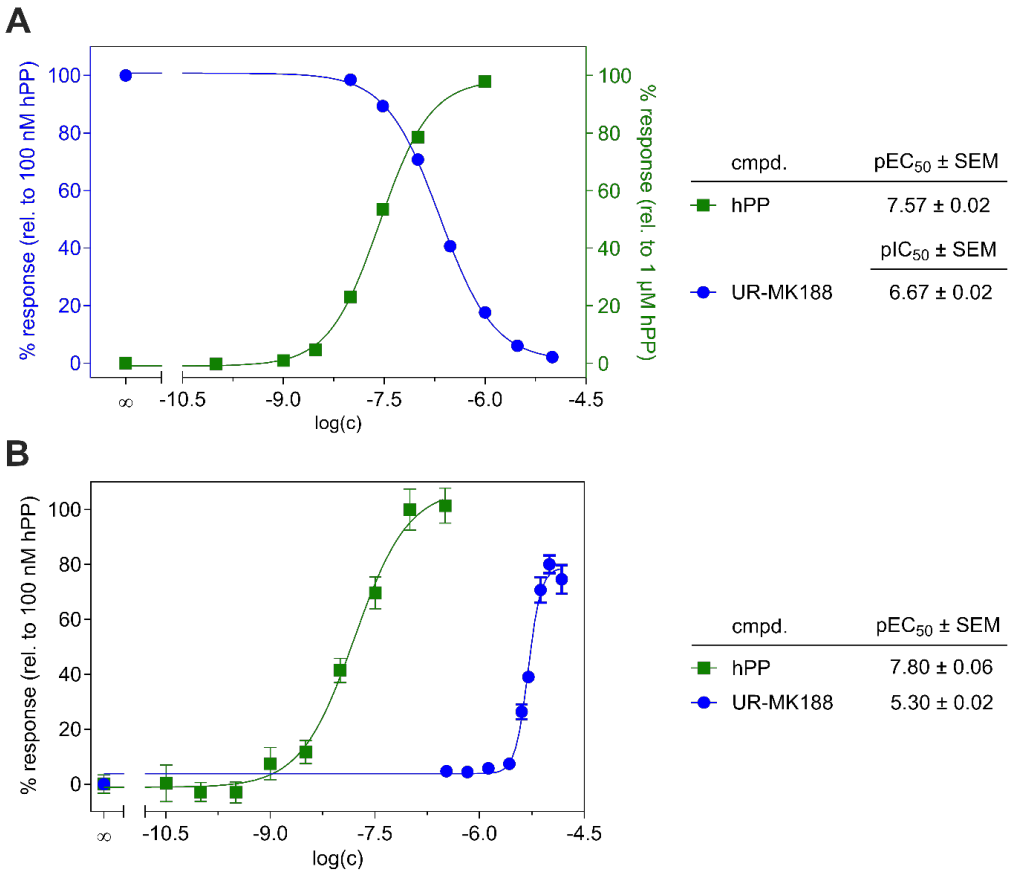

Figure 6.2. hPP and UR-MK188 studied in different functional Y_4R assays performed with CHO-hY_4-G_{qi5}-mtAEQ. (A) Ca^{2+} Aequorin assay measuring proximal cellular response. UR-MK188 acts as an antagonist capable of inhibiting the Y_4R-mediated Ca^{2+} response elicited by hPP. (B) Impedance-based assay measuring a distal cellular response associated with morphological changes of the cells. hPP and UR-MK188 act as agonists. Presented are mean values ± SEM from three independent experiments (performed in triplicate). In (A), data of hPP and UR-MK188 were taken from Konieczny *et al.*[65] and Keller *et al.*[30] In (B), data of hPP were taken from Wirth *et al.*[64]

Interestingly, hPP showed a considerably higher Y_4R binding affinity (ca. 3 log units, *cf.* Table 6.2) compared to pNPY, hNPY, and hPYY. This confirms that PP is the primary endogenous activator of Y_4R.[57, 58] On the other hand, the markedly lower Y_4R

binding affinities of NPY and PYY ($pK_i < 7$) compared to PP ($pK_i = 10.06$) questions the suggested physiological relevance of NPY and PYY (besides PP) for Y_4R activation59-61 as peptide concentrations above 0.5 nM are rather unlikely to occur under physiological conditions.62, 63

In contrast to Y_1R, Y_2R, and Y_5R, only a few antagonists of Y_4R have been reported. In this study, the Y_4R binding of the argininamide-type Y_4R antagonist UR-MK188[30] was investigated. The results showed that the Y_4R binding affinity in sodium-containing buffer was higher than that in sodium-free buffer ($P < 0.05$), suggesting that this antagonist prefers the inactive receptor conformation as hypothesized for the Y_1R antagonist BIBP3226 (Table 6.3). The obtained pK_i values of UR-MK188 were similar to reported data (Table 6.3). The Y_4R antagonism of UR-MK188 was concluded from the results of a functional assay with a proximal readout (Ca^{2+} aequorin assay).[30] In the present study, UR-MK188 was further investigated in an impedance-based functional Y_4R assay[64] representing a very distal readout to confirm its antagonistic effect at Y_4R. Interestingly, in the impedance-based assay, UR-MK188 behaved as a partial Y_4R agonist with an efficacy above 70%. (Figure 6.2). This suggests that functional assays with a distal readout can unmask receptor agonism that remains undetected in canonical functional assays.

6.3.4 Y_5R Binding

Y_5R binding studies in sodium-containing *buffer II* were conducted as previously reported[35] but using [K^4-[^{3}H]propionyl]hPYY[11] as the radioligand for the experiments instead of [K^4-[^{3}H]propionyl]pNPY. To note, [K^4-[^{3}H]propionyl]hPYY was recently introduced as a radioligand for Y_2R binding studies in sodium-containing buffer, but has not been used for Y_5R binding studies.[11] Since [K^4-propionyl]hPYY exhibits Y_5R binding affinity similar to that of [K^4-[^{3}H]propionyl]pNPY in sodium-containing buffer,[11] it was used for Y_5R binding experiments in *buffer II* in this study. Prior to the use of [K^4-propionyl]hPYY for the determination of ligand binding at Y_5R, it was characterized by saturation binding yielding a K_d of 9.5 nM (Figure A6.6D, Table A6.1; *Section 6.6 Appendix*). As a further control and validation of the assay, the Y_5R binding affinity of the non-tritiated analog [K^4-propionyl]hPYY in *buffer II* was determined using [K^4-[^{3}H]propionyl]hPYY as probe. This experiment afforded a pK_i value of 8.09 ± 0.05 (mean value ± SEM from three individual experiments performed in triplicate; expressed as K_i: 8.3 nM) being in excellent agreement with the K_d of 9.5 nM determined for [K^4-[^{3}H]propionyl]hPYY.

Regarding the Y_5R binding studies in sodium-free *buffer Ib*, the use of [K^4-[^{3}H]propionyl]hPYY was considered to be used as radioligand. However, its binding affinity was lower (K_d > 20 nM) compared to that obtained in *buffer II* (K_d = 9.5 nM), implying high amounts of radioligand to be used for the experiment and high unspecific binding relative to specific binding. Hence, its N-terminally extended histidyl analog [K^5-[^{3}H]propionyl]His-hPYY ([^{3}H]**6.1**), available in our lab, was also tested. [^{3}H]**6.1** was synthesized due to an unintended purchase of His-hPYY instead of hPYY as the labeling precursor (the lapse was noticed after the radiosynthesis of [^{3}H]**6.1**). Saturation binding experiments with [K^4-[^{3}H]propionyl]hPYY and [^{3}H]**6.1** at HEC-1B-hY_5R cells in *buffer Ib* yielded similar results (data of [K^4-[^{3}H]propionyl]hPYY not shown), however, [^{3}H]**6.1** appeared to be slightly more advantageous with respect to saturability (specific binding) and the extent of unspecific binding (a significant difference was not found based on the acquired data). Thus, the histidyl analog [^{3}H]**6.1** was used for Y_5R binding studies in *buffer Ib* to reduce the consumption of [K^4-[^{3}H]propionyl]hPYY. The K_d value obtained from saturation binding studies with [^{3}H]**6.1** in *buffer Ib* was 20 nM (for a representative saturation binding curve see Figure A6.6D, *Section 6.6 Appendix*). The synthesis of [^{3}H]**6.1** and its non-tritiated analog [K^5-propionyl]His-hPYY (**6.1**) is shown in Scheme A6.1 (*Section 6.6 Appendix*). Chromatograms of the RP-HPLC analysis of crude [^{3}H]**6.1** (reaction control), the micropreparative work-up of [^{3}H]**6.1** by RP-HPLC, and the determination of the radiochemical purity of [^{3}H]**6.1** are shown in Figures A6.3–6.5 (*Section 6.6 Appendix*). The suitability of [^{3}H]**6.1** for Y_5R competition binding studies in *buffer Ib* was evaluated by determining the pK_i value of **6.1** using [^{3}H]**6.1** as a probe. This control experiment gave a pK_i value of 7.88 ± 0.11 (mean value ± SEM from three individual experiments performed in triplicate; expressed as K_i: 14 nM), which confirmed the Y_5R binding affinity determined by saturation binding with [^{3}H]**6.1** (K_d = 20 nM).

In sodium-containing *buffer II*, all studied peptides displayed similar Y_5R binding affinities (pK_i = 7.96–8.55, Table 6.2, Figure 6.1H). The pK_i values obtained for pNPY, hNPY, and hPYY in sodium-free *buffer Ib* were slightly higher compared to the pK_i values determined in *buffer II*, but this was only significant for hNPY ($P < 0.05$) (Table 6.2, Figure 6.1G). For hPP, highly similar Y_5R binding affinities were observed for *buffer II* and *Ib*. Remarkably, all Y_5R binding affinities were in agreement with the reported data (< 1 log unit difference).

For the investigated Y_5R antagonist CGP71683A, the pK_i determined in *buffer II* was markedly higher (ca. 1.6 log units) than the pK_i determined in *buffer Ib,* indicating that this antagonist also prefers the inactive receptor conformation as hypothesized above for the reported Y_1R antagonist BIBP3226[66] and Y_4R antagonist, UR-MK188[30] (Table 6.3). Compared to literature, the pK_i of CGP71683A determined in sodium-containing buffer was about 0.4-1 log units higher than the reported pK_i values, whereas in sodium-free buffer, the determined pK_i was lower by 0.4 log units (Table 6.3).

6.3.5 Summary of the effect of sodium on YR binding of the ligands under study.

Taken together, the results of this study indicate that the effect of sodium on YR binding is dependent on the receptor subtype and type of ligand. It should be noted that none of the reported X-ray/cryo-EM structures of Y_1R, Y_2R, and Y_4R (note: to date, no Y_5R structure has been reported) shows the presence of sodium ion(s) in the receptor, as reported in the PDB, although the receptor preparations used for crystallization or vitrification contained sodium in most cases.[67-71] Consequently, the influence of sodium on receptor conformation is not addressed in the respective publications. As a comprehensive overview, the effect of sodium on YR binding of pNPY, hNPY, hPYY, and hPP, as well as the antagonists studied here, are summarized in Table 6.4.

Table 6.4. Summary of the effects of sodium on YR binding affinity (pK_i) of agonists and antagonists.

YR subtype	Ligands	Change in pK_i with $Na^+ \rightarrow Na^+$-free
Y_1R	pNPY	—
	hNPY	—
	hPYY	—
	hPP	↗
	BIBP3226	↘
Y_2R	pNPY	—
	hNPY	↗
	hPYY	—
	hPP	—
	JNJ31020028	—
	BIIE0246	↗
Y_4R	pNPY	↗
	hNPY	↗
	hPYY	↗
	hPP	—
	UR-MK188	↘
Y_5R	pNPY	—
	hNPY	↗
	hPYY	—
	hPP	—
	CGP71683A	↘

Arrows up (↗) and down (↘) indicate a significant increase and decrease, respectively ($P < 0.05$), in binding affinity for the comparison of the pK_i values determined in sodium-containing buffer with the pK_i values determined in sodium-free buffer (*cf.* Tables 6.2 and 6.3). The dash indicates that pK_i values were not significantly different ($P > 0.05$).

6.4 Conclusion

The neuropeptide Y receptor family and their endogenous ligands play several roles in numerous physiological processes, e.g., the regulation of anxiety, hormone release, stress, and food intake. This makes these receptors potential drug targets. Accordingly, *in vitro* studies of these receptors, such as the determination of ligand-receptor binding affinities, should be conducted in buffers containing sodium at a physiological concentration. However, for Y_1R, Y_2R, and Y_4R, receptor-ligand binding studies have been frequently performed in sodium-free buffers or buffers containing low sodium concentrations (≤ 30 mM). Since the binding of receptor agonists to class A GPCRs is often influenced by the absence or presence of sodium, a determination of binding affinities under sodium-free conditions might lead to a distorted picture of the binding profiles.

To gain a comprehensive view of the YR binding profiles of the endogenous agonists NPY, PYY, and PP, the Y_1R, Y_2R, Y_4R, and Y_5R binding affinities of these peptides were determined in radiochemical competition binding assays in both sodium-free and sodium-containing buffers. For these studies, well-characterized tritium-labeled radioligands were used, and binding data were obtained using procedures well-established in the same lab. To the best of our knowledge, this study is the first of its kind. A major finding from this study is that for the different YR subtypes, the binding of agonists was influenced differently by the absence or presence of sodium, known to allosterically modulate the activation of GPCRs. However, the effect of sodium depends not only on the individual receptor subtype but also on the type of agonist binding to the receptor. Notably, the reported YR binding profiles of NPY, PYY, and PP were generally confirmed. Nonetheless, the relevance of these peptides for activating the individual YR subtypes *in vivo* may need to be re-evaluated based on the YR binding affinities determined in the present study.

6.5 References

(1) Walther, C.; Morl, K.; Beck-Sickinger, A. G. Neuropeptide Y receptors: ligand binding and trafficking suggest novel approaches in drug development. *J. Pept. Sci.* 2011, *17* (4), 233-246. DOI: 10.1002/psc.1357.

(2) Yi, M.; Li, H.; Wu, Z.; Yan, J.; Liu, Q.; Ou, C.; Chen, M. A promising therapeutic target for metabolic diseases: neuropeptide Y receptors in humans. *Cell. Physiol. Biochem.* 2018, *45* (1), 88-107. DOI: 10.1159/000486225.

(3) Brothers, S. P.; Wahlestedt, C. Therapeutic potential of neuropeptide Y (NPY) receptor ligands. *EMBO Mol. Med.* 2010, *2* (11), 429-439. DOI: 10.1002/emmm.201000100.

(4) Pedragosa-Badia, X.; Stichel, J.; Beck-Sickinger, A. G. Neuropeptide Y receptors: how to get subtype selectivity. *Front. Endocrinol. (Lausanne)* 2013, *4*, 5. DOI: 10.3389/fendo.2013.00005.

(5) Katritch, V.; Fenalti, G.; Abola, E. E.; Roth, B. L.; Cherezov, V.; Stevens, R. C. Allosteric sodium in class A GPCR signaling. *Trends Biochem. Sci.* 2014, *39*, 233-244. DOI: 10.1016/j.tibs.2014.03.002.

(6) Maguire, J. J.; Kuc, R. E.; Davenport, A. P. Radioligand binding assays and their analysis. *Methods Mol. Biol.* 2012, *897*, 31-77. DOI: 10.1007/978-1-61779-909-9_3.

(7) Parker, M. S.; Sah, R.; Sheriff, S.; Balasubramaniam, A.; Parker, S. L. Internalization of cloned pancreatic polypeptide receptors is accelerated by all types of Y_4 agonists. *Regul. Pept.* 2005, *132* (1-3), 91-101. DOI: 10.1016/j.regpep.2005.09.008.

(8) White, K. L.; Eddy, M. T.; Gao, Z.-G.; Han, G. W.; Lian, T.; Deary, A.; Patel, N.; Jacobson, K. A.; Katritch, V.; Stevens, R. C. Structural connection between activation microswitch and allosteric sodium site in GPCR signaling. *Structure* 2018, *26*, 259-269. DOI: 10.1016/j.str.2017.12.013.

(9) Dukorn, S.; Littmann, T.; Keller, M.; Kuhn, K.; Cabrele, C.; Baumeister, P.; Bernhardt, G.; Buschauer, A. Fluorescence- and radiolabeling of [Lys^4,Nle^{17,30}]hPP yields molecular tools for the NPY Y_4 receptor. *Bioconjug. Chem.* 2017, *28*, 1291-1304. DOI: 10.1021/acs.bioconjchem.7b00103.

(10) Gleixner, J.; Gattor, A. O.; Humphrys, L. J.; Brunner, T.; Keller, M. [^{3}H]UR-JG102 – A Radiolabeled Cyclic Peptide with High Affinity and Excellent Selectivity for the Neuropeptide Y Y_4 Receptor. *J. Med. Chem.* 2023, *66* (19), 13788-13808. DOI: 10.1021/acs.jmedchem.3c01224.

(11) Schettler, F.; Gattor, A. O.; Koch, P.; Keller, M. Characterization of [^{3}H]propionylated human peptide YY – a new probe for neuropeptide Y Y_2 receptor binding studies. *ACS Pharmacol. Transl. Sci.* 2025. DOI: 10.1021/acsptsci.4c00666.

(12) Gerald, C.; Walker, M. W.; Vaysse, P. J.; He, C.; Branchek, T. A.; Weinshank, R. L. Expression cloning and pharmacological characterization of a human hippocampal neuropeptide Y/peptide YY Y_2 receptor subtype. *J. Biol. Chem.* 1995, *270* (45), 26758-26761. DOI: 10.1074/jbc.270.45.26758.

(13) Söll, R. M.; Dinger, M. C.; Lundell, I.; Larhammer, D.; Beck-Sickinger, A. G. Novel analogues of neuropeptide Y with a preference for the Y_1-receptor. *Eur.*

J. Biochem. 2001, *268* (10), 2828-2837. DOI: 10.1046/j.1432-1327.2001.02161.x.

(14) Krause, J.; Eva, C.; Seeburg, P. H.; Sprengel, R. Neuropeptide Y_1 subtype pharmacology of a recombinantly expressed neuropeptide receptor. *Mol. Pharmacol.* 1992, *41* (5), 817-821. DOI: 10.1016/S0026-895X(25)09119-9.

(15) Loh, K.; Shi, Y. C.; Bensellam, M.; Lee, K.; Laybutt, D. R.; Herzog, H. Y_1 receptor deficiency in beta-cells leads to increased adiposity and impaired glucose metabolism. *Sci. Rep.* 2018, *8* (1), 11835. DOI: 10.1038/s41598-018-30140-2.

(16) Lundell, I.; Blomqvist, A. G.; Berglund, M. M.; Schober, D. A.; Johnson, D.; Statnick, M. A.; Gadski, R. A.; Gehlert, D. R.; Larhammar, D. Cloning of a human receptor of the NPY receptor family with high affinity for pancreatic polypeptide and peptide YY. *J. Biol. Chem.* 1995, *270* (49), 29123-29128. DOI: 10.1074/jbc.270.49.29123.

(17) Rose, P. M.; Fernandes, P.; Lynch, J. S.; Frazier, S. T.; Fisher, S. M.; Kodukula, K.; Kienzle, B.; Seethala, R. Cloning and functional expression of a cDNA encoding a human type 2 neuropeptide Y receptor. *J. Biol. Chem.* 1995, *270* (39), 22661-22664. DOI: 10.1074/jbc.270.39.22661.

(18) Dumont, Y.; Fournier, A.; St-Pierre, S.; Quirion, R. Autoradiographic distribution of [^{125}I]Leu^{31},Pro^{34}]PYY and [^{125}I]PYY_{3-36} binding sites in the rat brain evaluated with two newly developed Y_1 and Y_2 receptor radioligands. *Synapse* 1996, *22* (2), 139-158. DOI: 10.1002/(SICI)1098-2396(199602)22:2<139::AID-SYN7>3.0.CO;2-E.

(19) Walker, M. W.; Smith, K. E.; Bard, J.; Vaysse, P. J.; Gerald, C.; Daouti, S.; Weinshank, R. L.; Branchek, T. A. A structure-activity analysis of the cloned rat and human Y_4 receptors for pancreatic polypeptide. *Peptides* 1997, *18* (4), 609-612. DOI: 10.1016/s0196-9781(97)00070-3.

(20) Berglund, M. M.; Lundell, I.; Eriksson, H.; Soll, R.; Beck-Sickinger, A. G.; Larhammar, D. Studies of the human, rat, and guinea pig Y_4 receptors using neuropeptide Y analogues and two distinct radioligands. *Peptides* 2001, *22* (3), 351-356. DOI: 10.1016/s0196-9781(01)00337-0.

(21) Balasubramaniam, A.; Mullins, D. E.; Lin, S.; Zhai, W.; Tao, Z.; Dhawan, V. C.; Guzzi, M.; Knittel, J. J.; Slack, K.; Herzog, H.*; et al.* Neuropeptide Y (NPY) Y_4 receptor selective agonists based on NPY_{32-36}: development of an anorectic Y_4 receptor selective agonist with picomolar affinity. *J. Med. Chem.* 2006, *49* (8), 2661-2665. DOI: 10.1021/jm050907d.

(22) Yan, H.; Yang, J.; Marasco, J.; Yamaguchi, K.; Brenner, S.; Collins, F.; Karbon, W. Cloning and functional expression of cDNAs encoding human and rat pancreatic polypeptide receptors. *PNAS USA* 1996, *93* (10), 4661-4665. DOI: 10.1073/pnas.93.10.4661.

(23) Eriksson, H.; Berglund, M. M.; Holmberg, S. K.; Kahl, U.; Gehlert, D. R.; Larhammar, D. The cloned guinea pig pancreatic polypeptide receptor Y_4 resembles more the human Y_4 than does the rat Y_4. *Regul. Pept.* 1998, *75-76*, 29-37. DOI: 10.1016/s0167-0115(98)00050-0.

(24) Borowsky, B.; Walker, M. W.; Bard, J.; Weinshank, R. L.; Laz, T. M.; Vaysse, P.; Branchek, T. A.; Gerald, C. Molecular biology and pharmacology of multiple

NPY Y_5 receptor species homologs. *Regul. Pept.* 1998, *75-76*, 45-53. DOI: 10.1016/s0167-0115(98)00052-4.

(25) Dumont, Y.; Thakur, M.; Beck-Sickinger, A.; Fournier, A.; Quirion, R. Characterization of a new neuropeptide Y Y_5 agonist radioligand: [^{125}I][cPP$_{1-7}$,NPY$_{19-23}$,Ala^{31},Aib^{32},Gln^{34}]hPP. *Neuropeptides* 2004, *38* (4), 163-174. DOI: 10.1016/j.npep.2004.04.007.

(26) Dumont, Y.; Thakur, M.; Beck-Sickinger, A.; Fournier, A.; Quirion, R. Development and characterization of a highly selective neuropeptide Y Y_5 receptor agonist radioligand: [^{125}I][hPP$_{1–17}$,Ala^{31},Aib^{32}]NPY. *Br. J. Pharmacol.* 2003, *139* (7), 1360-1368. DOI: 10.1038/sj.bjp.0705376.

(27) Grätz, L.; Müller, C.; Pegoli, A.; Schindler, L.; Bernhardt, G.; Littmann, T. Insertion of nanoluc into the extracellular loops as a complementary method to establish BRET-based binding assays for GPCRs. *ACS Pharmacol. Transl. Sci.* 2022, *5* (11), 1142-1155. DOI: 10.1021/acsptsci.2c00162.

(28) Keller, M.; Erdmann, D.; Pop, N.; Pluym, N.; Teng, S.; Bernhardt, G.; Buschauer, A. Red-fluorescent argininamide-type NPY Y_1 receptor antagonists as pharmacological tools. *Biorg. Med. Chem.* 2011, *19* (9), 2859-2878. DOI: 10.1016/j.bmc.2011.03.045 From American Chemical Society. All Rights Reserved. CAPLUS.

(29) Keller, M.; Weiss, S.; Hutzler, C.; Kuhn, K. K.; Mollereau, C.; Dukorn, S.; Schindler, L.; Bernhardt, G.; König, B.; Buschauer, A. N$^{\omega}$-Carbamoylation of the argininamide moiety: an avenue to insurmountable NPY Y_1 receptor antagonists and a radiolabeled selective high-affinity molecular tool ([^{3}H]UR-MK299) with extended residence time. *J. Med. Chem.* 2015, *58*, 8834-8849. DOI: 10.1021/acs.jmedchem.5b00925.

(30) Keller, M.; Kaske, M.; Holzammer, T.; Bernhardt, G.; Buschauer, A. Dimeric argininamide-type neuropeptide Y receptor antagonists: chiral discrimination between Y_1 and Y_4 receptors. *Biorg. Med. Chem.* 2013, *21* (21), 6303-6322. DOI: 10.1016/j.bmc.2013.08.065.

(31) Ertl, F. J.; Kopanchuk, S.; Dijon, N. C.; Veiksina, S.; Tahk, M. J.; Laasfeld, T.; Schettler, F.; Gattor, A. O.; Hubner, H.; Archipowa, N.*; et al.* Dually labeled neurotensin NTS_1R ligands for probing radiochemical and fluorescence-based binding assays. *J. Med. Chem.* 2024, *67* (18), 16664-16691. DOI: 10.1021/acs.jmedchem.4c01470.

(32) Ziemek, R.; Schneider, E.; Kraus, A.; Cabrele, C.; Beck-Sickinger, A. G.; Bernhardt, G.; Buschauer, A. Determination of affinity and activity of ligands at the human neuropeptide Y Y_4 receptor by flow cytometry and aequorin luminescence. *J. Recept. Signal Transduct.* 2007, *27*, 217-233. DOI: 10.1080/10799890701505206.

(33) Moser, C.; Bernhardt, G.; Michel, J.; Schwarz, H.; Buschauer, A. Cloning and functional expression of the hNPY Y_5 receptor in human endometrial cancer (HEC-1B) cells. *Can. J. Physiol. Pharmacol.* 2000, *78* (2), 134-142. DOI: 10.1139/y99-125.

(34) Cheng, Y.; Prusoff, W. H. Relationship between the inhibition constant (K_I) and the concentration of inhibitor which causes 50 per cent inhibition (I_{50}) of an enzymatic reaction. *Biochem. Pharmacol.* 1973, *22* (23), 3099-3108. DOI: 10.1016/0006-2952(73)90196-2.

(35) Kuhn, K. K.; Ertl, T.; Dukorn, S.; Keller, M.; Bernhardt, G.; Reiser, O.; Buschauer, A. High affinity agonists of the neuropeptide Y (NPY) Y_4 receptor derived from the C-terminal pentapeptide of human pancreatic polypeptide (hPP): synthesis, stereochemical discrimination, and radiolabeling. *J. Med. Chem.* 2016, *59*, 6045-6058. DOI: 10.1021/acs.jmedchem.6b00309.

(36) Sheikh, S. P.; O'Hare, M. M.; Tortora, O.; Schwartz, T. W. Binding of monoiodinated neuropeptide Y to hippocampal membranes and human neuroblastoma cell lines. *J. Biol. Chem.* 1989, *264* (12), 6648-6654. DOI: 10.1016/S0021-9258(18)83476-7.

(37) Frey, K. A.; Albin, R. L. Receptor binding techniques. *Curr. Protoc. Neurosci.* 2001, *Chapter 1*, Unit 1.4. DOI: 10.1002/0471142301.ns0104s00.

(38) Bylund, D. B.; Toews, M. L. Radioligand binding methods: practical guide and tips. *Am. J. Physiol.* 1993, *265* (5 Pt 1), L421-429. DOI: 10.1152/ajplung.1993.265.5.L421.

(39) Li, A. J.; Ritter, S. Functional expression of neuropeptide Y receptors in human neuroblastoma cells. *Regul. Pept.* 2005, *129* (1), 119-124. DOI: 10.1016/j.regpep.2005.02.003.

(40) Dumont, Y.; Cadieux, A.; Doods, H.; Fournier, A.; Quirion, R. Potent and selective tools to investigate neuropeptide Y receptors in the central and peripheral nervous systems: BIBO3304 (Y_1) and CGP71683A (Y_5). *Can. J. Physiol. Pharmacol.* 2000, *78* (2), 116-125. DOI: 10.1139/y99-119.

(41) Gehlert, D. R.; Beavers, L. S.; Johnson, D.; Gackenheimer, S. L.; Schober, D. A.; Gadski, R. A. Expression cloning of a human brain neuropeptide Y Y_2 receptor. *Mol. Pharmacol.* 1996, *49* (2), 224-228. DOI: 10.1016/S0026-895X(25)08702-4.

(42) Schneider, E.; Mayer, M.; Ziemek, R.; Li, L.; Hutzler, C.; Bernhardt, G.; Buschauer, A. A simple and powerful flow cytometric method for the simultaneous determination of multiple parameters at G protein-coupled receptor subtypes. *ChemBioChem* 2006, *7* (9), 1400-1409. DOI: 10.1002/cbic.200600163.

(43) Doods, H.; Gaida, W.; Wieland, H. A.; Dollinger, H.; Schnorrenberg, G.; Esser, F.; Engel, W.; Eberlein, W.; Rudolf, K. BIIE0246: a selective and high affinity neuropeptide Y Y_2 receptor antagonist. *Eur. J. Pharmacol.* 1999, *384* (2-3), R3-5. DOI: 10.1016/s0014-2999(99)00650-0.

(44) Gehlert, D. R.; Schober, D. A.; Beavers, L.; Gadski, R.; Hoffman, J. A.; Smiley, D. L.; Chance, R. E.; Lundell, I.; Larhammar, D. Characterization of the peptide binding requirements for the cloned human pancreatic polypeptide-preferring receptor. *Mol. Pharmacol.* 1996, *50* (1), 112-118. DOI: 10.1016/S0026-895X(25)09120-5.

(45) Berlicki, L.; Kaske, M.; Gutierrez-Abad, R.; Bernhardt, G.; Illa, O.; Ortuno, R. M.; Cabrele, C.; Buschauer, A.; Reiser, O. Replacement of Thr^{32} and Gln^{34} in the C-terminal neuropeptide Y fragment 25-36 by cis-cyclobutane and cis-cyclopentane beta-amino acids shifts selectivity toward the Y_4 receptor. *J. Med. Chem.* 2013, *56* (21), 8422-8431. DOI: 10.1021/jm4008505.

(46) Ziemek, R.; Brennauer, A.; Schneider, E.; Cabrele, C.; Beck-Sickinger, A. G.; Bernhardt, G.; Buschauer, A. Fluorescence- and luminescence-based

methods for the determination of affinity and activity of neuropeptide Y_2 receptor ligands. *Eur. J. Pharmacol.* 2006, *551* (1), 10-18. DOI: 10.1016/j.ejphar.2006.08.075.

(47) Bard, J. A.; Walker, M. W.; Branchek, T. A.; Weinshank, R. L. Cloning and functional expression of a human Y_4 subtype receptor for pancreatic polypeptide, neuropeptide Y, and peptide YY. *J. Biol. Chem.* 1995, *270* (45), 26762-26765. DOI: 10.1074/jbc.270.45.26762.

(48) Germain, A. R.; Carmody, L. C.; Nag, P. P.; Morgan, B.; Verplank, L.; Fernandez, C.; Donckele, E.; Feng, Y.; Perez, J. R.; Dandapani, S.*; et al.* Cinnamides as selective small-molecule inhibitors of a cellular model of breast cancer stem cells. *Bioorg. Med. Chem. Lett.* 2013, *23* (6), 1834-1838. DOI: 10.1016/j.bmcl.2013.01.025.

(49) Youngman, M. A.; McNally, J. J.; Lovenberg, T. W.; Reitz, A. B.; Willard, N. M.; Nepomuceno, D. H.; Wilson, S. J.; Crooke, J. J.; Rosenthal, D.; Vaidya, A. H.*; et al.* alpha-Substituted N-(sulfonamido)alkyl-beta-aminotetralins: potent and selective neuropeptide Y Y_5 receptor antagonists. *J. Med. Chem.* 2000, *43* (3), 346-350. DOI: 10.1021/jm990468g.

(50) Tough, I. R.; Holliday, N. D.; Cox, H. M. Y_4 receptors mediate the inhibitory responses of pancreatic polypeptide in human and mouse colon mucosa. *J. Pharmacol. Exp. Ther.* 2006, *319* (1), 20-30. DOI: 10.1124/jpet.106.106500.

(51) Hu, Y.; Bloomquist, B. T.; Cornfield, L. J.; DeCarr, L. B.; Flores-Riveros, J. R.; Friedman, L.; Jiang, P.; Lewis-Higgins, L.; Sadlowski, Y.; Schaefer, J.*; et al.* Identification of a novel hypothalamic neuropeptide Y receptor associated with feeding behavior. *J. Biol. Chem.* 1996, *271* (42), 26315-26319. DOI: 10.1074/jbc.271.42.26315.

(52) Keller, M.; Bernhardt, G.; Buschauer, A. [^{3}H]UR-MK136: A highly potent and selective radioligand for neuropeptide Y Y_1 receptors. *ChemMedChem* 2011, *6* (9), 1566-1571. DOI: 10.1002/cmdc.201100197.

(53) Vanderheyden, P. M.; Van Liefde, I.; de Backer, J. P.; Vauquelin, G. [^{3}H]-BIBP3226 and [^{3}H]-NPY binding to intact SK-N-MC cells and CHO cells expressing the human Y_1 receptor. *J. Recept. Signal Transduct.* 1998, *18* (4-6), 363-385. DOI: 10.3109/10799899809047752.

(54) Entzeroth, M.; Braunger, H.; Eberlein, W.; Engel, W.; Rudolf, K.; Wienen, W.; Wieland, H. A.; Willim, K. D.; Doods, H. N. Labeling of neuropeptide Y receptors in SK-N-MC cells using the novel, nonpeptide Y_1 receptor-selective antagonist [^{3}H]BIBP3226. *Eur. J. Pharmacol.* 1995, *278* (3), 239-242. DOI: 10.1016/0014-2999(95)00161-d.

(55) Shoblock, J. R.; Welty, N.; Nepomuceno, D.; Lord, B.; Aluisio, L.; Fraser, I.; Motley, S. T.; Sutton, S. W.; Morton, K.; Galici, R.*; et al.* In vitro and in vivo characterization of JNJ-31020028 (N-(4-4-[2-(diethylamino)-2-oxo-1-phenylethyl]piperazin-1-yl-3-fluorophenyl)-2-pyridin-3-ylbenzamide), a selective brain penetrant small molecule antagonist of the neuropeptide Y Y_2 receptor. *Psychopharmacology (Berl)* 2010, *208* (2), 265-277. DOI: 10.1007/s00213-009-1726-x.

(56) Pluym, N.; Brennauer, A.; Keller, M.; Ziemek, R.; Pop, N.; Bernhardt, G.; Buschauer, A. Application of the guanidine-acylguanidine bioisosteric

approach to argininamide-type NPY Y_2 receptor antagonists. *ChemMedChem* 2011, *6* (9), 1727-1738. DOI: 10.1002/cmdc.201100241.

(57) Michel, M. C.; Beck-Sickinger, A.; Cox, H.; Doods, H. N.; Herzog, H.; Larhammar, D.; Quirion, R.; Schwartz, T.; Westfall, T. XVI. International Union of Pharmacology recommendations for the nomenclature of neuropeptide Y, peptide YY, and pancreatic polypeptide receptors. *Pharmacol. Rev.* 1998, *50* (1), 143-150.

(58) Schüß, C.; Behr, V.; Beck-Sickinger, A. G. Illuminating the neuropeptide Y_4 receptor and its ligand pancreatic polypeptide from a structural, functional, and therapeutic perspective. *Neuropeptides* 2024, *105*, 102416. DOI: 10.1016/j.npep.2024.102416.

(59) Palanivel, V.; Gupta, V.; Chitranshi, N.; Tietz, O.; Vander Wall, R.; Blades, R.; Maha Thananthirige, K. P.; Salkar, A.; Shen, C.; Mirzaei, M.*; et al.* Neuropeptide Y receptor activation preserves inner retinal integrity through PI3K/Akt signaling in a glaucoma mouse model. *PNAS Nexus* 2024, *3* (8). DOI: 10.1093/pnasnexus/pgae299 (acccessed 3/3/2025).

(60) Cox, H. M.; Tough, I. R. Neuropeptide Y, Y_1, Y_2 and Y_4 receptors mediate Y agonist responses in isolated human colon mucosa. *Br. J. Pharmacol.* 2002, *135* (6), 1505-1512. DOI: 10.1038/sj.bjp.0704604.

(61) Anderson, Z. T.; Dawson, A. D.; Slominski, A. T.; Harris, M. L. Current insights into the role of neuropeptide Y in skin physiology and pathology. *Front. Endocrinol.* 2022, *13*, Review. DOI: 10.3389/fendo.2022.838434.

(62) Fletcher, M. A.; Rosenthal, M.; Antoni, M.; Ironson, G.; Zeng, X. R.; Barnes, Z.; Harvey, J. M.; Hurwitz, B.; Levis, S.; Broderick, G.*; et al.* Plasma neuropeptide Y: a biomarker for symptom severity in chronic fatigue syndrome. *Behav. Brain Funct.* 2010, *6* (1), 76. DOI: 10.1186/1744-9081-6-76.

(63) Lettgen, B.; Wagner, S.; Hänze, J.; Lang, R. E.; Rascher, W. Elevated plasma concentration of neuropeptide Y in adolescents with primary hypertension. *J. Hum. Hypertens.* 1994, *8* (5), 345-349. PubMed.

(64) Wirth, U.; Erl, J.; Azzam, S.; Höring, C.; Skiba, M.; Singh, R.; Hochmuth, K.; Keller, M.; Wegener, J.; König, B. Monitoring the reversibility of GPCR signaling by combining photochromic ligands with label-free impedance analysis. *Angew. Chem. Int. Ed.* 2023, *62* (21), e202215547. DOI: 10.1002/anie.202215547.

(65) Konieczny, A.; Braun, D.; Wifling, D.; Bernhardt, G.; Keller, M. Oligopeptides as neuropeptide Y Y_4 receptor ligands: identification of a high-affinity tetrapeptide agonist and a hexapeptide antagonist. *J. Med. Chem.* 2020, *63*, 8198-8215. DOI: 10.1021/acs.jmedchem.0c00426.

(66) Rudolf, K.; Eberlein, W.; Engel, W.; Wieland, H. A.; Willim, K. D.; Entzeroth, M.; Wienen, W.; Beck-Sickinger, A. G.; Doods, H. N. The first highly potent and selective non-peptide neuropeptide Y Y_1 receptor antagonist: BIBP3226. *Eur. J. Pharmacol.* 1994, *271* (2), R11-R13. DOI: 10.1016/0014-2999(94)90822-2.

(67) Kang, H.; Park, C.; Choi, Y. K.; Bae, J.; Kwon, S.; Kim, J.; Choi, C.; Seok, C.; Im, W.; Choi, H.-J. Structural basis for Y_2 receptor-mediated neuropeptide Y

and peptide YY signaling. *Structure* 2023, *31* (1), 44-57.e46. DOI: 10.1016/j.str.2022.11.010 (acccessed 2025/03/17).

(68) Park, C.; Kim, J.; Ko, S.-B.; Choi, Y. K.; Jeong, H.; Woo, H.; Kang, H.; Bang, I.; Kim, S. A.; Yoon, T.-Y.*; et al.* Structural basis of neuropeptide Y signaling through Y_1 receptor. *Nat. Commun.* 2022, *13* (1), 853. DOI: 10.1038/s41467-022-28510-6.

(69) Shen, S.; Deng, Y.; Shen, C.; Chen, H.; Cheng, L.; Wu, C.; Zhao, C.; Yang, Z.; Hou, H.; Wang, K.*; et al.* Structural basis of neuropeptide Y signaling through Y_1 and Y_2 receptors. *MedComm* 2024, *5* (7), e565. DOI: 10.1002/mco2.565.

(70) Tang, T.; Tan, Q.; Han, S.; Diemar, A.; Löbner, K.; Wang, H.; Schüß, C.; Behr, V.; Mörl, K.; Wang, M.*; et al.* Receptor-specific recognition of NPY peptides revealed by structures of NPY receptors. *Sci. Adv.* 2022, *8* (18), eabm1232. DOI: doi:10.1126/sciadv.abm1232.

(71) Yang, Z.; Han, S.; Keller, M.; Kaiser, A.; Bender, B. J.; Bosse, M.; Burkert, K.; Kögler, L. M.; Wifling, D.; Bernhardt, G.*; et al.* Structural basis of ligand binding modes at the neuropeptide Y Y_1 receptor. *Nature* 2018, *556* (7702), 520-524. DOI: 10.1038/s41586-018-0046-x.

6.6 Appendix

6.6.1 Scheme A6.1, Figures A6.1–A6.6 and Table A6.1

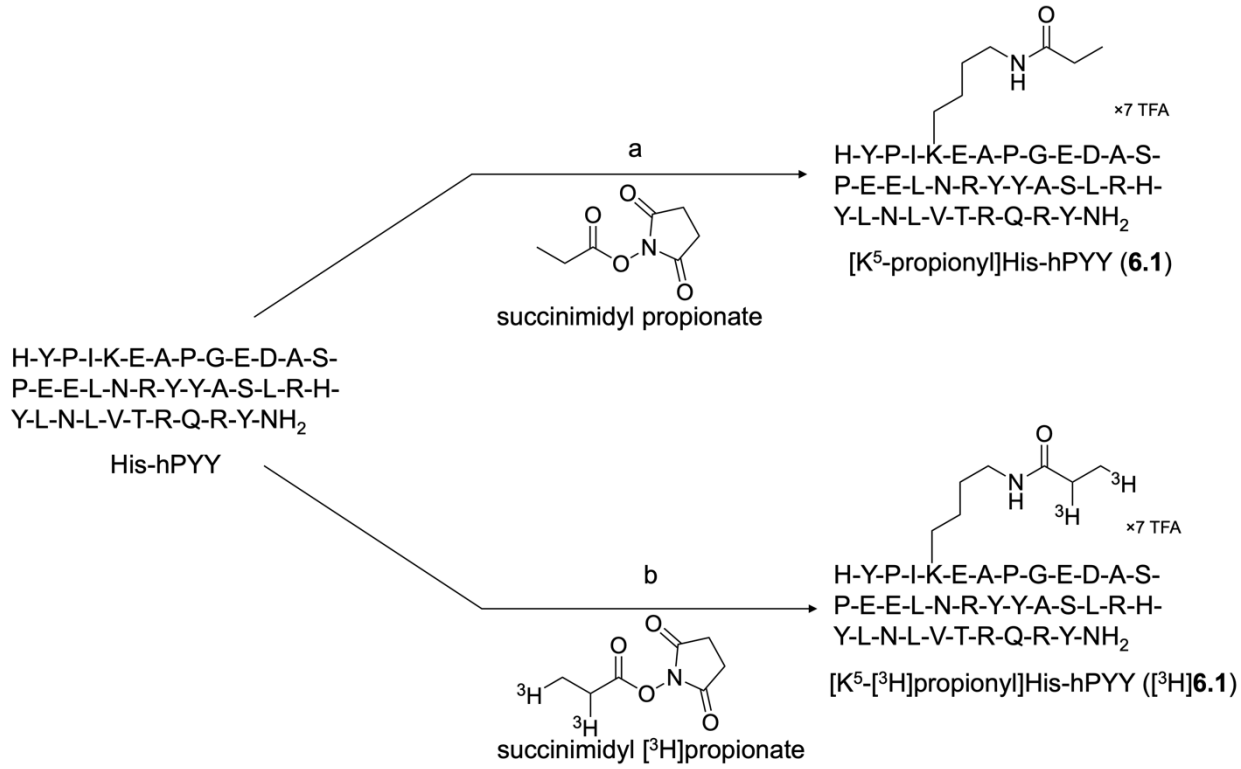

Scheme A6.1. Syntheses of [K^5-propionyl]His-hPYY (**6.1**) and [K^5-[^{3}H]propionyl]His-hPYY ([^{3}H]**6.1**). Reagents and conditions: (a) DIPEA, DMF/NMP/H_2O 60:25:15, rt, 1.5 h, 17%; (b) DIPEA, DMF/NMP/H_2O 60:25:15, rt, 1 h, radiochemical yield 12.8%.

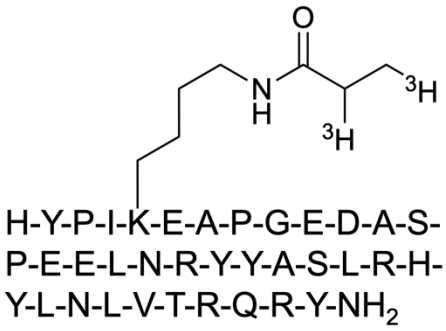

[^{3}H]**6.1** ([K^5-[^{3}H]propionyl]His-hPYY)

Figure A6.1. Structure of the [^{3}H]**6.1** used radioligand binding studies at Y_5R in sodium-free buffer.

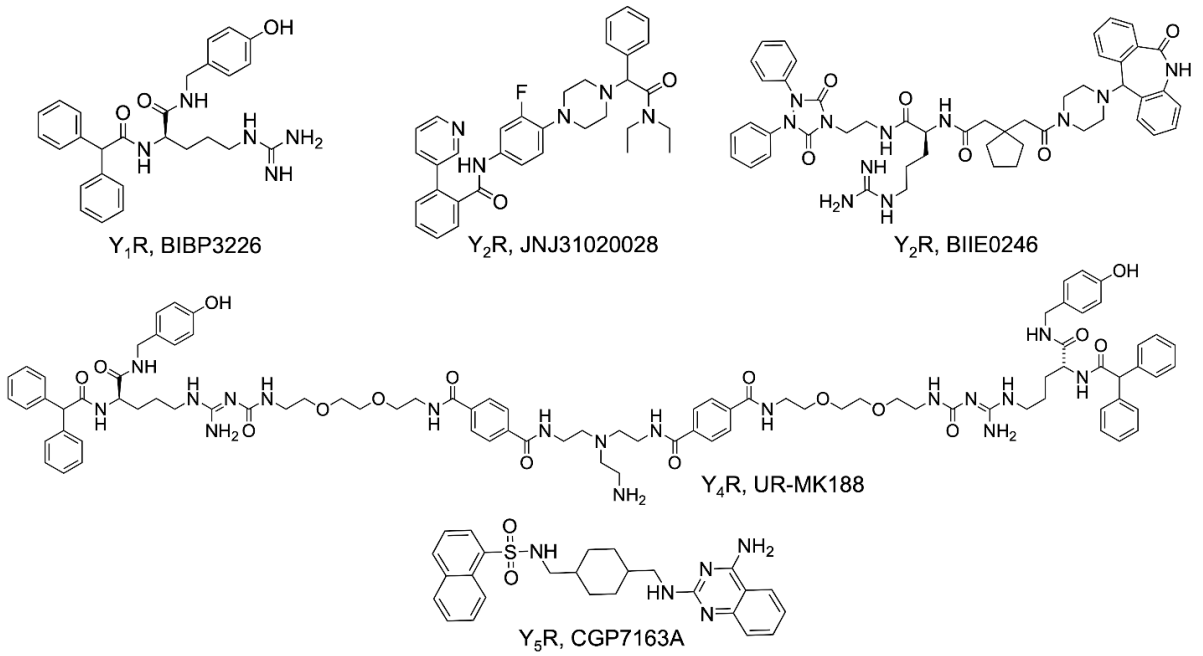

Figure A6.2. Structures of the used YR antagonists.

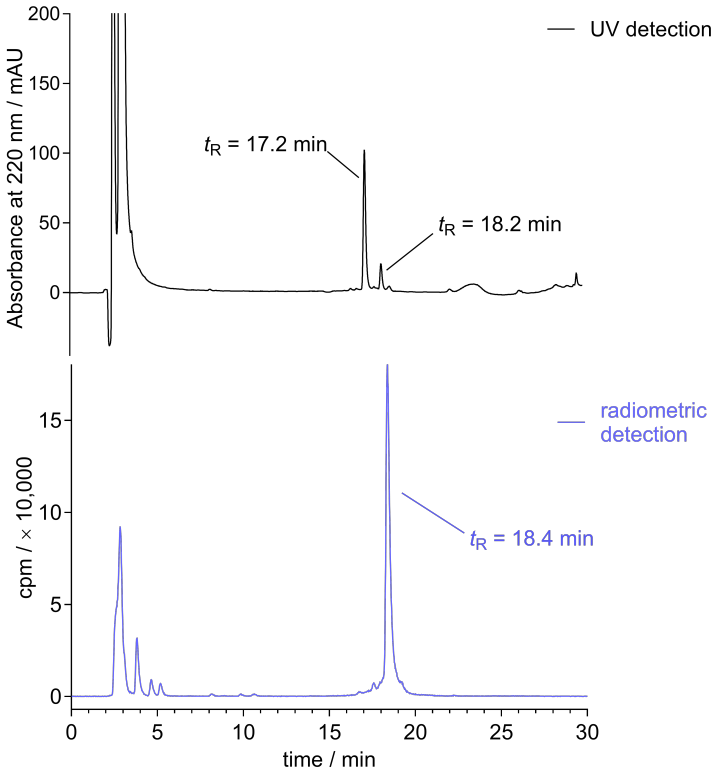

Figure A6.3. Chromatogram of the RP-HPLC analysis of crude [^{3}H]**6.1** obtained by the treatment of His-hPYY (3.5 equiv.) with succinimidyl [^{3}H]propionate (1 equiv.), showing a separation of the precursor His-hPYY (t_R = 17.2 min) and [^{3}H]**6.1** (t_R = 18.2/18.4 min). About. 0.2 µL of the reaction mixture were diluted with 100 µL of acetonitrile/0.05% aqueous TFA 10:90 and analyzed using the HPLC system and column described under *Synthesis of [K^5-[^{3}H]propionyl]His-hPYY ([^{3}H]**6.1**)* (*Section 6.2.2.4*). The following linear gradient was applied: 0-20 min: acetonitrile supplemented with 0.04% TFA/0.05% aqueous TFA 20:80-37:63, 20-22 min: 37:63-95:5, 22-30 min: 95:5 (isocratic).

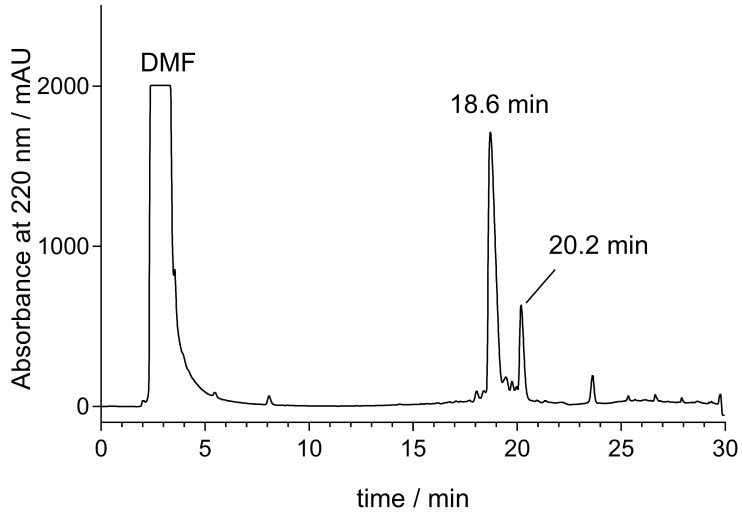

Figure A6.4. Chromatogram of a micropreparative RP-HPLC run performed to isolate [^{3}H]**6.1** from the mixture obtained by treatment of an excess of His-hPYY (3.5 equiv.) with succinimidyl [^{3}H]propionate (1 equiv.). The radioligand [^{3}H]**6.1** (t_R = 20.2 min) could be separated from the labeling precursor hPYY (t_R = 18.6 min). The identity of purified [^{3}H]**6.1** was confirmed by RP-HPLC analysis of a mixture of [^{3}H]**6.1** and [K^5-propionyl]His-hPYY (**6.1**) (see Figure A6.5). The HPLC system and conditions are provided under *Synthesis of [^{3}H]**6.1*** (*Section 6.2.2.4*).

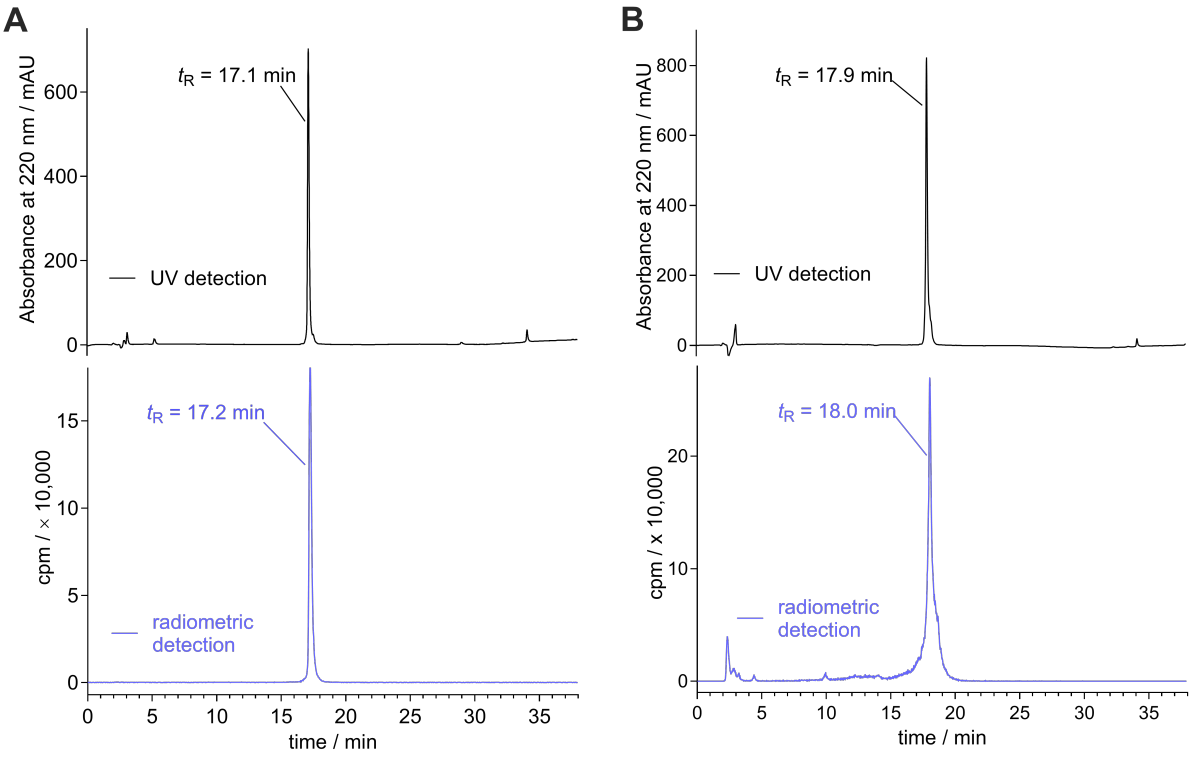

Figure A6.5. (A) Radiochemical purity (99%) of [^{3}H]**6.1** directly after synthesis determined by RP-HPLC analysis. (B) Radiochemical purity (ca. 80%) of [^{3}H]**6.1** determined 24 months after synthesis. Solutions of [^{3}H]**6.1** (0.32 µM) spiked with 19 µM [K^5-propionyl]His-hPYY (injection volume: 100 µL) were analyzed.

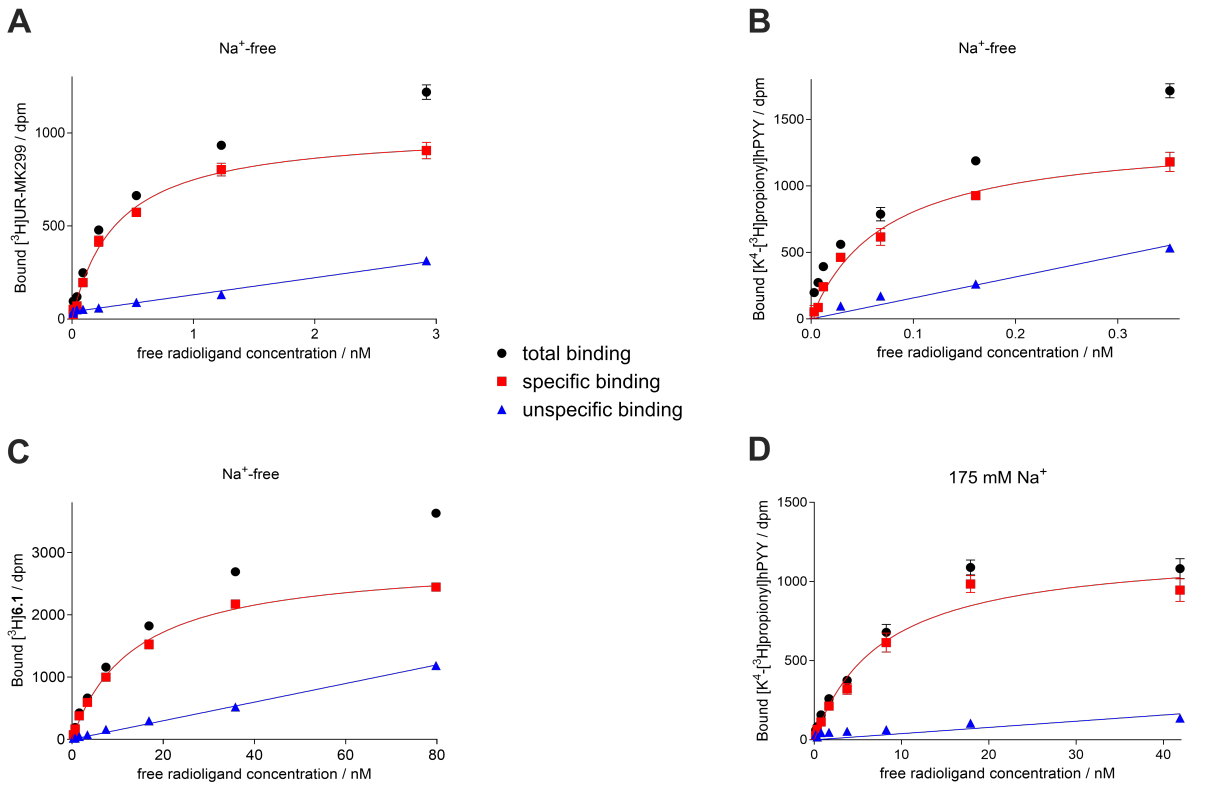

Figure A6.6. Representative saturation binding isotherms from saturation binding experiments. (A) Binding experiment was performed with the tritiated Y_1R antagonist [^{3}H]UR-MK299 at whole SK-N-MC cells in sodium-free *buffer Ib* (B) Binding experiment was performed with the tritiated Y_2R antagonist [K^4-[^{3}H] propionyl]hPYY at whole CHO-hY_2R cells in sodium-free *buffer Ib.* (C) Binding experiment was performed with [^{3}H]**6.1** at whole HEC-1B-hY_5R cells in sodium-free *buffer Ib* and (D) with [K^4-[^{3}H]propionyl]hPYY in sodium-containing *buffer II*. Experiments were performed in triplicate. Total and unspecific binding data represent mean values ± SEM. Specific binding data represent calculated values ± propagated error. For K_d mean values, see table A6.1.

Table A6.1. Summary of the binding affinities (K_d values) of radioligands used in the competition binding assays at human YR subtypes under sodium-free and sodium-containing conditions.

RReceptor subtype	RRadioligand	K_d (mean±SEM) / nM	
		Na^+	Na^+-free
Y_1R	[^{3}H]UR-MK299	0.058[1, a]	0.41 ± 0.02[1, b]
Y_2R	[K^4-[^{3}H]propionyl]hPYY	0.16[1, a]	0.078 ± 0.012[1, b]
Y_4R	[^{3}H]UR-JG102 ([^{3}H]**2.5**)	0.11[2, c]	0.012[2, d]
Y_5R	[K^5-[^{3}H]propionyl]His-hPYY ([^{3}H]**6.1**)	n.d.	20 ± 4[b]
Y_5R	[K^4-[^{3}H]propionyl]hPYY	9.5 ± 1.5[a]	n.d.

[a]Determined in *buffer II*. [b]Determined in *buffer Ib*. [c]Determined in *DPBS*. [d]Determined in *buffer Ia*. K_d values determined in this study are presented as mean values ± SEM (obtained from at least three independent experiments performed in triplicate). n.d. not determined.

6.6.2 References

(1) Schettler, F.; Gattor, A. O.; Koch, P.; Keller, M. Characterization of [^{3}H]propionylated human peptide YY – a new probe for neuropeptide Y Y_2 receptor binding studies. *ACS Pharmacol. Transl. Sci.* 2025. DOI: 10.1021/acsptsci.4c00666.

(2) Gleixner, J.; Gattor, A. O.; Humphrys, L. J.; Brunner, T.; Keller, M. [^{3}H]UR-JG102 – A Radiolabeled Cyclic Peptide with High Affinity and Excellent Selectivity for the Neuropeptide Y Y_4 Receptor. *J. Med. Chem.* 2023, *66* (19), 13788-13808. DOI: 10.1021/acs.jmedchem.3c01224.

Chapter 7

Summary

The neuropeptide Y (NPY) Y_4 receptor (Y_4R) represents a potential therapeutic target with respect to the treatment of diet-related diseases such as obesity due to its involvement in regulating food intake and gastrointestinal tract motility, among others. Within the family of NPY receptors, the Y_4 subtype is one of the least studied. There have been several efforts to develop Y_4R ligands, largely with the aim of obtaining potential therapeutics. Given the lack of high-affinity molecular probes that allow for the study of these ligands *in vitro* under conditions that are physiologically relevant, i.e. using sodium-containing buffers, the new Y_4R radioligand [^{3}H]**2.5** ([^{3}H]UR-JG102) was characterized in a sodium-containing and, for comparison, also in a sodium-free buffer. The findings from this study showed that [^{3}H]**2.5** is suitable for Y_4R ligand binding studies under physiological-like conditions (sodium-containing buffer). [^{3}H]**2.5** was also used in autoradiographic Y4R binding studies using tissues of rat brain and rat intestines, to assess its suitability for this technique. This study revealed low to moderate expression of Y_4R in certain brain regions, including the hypothalamus, midbrain, medulla, and brain stem. Also, Y_4R binding of [^{3}H]**2.5** was detected in rat intestines, known to express Y_4R. These findings suggested that this radioligand is suitable for autoradiographic Y_4R binding studies at cryosections of organs.

Another aspect of this thesis focused on identifying the proteolytic enzyme(s) and susceptible amide bond(s) associated with the proteolytic degradation of the cyclic hexapeptide **2.4** (UR-AK86C) (half-life in human plasma ca. 2 h), a potential lead compound for drug development. It also focused on developing plasma-stable analogs of **2.4** with improved stability in human plasma. By N^{α}-methylation of the proteolytically susceptible amide bond, replacement of the respective amino acids, or elongating the peptide backbone, 13 analogs of **2.4** were synthesized. The study revealed that angiotensin-converting enzyme (ACE), which cleaves the Leu^4-Arg^5 peptide bond in **2.4,** is responsible for the degradation of this peptide in human plasma. Concerning the development of plasma-stable analogs of **2.4**, eight peptides with significantly improved plasma stabilities (half-live ≥ 9 h) were obtained. However, the structural changes also led to significant decreases in their Y_4R binding affinities and agonism (up to 4 log units) compared to **2.4**. Out of these analogs, **4.9b** (UR-AG27), containing a cyclopentyl-Gly in position 4 instead of Leu, emerged as a potential lead structure candidate with significantly improved plasma stability (half-life ca. 19.5 h) while exhibiting partial Y_4R agonism (cAMP assay: pEC_{50} = 7.60, E_{max} = 93%) and

moderately high Y_4R binding affinity ($pK_i = 8.58$). New analogs of **2.4** and **4.9b** were also synthesized, with the guanidine groups in the peptides being replaced by weakly basic methyl-carbamoylguanidine moieties to reduce their positive net charge at pH 7.4, hence potentially increasing their penetration across biological membranes. While the analogs of **2.4** (**5.8b** (UR-AG13), **5.9b** (UR-AG11), and **5.10b** (UR-AG15)) showed increased lipophilicity but decreased Y_4R binding affinities (up to 1.5 log units), the analog of **4.9b** (**5.13b** (UR-AG41)) exhibited enhanced lipophilicity along with a Y_4R binding affinity and agonism similar to **4.9b**. Translocation studies of **4.9b** and **5.13b** using HBEC-5i cells revealed that these analogs were substantially proteolytically degraded by cellular enzymes within 24 h of incubation, producing degradation products similar to those found after their incubation (24 h) in human plasma. Further studies indicated that ACE and its variants were not responsible for their degradation, suggesting a need for additional investigations.

Lastly, part of this thesis focused on elucidating the effect of sodium on the NPY receptor (YR) binding profiles (Y_1R, Y_2R, Y_4R, Y_5R) of the endogenous agonists NPY, peptide YY, and pancreatic polypeptide, as well as of selected YR antagonists. The study showed that the presence of sodium generally reduces the binding of agonists to YRs while increasing the binding of antagonists. Notably, the effect of sodium on YR binding was dependent on the receptor subtype and the type of agonist or antagonist studied.

Chapter 8

Glossary

8.1 Abbreviations

ACE	angiotensin-converting enzyme
allo-Ile	2-((1*R*)-1-methylpropyl)-glycine
Arg(carb)	N^{ω}-carbamoylated arginine containing a tetramethylene spacer in the carbamoyl substituent
Boc	*tert*-butyloxycarbonyl
BSA	bovine serum albumin
br s	broad singlet (to describe the multiplicity of 1H-NMR signals)
BRET	bioluminescence resonance energy transfer
ca.	circa
calcd.	calculated
cAMP	cyclic adenosine monophosphate
CAMYEN	cAMP sensor using YFP-Epac-Nanoluciferase
CHO	Chinese hamster ovary
CNS	central nervous system
cpd. (= compd.)	compound
D_2O	deuterated water
DIC	*N,N'*-diisopropylcarbodiimide
DIPEA	*N*,*N*-diisopropylethylamine
DMF	*N*,*N*-dimethylformamide
DMSO	dimethylsulfoxide
DMSO-d_6	deuterated dimethylsulfoxide
DPBS	Dulbecco's phosphate-buffered saline
EDTA	ethylenediamine-tetraacetic acid
E_{max}	efficacy (maximum effect) of a receptor agonist determined in a functional assay
Epa	exchange protein activated by cAMP
EtOH	ethanol
FBS	fetal bovine serum
Fmoc	fluorenylmethyloxycarbonyl
Fmoc-amino acid	N^{α}-Fmoc protected and side chain protected (if required) amino acid
GABA	γ-aminobutyric acid
GPCR	G protein (= guanine nucleotide binding protein) coupled receptor

h	hour (s)
HBTU	3-[bis-(dimethylamino)methyliumyl]-3*H*-benzotriazol-1-oxide hexafluorophosphate
HEK293 / HEK293T	human embryonic kidney cells
HEC	human endometrial cancer
HEPES	4-(2-hydroxyethyl)-1-piperazineethanesulfonic acid
HOBt	hydroxybenzotriazole
HPLC	high performance liquid chromatography
HRMS	high resolution mass spectrometry
hPP	human pancreatic polypeptide
hPYY	human peptide YY
hNPY	human neuropeptide Y
HRMS	(high-resolution) mass spectrometry
hY_1R	human Y_1 receptor
hY_2R	human Y_1 receptor
hY_4R	human Y_4 receptor
hY_5R	human Y_1 receptor
k	retention (or capacity) factor (HPLC)
MeCN	acetonitrile
MeOH	methanol
MW	molecular weight
NMR	nuclear magnetic resonance (spectroscopy)
Nluc	Nanoluciferase
Pbf sulfonyl	2,2,4,6,7-pentamethyl-dihydrobenzofuran-5-
PBS	phosphate-buffered saline
pEC_{50}	negative decadic logarithm of the half maximal effective concentration (functional assays)
PET	positron emission tomography
pK_d	negative decadic logarithm of the dissociation constant K_d (in M) obtained from a saturation binding experiment
pK_i	negative decadic logarithm of the dissociation constant K_i (in M) obtained from a competition binding experiment
pNPY	porcine neuropeptide Y
ppm	parts per million

PS	polystyrene
PyBOP	benzotriazol-1-yl-oxytripyrrolidinophosphonium-hexafluorophosphate
RLU	relative luminescence units
RP	reversed phase
rt	room temperature
SEM	standard error of the mean
SPPS	solid-phase peptide synthesis
t_0	dead time
$t_{1/2}$	half-life
Tle	α-tert-butylglycine, tert-leucine
TFA	trifluoroacetic acid
t_R	retention time
YFP	yellow fluorescent protein
YR	NPY receptor
Y_nR	NPY receptor subtype n (n = 1, 2, 4 or 5)

8.2 Overview of bold compound numerals and their lab codes

Compound	Lab code	Compound	Lab code	Compound	Lab code
2.2	UR-KK193	**4.7b**	UR-AG37	**5.6**	UR-KS009 or LVK18
2.3	UR-KK200	**4.8a**	UR-AG32	**5.8a**	UR-AG12
2.4	UR-AK86C	**4.8b**	UR-AG33	**5.8b**	UR-AG13
2.5	UR-JG102	**4.9a**	UR-AG26	**5.9a**	UR-AG10
4.1	UR-MK134	**4.9b**	UR-AG27	**5.9b**	UR-AG11
4.2a	UR-AG1	**4.10a**	UR-AG6	**5.10a**	UR-AG14
4.2b	UR-AG2	**4.10b**	UR-AG7	**5.10b**	UR-AG15
4.3a	UR-AG24	**4.11a**	UR-AG38	**5.11**	UR-AG16
4.3b	UR-AG25	**4.11b**	UR-AG39	**5.12**	UR-AG17
4.4a	UR-AG28	**4.12a**	UR-AG42	**5.13a**	UR-AG40
4.4b	UR-AG29	**4.12b**	UR-AG43	**5.13b**	UR-AG41
4.5a	UR-AG30	**4.13a**	UR-AG46	**6.1**	UR-FS014
4.5b	UR-AG31	**4.13b**	UR-AG47		
4.6a	UR-AG34	**4.14a**	UR-AG48		
4.6b	UR-AG35	**4.14b**	UR-AG49		
4.7a	UR-AG36	**5.5**	UR-TB100		

I hereby declare in lieu of an oath that this thesis was written without the unauthorized assistance of third parties and without the use of other than the stated assistance; the data and concepts taken directly or indirectly from other sources are marked with citations.

Some of the experimental work was carried out in collaboration with other institutions and persons. Corresponding notes on the contributions of the persons concerned can be found at the beginning of the relevant chapter and under “Acknowledgments”.

No other persons were involved in the substantive production of this work. In particular, I did not make use of the paid assistance of a doctoral advisor or other persons. No one has received from me, either directly or indirectly, monetary benefits for work that was related to the content of the dissertation submitted.

This thesis has not yet been submitted in the same or a similar form to any other examination authority in Germany or abroad.

Regensburg, on

Albert Owusu Gattor